



**SEISMIC PERFORMANCE OF FLEXIBLE CONCRETE
STRUCTURES**

Approved by


Dissertation Committee:

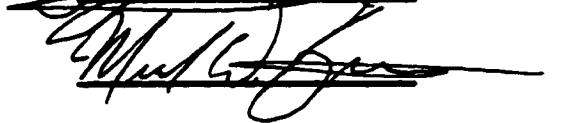


James D. Gann



R. L. Wood





R. L. Wood

**SEISMIC PERFORMANCE OF FLEXIBLE CONCRETE
STRUCTURES**

by

Habib Labib Feghali, Ingenieur de L'Ecole Centrale, MScE.

Dissertation

Presented to the Faculty of the Graduate School of

the University of Texas at Austin

in Partial Fulfillment

of the Requirements

for the Degree of

Doctor of Philosophy

The University of Texas at Austin

December 1999

To my beloved parents, Labib and Amale

ACKNOWLEDGMENTS

There are no words to describe my gratitude and special thanks to Dr. James O. Jirsa. I am deeply indebted to him for his guidance, support, encouragement, and friendly advice. He was like a parent when my parents were away. He is more than what one expects from his professor and mentor, offering me continuous help and encouragement, while guiding me in public relations and leadership. I have and will always appreciate his positive attitude and approach towards life. I am very fortunate to have had the opportunity to working with and for Dr. Jirsa.

I also would like to thank my dissertation committee members: Drs. M.D. Englehardt, M. E. Kreger, S.L. Wood, and S. Kyriakides for their time advice, and constructive criticism. Not to forget Dr. Roesset, whom I wish he could have stayed on my dissertation committee. I want to thank him, and will always gladly remember the joyful conversations we had, his high spirit, encouragement, and sense of humor.

I would like to thank Dr. Furlong, who was my supervisor for my Master's degree, for his support, and for his friendly and parentally concern.

I would like to thank all my professors who taught me math, physics and engineering, especially those at UT: Drs. J.O. Jirsa, R. Furlong, J.M. Roesset, M.E. Kreger, D. Wheat, R. Olson, N. Burns, S.L. Wood, Wright, R. Carrasquillo, S. Kinnas, R. Gilbert, T. Fowler, M.D. Englehardt, and last but not least Dr. J. Breen.

Many thanks to Dr. J. Pincheira for providing me with a copy of the analysis program DRAIN-2D. I appreciated his advice and all the messages we exchanged via the electronic mail. A special thanks goes to Dr Sashi Kunnath for providing a copy of IDARC and IDASS.

My sincere and special thanks to all the staff of the Civil Engineering Department, in particular: Martha, Lena, Elaine, Gilda, and Kathy.

I would also like to thank all my friends and those who believed in me at times when my system was failing me.

Finally, I would like to express my deepest thanks and gratitude to my parents, my brothers and sister, and to my Uncle Dr. Nabil Feghali. They have continuously supported me, and were here for me when I needed them most. Without their love and support, I would not be able to accomplish myself.

SEISMIC PERFORMANCE OF FLEXIBLE CONCRETE STRUCTURES

Publication No. _____

Habib Labib Feghali, PhD.
The University of Texas at Austin, 1999

Supervisor: James O. Jirsa

Concrete structures consisting of shallow slab and wall-like column elements are common in areas of low and moderate seismicity, and are the predominant structural system in the Eastern Mediterranean region. The structural members in the lateral force-resisting system are flexible but have limited ductility and low shear capacity. Recent earthquakes in Greece and Turkey have demonstrated the inadequacies of these systems. Since they constitute such a large portion of the building inventory throughout that region, the need for evaluation and retrofitting of existing structures is obvious.

Nonlinear dynamic time history analyses provide information on the magnitude and distribution of internal forces and deformations in yielding structures

but are very sensitive to assumptions and initial conditions. The objective of this study is to evaluate the influence of different earthquake ground motions, geometry of the structure, and material characteristics on the response of flexible concrete structures. The results are intended to provide guidance on use of nonlinear analyses for seismic design and evaluation.

A prototype basic reinforced concrete frame structure typical of practice in Lebanon was analyzed using scaled ground acceleration records from earthquakes that have occurred in the region. Variations in the basic structure include different mass distributions, variation of the column dimensions, orientation and layout of the wall-type columns, and inclusion of infill walls. The columns are of special interest because they are quite stiff in one direction and flexible in the other. Also, the performance of the prototype structure subjected to various representative ground motion records was studied. Retrofit schemes were investigated. Nonlinear static and nonlinear dynamic analyses were performed.

TABLE OF CONTENTS

ACKNOWLEDGMENTS	iv
ABSTRACT	vi
TABLE OF CONTENTS	viii
CHAPTER 1	
INTRODUCTION	1
1.1 General	1
1.2 Objective	3
1.3 Scope	4
CHAPTER 2	
LITERATURE REVIEW AND BACKGROUND INFORMATION	6
2.1 General	6
2.2 Earthquake Design Philosophy for Frame Structures.....	8
2.3 Soil Structure Interaction.....	11
2.4 Performance-Based Seismic Engineering	14
2.4.1 General	14
2.4.2 Performance Levels.....	16
2.4.3 Earthquake Design Levels.....	24
2.4.4 Design Performance Objectives.....	26
2.4.5 Component Modeling and Acceptance Criteria.....	29
2.4.6 Analysis Procedures	34
2.4.6.1 Linear Static Procedures (LSP)	35
2.4.6.2 Linear Dynamic Procedure (LDP).....	39
2.4.6.3 Nonlinear Static Procedures (NSP).....	43

2.4.6.4 Nonlinear Dynamic Procedure (NDP).....	47
--	----

CHAPTER 3

SEISMICITY AND COMMON STRUCTURAL PRACTICE IN THE MIDDLE EAST	52
3.1 General	52
3.2 Historic Events	52
3.3 Tectonics and Seismicity of the Area.....	53
3.4 Building Structural System.....	58
3.4.1 Columns	58
3.4.2 Slab-Beams	59
3.4.3 Construction Material	61
3.5 Vulnerability of the Structural System to Earthquake Induced Loads	62
3.5.1 Soil-Structure Interaction	63
3.5.2 Insufficient Stiffness, Strength and/or deformation Capacity	63
3.5.3 Building Irregularities	64
3.5.4 Poor Detailing and Quality Control	67
3.6 Case Study.....	70
3.6.1 General Building Description	71
3.6.2 Dimensions and Detailing of Structural Components.....	72

CHAPTER 4

ANALYTICAL TOOLS AND MODELS.....	77
4.1 General	77
4.2 Nonlinear Programs.....	78
4.2.1 RCCOLA	79
4.2.2 DRAIN-2D.....	80
4.2.2.1 Dynamic Equilibrium and Integration Solution	81

4.2.2.2	Static Incremental Loading.....	82
4.2.2.3	Viscous Damping	83
4.2.2.4	Beam Column Element	85
4.2.2.5	Hysteretic Behavior	86
4.2.3	SAP2000 NL-PUSH.....	88
4.2.3.1	Dynamic Analyses and Integration Procedure.....	88
4.2.3.2	Nonlinear Pushover Options	88
4.2.3.3	Viscous Damping	91
4.2.3.4	Nonlinear Link	91
4.3	Analytical Model	93
4.3.1	DRAIN-2D.....	94
4.3.1.1	Modeling Strength Degradation of Reinforced Concrete Members.....	94
4.3.1.2	Modeling of Shear Failure in Reinforced Concrete Members	96
4.3.1.3	Modeling Parameters and Procedure.....	101
4.3.1.3.1	Material Properties	101
4.3.1.3.2	Element Stiffness.....	102
 CHAPTER 5		
SENSITIVITY STUDY		111
5.1	General	111
5.2	Assumptions and Parametric Variables.....	111
5.2.1	Damping Coefficients	116
5.2.1.1	Conditions	116
5.2.1.2	Results	117
5.2.2	Strength of Materials.....	119
5.2.2.1	Conditions	119
5.2.2.2	Results	120

5.2.2.3 Steel Ductility.....	122
5.2.3 Effective Stiffness.....	124
5.2.3.1 Conditions	124
5.2.3.2 Results	126
5.2.4 Frame Geometry.....	128
5.2.4.1 Column Dimensions.....	128
5.2.4.2 Connection Rigidity (End Eccentricity)	130
5.2.4.3 Variation in Column Dimensions over Height of Structure.....	132
5.2.4.4 Column Layout.....	136
5.2.5 Mass Distribution	140
5.2.5.1 General	140
5.2.5.2 Analysis Results	140
5.2.6 Residual Column Strength	150
5.2.6.1 General	150
5.2.6.2 Analysis Results	151
5.2.7 Infill Action	157
5.2.8 Variations in Ground Motions.....	162
5.2.8.1 Ground Motion Characteristics	162
5.2.8.2 Structure Characteristics.....	169
5.2.8.3 Analysis Results	170

CHAPTER 6

NON LINEAR STATIC ANALYSES	175
6.1 General	175
6.2 Drawbacks of the Pushover Procedure.....	176
6.3 Load Pattern	177
6.4 Comparison Study	179

6.4.1 DRAIN-2D	179
6.4.1.1 Frame Structure	180
6.4.1.2 Soft Story Frame Structure	185
6.4.1.3 All Infill Frame Structure	189
6.4.1.4 Residual Strength	195
6.4.1.5 Geometric Variations	196
6.4.2 SAP2000	199
6.4.2.1 Modeling Assumptions	199
6.4.2.2 Results	200

CHAPTER 7

RETROFIT AND PERFORMANCE ENHANCEMENT SCHEMES FOR THE PROTOTYPE BUILDING.....	203
7.1 General.....	203
7.2 Performance of a Typical Building	203
7.2.1 Modeling Assumptions	203
7.2.2 Input and Building Description.....	207
7.2.3 Results	208
7.3 Retrofit	216
7.3.1 Conditions.....	216
7.3.2 Design Strategy for Seismic Retrofit	216
7.3.3 Retrofit Options/Techniques	217
7.3.4 Application of Retrofit	219
7.3.4.1 Addition of Shear Walls.....	221
7.3.4.2 Stiffness Reduction	227
7.3.5 Enhanced Design.....	232
7.3.5.1 Conditions	232
7.3.5.2 Results	232

7.4 Discussion and Design Implications	236
7.4.1 Uncertainties	236
7.4.2 Limitations.	239
7.4.3 Design Implications	241
CHAPTER 8	
CONCLUSIONS	243
8.1 Summary	243
8.2 Conclusions	249
8.3 Assumptions and Uncertainties	253
8.4 Suggestions For Further Research	254
REFERENCES	256
VITA	263

CHAPTER 1

INTRODUCTION

1.1 General

Reinforced concrete structural systems with concealed beams and ribbed slabs, slab-column systems and columns with large length to width ratio are often used for architectural reasons and because they are economical and/or traditional in some regions of the world. Under lateral forces, the flexibility of some elements in these structures may lead to large interstory or overall drifts. Flexible concrete structures have been used often in areas of low and moderate seismicity. In Lebanon and the Mediterranean region, such structures predominate. Many Lebanese buildings were designed according to codes where little attention was given to layout of the structures or to details, connections and irregularities. Common problems include:

- **Eccentric connections**
- **Poor detailing**
 - **90⁰ hooks**
 - **large spacing of ties in columns**
 - **splicing of reinforcement in probable plastic hinge location**
- **Stiffness and mass irregularities**
 - **soft story**

- concentrated mass on roof
- balconies
- discontinuous walls

An evaluation of the performance of these structures under seismic forces is essential for carrying out rehabilitation of existing systems or for design of new structures.

There is growing interest in the use of nonlinear static and nonlinear dynamic time history analysis procedures in design offices. These inelastic analyses yield information on the magnitude and distribution of internal forces and deformations in yielding structures but are very sensitive to assumptions and initial conditions. Such information is essential for evaluating the performance of a structure. Over the past 25 years, several nonlinear time history analysis programs have been developed. However, the applicability and accuracy of those programs need to be evaluated before they can be used in design offices.

The Federal Emergency Management Association has recently developed guidelines for seismic rehabilitation (FEMA 273). The document describes analytical

models for components and connections to be used in the evaluation and retrofit of existing buildings. The following material is included:

- Recommendations for analytical models of components and connections
- Four procedures for analysis
 - linear static
 - linear dynamic
 - nonlinear static (pushover)
 - nonlinear dynamic (time history)

The recommendations for modeling and the analytical procedures in FEMA 273 need to be examined regarding their applicability to flexible buildings.

1.2 Objective

The purpose of this study is to evaluate the influence of different parameters including earthquake ground motions, geometric and material characteristics, on the response of flexible concrete structures. The performance of flexible concrete structural systems typical in the Mediterranean basin will be investigated using available analytical tools and parameters that reflect the geometry of the systems. Based on the results, recommendations will be suggested for the parameters to be used in modeling flexible systems for evaluation of their performance and for retrofit schemes applicable to flexible reinforced concrete buildings.

1.3 Scope

The behavior of flexible buildings was studied by considering variations in geometry of the structural systems, in materials of construction, and in earthquake ground motions. Plans and details of typical existing and retrofitted systems were used. The parameters included were:

- **Geometric characteristics**
 - variations in plan layout: dimensions and orientation of long axis of columns
 - use of infill
 - effective moment of inertia for beams and columns
 - retrofit schemes, geometry and details
- **Characteristics of materials of construction**
 - steel
 - concrete
- **Earthquake ground motions**
 - peak ground acceleration
 - site-specific records

Nonlinear time history analyses were used to determine the performance of the systems under different ground motion records and different intensities of shaking. Results using nonlinear static procedures were compared with those using nonlinear time history procedures. Nonlinear static analyses in SAP2000 were compared with similar analyses conducted using DRAIN-2D.

CHAPTER 2

LITERATURE REVIEW AND BACKGROUND INFORMATION

2.1 General

Performance-based design has been defined as a set of procedures that yield structures with predictable performance and satisfy stated performance criteria. The major building codes currently in effect include the American Concrete Institute (ACI 318-95)⁹, the Uniform Building Code (ICBO-1994)¹⁰, BOCA Code (BOCA-1993)¹¹ and Standard Building Code (SBCCI-1993)¹². Each of these in turn is based either on the SEAOC Blue Book (SEAOC-1990)² or NEHRP Provisions (BSSC-1991)¹³, resource documents which themselves are closely tied to ATC 3-06 (ATC-1978)²⁶. Loads used in design are based on equivalent lateral forces and pseudo displacements²⁷: The base shear (loads) is equivalent to the forces that the building is expected to resist, but the building displacements using this base shear are less than the displacements likely to occur during a design earthquake. Experience with past earthquakes has indicated that this procedure is inadequate in controlling damage in buildings. The primary goal of current codes is to provide life-safety in severe, relatively rare earthquakes. Secondary goals include control of property damage and maintenance of function through drift limitations in moderate events, which are expected to occur more often. Codes have been developed empirically, based on observations of actual damage that has occurred in past earthquakes and on extensive research at various institutions. Therefore, they are considered as prescriptive

standards that yield actions assumed to result in acceptable performance with regard to strength resistance, however the damage control is poor. The extensive damage and economic losses that occurred during the 1994 Northridge and other recent moderate earthquakes have stimulated structural engineers to consider protecting economic investment in addition to meeting life safety requirements of structures. The Structural Engineers Association of California (SEAOC) recognized the need for performance evaluation even before the Northridge earthquake occurred. In 1992 the SEAOC Vision 2000 Committee was formed and subsequently (SEAOC 1995) presented recommendations concerning performance based seismic design and construction of buildings²⁸. Vision 2000 was based on the use of newly developing analytical techniques and methodologies for characterizing the behavior of structural systems subjected to ground motion, using non-linear analysis methods.

In determining the performance of a structure, inelastic response analyses were recognized as the most rigorous analysis procedure for seismic design¹. Inelastic response history analyses yield the needed information regarding distribution of internal forces and level of deformations in critical elements in yielding structures. Nevertheless, this procedure is a very difficult task to perform. However, simple non-linear models for structural systems were developed over the past 25 years. Since their use does not require particular mastery of numerical techniques, professional engineers may use them as an alternative to the linear models that have been adopted almost exclusively so far²⁹. Parameters to be used in

modeling a structure and determining a reliable response are the most difficult tasks facing the structural engineer.

In this chapter, the philosophy behind the design of structures to resist earthquake-induced forces is presented briefly. Performance-based design introduced by the NEHRP documents (FEMA 310 and FEMA 273), is defined. Four analytical design procedures are discussed, namely linear and nonlinear static and dynamic procedures.

2.2 Earthquake Design Philosophy for Frame Structures

SEAOC expressed the general philosophy of earthquake resistant design of buildings as follows²:

- 1- Resist minor earthquakes with no non-structural damage. Minor earthquakes may occur frequently in the service life of a structure.
- 2- Resist moderate earthquakes with no structural damage, some non-structural damage may take place.
- 3- Resist major earthquakes without collapse. The structure may sustain significant structural and non-structural damage. Major earthquakes are rare and should have long return periods.

Unlike standard design procedures for static loading, the structure is expected to yield and deform well beyond the elastic limit in a major earthquake. Frame members are expected to have a ductility that allows good energy absorption

capacity for the members. The ductility of a member is the ratio between the deformation of the member at ultimate and the deformation at yield. Although it is possible to design a structure to respond elastically during a major earthquake, it is economically and architecturally impractical.

Current design code procedures require most structures to deform in the inelastic range during a major earthquake by using reduction factors greater than unity for the design loads. Figure 2.1 shows the lateral force versus lateral displacement relationships for two structures A and B that are assumed to have the same initial stiffness but different lateral strengths. A behaves elastically while B can deform beyond its elastic range. It can be seen from Fig. 2.1 that structure B can be designed for a lower strength than structure A, provided that the inelastic deformation of structure B is controlled. The higher the ductility of structure B, the larger its energy dissipation capacity and the lower the required strength.

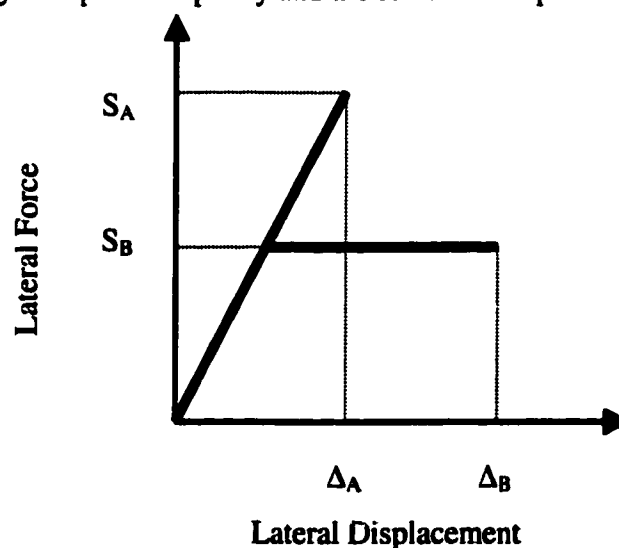


Figure 2.1 Force-displacement relationship

Current codes account for nonlinear seismic response in a linear static analysis procedure by including a response modification factor in calculating a reduced equivalent base shear to reproduce a rough approximation of the internal forces during a design earthquake. This modification factor is function of the ductility of the structure. Other modification factors can be used to account for the importance (use) of the structure and to represent the soil interaction with the structure. The ductility of the structure depends on the structural system and the material of construction. Building displacements using this base shear are significantly less than the displacements the building will actually experience during an earthquake, thus this method introduces another modification factor for estimating the drift and ductility demands.

To ensure ductile behavior for a reinforced concrete structure, current design provisions require special detailing of frame members and connections. The philosophy of forcing the beams to yield before columns also known as weak-beam strong-column provision is implemented by the formulae (2.1)⁹

$$\frac{\sum M_{col}}{\sum M_{beam}} \geq \frac{6}{5} \quad (2.1)$$

This design provision is based on the capacity of the member section, where $\sum M_{col}$ is the sum of column capacities at the frame connection and $\sum M_{beam}$ is the sum of beam capacities at the connection. Figure 2.2 shows the possible failure mechanisms for a frame structure.

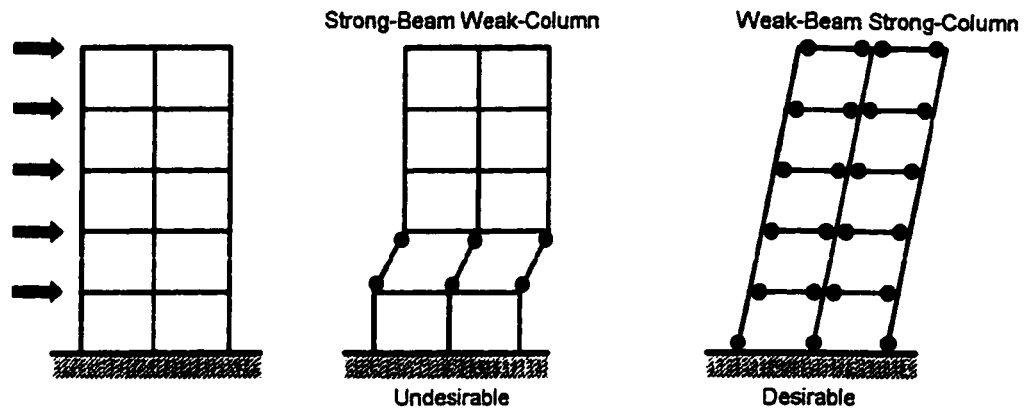


Figure 2.2 Possible Failure mechanisms for frame structures subjected to lateral forces¹⁵.

The strong-beam weak-column mechanism is undesirable mainly because yielding of columns in a given story means increased likelihood of collapse of the entire building. The weak-beam strong-column mechanism increases the likelihood of flexural yielding in beams prior to hinging of columns which allows energy dissipation with less likelihood of collapse of the building.

2.3 Soil Structure Interaction

The estimation of earthquake motions at the site of a structure is the most important phase of the design or retrofit of a structure. Many methods were developed to conduct accurate earthquake analysis of a soil-structure system in the time domain, including many realistic nonlinear properties^{6,7,23}. These methods vary in complexity, from finite element modeling that accounts for the effects of foundation embedment, variations of soil properties with depth, etc, to simplified

procedures that utilize axial and rotational springs and corresponding dashpots to simulate the stiffness and damping of the foundation soil. Two simplified procedures can be used to account for the effects of the soil-structure interaction³⁰:

- The first approach involves modifying the dynamic properties of the structure and the evaluation of the response of a modified structure to the free-field motion. Interaction effects are introduced by the addition of springs and dashpots as a model for the effective stiffness and damping of the interacting soil-structure system. This model produces an increase in the fundamental period of the structure as a result of the flexibility of the foundation soil. The change in damping results mainly from the effects of energy dissipation in the soil due to radiation damping and inelastic action in the soil. Despite the simplifications in modeling, this procedure yields results that are in close agreement with those of more “accurate” but expensive procedures, such as finite element method³⁰. Table 2.1 shows formulas that can serve in computing the spring stiffness and the effective mass and damping factors used in modeling the foundation soil under a rigid circular plate on the surface of a half-space.

DIRECTION	STIFFNESS	DAMPING	MASS
Vertical	$k = \frac{4Gr}{1-\nu}$	$1.79 \sqrt{k\rho r^3}$	$1.50 \rho r^3$
Horizontal	$18.2Gr \frac{(1-\nu^2)}{(2-\nu)^2}$	$1.08 \sqrt{k\rho r^3}$	$0.28 \rho r^3$
Rotation	$2.7Gr^3$	$0.47 \sqrt{k\rho r^5}$	$0.49 \rho r^5$
Torsion	$5.3Gr^3$	$1.11 \sqrt{k\rho r^5}$	$0.70 \rho r^5$

ρ = mass of unit volume

ν = Poisson's ratio

r = plate radius

G = shear modulus

Table 2.1 Properties of Rigid Circular Plate on Surface of Half-Space²³

- The second procedure involves modifying the free-field ground motion and analyzing the response of the fixed-base structure using the modified ground motion.

If a lightweight flexible structure is founded on very stiff rock, the assumption that the input motion at the base of the structure is the same as the free field earthquake motion is valid. This assumption is valid for most building structures, since buildings are approximately 90% voids, and very often, the weight of the soil excavated is excavated before the structure is built and is equal to or

greater than the weight of the structure^{23,31}. However, if the structure is very massive and stiff, and the soil is relatively soft, then interaction between the soil and the structure in the proximity of the foundation is expected to occur.

For most structures, particularly buildings, simplified procedures will yield acceptable results, except for very massive structures such as dams where the soil need to be modeled more accurately, using finite element methods for example.

Large structures can cause the surrounding terrain to move. This effect is not of great significance for most buildings and can be ignored in their fundamental mode. However, the effect can be large for high modes of vibration, in particular for large buildings where the participation factor of high modes is not negligible^{1,31,32}. In this study, the effect of soil-structure interaction will be neglected.

2.4 Performance-Based Seismic Engineering

2.4.1 General

The civil engineering community has developed techniques to design structures to behave elastically even in the most severe earthquakes. However, severe earthquakes are relatively infrequent events with low probability of occurring during the life of a building. Therefore, it is generally unnecessary and uneconomical to design all buildings to remain elastic in such rare events. Only critical facilities and facilities that contain hazardous material need to remain undamaged during severe earthquakes.

Hence, engineers have been designing buildings that can survive severe earthquakes without collapse but with some damage occurring. Life safety has been the primary concern for designers. Following the experience gained from recent earthquakes in California and Japan, structural engineers and building owners are realizing the need to control economic losses due to non-structural damage and business interruption from minor to moderate earthquakes in addition to satisfying requirements for life safety. Sozen⁴⁸ states that the most relevant performance criterion for a building structure that has survived an earthquake is the cost of all damage, not only damage to structural elements. Much of the earthquake damage in buildings that do not collapse has been observed to be related to the distortion of the building³³. An acceptable measure of the distortion is given by the story drift ratio. The higher the drift ratio, the higher the amount of damage in the structure. Simple techniques for estimating structural displacements helped to develop design based explicitly on expected displacements. Displacement-based or performance-based design is useful for the owner or the designer in setting a performance level that is based on controlling displacement demands. The goal is to minimize earthquake related cost to the building owner over the life of the building by finding a balance between the cost related to providing minimum earthquake resistance to satisfy life safety and the cost related to damage in possible future earthquakes¹⁴. Consequently, performance-based standards for structural design can be considered to depend on three major elements:

- Definition of performance levels or damage states.
- Definition of actions or events that are likely to affect the structure.
- Definition of acceptable or satisfactory performance.

2.4.2 Performance Levels

The Structural Association Engineers of California (SEAOC) recognized five performance levels for buildings in the Vision 2000 report³⁴ published in 1995. SEAOC recommended the use of maximum transient interstory drift ratio to relate the displacements in a building to the performance level of the building. Each performance level is related to a range of damage. Figure 2.3 shows the spectrum of damage states that a building may experience when subjected to ground motions of increasing severity. Table 2.2 illustrates permissible levels of damage to the various systems and sub-systems in buildings, for each of the performance levels. It also shows typical transient and permanent drift ratios for the corresponding level of performance.

Damage Range & Damage Index **Damage States and Performance Level Thresholds**

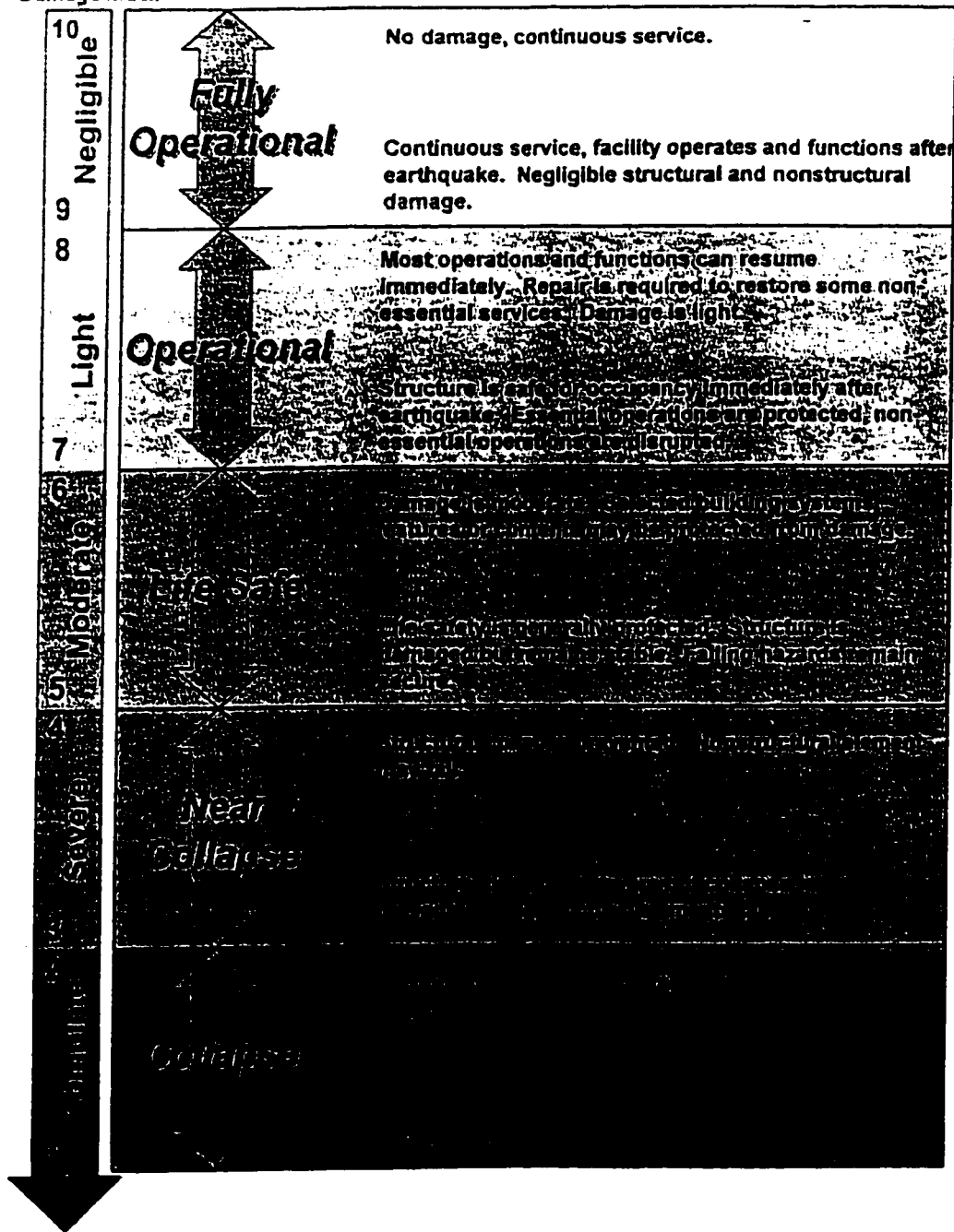


Figure 2.3 Spectrum of Damage States³⁴

System Description	Performance Level									
	10 Fully Operational	9	8 Operational	7	6 Life Safe	5	4 Near Collapse	3	2 Collapse	1
Overall building damage	Negligible		Light		Moderate		Severe		Complete	
Permissible transient drift	< 0.2%+/-		< 0.5%+/-		< 1.5%+/-		< 2.5%+/-		> 2.5%+/-	
Permissible permanent drift	Negligible.		Negligible.		< 0.5%+/-		< 2.5%+/-		> 2.5%+/-	
Vertical load carrying element damage	Negligible.		Negligible.		Light to moderate, but substantial capacity remains to carry gravity loads.		Moderate to heavy, but elements continue to support gravity loads.		Partial to total loss of gravity load support	
Lateral Load Carrying Element damage	Negligible - generally elastic response; no significant loss of strength or stiffness.		Light - nearly elastic response; original strength and stiffness substantially retained. Minor cracking/yielding of structural elements; repair implemented at convenience.		Moderate - reduced residual strength and stiffness but lateral system remains functional.		Negligible residual strength and stiffness. No story collapse mechanisms but large permanent drifts. Secondary structural elements may completely fail.		Partial or total collapse. Primary elements may require demolition.	
Damage to architectural systems	Negligible damage to cladding, glazing, partitions, ceilings, finishes, etc. Isolated elements may require repair at users convenience.		Light to moderate damage to architectural systems. Essential and select protected items undamaged. Hazardous materials contained		Moderate to severe damage to architectural systems, but large falling hazards not created. Major spills of hazardous materials contained.		Severe damage to architectural systems. Some elements may dislodge and fall.		Highly dangerous falling hazards. Destruction of components.	
Egress systems	Not impaired.		No major obstructions in exit corridors. Elevators can be restarted perhaps following minor servicing.		No major obstructions in exit corridors. Elevators may be out of service for an extended period.		Egress may be obstructed		Egress may be highly or completely obstructed.	

Table 2.2 General Damage Description by Performance Levels and System³⁴

System Description	Performance Level									
	10 Fully Operational	9	8 Operational	7	6 Life Safe	5	4 Near Collapse	3	2 Collapse	1
Mechanical/Electrical/ Plumbing/Utility Systems	Functional.		Equipment essential to function and fire/life safety systems operate. Other systems may require repair. Temporary utility service provided as required..		Some equipment dislodged or overturned. Many systems not functional. Piping, conduit ruptured.		Severe damage and permanent disruption of systems.		Partial or total destruction of systems. Permanent disruption of systems.	
Damage to contents	Some light damage to contents may occur. Hazardous materials secured and undamaged.		Light to moderate damage. Critical contents and hazardous materials secured.		Moderate to severe damage to contents. Major spills of hazardous materials contained.		Severe damage to contents. Hazardous materials may not be contained.		Partial or total loss of contents.	
Repair	Not required.		At owners/tenants convenience.		Possible - building may be closed.		Probably not practical.		Not possible.	
Effect on occupancy	No effect.		Continuous occupancy possible.		Short term to indefinite loss of use.		Potential permanent loss of use.		Permanent loss of use.	

Table 2.2 (continued)

Four building performance levels were adopted in the NEHRP document, Guidelines for the Seismic Rehabilitation of Buildings (FEMA 273 and FEMA 274)¹. Each building performance level is made up of a structural performance level that describes the limiting damage state of the structural systems and a nonstructural performance level that describes the limiting damage state of the nonstructural systems.

There are five structural performance levels:

- S-1 Immediate Occupancy Performance Level.
- S-2 Damage Control Performance Range.
- S-3 Life Safety Performance Level.
- S-4 Limited Safety Performance Range.
- S-5 Collapse Prevention Performance level.

And five nonstructural performance levels:

- N-A Operational Performance Level.
- N-B Immediate Occupancy Performance Level.
- N-C Life Safety Performance Level.
- N-D Hazards Reduced Performance Level.
- N-E only structural improvements are made.

Figure 2.4 illustrates the building performance levels and ranges and Table 2.3 shows the damage control within a building performance level.

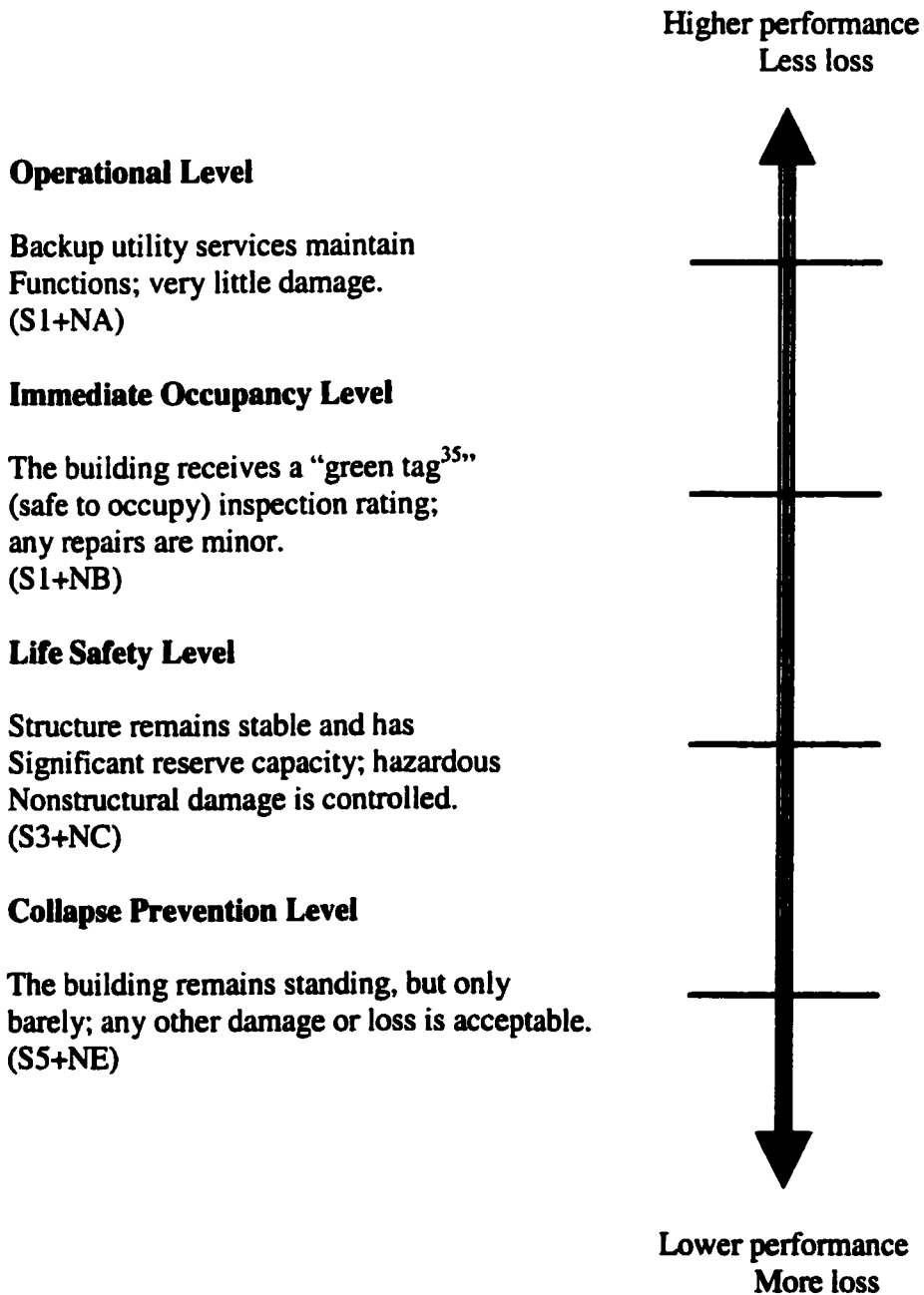


Figure 2.4 Spectrum of Damage States¹

Damage Control and Building Performance Levels

	Building Performance Levels			
	Collapse Prevention Level	Life Safety Level	Immediate Occupancy Level	Operational Level
Overall Damage	Severe	Moderate	Light	Very Light
General	Little residual stiffness and strength, but load-bearing columns and walls function. Large permanent drifts. Some exits blocked. Infills and unbraced parapets failed or at incipient failure. Building is near collapse.	Some residual strength and stiffness left in all stories. Gravity-load-bearing elements function. No out-of-plane failure of walls or tipping of parapets. Some permanent drift. Damage to partitions. Building may be beyond economical repair.	No permanent drift. Structure substantially retains original strength and stiffness. Minor cracking of facades, partitions, and ceilings as well as structural elements. Elevators can be restarted. Fire protection operable.	No permanent drift; structure substantially retains original strength and stiffness. Minor cracking of facades, partitions, and ceilings as well as structural elements. All systems important to normal operation are functional.
Nonstructural components	Extensive damage.	Falling hazards mitigated but many architectural, mechanical, and electrical systems are damaged.	Equipment and contents are generally secure, but may not operate due to mechanical failure or lack of utilities.	Negligible damage occurs. Power and other utilities are available, possibly from standby sources.
Comparison with performance intended for buildings designed, under the NEHRP Provisions, for the Design Earthquake	Significantly more damage and greater risk.	Somewhat more damage and slightly higher risk.	Much less damage and lower risk.	Much less damage and lower risk.

Table 2.3 General Damage Descriptions by Performance Levels¹.

The four building performance levels described in Table 2.3 and Fig. 2.4 are summarized below:

- **Operational Level (1-A):** The building is occupiable and all equipment and services related to the building’s basic occupancy and functionality are available

for use. In general, the damage is negligible and repair is not required. Under low levels of ground motion, most buildings should be able to meet or exceed this performance level. However, it will not be economically practical to design for this performance under severe levels of ground shaking, except for buildings that house essential services.

- **Immediate Occupancy Level (1-B):** The building is expected to sustain minimal or no damage to its structural elements. (In a concrete frames, this kind of damage corresponds to minor hairline cracking, limited yielding and generally strains below 0.003.) The building remains safe to occupy for its normal intended function, immediately following the earthquake. However, damage to some contents, utilities and non-structural components may disrupt some normal functions. Back-up systems and procedures may be required to permit continued use. Repairs may be instituted at the owners' and tenants' convenience. Many building owners may wish this level of performance when the building is subjected to moderate earthquake ground motion. Some owners may desire such performance for very important buildings under severe levels of earthquake ground shaking.
- **Life Safety Level (3-C):** The building may experience extensive damage to structural and nonstructural components. (In a concrete frame, this damage represents extensive damage to beams, spalling of cover, shear cracking (1/8" or less), minor column-spalling, joints cracked.) The structure's lateral stiffness and

ability to resist additional lateral loads have been reduced, possibly to a great extent, however, some margin against collapse remains. Repairs may be required before reoccupancy, and repair may be deemed economically impractical. Many building owners will desire to meet this performance level for a severe level of ground shaking.

- **Collapse Prevention Level (5-E):** An extreme damage state in which the lateral and vertical load resistance of the building have been substantially compromised. Aftershocks could result in partial or total collapse of the structure. Many buildings meeting this level will be complete economic losses. (In a concrete frame, this damage can be seen as extensive cracking and hinge formation in ductile elements, limited damage to non-ductile elements and severe damage to short columns.) This performance level has sometimes been selected as the basis for mandatory seismic rehabilitation ordinances enacted by municipalities as it reduces the severe life-safety hazards at relatively low cost.

In order to determine the level of performance for a structure, the level of ground motion that the structure is expected to be subjected to, must be selected.

2.4.3 Earthquake Design Levels

Four earthquake design levels are recognized by SEAOC in VISION 2000³⁴. These levels are expressed in terms of a mean recurrence interval or a probability of exceedance as shown in Table 2.4³⁴. The mean recurrence interval (e.g. 475 years) is

an expression of the average period of time, expressed in years, between the occurrence of earthquakes which produce effects of the same, or greater, severity. The probability of exceedance (e.g. 10% in 50 years) is a statistical representation of the chance that earthquake effects exceeding a given severity, will be experienced at the site within a specified number of years. The relationship between the recurrence interval and the probability of exceedance in a specified number of years is given by equation (2.2):

$$P_R = \frac{1}{1 - e^{\frac{1}{n} \ln(1 - P_{En})}} \quad \text{Eq.(2.2)}$$

Where,

P_R is the mean return period in years.

P_{En} is the probability of exceedance in n years.

In FEMA 273, two levels of earthquake shaking hazard are used to satisfy the basic safety objectives, namely, Basic Safety Earthquake 1 (BSE-1) and Basic Safety Earthquake 2 (BSE-2) also called Maximum Considered Earthquake ground motion (MCE). The United States Geological Survey (USGS) had developed, in 1996, national probabilistic maps of expected seismic ground shaking for ground motions with a 10% chance of exceedance in 50years, a 5% chance of exceedance in 50 years and a 2% chance of exceedance in 50 years. These maps plot key ordinates of a ground acceleration response spectrum, allowing development by the user of a complete spectrum at any site. In most areas of the United States, BSE-2 earthquake

ground motion has a 2% probability of exceedance in 50 years¹ (the corresponding return period is 2,475 years). The BSE-1 earthquake is defined as that ground shaking having 10% probability of exceedance in 50 years (the corresponding return period is 474years). For BSE-1, ground motions need not exceed those used for new buildings, defined as 2/3 of the BSE-2 motion¹.

Table 2.4 Earthquake Design Levels³⁴

Earthquake Design Level	Recurrence Interval	Probability of Exceedance
Frequent	43 years	50% in 30 years
Occasional	72 years	50% in 50 years
Rare	475 years	10% in 50 years
Very Rare	970 years ²⁶	10% in 100 years ²⁶

2.4.4 Design Performance Objectives

The combination of a target performance level and a specific intensity of ground motion at which the performance is to be achieved is termed a Performance Objective. Figure 2.5³⁴ is a graphical summary of the recommendations for minimum

design performance objectives for buildings of different occupancies and uses. Similar figures can be drawn to illustrate the design performance for buildings with the performance levels defined in FEMA 273¹, as shown in Table 2.5.

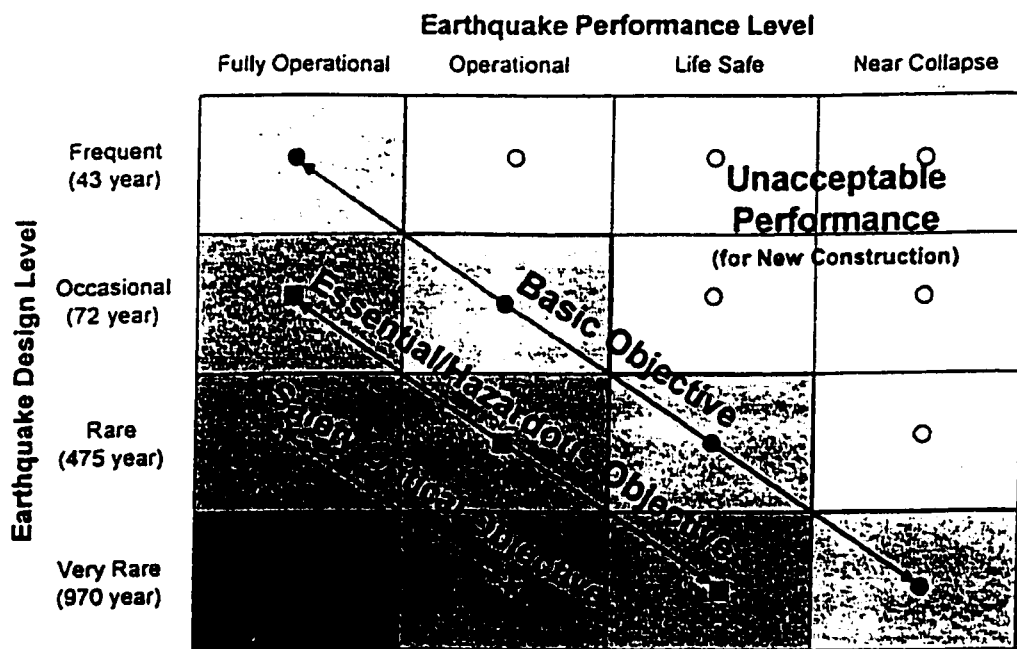
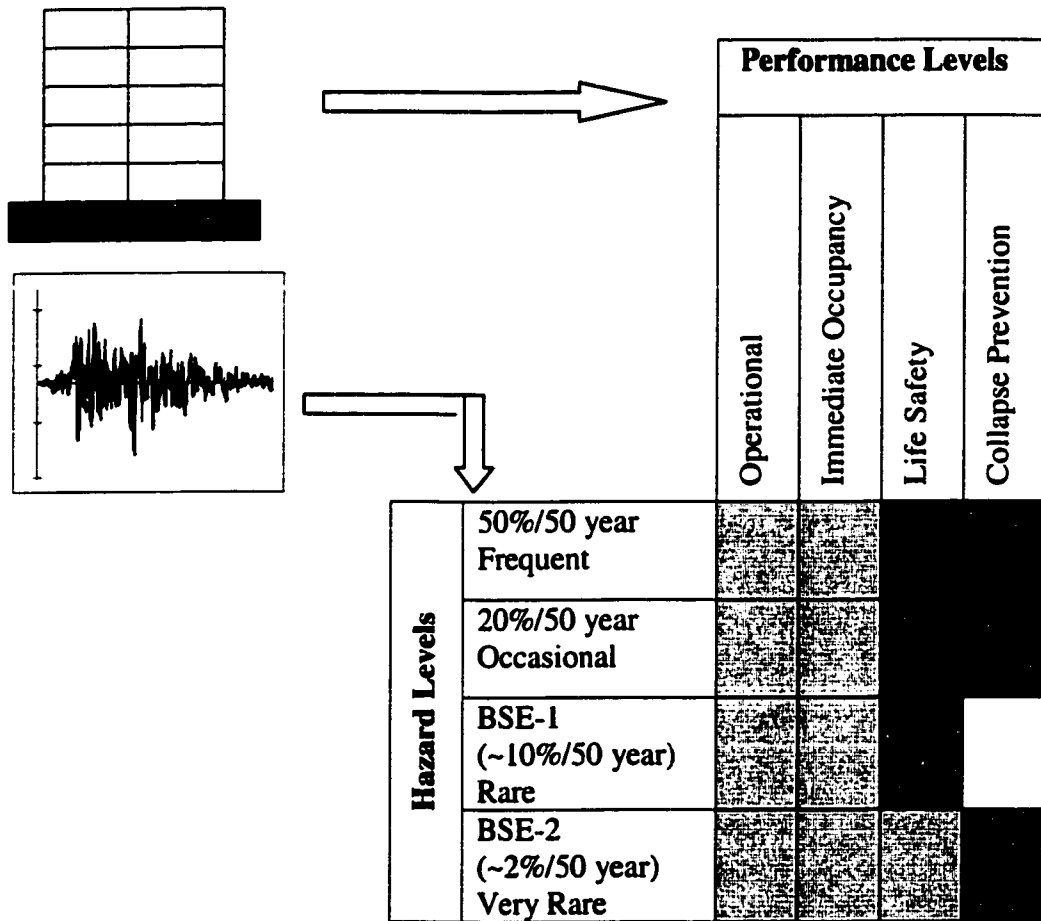


Figure 2.5 Recommended Performance Objectives for Buildings³⁴.






-  Enhanced Objectives
-  Basic Safety Objectives
-  Limited Objectives

Table 2.5 Rehabilitation objectives as by FEMA 273¹

In Table 2.5, basic safety objective, BSO, is a performance level intended to provide a low risk of life endangerment for any earthquake likely to affect the structure. However, buildings meeting the BSO are expected to experience little

damage from relatively frequent, moderate earthquakes, but significant damage may occur in severe earthquakes.

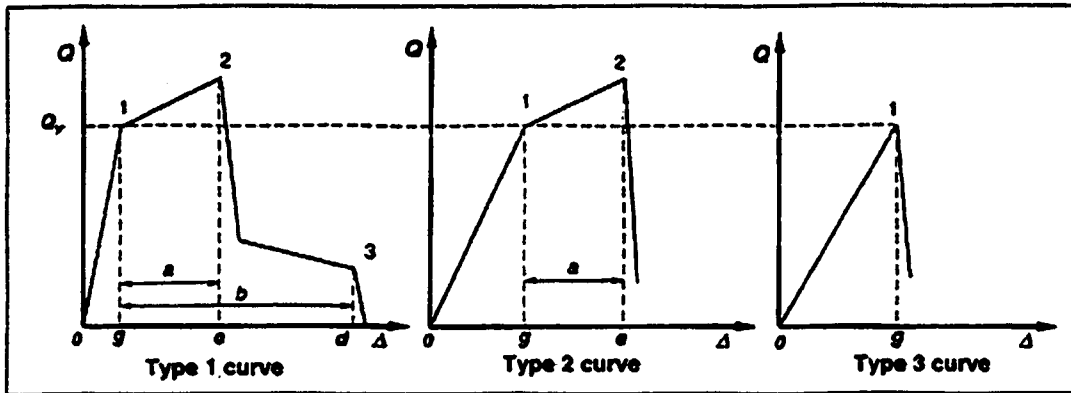
On the other hand, the enhanced rehabilitation objectives are intended to provide performance superior to that of the BSO. Enhanced objectives lead to design in which damage is limited and losses associated with that damage are reduced or eliminated. The limited rehabilitation objectives are intended to provide performance inferior to that of the BSO. Limited objectives are intended primarily for cases where existing inadequate structures are improved but to standards less than those required for new buildings.

Basically, conducting performance-based design is matching expected performance with the needed performance in order to minimize the total building cost over its life span. For such a design approach, computational tools are needed, that permit inelastic analysis of systems and are based on an understanding of structural behavior of the system and the construction materials.

2.4.5 Component Modeling and Acceptance Criteria

A critical section of a structural member that can control the mode of failure of the member is termed component. For the purpose of conducting analysis of structural systems, FEMA 273 provides designers with typical component behavior and acceptance criteria corresponding to different performance objectives.

Idealized load-deformation curves (Fig. 2.6) for various types of component actions are recommended in FEMA 273.



Where,

Q_y is the yield strength of the component.

Q is the load exerted on the component.

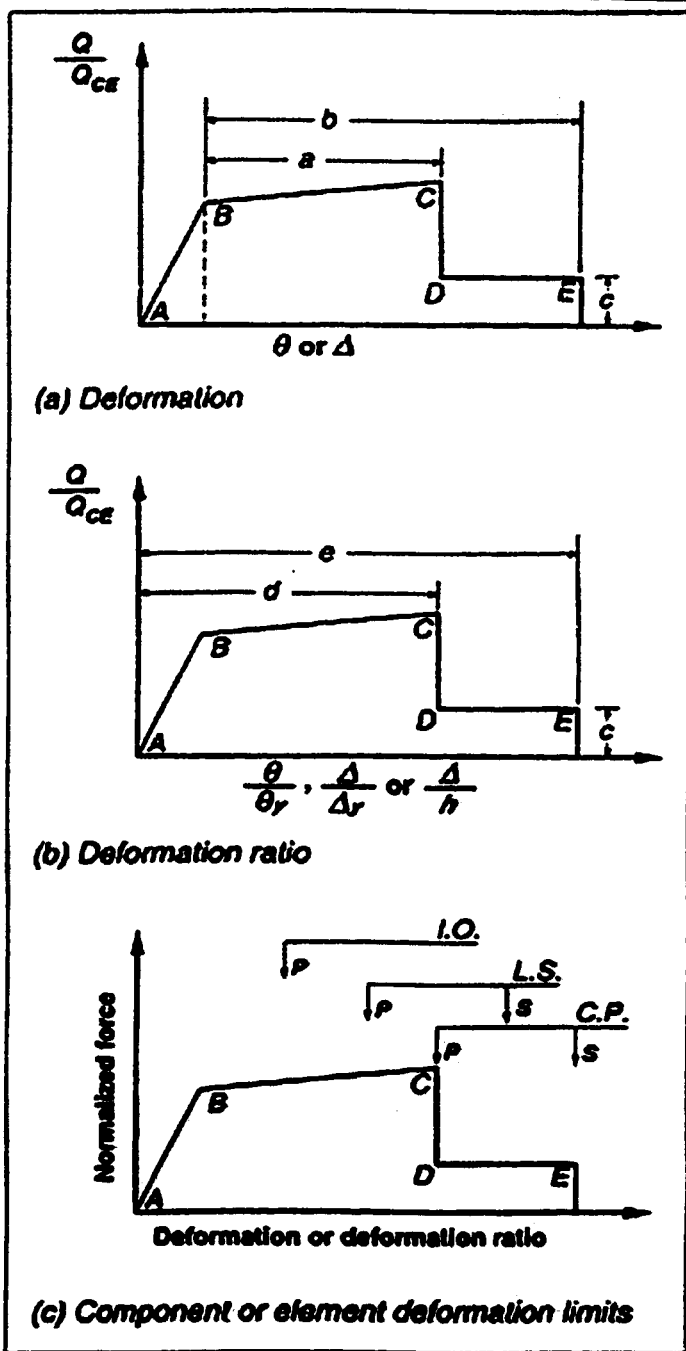
Δ is the deformation of the component.

Figure 2.6 General Component Behavior¹

Type 1 represents typical ductile behavior of component that has residual capacity after the peak load is reached. Type 2 is representative of ductile behavior up to a peak load but sudden, total loss of capacity thereafter. Acceptance criteria for elements that exhibit type 1 or type 2 behavior are typically within the elastic or plastic ranges between points 1 and 2, depending on the performance level. In FEMA 273, component actions exhibiting type 1 or type 2 behavior are considered deformation-controlled if the strain hardening or strain softening range is sufficiently large $e > 2g$, otherwise they are considered force-controlled. Type 3 is

representative of brittle behavior with no inelastic deformation prior to failure. Component actions displaying this behavior are always considered force-controlled. Acceptance criteria for components exhibiting force-controlled behavior must always be within the elastic range.

Figure 2.7 shows idealized load deformation relationship used in FEMA 273 to model and to specify acceptance criteria for deformation-controlled component. Tables recommending values for a, b, c, d and e are also provided¹.



Q_{CE} is the expected strength of the component

θ is the rotation

Δ is the displacement

h is the length of the component

I.O.= Immediate Occupancy

L.S.= Life Safety

C.P.= Collapse Prevention

P is primary component

S is secondary component

Figure 2.7 Idealized Component Load versus Deformation curves for Modeling and Acceptability¹

In FEMA 273, acceptance criteria rely on component behavior rather than global structural behavior even though the performance levels are described in terms of global behavior. Thus, the probable performance of the structure might be underestimated because system effects are neglected. Hamburger⁴⁹ emphasized the conservatism in FEMA 273 due to component-based approaches through the following example:

A structure comprised of three vertical components, labeled 1, 2, and 3 respectively acting in parallel as shown in Fig. 2.8. For each of the three components, the element shear and lateral deflection relationship is drawn in Fig. 2.8.

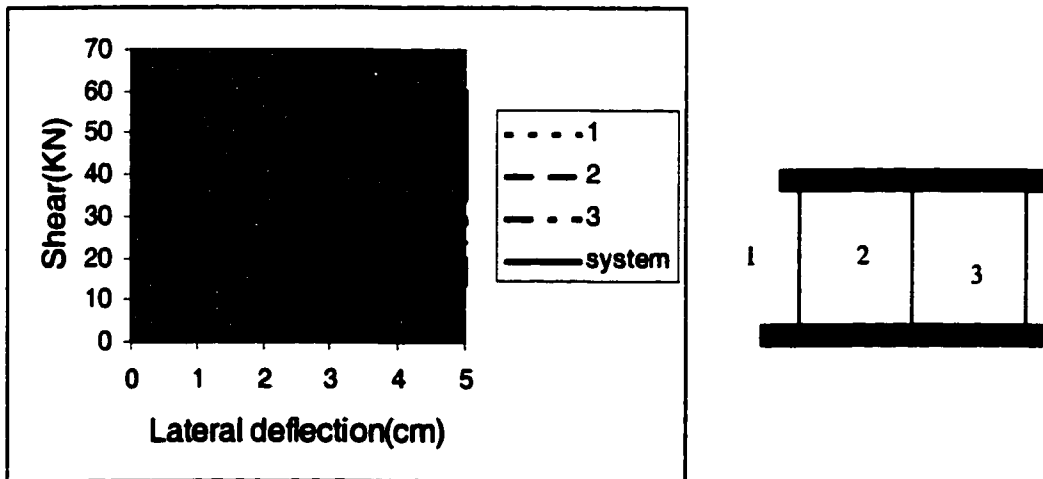


Figure 2.8 Effect of Parallel Components on System Behavior⁴⁹

Hamburger⁴⁹ states, “using FEMA 273, the acceptable displacement for Collapse Prevention performance would be defined as 4 cm, beyond which displacement component 1 degrades in strength. The permissible deformation for Life Safety performance would be 75% of the deformation for Collapse prevention performance, or 3 cm. However, critical review of the pushover curve for the structure indicates that a more realistic estimate of the Collapse Prevention performance for this structure would occur at a displacement of 5cm, beyond which the structure as a whole, rather than a single component, degrades in strength. Similarly, for the Life Safety level, it would appear that a deformation of 3.75cm would more realistically provide the intended margin of 1.33 against collapse. The structure shown in Fig. 2.8, in which components act in parallel is a redundant structure, in which the failure of one component doesn’t compromise the behavior of the structure.”

2.4.6 Analysis Procedures

Many analytical procedures have been developed in order to determine the forces and deformations in structures^{6,7,37}. These methods include elastic static and dynamic procedures, as well as pushover and dynamic nonlinear time-history analysis. A brief summary of some of these methods is given below.

2.4.6.1 Linear Static Procedures (LSP)

This procedure is the only one feasible for hand calculations. The vast majority of structures are designed using equivalent static lateral loads in accordance with the Uniform Building Code or other model codes.

For LSP, the building is modeled with linear-elastic stiffness and equivalent viscous damping. Design earthquake demands are represented by static lateral forces. In FEMA 273, the sum of these static lateral forces is equal to the pseudo lateral load. In UBC-94, the sum of these forces is equal to the equivalent base shear. In FEMA 273, this procedure is based on equivalent displacement and pseudo lateral forces while in UBC-94 it is based on equivalent lateral forces and pseudo displacements.

In designing a building following UBC-94, lateral forces are determined by first calculating the design base shear, which is proportional to the weight of the building as described in equation (2.3):

$$V = \frac{ZIC}{R_w} W \quad (2.3)$$

where Z = seismic zone coefficient.

I = importance factor.

C = site coefficient.

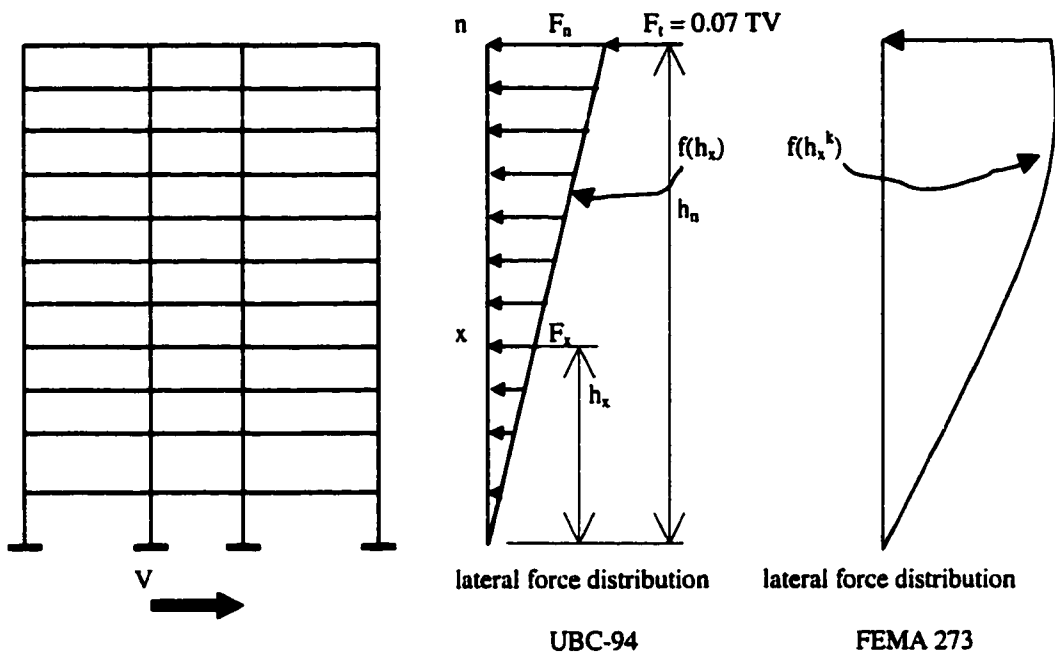
R_w = structural system coefficient.

W = total seismic dead load.

Z, C, R_w , and I are function of zoning, site characteristics, occupancy, configuration, structural system, building height, and building weight

The design base shear is distributed over the height of a building. A portion of the design base shear is concentrated at the top of a flexible building (if building fundamental period of vibration, $T > 0.7$ sec.), to account for the higher mode effects. The rest of the design base shear is distributed in proportion to the story masses, varying from a maximum value at the top to a minimum at the bottom, in correspondence with fundamental mode response. If the story masses are the same, the rest of base shear is distributed linearly over the height of the structure. Story shear can be calculated using equation (2.4). The distribution of shear along the height of the building is graphically represented in Fig. 2.9.

$$V_x = F_x + \sum_{i=x}^n F_i \quad (2.4)$$



- F_i, F_n, F_x = lateral force applied to level i, n or x , respectively.
- F_t = portion of V considered concentrated at top of structure in addition to F_n .
- h_i, h_x = height in ft above base to level i , or x , respectively.
- w_i, w_x = that portion of w which is located at or assigned to level i or x , respectively.
- W = total seismic dead load.
- T = fundamental period of vibration of structure in seconds in direction of analysis.
- V = total lateral force or shear at the base for which a building is to be designed.

Figure 2.9 Lateral Force Distribution

In designing a building following FEMA 273, lateral forces are determined by first calculating the pseudo lateral load, which is proportional to the weight of the building as described in equation (2.5):

$$V = C_1 C_2 C_3 S_a W$$

(2.5)

Where

W is the total seismic dead load.

C₁ is function of the period, T, of the building.

T is function of the building height, the structural system and material of construction of the building.

C₂ reflects the effect of strength and stiffness degradation

C₃ represents an adjustment for increased displacements due to P-Δ effects.

S_a is the response spectrum acceleration at the fundamental period and damping ratio of the building in the direction under consideration. In FEMA 273, section 2.6.1.5 provides equations and modification factors that can be applied to key ordinates of ground motion response spectrum that are plotted in the maps developed by USGS in 1996. S_a can be determined directly from the complete response spectrum plotted using the modified key ordinates and the corresponding equations.

The pseudo lateral load is distributed over the height of a building as described by equation (2.6)

$$F_x = C_{vx} V \quad (2.6)$$

$$C_{vx} = \frac{w_x h_x^k}{\sum_1^n w_i h_i^k}$$

Where:

k is function of T

C_{vx} = vertical distribution factor

V = pseudo lateral load

w_i = portion of the total building weight W located at floor level i

w_x = portion of the total building weight W located at floor level x

h_i = height from the base to floor level i

h_x = height from the base to floor level x

2.4.6.2 Linear Dynamic Procedure (LDP)

The LDP includes two analysis methods, namely, the response spectrum and time-history analysis.

1- *The response spectrum method* was first introduced by Housner³⁸ and Biot^{39,40}. This method uses peak modal responses calculated from dynamic analysis of a damped single-degree-of-freedom oscillator. Figure 2.10 illustrates the procedure for computing and constructing the response spectrum for a given ground motion and a specified damping ratio. For multi-degree-of-freedom systems, the response of the structure is represented as a linear superposition of mode shapes, for

each mode shape, the structure is treated as a single-degree-of-freedom system. To combine the modal responses, techniques such as the square root of the sum of squares (SRSS) were developed. However, the SRSS method fails when the modes of the structure are very close. Then other techniques such as the complete quadratic combination (CQC) which take into account the correlation between modes need to be used³⁷. Only those modes contributing significantly to the response need to be combined (most codes allow considering those modes that cause 90% of the participating mass to vibrate). The response spectrum method is used only to determine the maximum responses of structures.

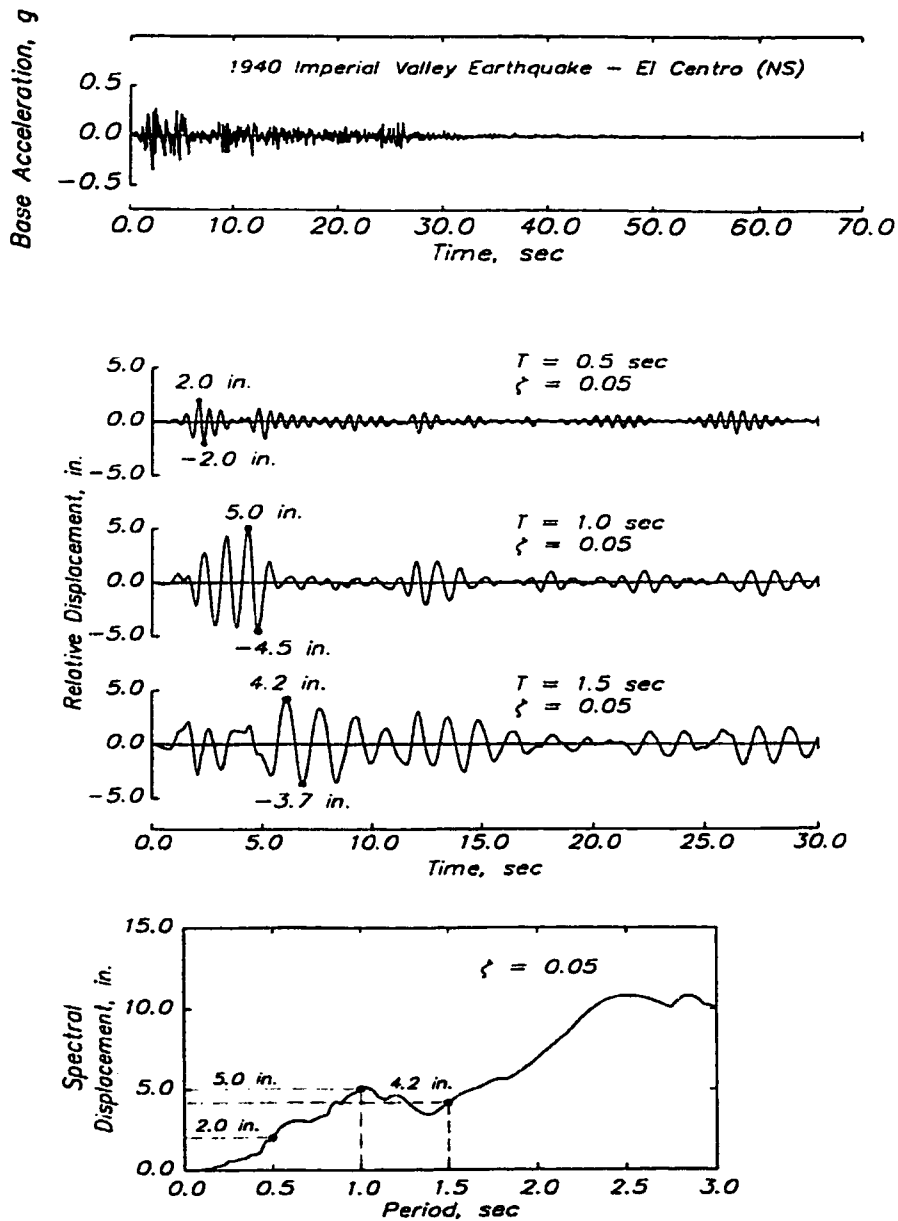


Figure 2.10 Computation of Displacement Response Spectrum for the 1940 El Centro NS Component with 0.05 damping ratio⁷⁵.

Current codes recommend that a smooth curve of the normalized spectral response be used for design and evaluation of buildings⁴¹. Typically, a curve for the spectral acceleration consists of a constant value corresponding to low periods and a hyperbolically declining curve for higher periods. Figure 2.11 shows calculated and idealized response spectra for the N90E component of the San Francisco Presidio earthquake with 5% damping.

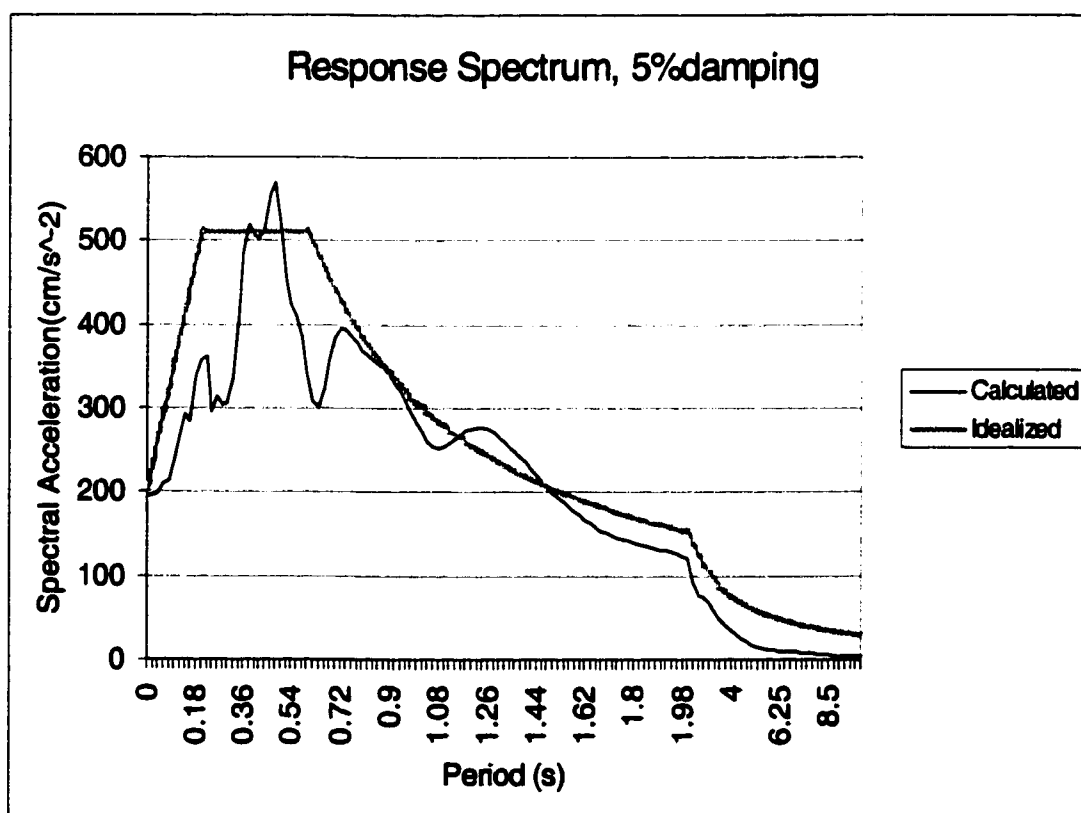


Figure 2.11 San Francisco Presidio Spectra with 5% damping on hard rock.

In UBC-94, the declining curve includes the higher mode contribution to the response of the structure. Soil structure interaction is introduced through the spectral displacement or acceleration curve.

2- *The Time-History method* involves a time-step-by-time-step evaluation of building response using discretized recorded or synthetic ground motion records. This method is particularly useful in nonlinear analysis and in cases where the characteristic modes of the structure are very close. Time-history procedures will be detailed in section 2.4.6.4

2.4.6.3 Nonlinear Static Procedures (NSP)

The non-linear static analysis also known as Pushover analysis, is a simple and efficient technique to predict the response under lateral forces of a structure without the need to conduct a dynamic analysis. A pushover analysis is expected to establish the sequence of component yielding and/or failure, the global ductility, and the adequacy of the structure by providing a relationship between the roof displacement and the base shear of the structure. The method consists of the application of an increasing monotonic static lateral load with a specified lateral load distribution along the height of the structure. The lateral load is increased until either a mechanism forms or a target displacement for a specific part of the structure is reached. The response varies depending on the pattern of the load applied. There are

several patterns used, including uniform distribution, inverted triangular distribution and modal adaptive distribution⁴. The former two patterns bound the response and are the most commonly used. The modal adaptive distribution captures the different modes of deformation and the influence of higher modes in the response but is more difficult to implement in existing analytical programs as it needs to be updated at each event of the analysis. Moghadam⁴² and Nicoletti⁴³ suggested methods for using 3D-pushover analysis for asymmetric buildings based on the modal adaptive distribution method.

Two lateral load patterns were assumed in FEMA 273: The first pattern is the “uniform” pattern. The second is the “modal” pattern corresponding to the initial elastic modal response. In FEMA 273, pushover analysis is recommended for buildings with irregularities without significant higher-mode response. The NSP should be implemented with caution and after comprehensive knowledge of the structure and its components has been obtained.

Another nonlinear static procedure, the *Capacity Spectrum Method (CSM)* was adopted in ATC 40. The procedure compares the capacity of the structure (in the form of a force deformation relationship based on a pushover analysis) with the demands on the structure (in the form of response spectra). The graphical intersection of the two curves represents the expected response of the structure⁴⁴. In order to account for inelastic behavior of the structure, effective damping values are applied to the elastic response spectrum to produce an inelastic response spectrum.

5% damping is assumed to represent a linear elastic response and 20% damping a response at an approximate displacement ductility of 3 using the procedure in ATC 40. If the capacity curve intersects the demand envelope, the building is expected to survive the earthquake. It is a simple method for rapid evaluation of structures.

In checking a structure using the capacity spectrum method, first, a pushover analysis is conducted to relate the roof displacement, Δ_R , of the structure to the base shear, V/W . Then, Δ_R and V/W are converted to spectral displacement, S_d , and spectral acceleration, S_a , respectively, by use of modal participation factors and effective modal weight ratios as determined from dynamic characteristics of the fundamental mode of the structure (ATC-40). Each mode of vibration is related to the corresponding spectral acceleration and spectral displacement by Eq (2.7)

$$T_i = 2\pi \sqrt{\frac{S_{di}}{S_{ai} g}} \quad (2.7)$$

The inelastic response spectra can be deduced from the elastic response spectrum using the method developed by Newmark and Hall⁴⁶:

In the constant acceleration range, the inelastic spectrum can be approximated by the elastic response spectrum reduced by $\frac{1}{\sqrt{2\mu-1}}$

In the constant velocity and displacement ranges, the inelastic response spectrum can be approximated by the elastic spectrum reduced by $\frac{1}{\mu}$

Where μ is displacement ductility ($\mu = \frac{\text{maximum_displacement}}{\text{displacement_at_yield}}$).

The relationship between damping and ductility can be found in tables from research studies^{46, 47} or ATC-40.

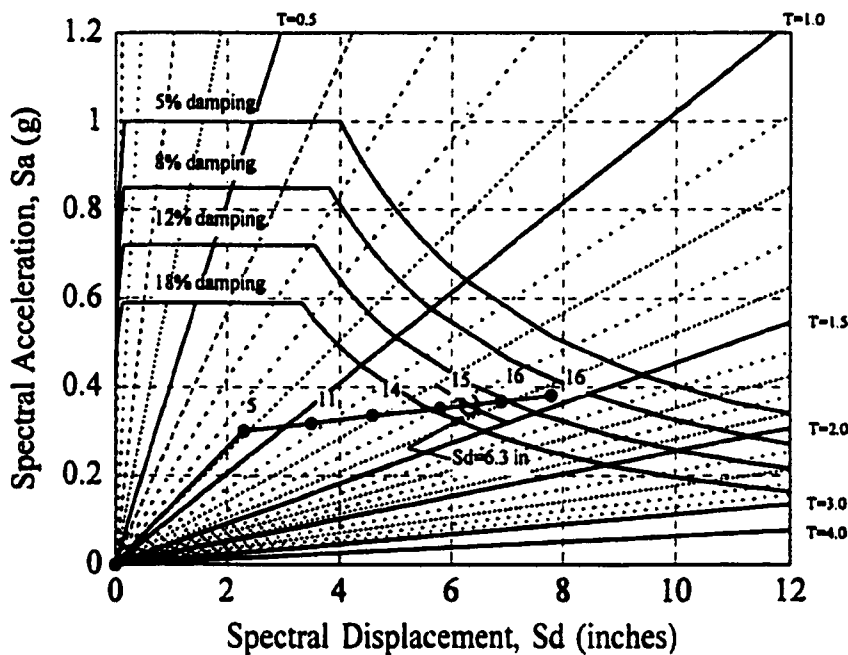


Figure 2.12 Idealized capacity spectrum method for an ideal structure⁴⁶.

In Fig. 2.12, idealized capacity spectra are plotted for an ideal structure. Four capacity demand curves are shown, corresponding to damping ratio of 5, 8, 12 and 18%. Note that the elastic limit ($S_d=2.3''$) of the capacity curve does not intersect the response spectrum curve corresponding to 5% damping (elastic range). Therefore, the elastic demand exceeds the elastic capacity, and the structure is in the inelastic range. For example, the structure is expected to sustain an earthquake with a spectral acceleration of 0.36g and a spectral displacement of 6.3'' corresponding to the point

where the capacity curve of a ductility corresponding to 15.5% damping meets the demand curve corresponding to 15.5% damping.

2.4.6.4 Nonlinear Dynamic Procedure (NDP)

To better understand the nonlinear dynamic procedure, a review of nonlinear time-history analyses is needed. As stated in section 2.4.6.2, nonlinear time history dynamic analysis involves a time-step-by-time-step direct integration of the equilibrium equation. At any time step, the incremental dynamic forces acting on a structure during a time step Δt should satisfy equilibrium, Eq 2.7:

$$M\Delta\ddot{x}(t) + C\Delta\dot{x}(t) + K\Delta x = \Delta F(t) \quad (2.7)$$

For the numerical solution of equilibrium equations in the time domain, there are two fundamentally different groups of algorithms available: explicit and implicit integration schemes⁴⁵. In explicit integration, the equation of motion, Eq.(2.7) is established for time t , accelerations and velocities at t are approximated using the central difference operator as follows:

$$\ddot{x}_t = \frac{1}{\Delta t^2} (x_{t-\Delta t} - 2x_t + x_{t+\Delta t}) \quad (2.8)$$

$$\dot{x}_t = \frac{1}{2\Delta t} (-x_{t-\Delta t} + x_{t+\Delta t}) \quad (2.9)$$

Substitution of Eqs. (2.8) and (2.9) into Eq. (2.7) leads to

$$\left(\frac{1}{\Delta t^2} M + \frac{1}{2\Delta t} C\right)x_{t+\Delta t} = F_t - \left(K - \frac{2}{\Delta t^2} M\right)x_t - \left(\frac{1}{\Delta t^2} M - \frac{1}{2\Delta t} C\right)x_{t-\Delta t} \quad (2.10)$$

This set of equations can be solved directly for $x_{t+\Delta t}$, the unknown displacements at time $t+\Delta t$. For diagonal matrices M and C , this task is trivial and does not require the factorization of the stiffness matrix K of the structure.

In implicit integration, accelerations and velocities are approximated using the Newmark method as follows:

$$\ddot{x}_{t+\Delta t} = \frac{6}{\Delta t^2}(x_{t+\Delta t} - x_t) - \frac{6\dot{x}_t}{\Delta t} - 2\ddot{x}_t \quad (2.11)$$

$$\dot{x}_{t+\Delta t} = \frac{3}{\Delta t}(x_{t+\Delta t} - x_t) - 2\dot{x}_t - \frac{\Delta t}{2}\ddot{x}_t \quad (2.12)$$

Substitution of Eqs. (2.11) and (2.12) into Eq. (2.7) leads to

$$K^* x_{t+\Delta t} = F_{t+\Delta t}^* \quad (2.13)$$

where

$$K^* = K + \frac{6}{\Delta t^2} M + \frac{3}{\Delta t} C \quad (2.14)$$

$$F_{t+\Delta t}^* = F_{t+\Delta t} + \left(\frac{6}{\Delta t^2} x_t + \frac{6}{\Delta t} \dot{x}_t + 2\ddot{x}_t\right)M + \left(\frac{3}{\Delta t} x_t + 2\dot{x}_t + \frac{\Delta t}{2}\ddot{x}_t\right)C \quad (2.15)$$

Eq. (2.13) can be solved for the displacements $x_{t+\Delta t}$. But this task involves factorization of the effective stiffness matrix K^* , which is a computationally expensive task. Moreover, K^* changes whenever K changes, such as due to inelastic behavior or when Δt is varied. The piecewise linearization of response histories

causes unbalanced forces at each time step which can be resolved using various numerical analysis techniques⁴⁵.

To provide stability in the explicit algorithm, the time step should satisfy the Courant condition, $\Delta t < T_n / \pi$, where T_n is the smallest natural period of the structure. Physically, this requirement means that Δt should be on the order of the time required by sound waves to travel through the smallest member or element in the structure. This time step can be extremely small. For example, the sound velocity in steel is 16,800 ft/sec. Thus, a sound wave travels along a 12 ft column in 0.7×10^{-3} sec, so that the stability criterion requires $\Delta t < 0.2 \times 10^{-3}$ sec. In the case of structures with massless degrees of freedom, the method breaks down because $T_n = 0$, unless such degrees of freedom are condensed out prior to the time step solution. Thus, even though the solution of Eq. (2.10) requires relatively little effort, a time history analysis of a 10-second earthquake record may involve at least 50,000-time steps⁴⁵.

Implicit algorithms generally are unconditionally stable, regardless of the Courant condition. The time step size may be several orders of magnitude larger than T_n . Physically, these algorithms have the effect of suppressing the higher modes through artificial damping. It is of interest to note that these higher modes generally contribute little to the structural response. But when an unstable integration method is used, a violation of the stability criterion causes these high

frequency modes to drown out the responses of the significant lower modes, thus making the results useless.

In summary, the choice of a numerical solution algorithm has to reflect a balance between accuracy and stability requirements. The apparent computational advantage associated with the larger time steps of an implicit integration scheme can in general be realized only by sacrificing accuracy. Fortunately in the case of building structures, the role of higher modes is usually not very significant.

The NDP is the most “accurate” analysis method available. Calculated response can be highly sensitive to characteristics of particular ground motions and the nonlinear stiffness behavior of the elements, therefore, representative or generalized ground motions need to be used and the NDP should be applied with caution and after comprehensive knowledge of the structure and its behavioral characteristics are obtained.

It should be noted that uncertainties are involved in the seismic input, and in the strength and deformation capacities of elements and structures. Therefore, uncertainties in the results will be must be recognized regardless of the evaluation procedures. While equivalent elastic procedures may be preferred by practitioners for the design of most new structural systems, inelastic analysis procedures will be essential for implementation of performance-based design. Such analytical capability

will be important for the evaluation of structural behavior at low performance levels (damage likely) where significant inelastic deformations are expected³⁶ and for high performance levels where accurate determination of even small deformations will be needed to determine compliance.

CHAPTER 3

SEISMICITY AND COMMON STRUCTURAL PRACTICE IN THE MIDDLE EAST

3.1 General

Evidence of earthquakes in the eastern basin of the Mediterranean Sea has been reported since 2000 BC. Earthquakes of moderate to high intensities have and continue to occur in the Middle East. The structural systems commonly used in Lebanon, Greece, Turkey and elsewhere in this region are constructed using lateral-force resisting elements that have limited or no ductility and insufficient strength. These structures are vulnerable even to moderate intensity ground motions. In addition to the low strength of the lateral-force resisting systems, vertical and horizontal geometric and strength irregularities are frequently encountered in the construction practice in the Middle East.

In this chapter, a brief description of the seismicity of the area is presented. Common structural systems and deficiencies in the systems are discussed, and a building for case study is described.

3.2 Historic Events

Based on historical accounts, earthquakes have been occurring in the eastern Mediterranean region for the past four millennia. In Lebanon, three of the powerful earthquake events in recorded seismic history are those of 551 A.D., 1202 A.D., and

1759 A.D. From historical accounts, the estimated magnitudes were in excess of 7 and lead to major destruction in the coastal cities of Lebanon. In Turkey, the region of Celainai, which is known today as Dinar, was destroyed in the 8th century B.C. The town of Apameia was devastated by a strong earthquake in 84B.C., and 225-235 A.D. In the 20th century, major earthquakes occurred in the region, the 1925 and 1995 earthquake in Dinar, the 1956 earthquake in Lebanon, the 1998 earthquake in Ceyhan and finally the August 17th, 1999 earthquake in Izmit, Turkey.

3.3 Tectonics and Seismicity of the Area

The Dead Sea fault system, also known as the Levant fracture system, is a major tectonic feature that accounts for the bulk of seismic activities in the Eastern Mediterranean. It forms a plate boundary that links the Arabian plate convergence in south Turkey with active seafloor spreading in the Red Sea. The Arabian plate moves northward and collides with the Eurasian plate in northeast Iraq. The southern segment of the Dead Sea fault system, which extends from the gulf of Aquaba to the Sea of Galilee and the south of Lebanon, strikes in a more or less N-S direction. When entering Lebanon through the Galilee heights, it changes into a more complex system of strike-slip faults. See Figs. 3.1, 3.2 and 3.3. The Levant fracture system is believed to be similar, to a great extent, to the San Andreas fault system. Historically, it has given rise, at different segments along its length and in different time intervals, to major destructive earthquakes of varying magnitudes. Although the

quaternary displacements of these faults have not been carefully studied, the destruction due to major historical earthquakes as described in the literature leads one to believe that these faults can be a potential source of future strong earthquakes^{50,51,52}.

Other important active faults such as the Cyprus Arc, which extends from the island of Cyprus to join the Taurus-Zagros thrust in southern Turkey, affect the seismic activity in Lebanon. Earthquake events on the seabed between Cyprus and Lebanon, sometimes close to the coast, are very frequent. These earthquakes may affect almost all cities along the Lebanese coast.

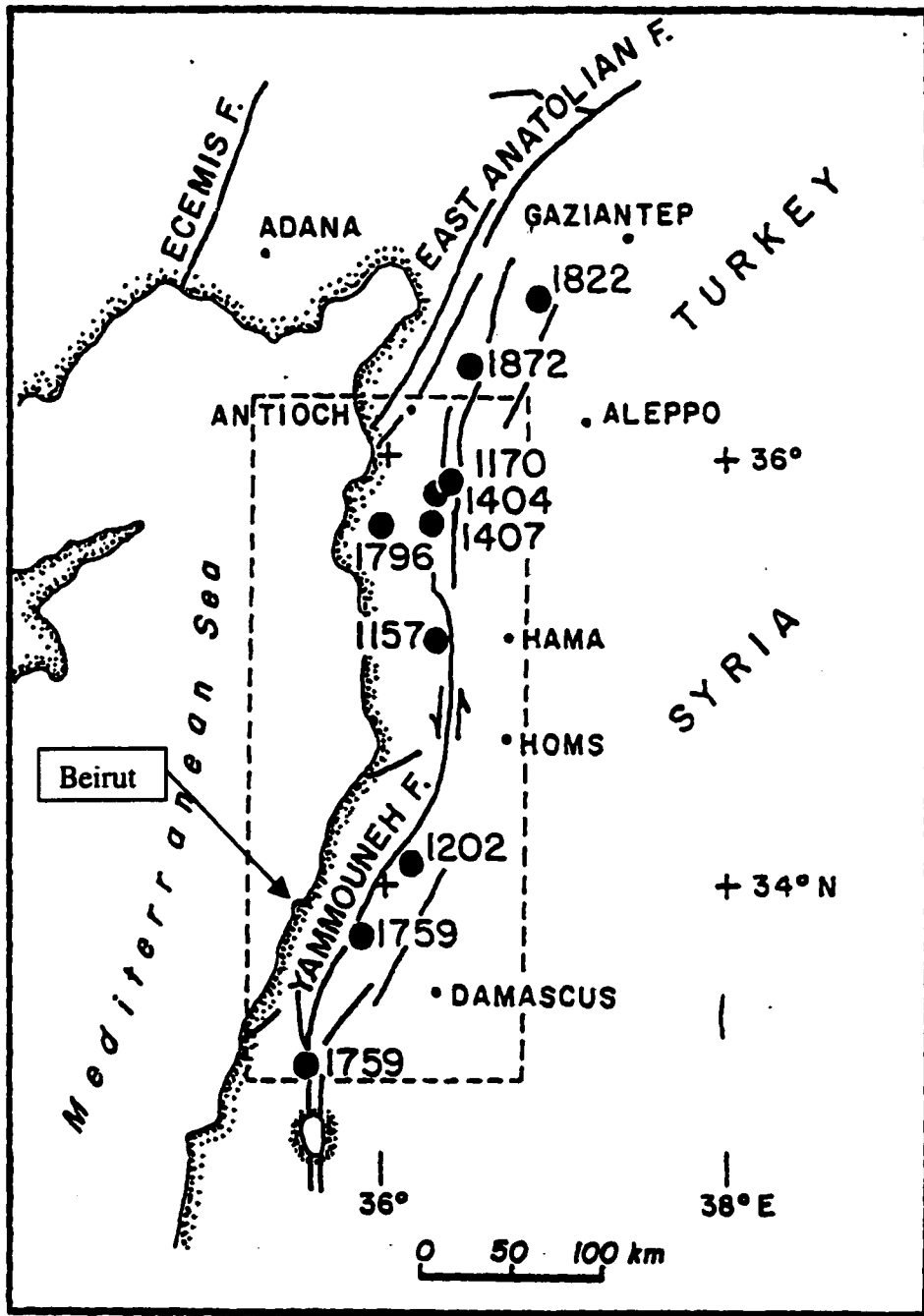


Figure 3.1 Map of the Eastern Mediterranean region⁵¹

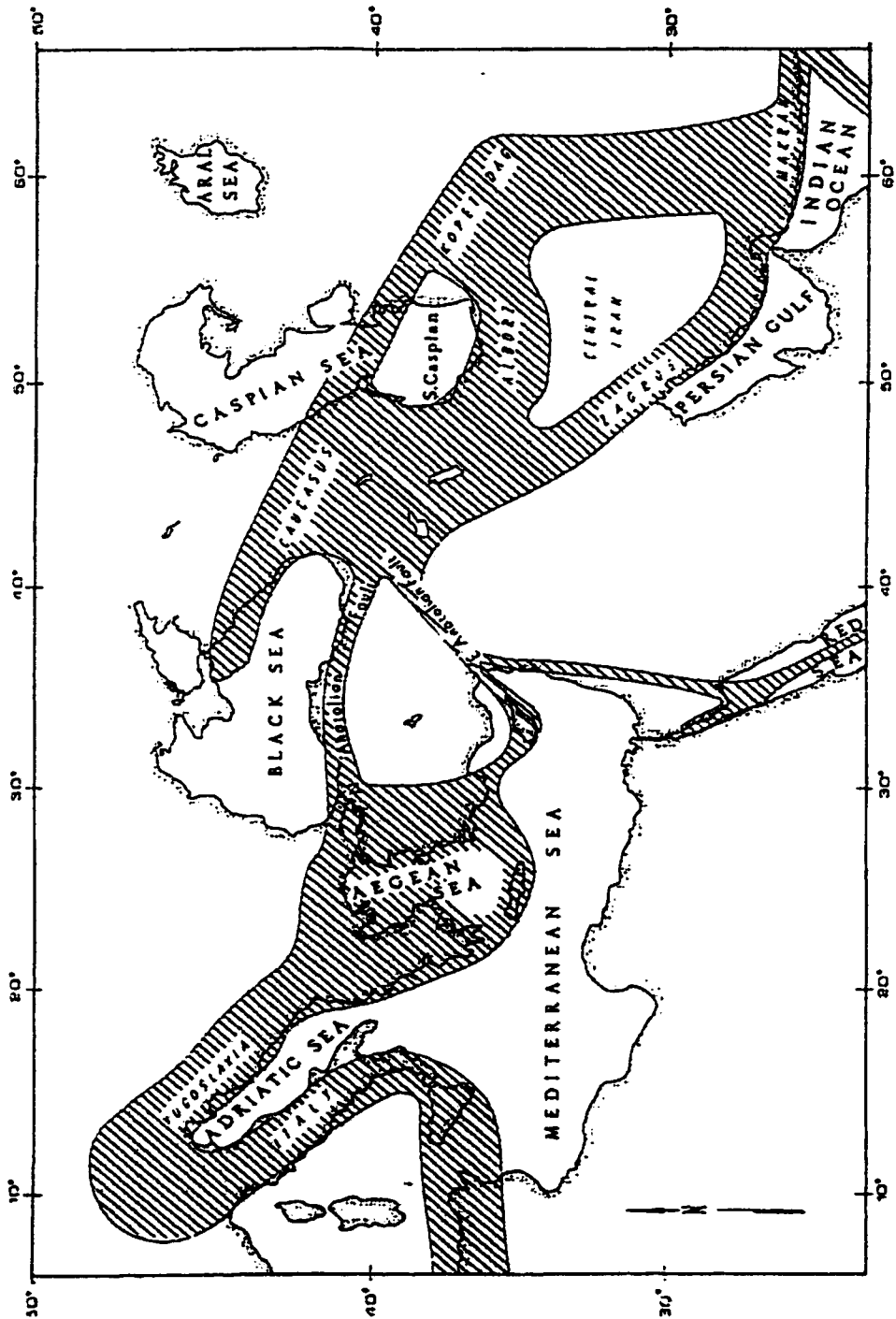


Figure 3.2 The principle seismic belts (shaded) in the Mediterranean and Middle East⁵³

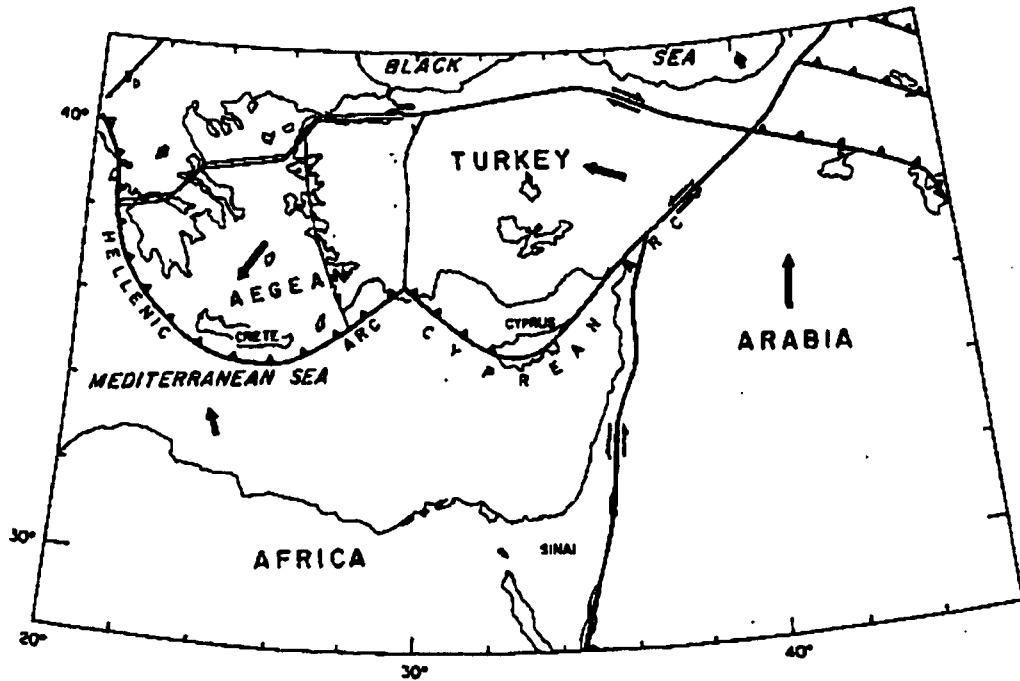


Figure 3.3 Simplified tectonics of the Eastern Mediterranean⁵¹

Despite the exposure of the Eastern Mediterranean to seismic activities, most of the building structures are designed for gravity loading only and continue to be designed with little attention to lateral resistance against earthquake induced displacements. Studies^{54,63} have been conducted to determine earthquake hazard levels in Lebanon and Turkey. For the purpose of seismic design of structures, it was recommended⁵⁴ that Lebanon be divided into two seismic zones with minimum design peak ground acceleration on rock equal to 0.15g and 0.2g (g being the gravitational acceleration). Since Lebanon is a small country, design ground

acceleration equal to 0.2g across the entire territory may be preferable⁵⁴. A value of 0.2g corresponds to moderate seismic zone 2B of the Uniform Building Code 1994.

3.4 Building Structural System

Flexible reinforced concrete structures have been used often in areas of low to moderate seismicity, and in the Mediterranean Basin, they are the predominant structural system. The lateral load resisting system consists of slab-column frames with concealed beams and ribbed slabs.

3.4.1 Columns

The columns are designed to support gravity loads. They are wall-like elements with large depth to width ratios (2-5). The aspect ratio is selected for architectural reasons. Typically, the width of a column will be in the range of 20 to 40 centimeters (8 to 16 inches), the same as adjoining partition walls. The structural behavior of these columns is similar to flexible walls with uniformly spaced reinforcement on both faces and both directions and no boundary elements. They are very stiff in one direction and very flexible in the other. Figure 3.4 shows typical dimension ratios for a column section.

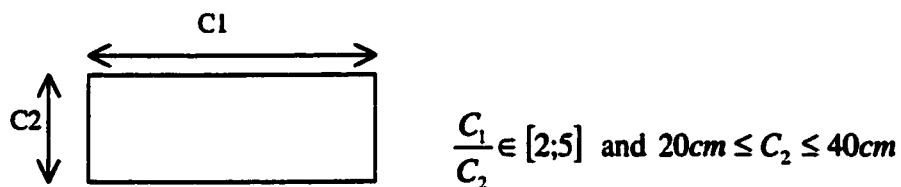


Figure 3.4 Typical column cross section

3.4.2 Slab-Beams

The majority of slabs are one way joist system with beams concealed within the thickness of the slab and hollow core concrete blocks (“Hourdis”) between joists. Typical slab thickness is 20 to 40 cm. The beams are wide and shallow. The width of the beams may vary between 2.5 and 5 times the slab thickness depending on the span length and applied loads. The beams are designed only for gravity loads. Figure 3.5 shows a schematic slab cross section showing a triangular joist cross section and a hollow core concrete block topped with a three inch layer of concrete reinforced for shrinkage only. Figure 3.6 shows an unfinished ceiling with a wall/column. Figure 3.7 shows the formwork with the steel for the beam and the hollow core concrete blocks prior to placing the joists and pouring the concrete.

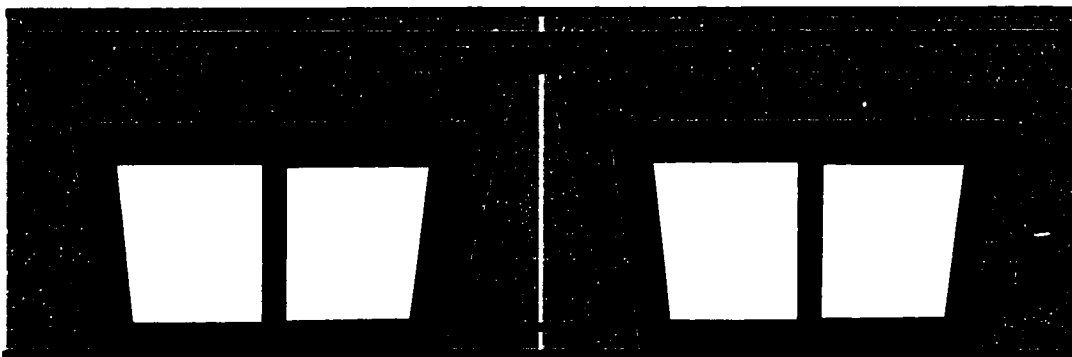


Figure 3.5 A schematic slab cross section

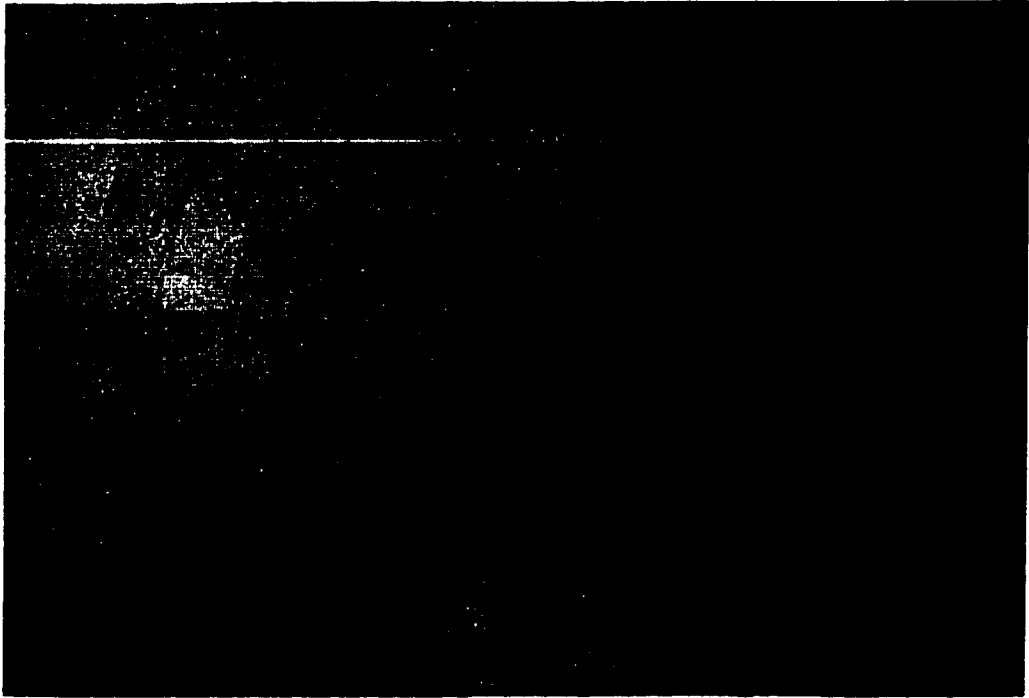


Figure 3.6 Unfinished ceiling and wall-like column

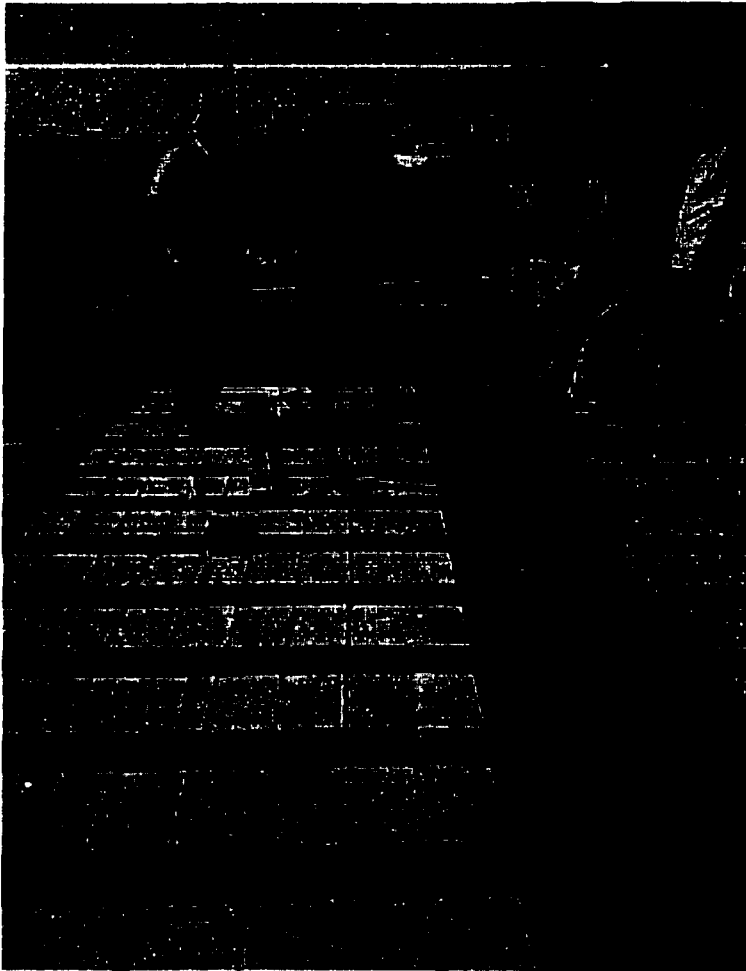


Figure 3.7 A slab under construction

3.4.3 Construction Material

Most buildings in the Middle East are constructed using cast in place concrete. The concrete strength varies between 1.7 Ksi and 3 Ksi. The low range of

concrete strength is due mainly to the consistence on high water-cement ratios for ease of placement and workability. The use of ready-mixed concrete has increased since late eighties, however, concrete strength is still in a low range from 2.5 to 3.5 Ksi.

Most of the reinforcing steel used since the early eighties is Grade 60 deformed steel bars if bar diameter is larger than 8mm and Grade 60 plain steel bars for diameters smaller or equal to 8 mm. The steel is imported primarily from Eastern Europe and has low ductility.

3.5 Vulnerability of the Structural System to Earthquake Induced Loads

The damage to buildings caused during earthquakes in Turkey, Jordan, Greece and Lebanon shows that the structural system used in these areas is vulnerable to seismic loads, especially since most of the buildings designed with the slab-column structural system were intended to support gravity loads only. The flexible structures undergo large deformations when subjected to lateral loads. Given the aspect ratio and the small amount of reinforcement for columns and beams, deformation capacities are low and result in low global ductility of buildings. Hence, their ability to absorb and dissipate energy through plastic deformation is reduced. Many deficiencies in geometry, strength and materials raise concern about the performance of such structures in a seismic event.

3.5.1 Soil-Structure Interaction

In most areas in Lebanon, the bedrock is believed to be shallow. Therefore, the ground acceleration amplification due to loose soil deposits may not be significant and can be ignored in most cases. However, Beirut and the south coast of Lebanon, offer a great diversity of soil types, particularly loose sand alluvium with a relatively shallow water table. Thus in areas of loose sands and high water level, there is a potential threat of soil liquefaction in the event of moderate to strong ground motion.

3.5.2 Insufficient Stiffness, Strength and/or Deformation Capacity

As stated above, most building structures are designed for gravity loads. Hence, they have low lateral resistance. In Lebanon, shear walls are mostly used in tall buildings (above 12 stories) for wind resistance. In many tall buildings, shear walls are oriented in only one direction (predominant wind) while the perpendicular direction can be very flexible. Elevator shafts and staircases are frequently constructed with reinforced concrete walls designed mainly for gravity loads. Because of their high stiffness, they attract most of the lateral forces. If their strength capacity is not enough, they may fail and cause partial or total collapse of the structure.

Because of the large aspect ratios of beams and columns, framing action is not well understood. Beams are estimated to be stronger than columns in one

direction and weaker in the other. Shallow beams may have low ductility and may fail in flexure (local failure) at low global deformation of the structure.

3.5.3 Building Irregularities

Irregularities include vertical and horizontal mass distribution and varying strengths of resisting elements. In many structures, walls can be found on one side of the building. As a result, there is a concentration of stiffness on one side which causes large eccentricity between the center of rigidity and the center of mass and creates potential torsional problems in the structure.

Most water reservoirs can be found on the roof of buildings in the Middle East. The reason is to use gravity to provide water pressure for the building. However, a concentration of mass on the roof induces a large inertial force on the roof increasing overturning moments at the base of the structure. Such reservoirs may also increase torsional problems.

Partition walls can be placed at different locations from one story to another and may not be included in the structural design of the lateral force resisting system. Partition walls often are only considered as additional dead loads on the supporting slab. In most cases, partition walls are unreinforced infill walls constructed with concrete blocks. Under low lateral deformations, the infill walls are not damaged and will function in a manner similar to reinforced concrete shear walls. While the weight of partition walls increases inertial forces, the lateral drift of the building may

be decreased and structural damage reduced. The added strength and stiffness of the infills may also induce torsion and alter the behavior of the total structure. In the Eastern Mediterranean, infill walls generally are not used on the first floor. The resulting soft first story may suffer large deformations that could cause total collapse of the structure (Turkey and Taiwan 1999 earthquakes). If the structure is subjected to lateral forces normal to the plane of the partition walls, these walls may fail and cause life hazards since they are unreinforced. Figures 3.8 and 3.9 show buildings with no infill walls on the first story to provide openings and space for commercial use.

In many structures, walls or columns may be interrupted between stories (to satisfy space requirements of the occupants) leading to serious vertical irregularities. Column orientation may be altered, for architectural reasons, between stories or even at the same floor, as shown in Fig. 3.9.

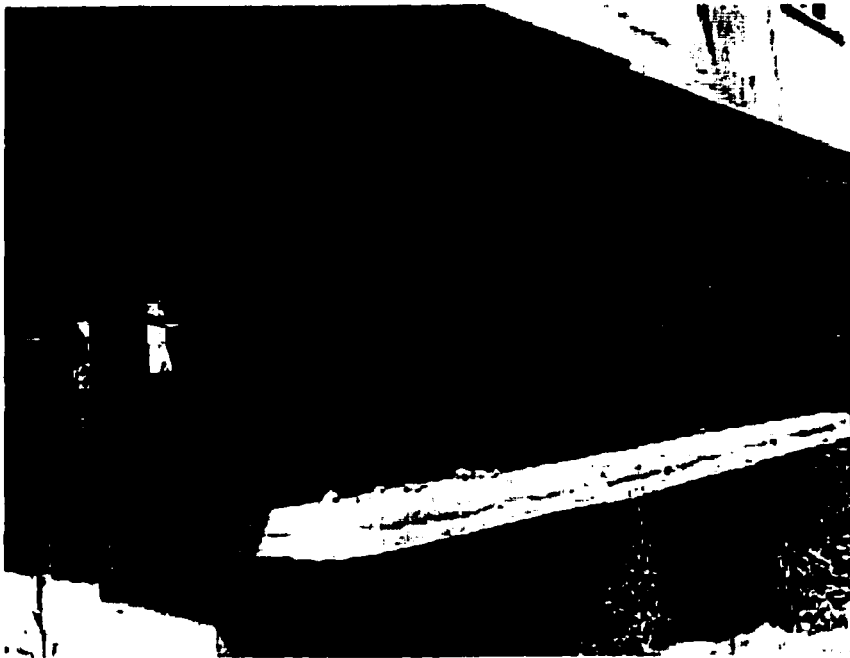


Figure 3.9 Columns with different orientations

3.5.4 Poor Detailing and Quality Control

Commonly encountered detailing shortcomings include inadequate confinement for columns. Column ties are not anchored in the core. Typical construction practice is to use 90° hoops. Column ties are spaced at large distances,

thus the unsupported length of longitudinal bars is excessive, eventually leading to local buckling of longitudinal reinforcing bars and also creating elements that must rely solely on the concrete for shear strength. Cross ties are not provided on every other longitudinal bar as recommended in the ACI 318-95 code. Given the low amount of transverse reinforcement provided in columns, the poor concrete quality and strength, and the thin concrete cover, spalling of concrete cover is observed at low deformation levels. Figure 3.10 shows failure in a column with large tie spacing and the concrete cover.



Figure 3.10 Column failure due to poor detailing and irregular in-plan layout

Another detailing problem is splicing of reinforcement in probable plastic hinge location, and the use of short splice lengths. Little care is given to reinforcement anchorage especially at the exterior beam column joints. No transverse reinforcement is used in beam-column joints making the joint vulnerable to shear failure.

Torsion at joints is a potential problem, especially at eccentric beam column joints as shown in Fig. 3.11

Little attention is given to material quality and control. The steel ductility and concrete strength may be very low. Concrete and steel properties are seldom verified through quality control and verification testing.



Figure 3.11 Eccentric beam-column connection

An evaluation of the performance of flexible concrete slab-column structure under seismic forces is needed for rehabilitation of existing systems or for the design of new structures.

3.6 Case Study

A theoretical eight-story reinforced concrete building⁵⁵ typical of Lebanese construction practice was selected for a study to evaluate the performance of the system under different combinations of input parameters.

3.6.1 General Building Description

The eight-story structure is about 25 meters by 13.5 meters in plan dimensions. It has five bays in the long direction and three bays in the short direction. The total story height is 3.2 meters. The location of infill walls may vary on each floor. For this study, they will be considered only around the perimeter. The building is supposed to have a fixed base (rigid foundation on bedrock). Figure 3.12 shows the layout of a typical floor.

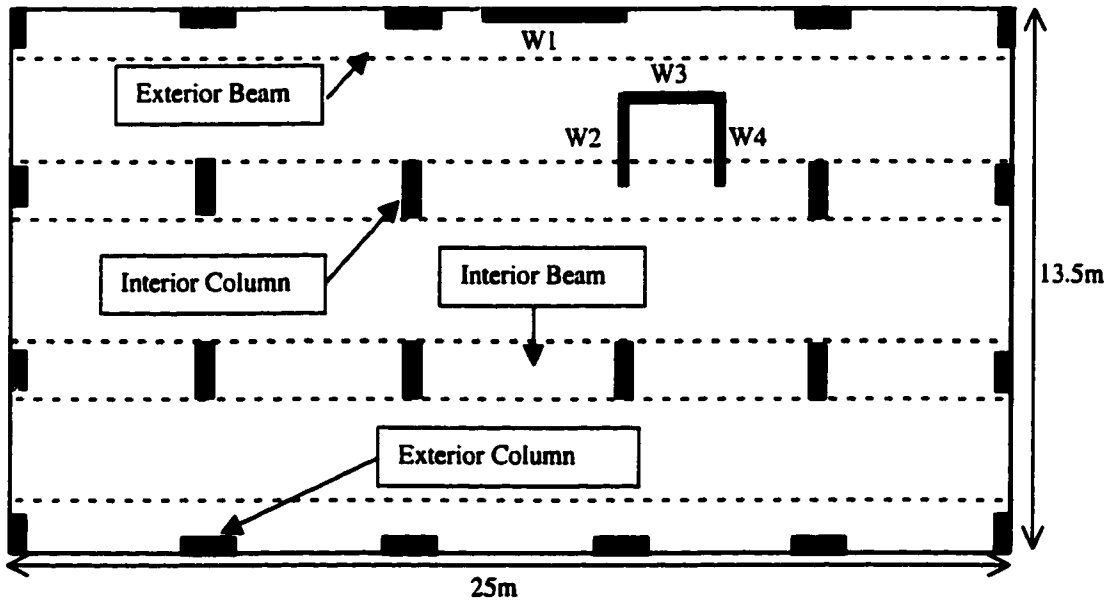


Figure 3.12 Floor layout

The floor system consists of one-way “Hourdis” ribbed slabs supported on concealed wide beams spanning between columns as shown in Fig. 3.12. The thickness of the slab is 24 centimeters (8.16 inches). Construction material properties are appropriate to the local design and construction practice, hence the concrete

strength $f'_c = 176 \text{ Kg/cm}^2$ (2.5 Ksi), the reinforcing steel strength $f_y = 4200 \text{ Kg/cm}^2$ (60 Ksi).

The building is designed to carry typical residential live loads ($200 \text{ Kg/m}^2 = 40 \text{ lbs/ft}^2$) and dead loads ($760 \text{ Kg/m}^2 = 151 \text{ lbs/ft}^2$). The dead load includes the self-weight of the slab ($410 \text{ Kg/m}^2 = 81 \text{ lbs/ft}^2$), self-weight of tiling and ceiling plastering ($150 \text{ Kg/m}^2 = 30 \text{ lbs/ft}^2$), and the weight of partition walls and plaster ($200 \text{ Kg/m}^2 = 40 \text{ lbs/ft}^2$).

3.6.2 Dimensions and Detailing of Structural Components

The widths of the concealed beams (24 centimeters deep) are 75 centimeters for the edge beams and 120 centimeters for the interior beams. Figure 3.12 shows the layout of the beams. The joists span perpendicular to the main grids. The longitudinal reinforcement in beams and slab ribs is shown in Figs. 3.13 to 3.15. The shear reinforcement in beams and joists consists of 6 mm plain bars spaced at 20 centimeters.

Notation: X Φ Y: Number of bars is X. Diameter of a bar is Y mm.

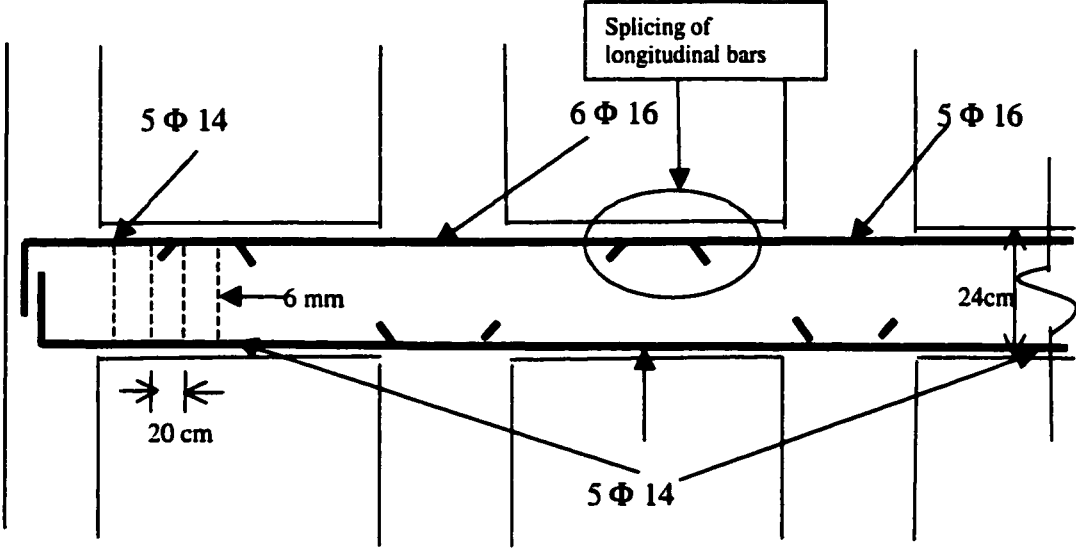


Figure 3.13 Longitudinal reinforcement in exterior beams⁵⁵

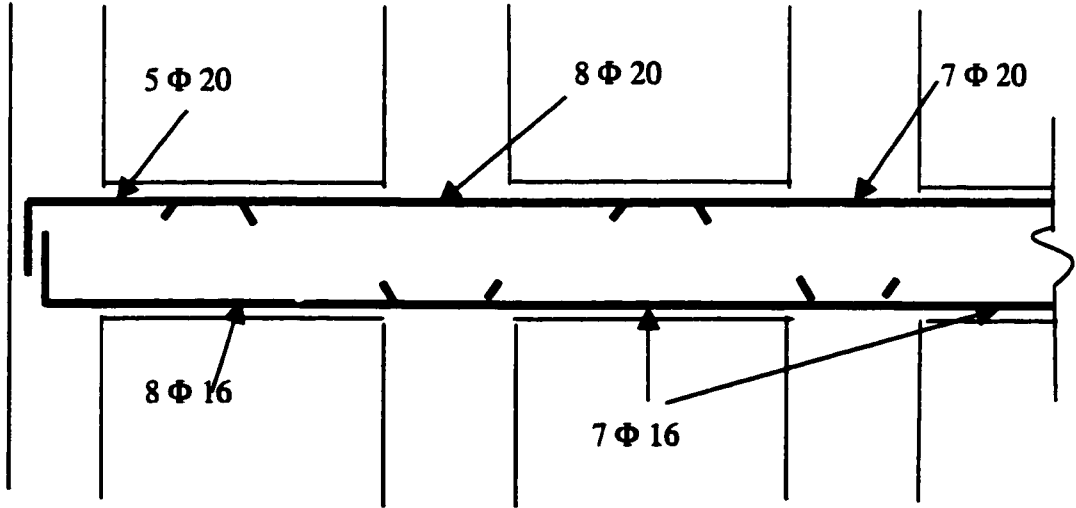


Figure 3.14 Longitudinal reinforcement in interior beams⁵⁵

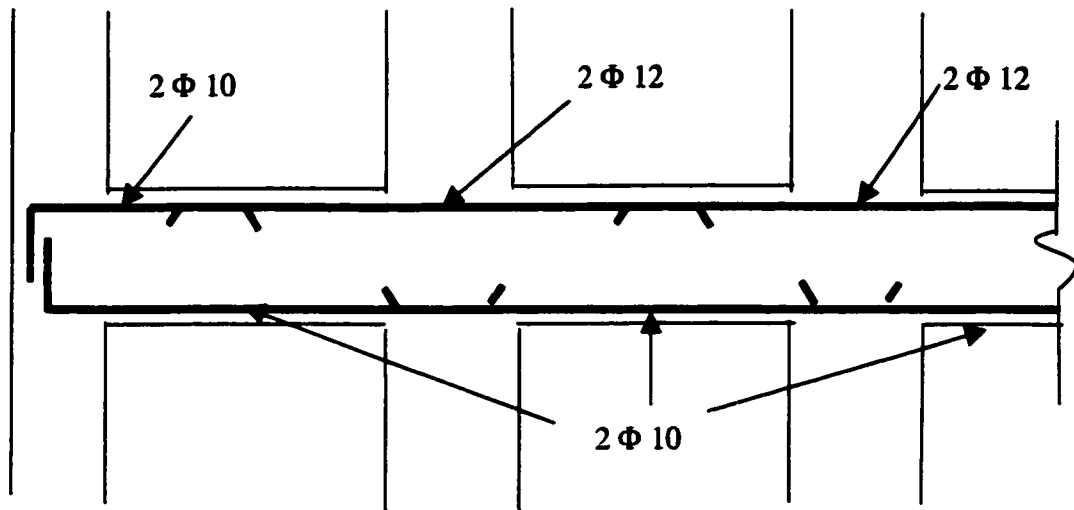


Figure 3.15 Longitudinal reinforcement in joists⁵⁵

The dimensions of columns and reinforcement are given in Table 3.1. Column reinforcement is spliced just above the floor level. Ties are 8 millimeters (0.32 inches) in diameter and spaced at 20 centimeters (8 inches).

Column	Story	Dimensions (centimeters)	Longitudinal reinforcement	Transverse reinforcement
Corner	1 to 4	20 x 70	8 T 20	4 T 8 @ 20 cm
	5 to 8	20 x 60		
Edge	1 to 4	20 x 80	8 T 22	4 T 8 @ 20 cm
	5 to 8	20 x 70		
Interior	1 to 4	30 x 100	12 T 22	6 T 8 @ 25 cm
	5 to 8	25 x 70		

Table 3.1 Columns dimensions and reinforcement⁵⁵

Notation: X T Y: Number of bars is X. A bar diameter is Y millimeters. (T is twisted)

The walls constituting the elevator shafts and the stair wall are 20 centimeters (8 inches) thick. Walls dimensions and reinforcement are shown if Table 3.2.

Wall	Length (meters)	Thickness (cm)	Vertical reinforcement	Horizontal reinforcement
W1	2.6	20	T 12 @ 40 cm	T 12 @ 45 cm
W2	1.8	20	T 12 @ 40 cm	T 12 @ 45 cm
W3	1.8	20	T 12 @ 40 cm	T 12 @ 45 cm
W4	1.8	20	T 12 @ 40 cm	T 12 @ 45 cm

Table 3.2 Walls dimensions and reinforcement⁵⁵

CHAPTER 4

ANALYTICAL TOOLS AND MODELS

4.1 General

Many models have been proposed to represent the inelastic behavior of structural members or systems. These models can be classified in three major groups depending on their level of complexity.

A general model is based on material response. For reinforced concrete structures, the structure is divided into finite elements, with different elements for the concrete and the steel bars. Special element models are used to represent the bond between these different elements. Given a set of constitutive equations for material response, any kind of structure, regardless of its complexity, can be modeled by finite elements. The definition of the constitutive equations is crucial. This approach requires large computer memory. Thus, it is often applied to the analysis of a single element structure or portion of a system.

The second model is referred to as a fiber model. Each element of the structure is divided into segments. For each segment, the cross section is discretized into a number of "fibers"¹⁷. The stiffness of segments is obtained by numerically integrating the stiffness of the cross-section of elements in which fibers may be in the elastic, inelastic, or strain-hardening range. This technique is also called spread plasticity and is computationally intensive.

The third model is referred to as member type model. For moment resisting frame structures, each member of the frame is considered as an element where inelastic behavior is, in general, concentrated at the two ends of structural element (beam or column). Thus, inelastic behavior is assumed to occur at member ends only (lumped plasticity). Between the ends, elements are assumed to behave elastically. Although the discretization of the structural members is not refined, the results of using these models for the behavior of members with uniaxial bending and constant axial load generally are satisfactory because experience has been gained through calibration using experimental results^{14,18,19}. For dynamic analyses of structures under earthquake excitations, member-type models are most commonly used. However, these models are very sensitive to the definition of properties in the inelastic areas.

In this chapter, three nonlinear programs are presented and analytical models used for the structural members are introduced.

4.2 Nonlinear Programs

Over the past 25 years, a number of nonlinear time history analysis programs have been developed at various research institutions. Kanaan and Powell³ developed one of the most commonly used programs, DRAIN-2D in the 1970's at the University of California at Berkeley. Another program for reinforced concrete structure analysis, IDARC, was developed in the 1980's at the State University of

New York at Buffalo by Park, Reinhorn and Kunnath⁵. Numerous modifications have been made to both programs since their initial release. Most recently, more general-purpose analysis programs, such as SAP2000 have added non-linear time history analysis to their features. In this study, only DRAIN-2D and SAP2000 will be used for analysis because they offer the possibility of modeling a brittle shear failure of a member. RCCOLA is a computer code, that was originally developed by Mahin at the University of California at Berkeley in 1977 and modified in 1983 at the University of Texas at Austin¹⁶, for the analyses of reinforced concrete cross sections.

4.2.1 RCCOLA

The input file for RCCOLA includes the stress strain characteristics for both concrete and steel. Also the cross section geometry needs to be defined in the input file. RCCOLA analyzes the section by dividing it into a large number of fibers where the stress is constant over each fiber. Fibers can be in the elastic range, plastic range or strain hardening, depending on the value of strain at the considered fiber. Hence, it can analyze the cross section of a complex shape. The output file generated by RCCOLA can include the moment-curvature relationship of a cross section. RCCOLA can be used to calculate the moment capacity, the shear capacity, yield ductility and curvatures at a series of given axial loads, for different specified extreme compressive strains of concrete.

4.2.2 DRAIN-2D

The DRAIN-2D program consists of a main program and several element subroutines. The main program involves processing of structural data (member properties, load conditions), assembly of the stiffness matrix of the structure, and the solution algorithm of the simultaneous equations. The element subroutines are intended to model the behavior of different types of structural members (reinforced concrete or steel elements). Analysis of the structures considered in this study was carried out using a modified version of DRAIN-2D. A modification of the original version to include a model for brittle shear failure of a beam-column element was made at the University of Texas at Austin by Pincheira and Jirsa¹⁵.

To analyze a structure using DRAIN-2D, the structure is idealized as a planar assemblage of discrete elements connected at every floor level with a rigid diaphragm. Therefore, torsional response is neglected. Analysis is carried out by the direct stiffness method, with nodal displacements as unknowns. Each node possesses up to three displacement degrees of freedom. The earthquake excitation is defined by time histories of ground acceleration. Static loads may be applied prior to the dynamic loading, but no yielding is permitted under static loads. The effects of gravity loads and initial prestressing on the elements are considered as initial member end actions. Any end forces due to dynamic loading are simply added to these initial forces.

The dynamic response is determined by step-by-step integration. A constant acceleration is assumed within any step. The tangent stiffness of the structure is used for each step, and linear structural behavior is assumed during the step. If an element yields or unloads, information will be returned from the element subroutine. Changes are then made to the tangent stiffness matrix and the triangularization operation of Gauss elimination is repeated. Applying corrective loads in the subsequent time step will eliminate any unbalanced loads resulting from errors in the assumed linear behavior within the step. Second order effects can be taken into account by including geometric stiffness in the element stiffness matrix.

The structure mass is assumed to be lumped at nodes so that the mass matrix is diagonal. Axial deformations and shear deformations of structural elements are included in the analysis. Beam-column joint regions are assumed infinitely rigid. All support nodes are assumed to move in phase.

4.2.2.1 Dynamic Equilibrium and Integration Solution

For a multi-degree-of-freedom system, the dynamic equilibrium at any time t , and for any time step Δt , can be expressed by:

$$[M]\{\Delta\ddot{r}\} + [C_T]\{\Delta\dot{r}\} + [K_T]\{\Delta r\} = \{\Delta F\} \quad (4.1)$$

in which, $[M]$ is the mass matrix, and $[C_T]$, $[K_T]$ are the tangent values of the damping and stiffness matrices for the structure at the beginning of the time step. The vectors $\{\Delta\ddot{r}\}$, $\{\Delta\dot{r}\}$ and $\{\Delta r\}$ are the increments of acceleration, velocity and

displacement, respectively, at nodes; $\{\Delta F\}$ is the increment in applied loading. In the case of an earthquake, $\{\Delta F\} = -[M] \{\Delta \ddot{r}_g\}$, in which $\{\Delta \ddot{r}_g\}$ is the increment of ground acceleration.

Using an approximation that within the time step acceleration remains constant, the dynamic equilibrium Equation (4.1) is solved. The constant acceleration method has the advantage of being stable for all periods and time steps. However, the accuracy of the results depends largely on the integration time step used. The smaller the time step, the more accurate are the expected results. On the other hand, it is important to select as long a time step as possible in order to minimize the computational effort. Previous research has shown that a time step of 0.005 second will generally yield enough accuracy^{3,15,20}, therefore an integration time step of 0.005 is used for the subsequent dynamic analyses.

4.2.2.2 Static Incremental Loading

The modified version of DRAIN-2D at the University of Texas allows the user to compute the inelastic response of a structure under static loads. To obtain inelastic behavior under static lateral loading, the program uses the same subroutines used for computing the dynamic behavior, but eliminates the acceleration and velocity terms from the dynamic equilibrium equation (4.1). The dynamic equations are reduced to those corresponding to static equilibrium in which the multiplication

of the mass matrix and the increment of the ground acceleration vector represent incremental static lateral forces. Hence, only force controlled loading is permitted.

4.2.2.3 Viscous Damping

Damping of the structure is considered through the damping matrix $[C_T]$. DRAIN-2D assumes that viscous damping is a linear combination of the mass and tangent stiffness matrices (Rayleigh damping) as expressed in equation (4.2):

$$[C_T] = \alpha [M] + \beta [K_T] \quad (4.2)$$

where α and β are the mass and stiffness damping coefficients, respectively. If the system is assumed to be uncoupled into normal modes, these coefficients can be specified at two different modes of vibration i and j , through the following relationships:

$$\alpha = \frac{4\pi(T_j\xi_j - T_i\xi_i)}{T_j^2 - T_i^2} \quad (4.3)$$

$$\beta = \frac{T_i T_j (T_j \xi_i - T_i \xi_j)}{\pi(T_j^2 - T_i^2)} \quad (4.4)$$

in which T_i, T_j are the respective periods of the two modes of vibration selected, and ξ_i, ξ_j are the respective damping ratios for these two modes. Typically, the first two modes of vibration are selected, because they dominate the dynamic behavior of building structures. Since the stiffness of the structure varies as members start yielding, the tangent stiffness matrix and the viscous damping matrix will vary as the structure moves into the inelastic range.

Figure 4.1 shows the relationship between the damping ratio and period of vibration that is obtained using Equations (4.3) and (4.4).

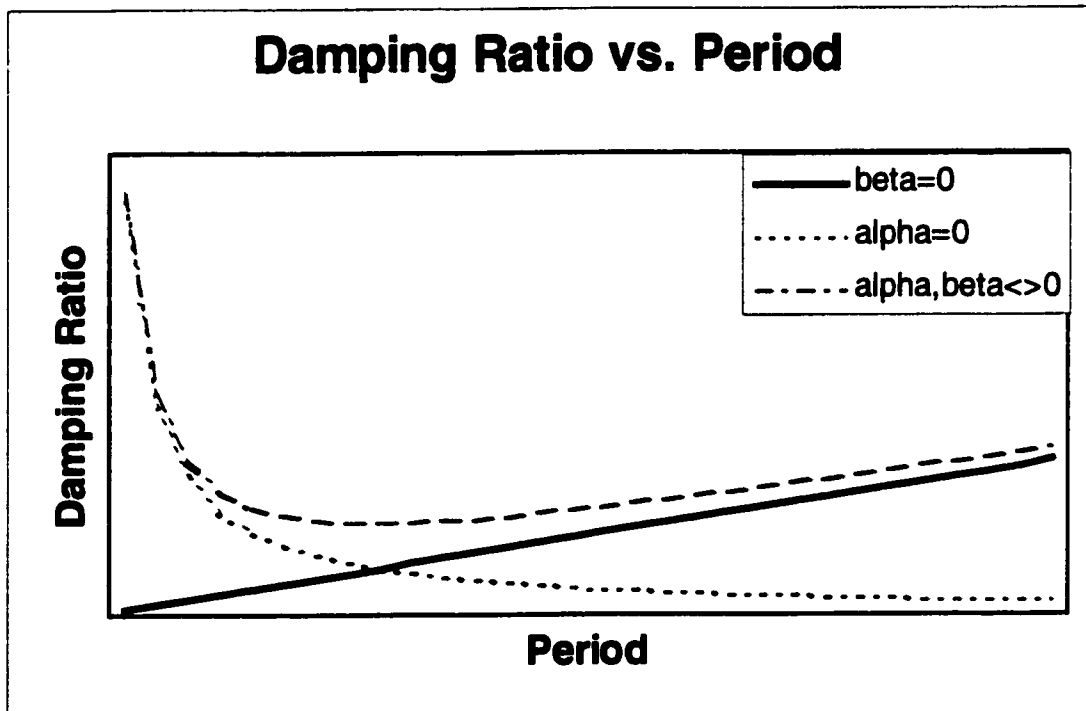


Figure 4.1 Relationship between damping ratio and period for Rayleigh damping.

If the damping ratios for the first two modes are chosen to be equal, $\xi_1 = \xi_2 = \xi$, Fig. 4.1 shows that the damping ratio for higher modes will be larger than ξ . Responses of high frequency modes are effectively eliminated by the higher damping ratios^{6,7}.

4.2.2.4 Beam Column Element

A beam-column element with degrading stiffness was formulated to model reinforced concrete frame elements.

In DRAIN-2D, the one-component model proposed by Giberson²¹ was adopted to represent reinforced concrete frame members (beams and columns) as shown in Fig. 4.2. The element was assumed to consist of a linear elastic beam element with non-linear rotational springs at each end. Yielding is assumed to be concentrated in plastic hinge regions at the element ends. All plastic deformations, including the effects of stiffness degradation, were introduced by means of the moment-rotation relationships for the inelastic springs, while the central element deforms elastically.

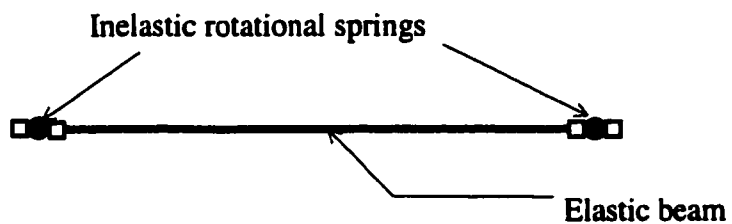


Figure 4.2 Element Idealization - One Component Model

4.2.2.5 Hysteretic Behavior

To model the inelastic behavior of reinforced concrete members under reversed cyclic loading, an extended version of Takeda's model²² was adopted, as illustrated in Fig. 4.3.

While the original Takeda's model is based on a bilinear relationship in which the initial stiffness and strain hardening ratio are determined from monotonic loading conditions for flexural deformations only, the modified version included two major changes as shown in Figs. 4.4 and 4.5.

- (1) A reduction of the unloading stiffness as a function of the largest previous spring rotation.
- (2) An increase in the reloading stiffness that depends on previous spring rotations.

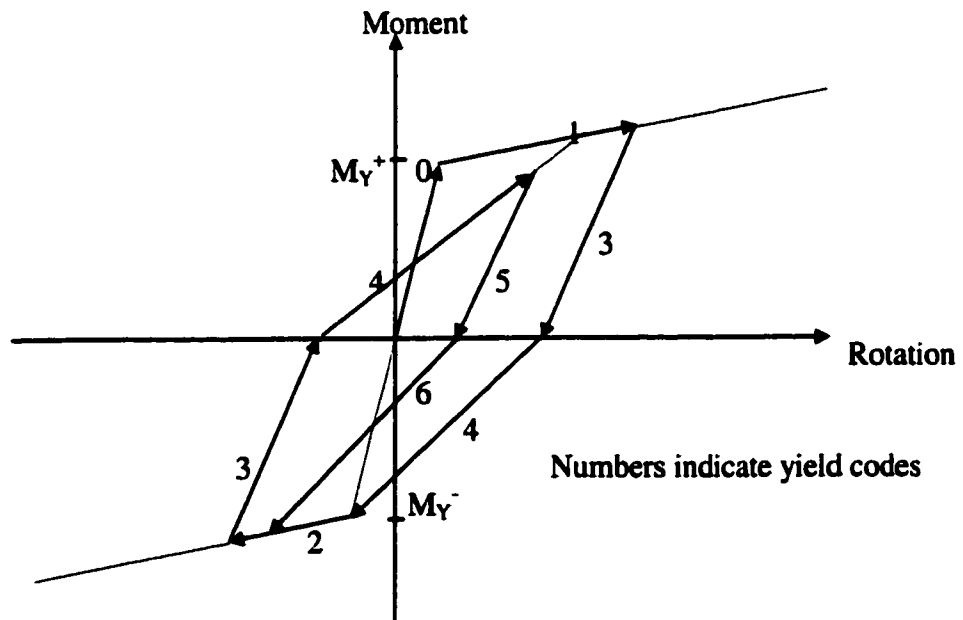


Figure 4.3 Inelastic Spring Moment-Rotation Relationship Extended from Takeda's Model

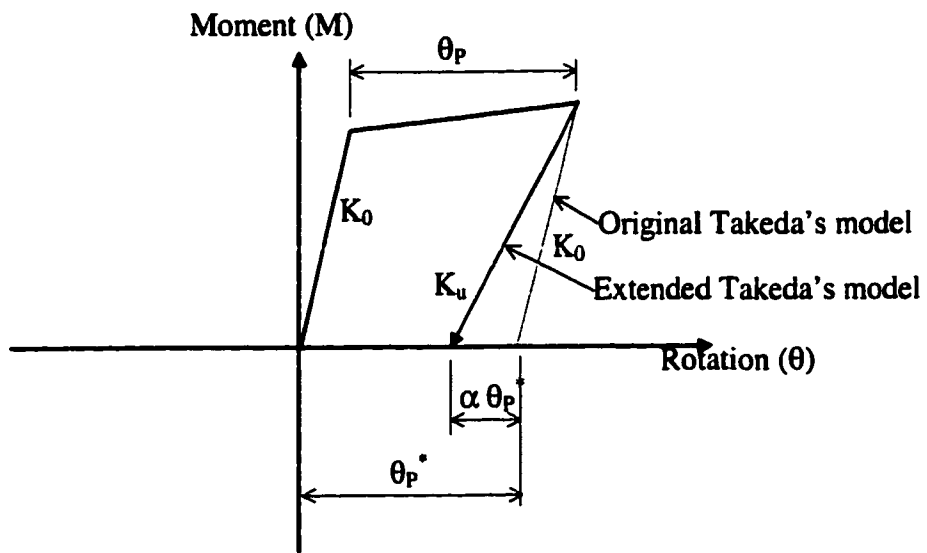


Figure 4.4 Unloading Stiffness for Extended Takeda's Model

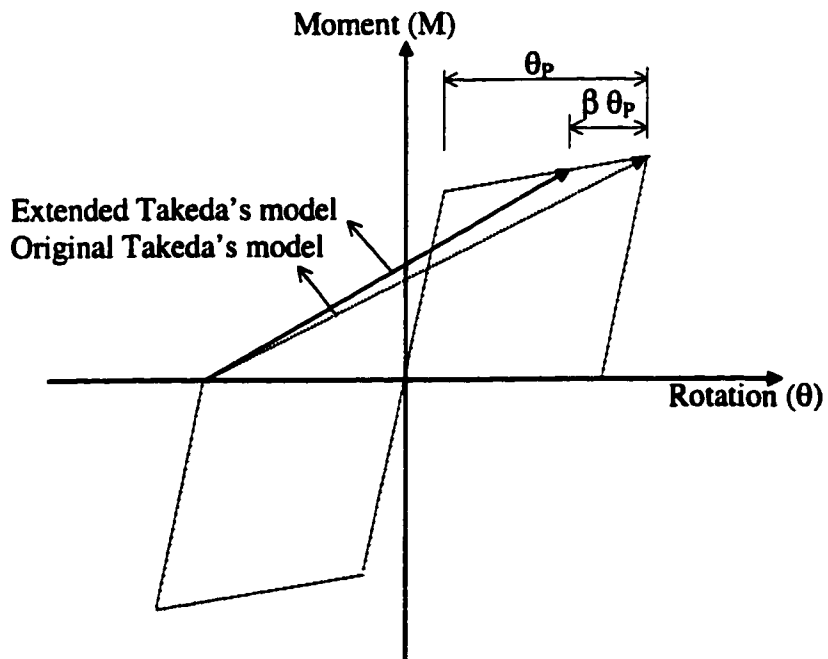


Figure 4.5 Reloading Stiffness for Extended Takeda's Model

4.2.3 SAP2000 NL-PUSH

SAP2000 represents the state-of-the-art in three-dimensional finite element technology for structural engineering⁸. SAP2000 provides powerful capabilities for modeling a wide range of structures, including bridges, dams, tanks and buildings. Element types range from Frame/Truss to Shell/Plate to Solid to Nonlinear Link elements.

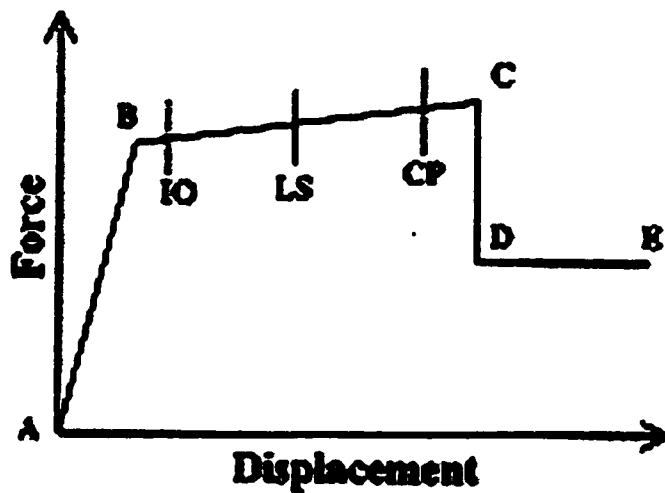
4.2.3.1 Dynamic Analyses and Integration Procedure

Dynamic loading can be in the form of multiple base response spectrums, or multiple time varying loads and base excitations. The programs support Eigen and Ritz analysis, as well as modal combinations by the square root of the sum of the squares, SRSS, the complete quadratic combination, CQC, or the general CQC3 method, GMC. In the case of response spectrums, modal superposition is used in solving the dynamic equilibrium. For time varying loads and base excitations, the same equilibrium equation (4.2) solved in DRAIN-2D is solved using constant acceleration with $\beta=1/2$.

4.2.3.2 Nonlinear Pushover Options

Static loading options allow for nodal loading with specified forces or displacements. New computational techniques have been integrated into SAP2000

Nonlinear Version 7 to allow a static pushover analysis to be performed in a simple and practical manner. Nonlinear hinges may be defined anywhere in the frame, and properties may be user defined or calculated automatically by the program as shown in Figs. 4.6 and 4.7. Analyses may be force or displacement controlled.



IO = Immediate Occupancy

LS = Life Safety

CP = Collapse Prevention

Figure 4.6 Component modeling and acceptability (FEMA 273)

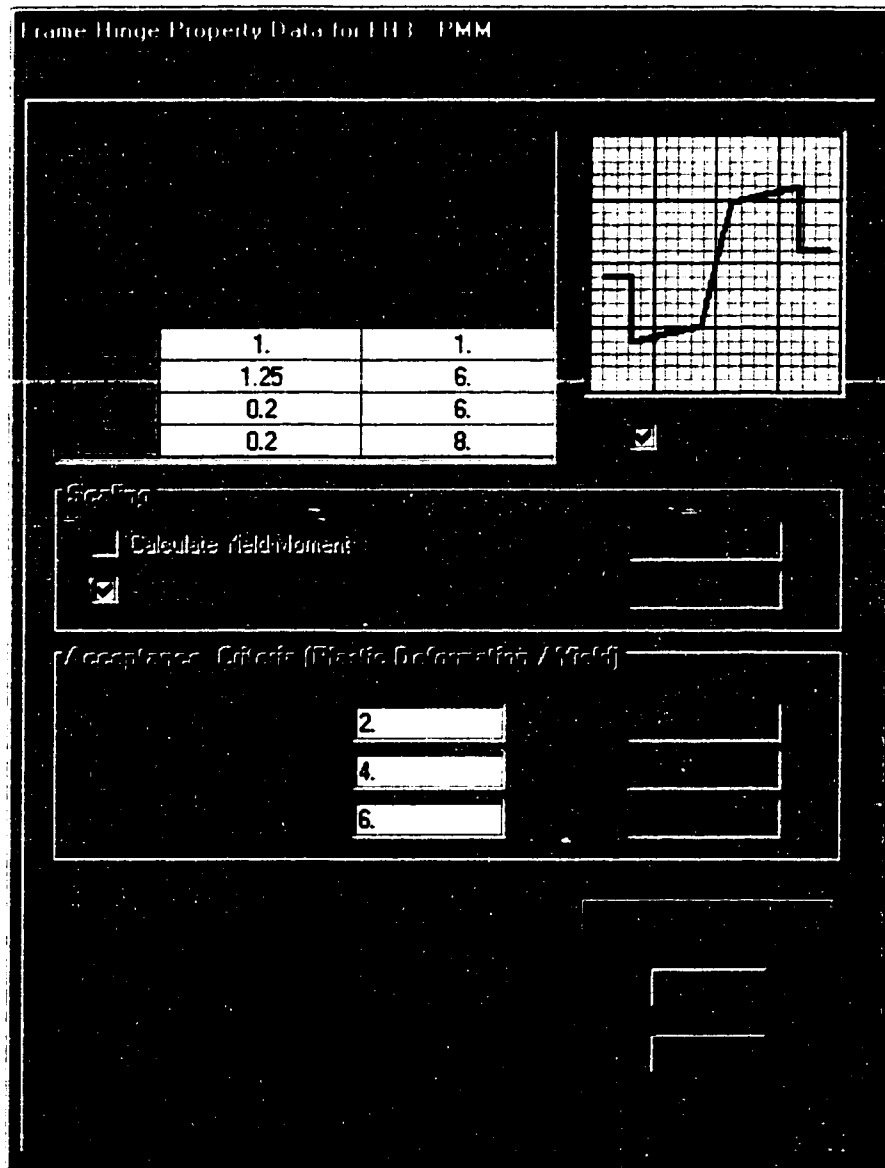


Figure 4.7 Hinge properties for Pushover Analysis (SAP2000).

Nonlinear pushover analysis based on ATC-40 and FEMA-273 is fully integrated into the SAP2000 NL-PUSH. Nonlinear Pushover Analysis results can be used with the integrated steel and concrete design postprocessor options. Default and

user defined Moment, Shear, Axial and PMM (biaxial moment axial-load interaction diagram) hinges at any location along a frame member. A highly interactive capacity spectrum curve display form allows study of the effects of parameter changes instantaneously.

4.2.3.3 Viscous Damping

Although the developer of SAP2000, E. Wilson, disagrees with the use of Rayleigh damping, it is used by SAP2000 in order to obtain results for numerically sensitive structural systems. Wilson argues that the assumption of proportional damping implies the existence of external supported dampers that are physically impossible for a base supported structure. The use of stiffness proportional damping has the effect of increasing the damping in higher modes of the structure for which there is no physical justification and can result in significant errors in some cases²³. On the other hand, mass proportional damping cannot be justified because it causes external forces to be applied to the structure that reduce the base shear for seismic loading²³.

4.2.3.4 Nonlinear Link

The nonlinear link (NL-Link) element is an exponentially plastic element (Fig. 4.8). For a large selected value of the exponential, the element could be considered bilinearly plastic. It may be used to model local structural nonlinearities

for dynamic analysis involving base isolators, dampers, and hook and gap elements. Each NL-Link element may be either one-joint grounded spring specified at one end of a member or a two-joint link connecting two different nodes of the structure. Each element is assumed to be composed of six separate “springs”, one for each degree of six deformational degrees of freedom (axial, shear, torsion, and pure bending). Figure 4.9 shows the hysteretic behavior of plastic1 NL-Link in two orthogonal directions used for 3D nonlinear time history analyses.

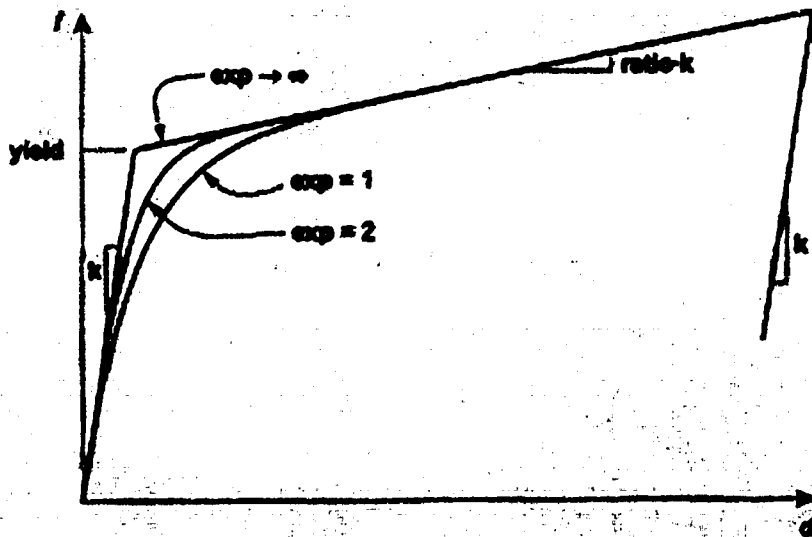


Figure 4.8 Uniaxial hysteretic behavior of plastic-1 NL-Link(SAP2000).

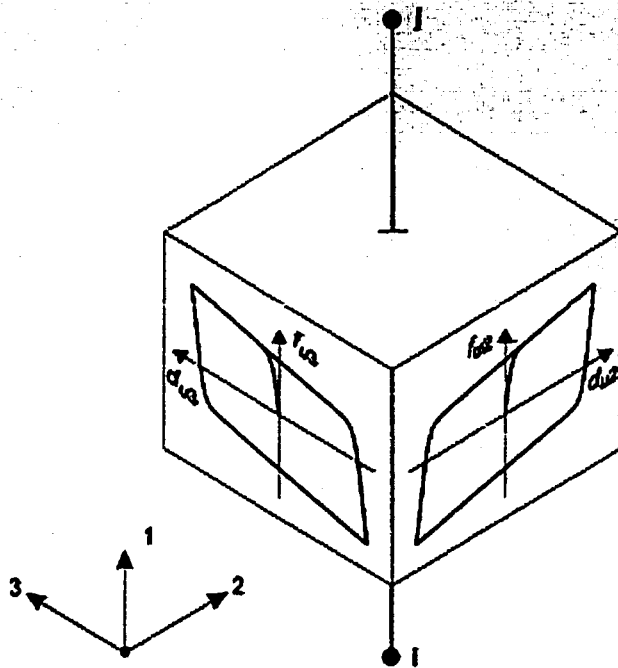


Figure 4.9 Hysteretic behavior of the biaxial plastic-1 NL-Link(SAP2000).

4.3 Analytical Model

The lumped plasticity model used to analyze the inelastic behavior of the reinforced concrete members of buildings selected for this study, is described in this section. Material properties as well as hysteretic behavior of such members are presented. Also, assumptions used in assigning member stiffness properties are discussed.

4.3.1 DRAIN-2D

Since the structures analyzed in this study are mainly frame structures, the element subroutine 11 developed by Pincheira and Jirsa¹⁵ for reinforced concrete beams and columns was used to model members in buildings. The degrading stiffness element has two additional deformation modes, namely additional rotational deformations associated with each of the two rotational springs, as shown in Fig. 4.2. For each element, deformations consist of inelastic hinge rotations of springs and deformations of elastic beams connecting the springs. However the additional degrees of freedom due to spring rotations are condensed out in the element stiffness matrix formulation, so they do not appear as structural degrees of freedom³. Yield moments specified at the ends of elements consider no interaction between axial force and bending moment in producing yield¹⁵.

4.3.1.1 Modeling Strength Degradation of Reinforced Concrete Members

To represent failure of reinforced concrete members due to the short embedment lengths in beams or short lap splices in columns, modifications to the original Takeda's model were introduced to reproduce the variations in stiffness with load reversals. Typically, these modes of failure are characterized by a sudden loss of the flexural strength of the section after reaching peak moment capacity. Figure 4.10 shows the main features of the moment-rotation envelope for the Takeda model modified by Pincheira¹⁵.

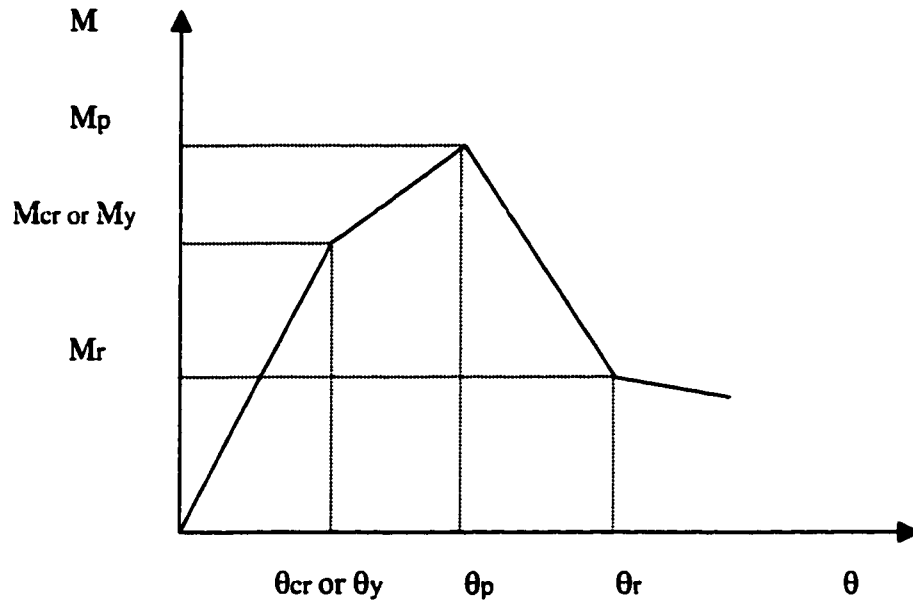


Figure 4.10 Moment-rotation envelope for beam-element-1

Where,

M_p = peak moment

M_{cr} or M_y = moment at cracking or at yield

M_r = the residual moment

θ_p = is the rotation at peak moment

θ_{cr} or θ_y = the rotation at cracking or at yield

θ_r = is the rotation at residual moment

The negative slope after θ_r is reached is to prevent moment reversal beyond this point¹⁵.

4.3.1.2 Modeling of Shear Failure in Reinforced Concrete Members

The same model used in the previous section can be used to represent shear failure modes of reinforced concrete members²². In such a model, shear failure is introduced by activating the descending branch of the moment-rotation relationship at both ends of the member when the specified shear capacity is reached. However, to specify a shear capacity for a section, it is assumed that the member is subjected to equal and opposite end moments. Another disadvantage of this method is the instability that may be introduced when several members reach shear capacity and negative tangent stiffness at the same time. To eliminate the problem of instability introduced by the negative stiffness, Pincheira and Jirsa¹⁵ suggested a brittle shear model as shown in Fig. 4.11.

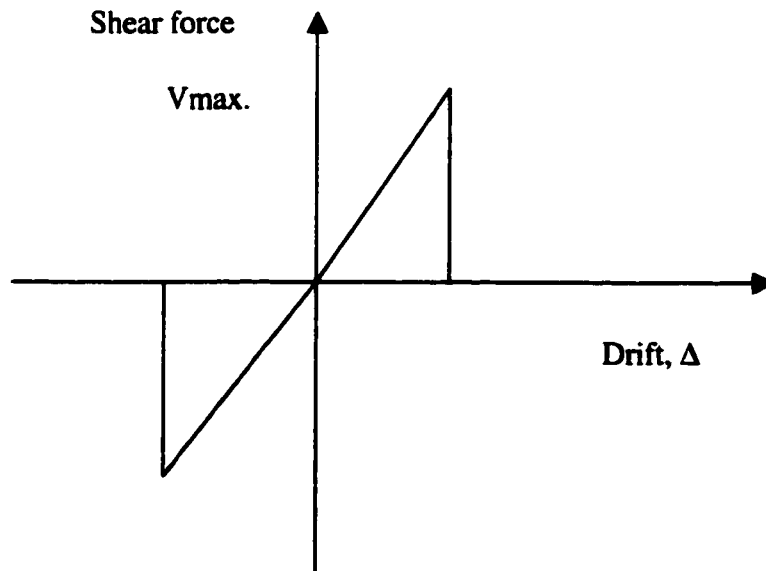


Figure 4.11 Hysteretic behavior of the simplified shear model¹⁵.

Figure 4.11 shows typical hysteretic behavior of the simplified shear model suggested by Pincheira. The member exhibits linear shear behavior until the shear capacity is reached. It then loses its lateral strength but maintains its axial compression strength. With this model, the behavior of the element after shear failure is essentially that of a truss element. However, previous research have shown that columns with axial loads of 20% of the ultimate compression capacity were able to sustain lateral drifts of at least twice that at peak shear capacity with no sign of axial failure²⁴.

To account for the ability of the member to maintain a certain fraction of its stiffness and strength after shear failure is reached, Li and Jirsa suggested the parallel element model¹⁴. As shown in Fig. 4.12, every column element is divided into two sub-elements, column 1 and column 2. After the shear capacity of the original column element is exceeded, column 2 loses its lateral load resisting capacity by changing to a truss member. The shear capacity of column 1 can be set to a very large value so that it does not fail in shear. The shear capacity of column 1 becomes the residual shear capacity after the original column element fails in shear. The hysteretic behavior of the column with shear failure is demonstrated schematically in Fig. 4.13. After the shear failure occurs, a sudden loss of shear capacity from the peak capacity V_{max} to a residual capacity V_{res} is assumed.

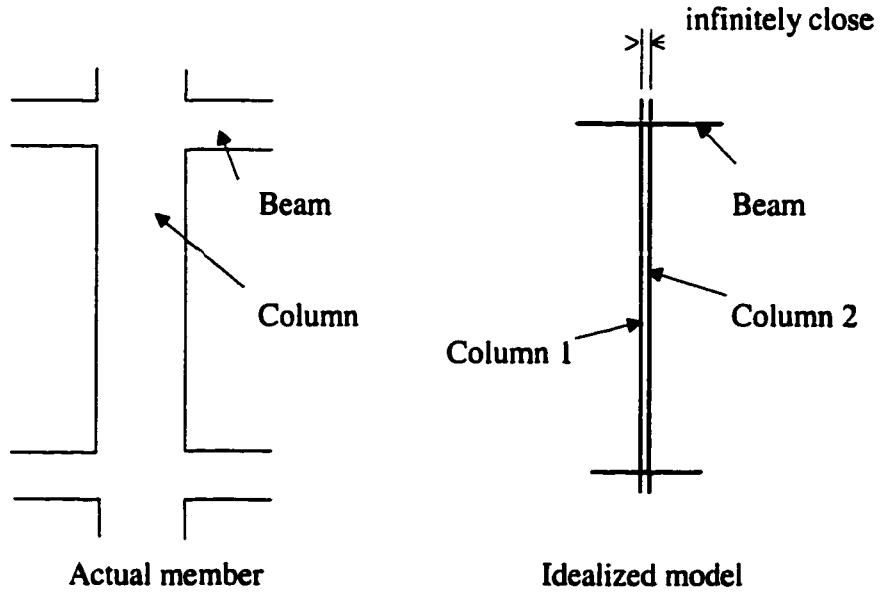
Previous research⁶¹ has shown that shear failure modes can be categorized as Shear compression failure, shear bond failure and shear flexure failure. Shear

compression failure occurs under moderate axial load and a large shear reinforcement ratio in the columns. Shear-compression failure is characterized by small drift capacity and a large loss of strength after peak shear is reached. Shear bond failure occurs when large longitudinal reinforcement ratio, large bar sizes and low concrete strength are used. A gradual loss of strength and the capacity of the member to sustain large drift after peak shear characterize this mode of failure. Shear flexure failure occurs when the longitudinal reinforcement ratio and axial load are low. Members failing in this mode can withstand large deformation with moderate strength degradation. By using different values for the residual shear capacity in the simplified parallel-element model, it is possible to model different shear failure modes as described above.

In this study, residual shear capacity was assumed to remain constant after shear failure has occurred. The column was assumed to be able to sustain very large lateral deformations. The shear capacity V_{max} was computed using ACI 318-95 Code⁹ equation (11-4) for members subject to axial compression.

$$V_c = 2\left(1 + \frac{N_u}{2000A_g}\right)\sqrt{f_c}b_wd \quad (4.5)$$

Before shear failure



After shear failure

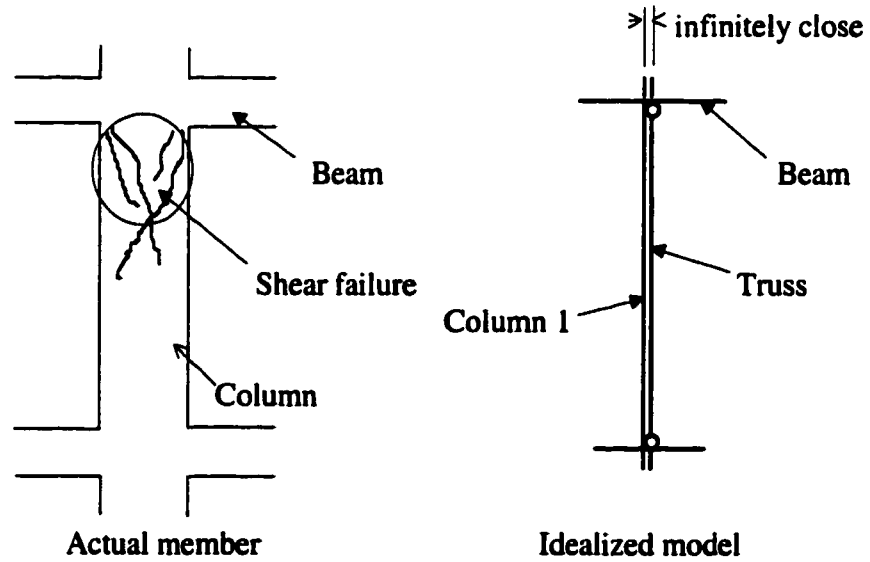
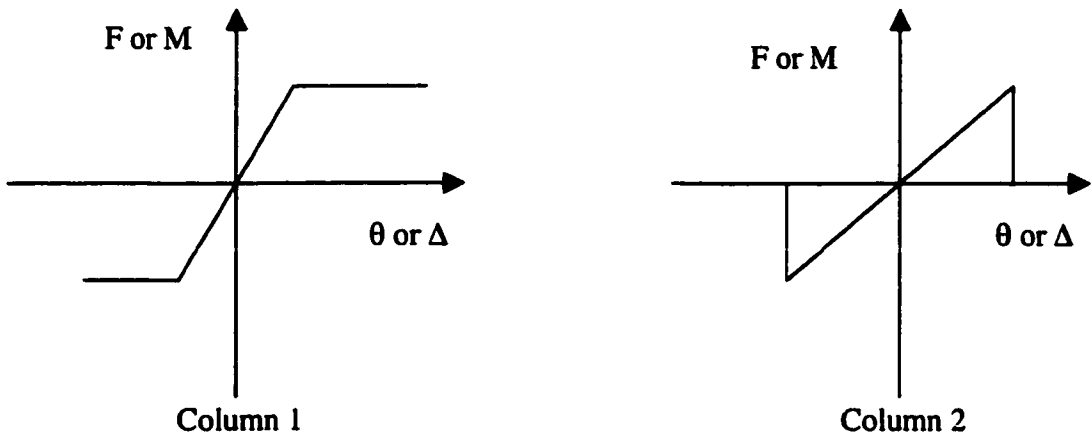


Figure 4.12 Parallel-Element Model for Shear Failure proposed by Li¹⁴



Moment-rotation or force-displacement envelope for beam-element

- Before shear failure
- After shear failure

V_{max} : original shear capacity
 V_{res} : residual shear capacity

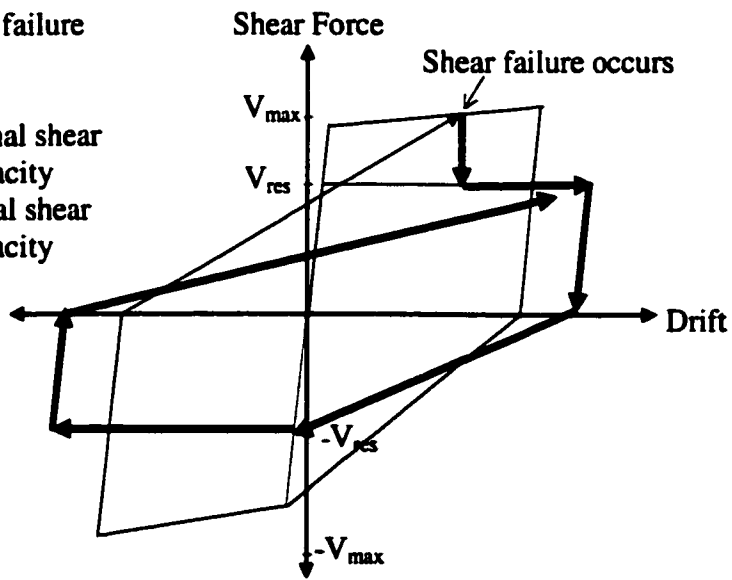
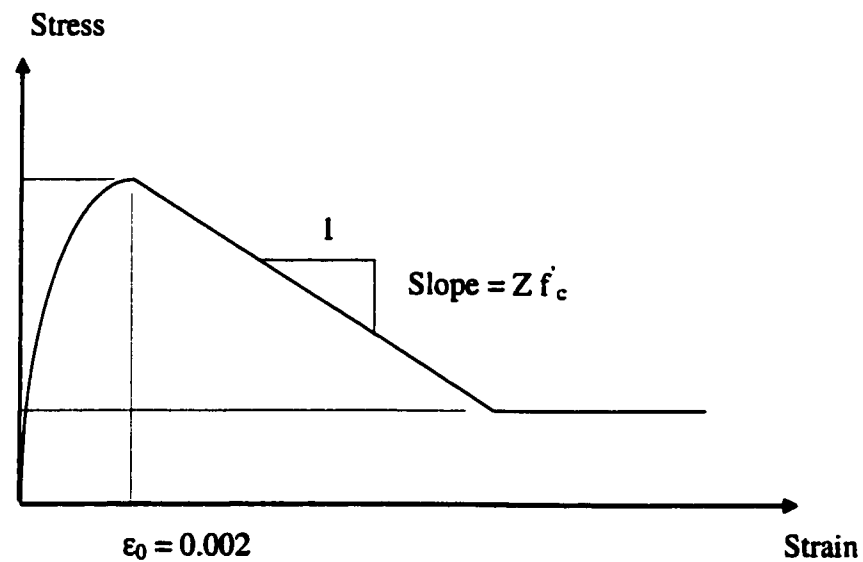


Figure 4.13 Model of hysteretic behavior of column failing in shear

4.3.1.3 Modeling Parameters and Procedure

4.3.1.3.1 Material Properties

For concrete, the stress-strain relationship was assumed to follow the Park and Kent model²⁵ as shown in Fig. 4.14. The stress-strain relationship for reinforcing steel was idealized as presented in Fig. 4.15.



$$Z = \frac{0.5}{\epsilon_{50u} + \epsilon_{50h} - 0.002}$$

in which, $\epsilon_{50u} = \frac{3 + 0.002 f'_c}{f'_c - 1000}$, (f'_c in psi)

$$\epsilon_{50h} = \frac{3}{4} \rho_s \sqrt{\frac{b''}{s}}$$

ρ_s is the ratio of transverse reinforcement over the volume of confined concrete;

b'' is the width of confined core;

s is the transverse reinforcing steel spacing.

Figure 4.14 Stress-Strain Relationship for Concrete. DRAIN-2D

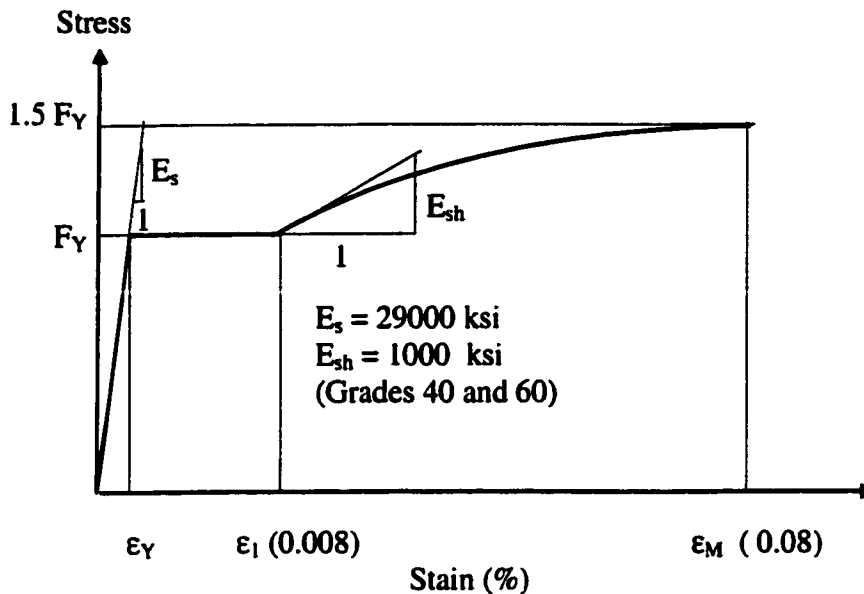


Figure 4.15 Stress-Strain Relationship for Reinforcing Steel. DRAIN-2D

4.3.1.3.2 Element Stiffness

To determine the cross section properties of reinforced concrete members to be used in DRAIN-2D, It was assumed that the material is homogeneous and the members bend in double curvature with equal moment at both ends as shown in Fig. 4.16. That is equivalent to saying that during the entire loading, the bending distribution of the member is such that the point of inflection remains fixed at mid-span. This assumption allows the use of the same stiffness formulation for the rotational springs.

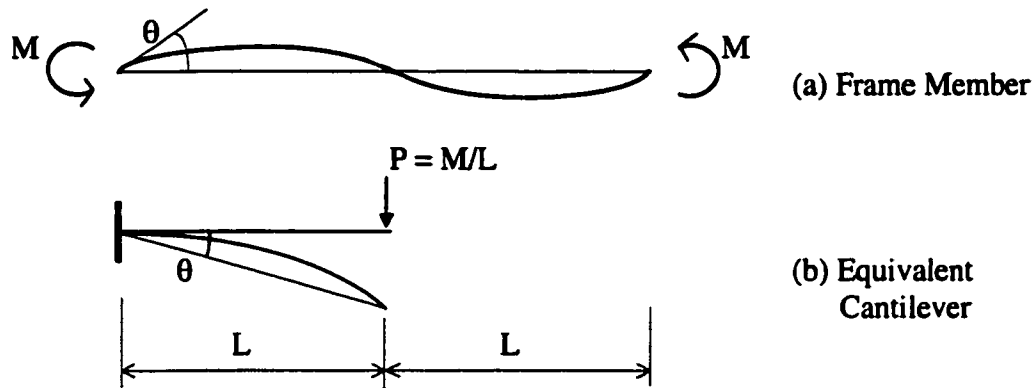


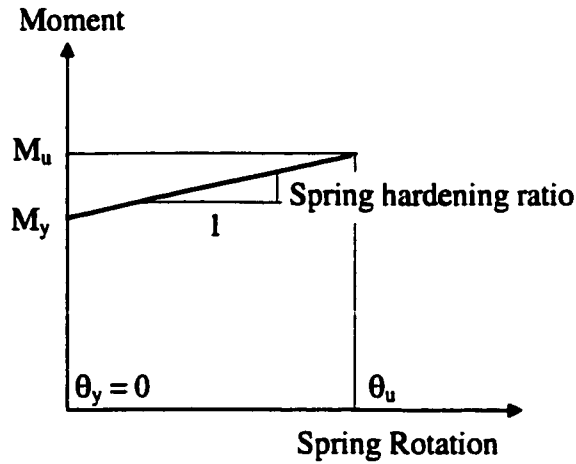
Figure 4.16 Equivalent Cantilever

Within the equivalent cantilever, section properties, including material, dimension, and reinforcement do not change.

Two options are available in DRAIN-2D for assigning element stiffness properties³.

The first option is to specify an effective flexural stiffness $(EI)_{\text{eff}}$ for the linear elastic element, that takes into account cracking. Also an axial stiffness (EA) and a shear stiffness (GA') are specified based on gross section properties.

A very large initial elastic stiffness is assigned to the spring (10^{16} kip-inches), so that each hinge is practically rigid up to yield (Fig. 4.17).



$$\text{Spring hardening ratio} = \frac{M_u - M_Y}{\theta_u - \theta_Y} = \frac{M_u - M_Y}{\theta_u}$$

Figure 4.17 Assumed Spring Moment-Rotation Relationship

The moment-rotation relationships for the cross-section are obtained by direct integration of the moment-curvature relationships. The moment-curvature relationship for columns was computed using the program RCCOLA¹⁶, considering the columns subjected to an axial load equal to the gravity load carried by the columns. In computing the moment-curvature relationships for beams, axial load was neglected. The multi-line moment curvature diagram obtained from the RCCOLA program was represented by a bi-linear relationship (Fig. 4.18). The yield point (M_Y , Φ_Y) and the ultimate point (M_u , Φ_u) for the bi-linear relationship correspond to the first yielding of the tension reinforcement and the ultimate capacity of the section respectively, as computed by RCCOLA.

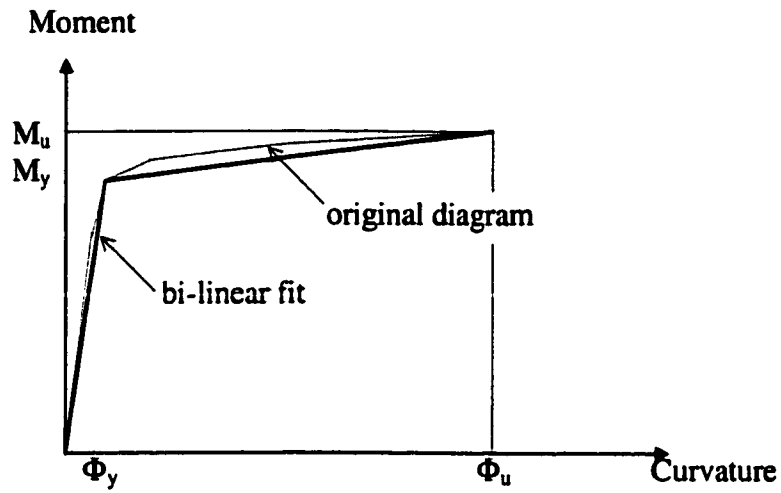


Figure 4.18 Bi-Linear Fit for the Moment-Curvature Relationship of Reinforced Concrete Cross Sections

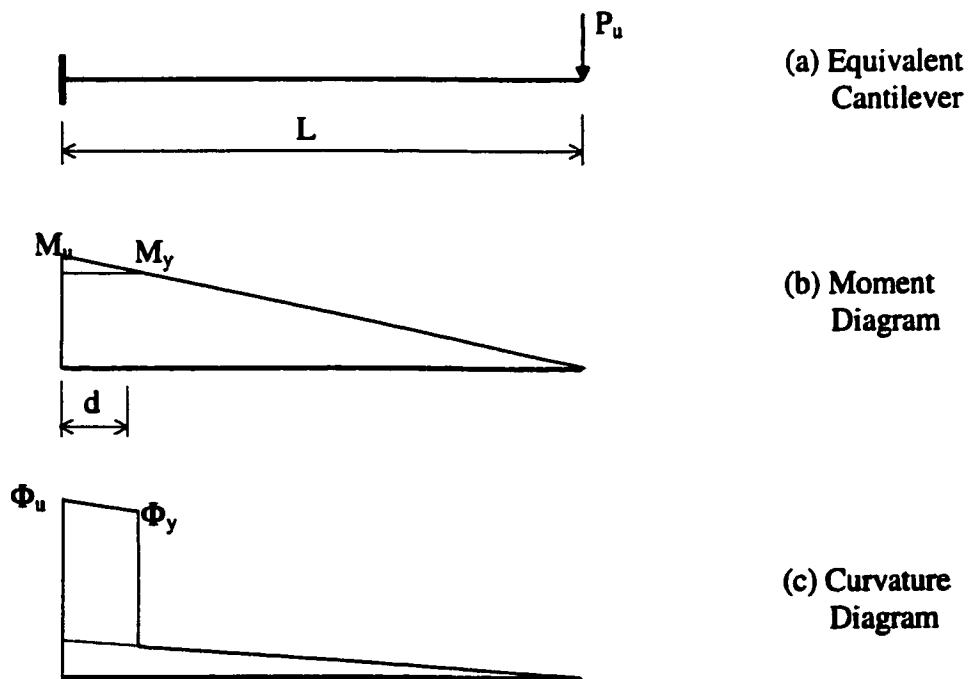


Figure 4.19 Moment and Curvature Diagrams for the Equivalent Cantilever

In determining the ultimate rotation capacity for the spring, θ_u , plastic hinges were assumed to be concentrated along a distance d from the end of the member (d is the effective depth of the cross section) as shown in Fig. 4.19. Therefore, using the moment area theorem, the plastic hinge rotation θ_u was calculated as follows (Fig. 4.20).



Figure 4.20 Calculation of Ultimate Rotation Capacity

$$\theta_U = \frac{\delta_U}{L} \quad (4.6)$$

$$\delta = (\Phi_U - \Phi_Y)d(L - \frac{d}{2}) \quad (4.7)$$

After substituting (4.7) into (4.6):

$$\theta_U = \frac{(\Phi_U - \Phi_Y)d(L - \frac{d}{2})}{L} \quad (4.8)$$

The second option is to determine the effective flexural stiffness of the member (EI) directly from the bilinear fit moment-curvature relationship: First, the equivalent cantilever was represented with an idealized cantilever as shown in Fig.

4.21. The effective stiffness (EI), initial spring stiffness K_{sp} , and spring strain hardening ratio p were computed by setting the tip displacement δ_y and tip rotation α_y of the idealized cantilever equal to those of the equivalent cantilever as shown in Fig. 4.21 when the fixed-end moment reaches yield. The following equations can be used to obtain the effective stiffness, initial spring stiffness and spring hardening ratio³:

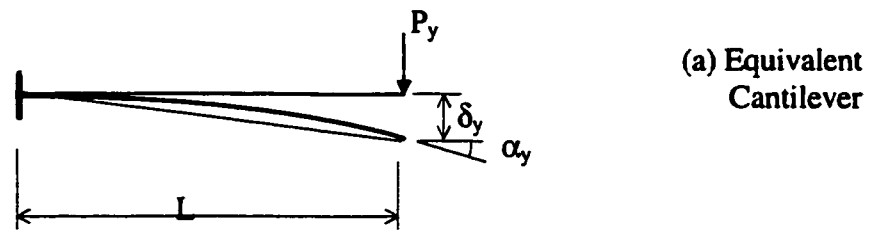
$$EI = \frac{M_y L}{3(2\alpha_y - 2\frac{\delta_y}{L})} \quad (4.9)$$

$$K_{sp} = \frac{M_y L}{(\delta_y - \frac{M_y L^2}{3EI})} \quad (4.10)$$

$$p = \frac{(P_u L - M_y)L}{(\delta_u - \delta_y - \frac{(P_u L - M_y)L^2}{3EI})} \quad (4.11)$$

in which, δ_u is any cantilever tip displacement when the fixed-end moment is strain hardening; M_y is the yield moment at the fixed-end of the cantilever.

Figure 4.22 shows the $P-\delta$ relationship of the cantilever and the $M-\theta$ relationship of the spring.



(a) Equivalent Cantilever



(b) Idealized Cantilever

- P_y : Load when fixed-end moment L reaching yield;
 δ_y : Cantilever tip displacement;
 δ_1 : Cantilever tip displacement due to spring rotation only;
 δ_2 : Cantilever tip displacement due to beam bending only;
 α_y : Cantilever tip rotation;

Figure 4.21 Idealized Cantilever

By assuming the section moment-curvature relationship as shown in Fig. 4.23, tip displacement and tip rotation for the equivalent cantilever can be calculated using Equations (4.12), (4.13) and (4.14).

$$\delta_y = \frac{1}{3} \Phi_y L^2 - \frac{1}{3} \left(\frac{M_{cr}}{M_y} \right)^2 L^2 \left(\frac{M_{cr}}{M_y} \Phi_y - \Phi_{cr} \right) \quad (4.12)$$

$$\alpha_y = \frac{1}{2} \Phi_y L - \frac{1}{2} \left(\frac{M_{cr}}{M_y} \right) L \left(\frac{M_{cr}}{M_y} \Phi_y - \Phi_{cr} \right) \quad (4.13)$$

$$\begin{aligned} \delta_u = & \frac{1}{3} \Phi_y \left(\frac{M_y}{M_u} L \right)^2 - \frac{1}{3} \left(\frac{M_{cr}}{M_y} \Phi_y - \Phi_{cr} \right) \left(\frac{M_{cr}}{M_u} L \right)^2 + \frac{1}{6} (\Phi_u - \Phi_y) \left(1 - \frac{M_y}{M_u} \right) \left(2 + \frac{M_y}{M_u} \right) L^2 \\ & + \frac{1}{2} \Phi_y \left(1 - \frac{M_y}{M_u} \right) \left(1 + \frac{M_y}{M_u} \right) L^2 \end{aligned} \quad (4.14)$$

Values for M_{cr} , M_y , M_u , and Φ_{cr} , Φ_y , Φ_u , were calculated using RCCOLA.

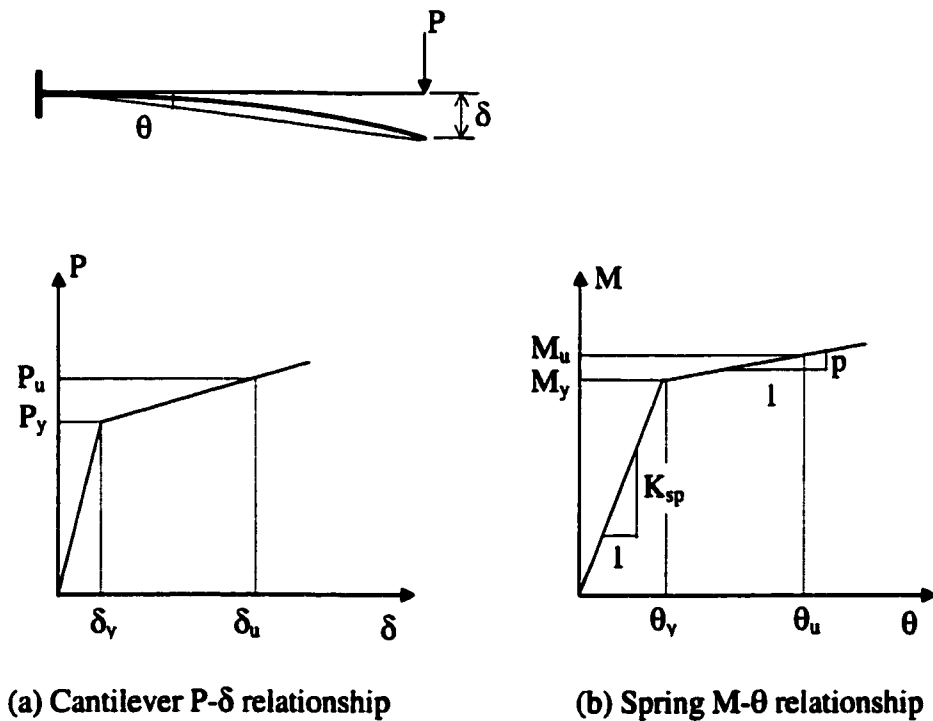


Figure 4.22 Idealized Cantilever Behavior

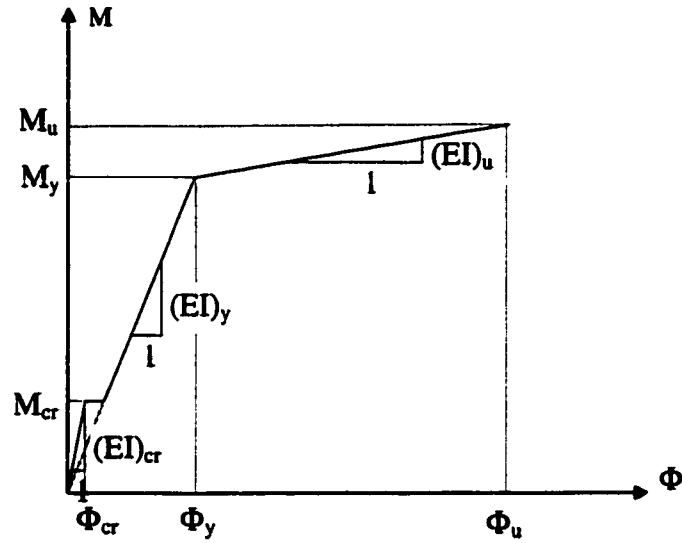


Figure 4.23 Section M- Φ Diagram

The analytical tools presented in this chapter, and the analytical models discussed above were used to conduct a parametric study of reinforced concrete structures. Modifications to the analytical models were introduced in chapter 7 and used in the analyses. Suggestions on the use and enhancements of the nonlinear analysis programs were made in Chapter 8.

CHAPTER 5 SENSITIVITY STUDY

5.1 General

In the absence of field data necessary to calibrate analytical models and tools, a parametric study is essential to better understand the results of analysis and the parameters that most effect those results. In this chapter, a sensitivity study involving selected critical structural parameters is discussed using the results of nonlinear time history analyses.

5.2 Assumptions and Parametric Variables

For the sensitivity study, only DRAIN-2D was used to perform the analyses. Option 1 discussed in section 4.3.1.3.2 was used for assigning element stiffness. Because of limitations in DRAIN-2D, only a planar representation of the structure was analyzed. The beam element model available with DRAIN-2D and described in Chapter 4 was used. Columns were modeled using the parallel element model suggested by Li and Jirsa¹⁴, with the boundary conditions modified as discussed in Chapter 7. Unreinforced masonry walls were modeled using the infill panel element available with DRAIN-2D. The infill panel element is intended to permit contribution of the infill masonry panels to the lateral stiffness of the structure. The infill element is assumed to act in shear only. Figure 5.1 shows the load deformation

characteristics for the infill panel element.

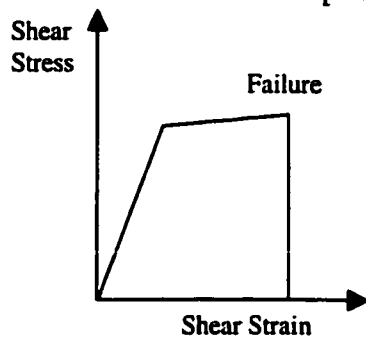


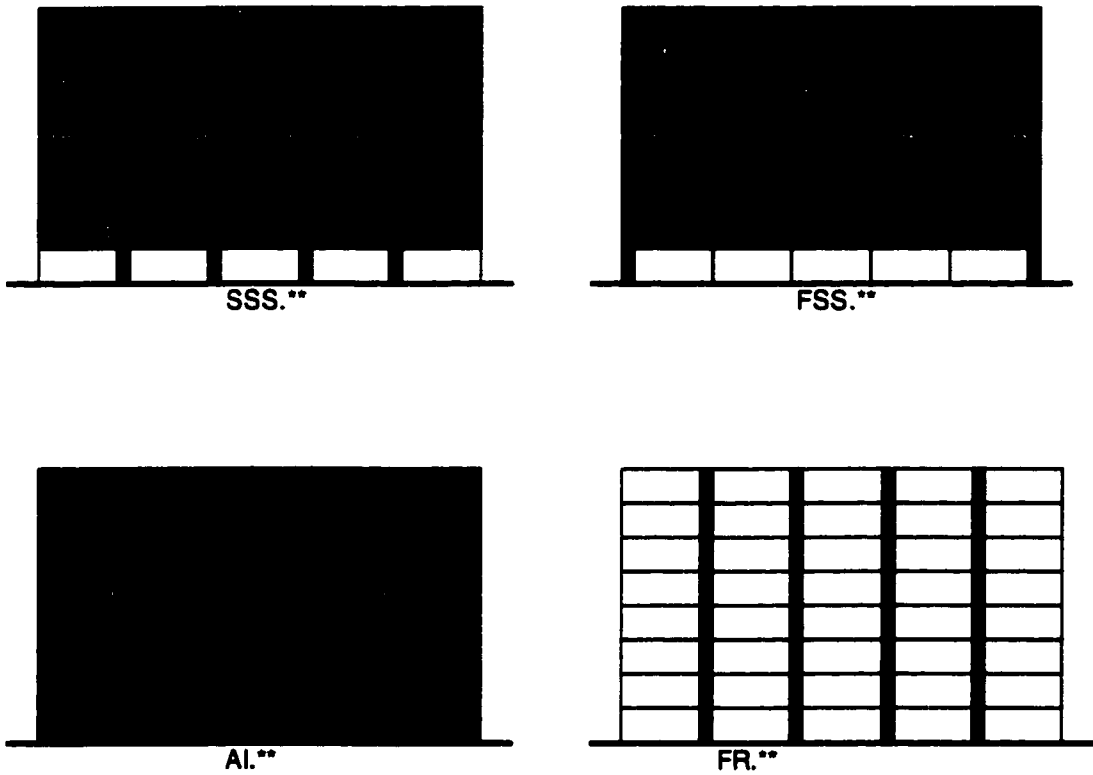
Figure 5.1 Force-Deformation relationship for infill panel element.

Section properties for beams and columns were analyzed using RCCOLA as described in Chapter 4.

The exterior frame in the long direction with no stair-wall (as shown in Fig. 3.12) was used in the analyses. Four elevation configurations were used to model the building as shown in Fig. 5.1. A frame system with no infill is noted FR. A frame building with infill panels from the second story to the roof with the strong axis of the interior columns oriented along the frame direction is noted as a stiff soft story (SSS). A frame building with infill panels from the second story to the roof with the weak axis of the interior columns oriented along the frame direction is noted as a flexible soft story (FSS). And a frame building with infill panels at all levels is noted as AI.

The parameters being investigated include damping ratio, material strength, effective stiffness of structural elements, residual strength of failed elements and variations in geometry of the structure and earthquake ground motions. In Table 5.1,

a list of analyses with the associated parameters investigated is shown.



- SSS stiff soft story
- FSS flexible soft story
- FR frame
- AI all infill
- ** mass of frame as% of total building mass

Figure 5.1 Building models

Run	#2	f_c (ksi)	f_y (ksi)	E_b (E _b)	E_c (E _c)	#7	#8	NFL1ST STO.	NFL 2-8 STO.	End Ecc.	#12	#13	T1(s)	Weight(kN)
1	386	25	60	1	1	005	015	NO	NO	NO	4	2/3	1.349	2920
102	386	25	60	1	1	002	015	NO	NO	NO	4	2/3	1.349	2920
110	386	25	60	1	1	01	015	NO	NO	NO	4	2/3	1.349	2920
2	287	3125	80	1	1	005	015	NO	NO	NO	4	2/3	1.272	2920
3	287	225	80	1	1	005	015	NO	NO	NO	4	2/3	1.382	2920
4	143	225	80	1	1	005	015	NO	NO	NO	4	2/3	1.382	2920
8	386	25	60	1	1	005	015	NO	NO	NO	3	2/3	1.379	2920
9	386	25	60	1	1	005	015	NO	NO	NO	2	2/3	1.417	2920
10	143	225	80	0.5	0.7	005	015	NO	NO	NO	4	2/3	1.882	2920
11	143	225	80	0.35	0.7	005	015	NO	NO	NO	4	2/3	2.113	2920
12	143	225	80	0.5	0.7	005	015	NO	NO	YES	4	2/3	1.606	2920
13	143	225	80	0.5	0.7	005	015	NO	YES	YES	4	2/3	0.947	2920
14	143	225	80	0.5	0.7	005	02	NO	YES	YES	4	2/3	1.093	3990
15	143	225	80	0.5	0.7	005	02	YES	YES	YES	4	2/3	1.061	3990
16	143	225	80	0.5	0.7	005	015	NO	YES	YES	4	1/3	0.947	2920
17	143	225	80	0.5	0.7	005	02	YES	YES	YES	4	1/3	1.061	3990
18	143	225	80	0.5	0.7	005	015	YES	YES	YES	4	2/3	0.91	2920
19	143	225	80	0.5	0.7	005	015	NO	YES	YES	4	2/3	0.939	2920
20	143	225	80	0.5	0.7	005	015	NO	YES	YES	4	2/3	1.094	2920
21	143	225	80	0.5	0.7	005	02	NO	YES	YES	4	2/3	1.062	3990
22	143	225	80	0.5	0.7	005	015	NO	YES	YES	4	2/3	1.346	2920

Table 5.1 Test parameters

RUN	#2	f _c (Ksi)	f _y (Ksi)	E _b (E-sh)	E _c (E-sh)	#7	#8	NFLL 1ST STO.	NFLL 2-8 STO.	End Ecc.	#12	#13	T ₁ (s)	Weight(KN)
23	143	225	80	05	07	005	03	NO	YES	YES	4	2/3	0514	5840
24	143	225	80	05	07	005	03	NO	YES	YES	4	2/3	0774	5840
19	1	—	—	—	—	1		SAME COLUMN DIMENSION AT ALL LEVELS						
20	—	1	1	1	1	—		SAME COLUMN DIMENSION AT ALL LEVELS						
21	—	—	—	—	—	—		SAME COLUMN DIMENSION AT ALL LEVELS						
22	1	1	1	1	1	1		SAME COLUMN DIMENSION AT ALL LEVELS						
23	1	—	—	—	—	1		FIXED BASE WALL, COLUMN SIZE CHANGE OVER HEIGHT						
24	1	—	—	—	—	1		PINNED BASE WALL, COLUMN SIZE CHANGE OVER HEIGHT						

ELCENTRO-12M1T - NORTH BRIDGE SCALED TO 0.445G SAME MODEL AS 13

#2 = Steel Ductility = ϵ_l/ϵ_y (see Fig. 5.6)

#7 = Viscous Damping Ratio = ξ

#8 = Mass of Frame/ Total Building Mass

#12 = Aspect ratio of column = C_1/C_2 (see Fig. 3.4)

#13 = Residual Strength = V_{res}/V_{max} (see Fig. 4.13)

Table 5.1 (continued)

The building models were subjected to the horizontal ground motions (0.223g peak acceleration) from the 1998 Ceyhan earthquake in Turkey (see Figs. 5.41, 5.43 and 5.44). The amplitude of ground motions was magnified by a factor of two in order to produce failures that demonstrate effects of the parameters under consideration.

5.2.1 Damping Coefficients

5.2.1.1 Conditions

The use of approximate “equivalent viscous damping ratio” has little theoretical or experimental justification²³. However, viscous damping ratios are still used to approximate material damping, joint friction, and radiation damping. Depending on the level of deformation and strain induced in the structure, viscous damping ratio values varying from 2% to 10% have been recommended⁴⁶. High viscous damping ratio values are intended to compensate for the inability of including the hysteretic energy dissipation in elastic analyses^{42, 56}.

For structure FR, three different damping ratios were considered 2, 5 and 10%. The effective stiffnesses were based on gross concrete sections. Design material strengths were used, 2.5 ksi for the concrete and 60 ksi for the reinforcing steel. The column aspect ratio was 4. The effect of end eccentricities (rigid beam-column connection) was neglected and the residual shear strength was assumed to be equal to 2/3 of the maximum strength, even though no shear failure in columns was observed.

The weight of the frame was 2920 KN and the height of the building was 25.6 meters.

5.2.1.2 Results

Figures 5.2 and 5.3 show respectively the time history of roof displacement and base shear for D02, D05 and D10 (from Runs 102,1,and 10, Table 5.1).

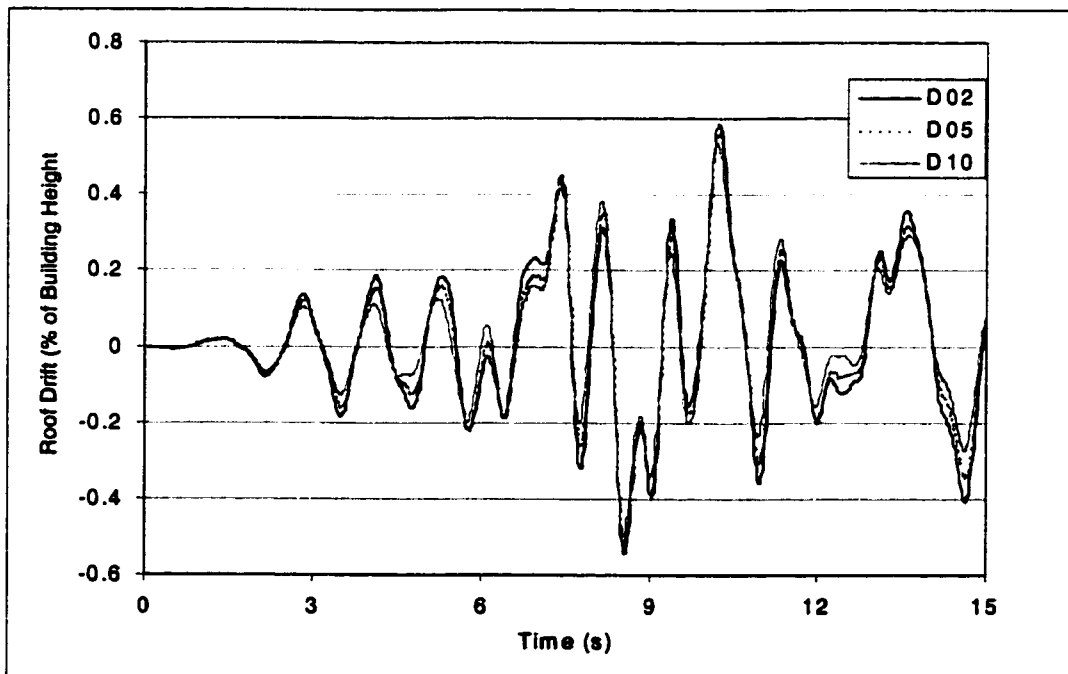


Figure 5.2 Time history of roof drift - different viscous damping ratios.

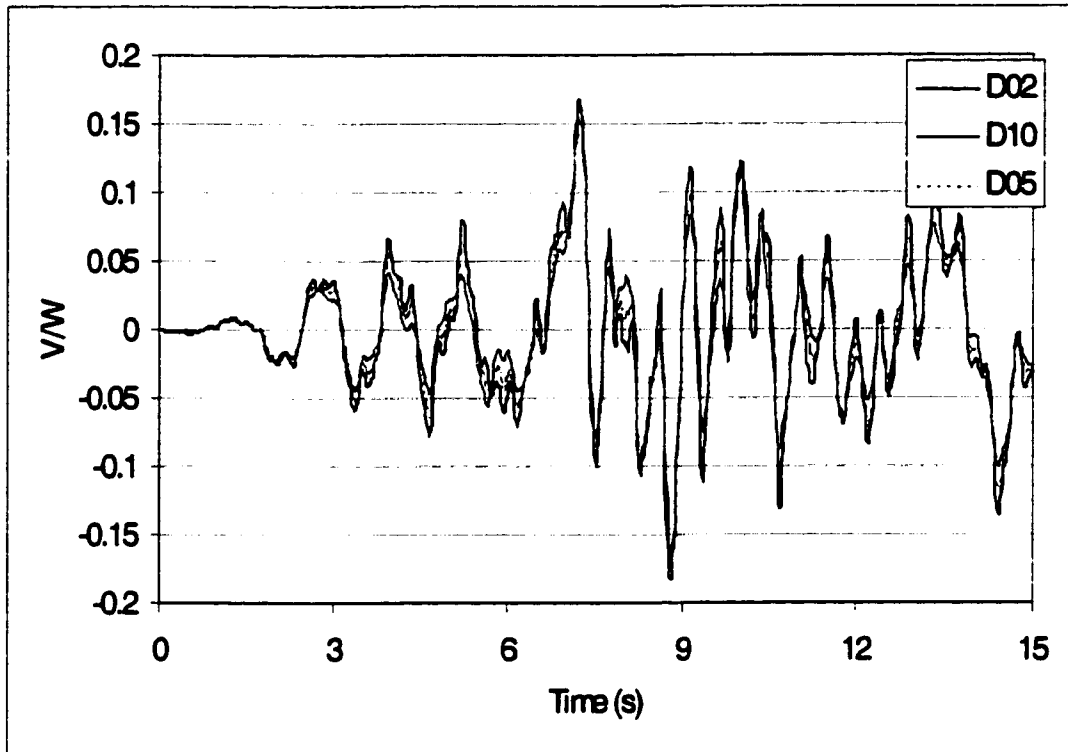


Figure 5.3 Time history of base shear - different viscous damping ratios.

From Figs. 5.2 and 5.3, it can be seen that damping coefficients had no influence on the structural period. As expected, the shape of roof displacement and base shear did not change with the damping ratio since no shear or flexural failure was recorded. Low damping resulted in slightly larger displacements and base shears. Slightly more damage could be expected as damping is reduced. Previous studies^{14,15} have concluded that a 5% damping could be used as an average value for viscous damping for reinforced concrete structures.

5.2.2 Strength of Materials

5.2.2.1 Conditions

Strength of concrete in structures may vary from design values⁵⁷. Concrete gains strength as it ages, thus in most cases, actual concrete strength in a building is higher than the design values. However, in case of poor quality control, particularly in case of high water-cement ratio during construction for workability reasons, concrete strength might be significantly lower than design values.

The actual steel yield strength is usually higher than the specified nominal yield strength. If the reinforcing bar can undergo large deformations, steel strength can reach values 50% higher than the yield strength due to strain hardening. Reinforcing bars in beams can undergo large deformations when plastic hinges occur in beams.

In addition, concrete and steel exhibit increases in strength when loaded at increased strain rates. Higher rates of loading may increase the strength of concrete obtained from standard cylinder tests by as much as 15-20%^{58,59,60}. The rate of loading in a structure subjected to seismic action may differ between members depending on their location in the structure. The rate of loading depends on the period of the structure and the ground motion characteristics. Concrete exhibits an increase in stiffness as well when loaded at high strain rates⁵⁹ since the modulus of elasticity of concrete is a function of concrete strength.

Therefore, the use of 0.9, 1.0 and 1.25 times the specified concrete

strength in evaluating the behavior of a structure can be justified. The amount of strain hardening in steel during an earthquake is difficult to predict, but a value of $4/3$ the nominal yield strength represents a realistic increase reflecting reinforcing bar production and quality control procedures.

5.2.2.2 Results

The standard FR building was analyzed using three different combinations of material strength. Concrete strength was assumed to be 1.0, 1.25 and 0.9 times the nominal design value. Steel was taken as 1.0 and 1.33 times the nominal design value. The following combinations were used considering nominal concrete strength of 2500 psi and steel yield of 60 ksi. C2.5S60 is intended to represent structure FR with the nominal design strengths of 2.5 ksi for concrete and 60 ksi for the reinforcing steel bars (Run 1). C3.125S80 is intended to represent over-strength in concrete and steel (Run 2) and C2.25S80 is intended to represent over-strength in steel and strength deficiency in concrete (Run 3). Figures 5.4 and 5.5 show the time history of roof and the time history of base shear.

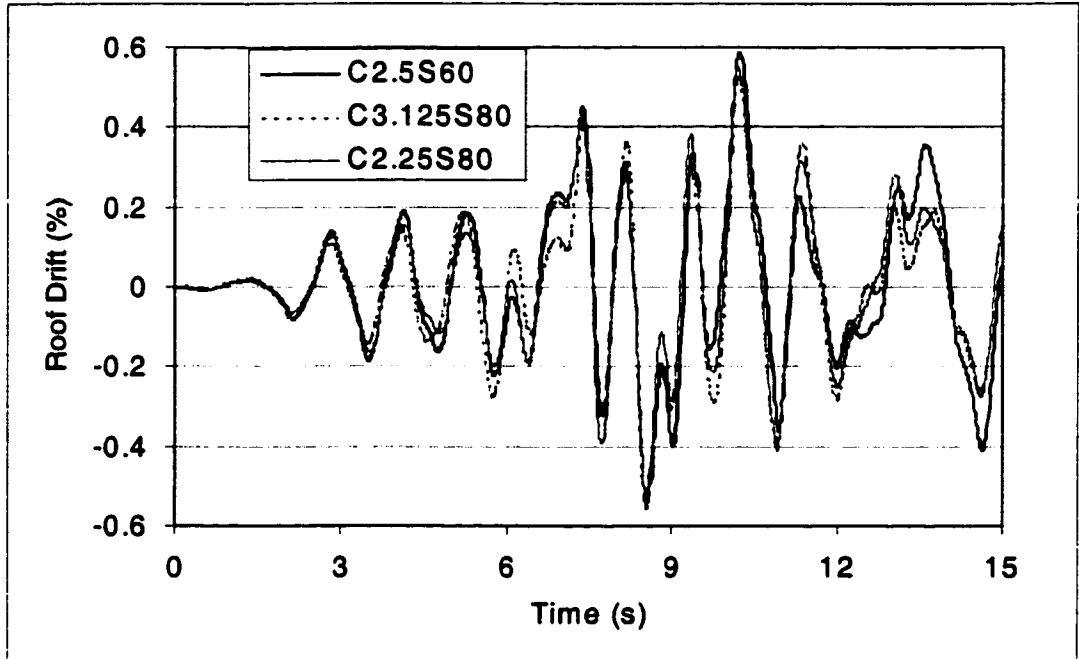


Figure 5.4 Time history of roof drift - different material strengths.

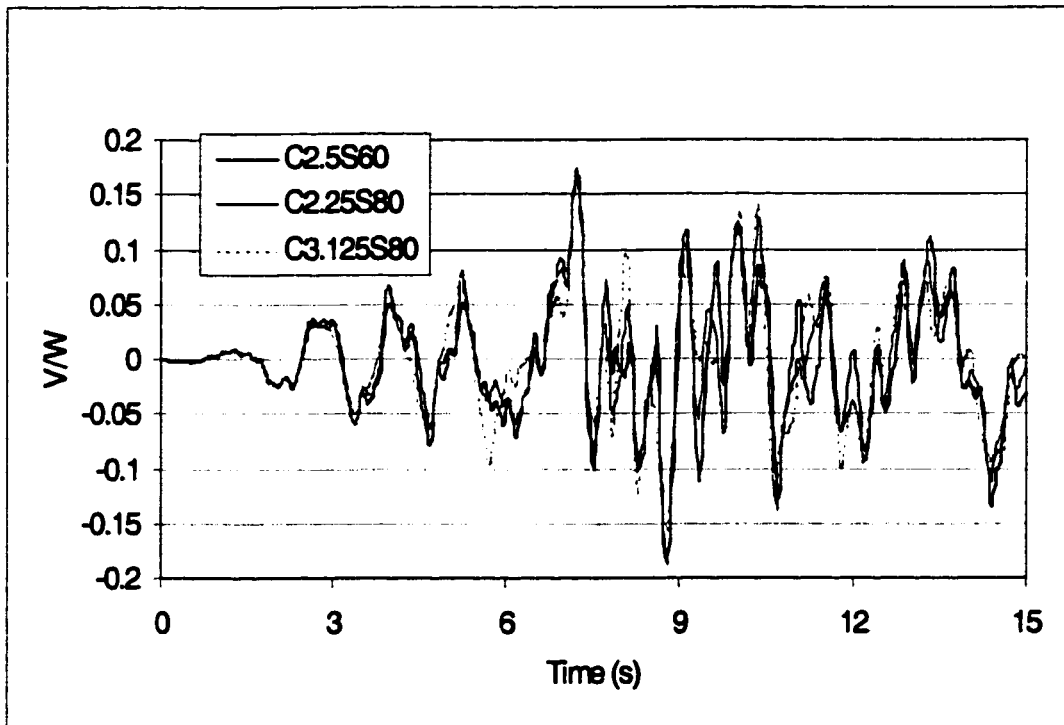


Figure 5.5 Time history of base shear - for different material strengths.

The results shown in Figs. 5.4 and 5.5 demonstrate that strength of material had little influence on the period of the structure or the peak roof displacement and peak base shear. Although higher concrete strength was expected to result in shorter periods, the difference is too slight to be observed. With higher material strengths, plastic rotations in beams were smaller.

5.2.2.3 Steel Ductility

In defining the material properties in RCCOLA for the calculation of the section characteristics, the stress strain relationship for the reinforcing steel was described in section 4.3.1.3.1 and Fig. 5.6. Since some steel sources in the

Middle East, and in Lebanon in particular, provide low ductility reinforcing bars, the effect of the steel ductility on the general behavior was investigated. The standard model was considered with two combinations of critical strains (ϵ_1 ; ϵ_M) namely (0.008; 0.08) and (0.004; 0.04) (Runs 3 and 4) for the same F_Y of 80 ksi (Fig. 5.6). The results showed no influence of the steel ductility on the period of the structure, peak roof displacement or the peak base shear. Also the results showed no significant failures or inelastic strains. Since both models exhibit the same moment curvature relationship in the elastic range until yield is reached, and the structural elements remained mostly in the elastic range under the ground motions used in the analysis, difference in steel deformation range did not have an effect on response. A peak ground motion of 0.445 g was used in the analysis. Higher values are unlikely to occur in the Mediterranean region⁶³. However, in case larger peak ground are experienced, higher steel ductility should provide better performance by allowing larger plastic deformations.

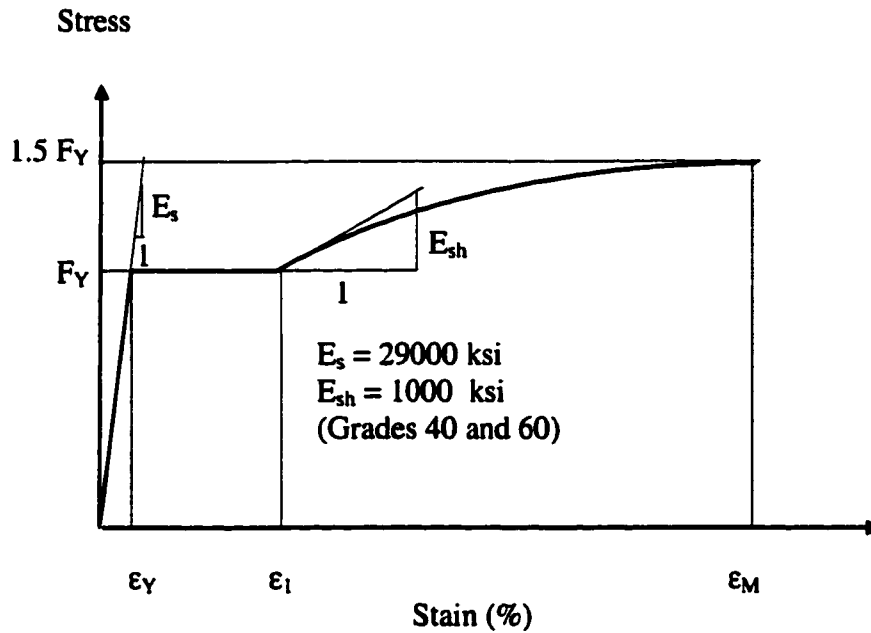


Figure 5.6 Stress-Strain Relationship for Reinforcing Steel

5.2.3 Effective Stiffness

5.2.3.1 Conditions

The contribution of the slab to the beam stiffness was ignored because the slab deck is very thin (about 2.5 inches) and lightly reinforced to resist only temperature variations and shrinkage and the ribs (joists) were normal to the plane of the frame. The slab contribution to the stiffness and strength of the building will be discussed further in Chapter 7.

An average stiffness of a member after it cracks generally is designated as the effective stiffness of a member. Ideally, analysis should be carried out using the stiffness of the gross section as an initial value and modified as the structure undergoes cracking. However, in the absence of a reliable tool to handle degrading stiffness “accurately”, approximate values are used to determine or represent the effective stiffness of reinforced concrete members. An approximate value of the effective stiffness of a concrete member, $E_c I_e$, is given by equation 5.1.

$$I_e = \left(\frac{M_{cr}}{M_a} \right)^3 I_g + \left[1 - \left(\frac{M_{cr}}{M_a} \right)^3 \right] I_{cr} \quad (5.1)$$

where,

E_c is the modulus of elasticity of concrete

I_e is the effective moment of inertia of the member

I_g is the moment of inertia of gross concrete section about centroidal axis, neglecting reinforcement

I_{cr} is the moment of inertia of cracked section transformed to concrete

M_{cr} is the cracking moment

M_a is maximum moment in member

Alternatively, the ACI code⁹ permits the use of $0.35E_c I_g$ as an effective stiffness for beams and $0.7E_c I_g$ for columns. In FEMA 273¹, it is suggested that the effective stiffness be taken as $0.5E_c I_g$ for beams and $0.7E_c I_g$ for columns. The effect of effective stiffness was investigated using three models noted 100/100 (I_g for

beams and columns), 35/70 (ACI), and 50/70 (FEMA) where the values represent the percentage of I_g for beams and columns respectively (Runs 4, 10 and 11).

5.2.3.2 Results

The effective stiffness was found to affect the response of the structure significantly as shown in Figs. 5.7 and 5.8. The lower the effective stiffness the longer the period of the structure. Peak roof displacements were higher using low effective stiffnesses. Using the Ceyhan earthquake record, the peak base shear for the stiffer model was lower than for the more flexible model. Li¹⁴ has found that the same trend was obtained using other earthquake motions. In the present case, the acceleration spectra for the fundamental periods in 35/70, 50/70 and 100/100 were very similar (1100, 1045 and 990 mm/s² respectively). However, for the second mode, acceleration spectra for 35/70, 50/70 and 100/100 were 8920, 6540 and 5240 mm/s² respectively. Therefore, the higher base shear for the least stiff structure can be attributed to second mode contributions.

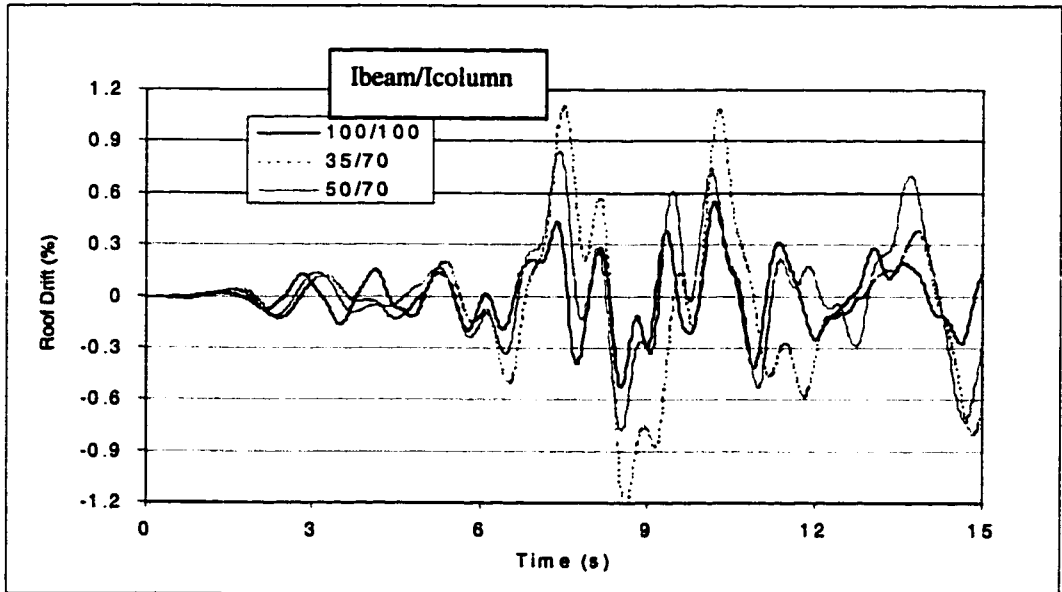


Figure 5.7 Time history of roof drift - different effective stiffness values.

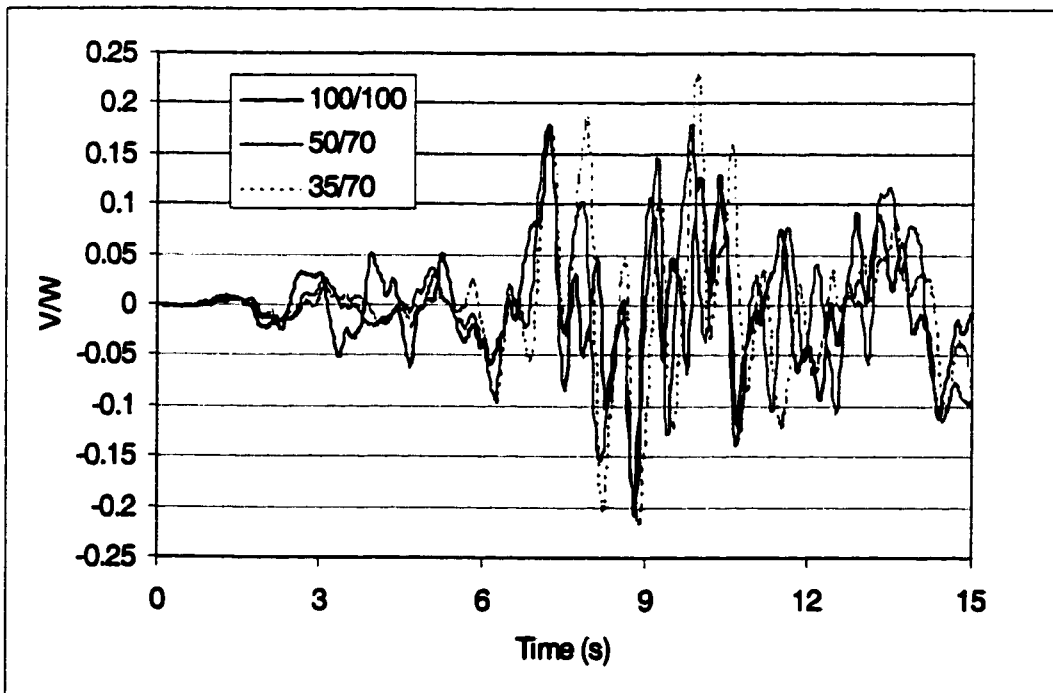


Figure 5.8 Time history of base shear - different effective stiffness values.

5.2.4 Frame Geometry

The geometric variations investigated include, geometric aspects (column depth to width ratio), the effect of rigid connections and different elements layout.

5.2.4.1 Column Dimensions

In Lebanese practice, columns are designed for gravity loads only. Thus, the total concrete area and amount of reinforcement is determined from gravity loads. In order to obtain functional space, the widths of columns often are designed to merge with partition walls. However, when such constraint is waived, the depth to width ratio of a column cross section may vary between 1 and 5, but practically varies between 2.5 and 5. For the comparisons discussed here, the area of a column section was maintained constant while the width and depth were varied to produce three different aspect ratios (column depth to width) of 2, 3 and 4 (Runs 4, 8 and 9). The column layout was the same for the three structures (FR Fig.5.1). For the same cross sectional area, elements with larger aspect ratios are stiffer in their long directions and much more flexible in the shorter direction than elements with smaller aspect ratios. The column aspect ratio had little influence on the period of the structure (Table 5.1) and on the roof displacements (as shown in Fig.5.9). Figure 5.10 shows that the base shear for the smaller column aspect ratio is slightly lower than the base shear for the larger aspect ratio. When the column ratio was large, the stiffness

along the column depth direction is larger than for smaller aspect ratio. Since stiffer columns attract more shear than flexible ones, the base shear for the stiffer structure was larger than for the more flexible structure.

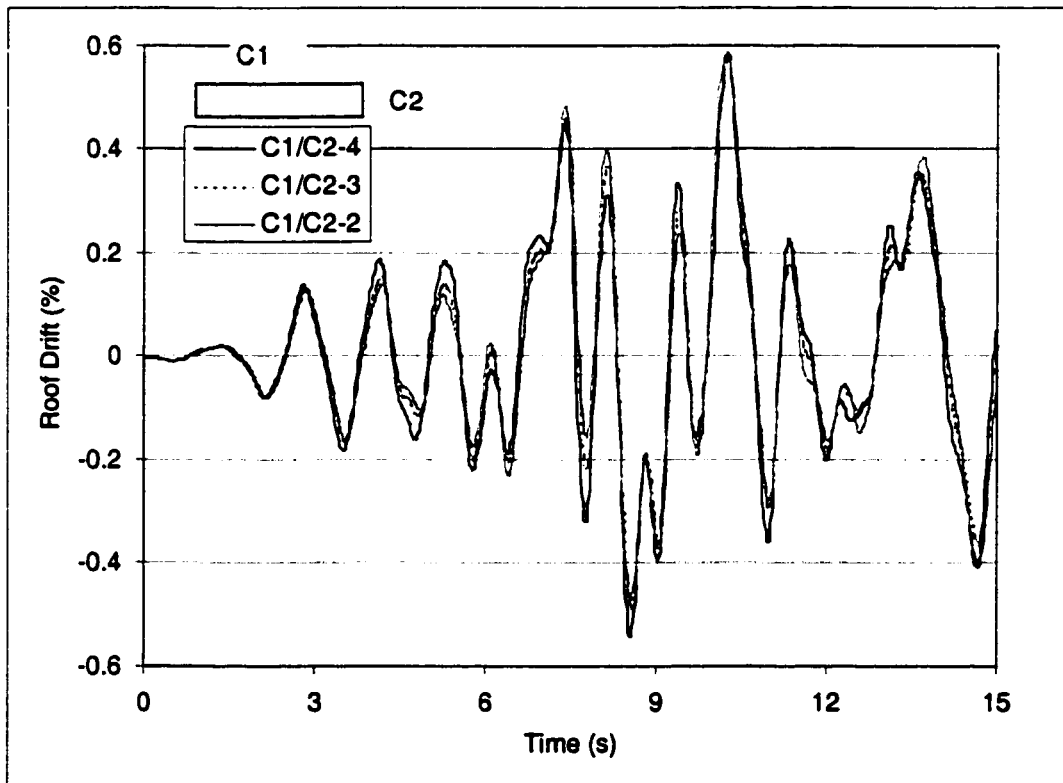


Figure 5.9 Time history of roof drift - different column aspect ratios.

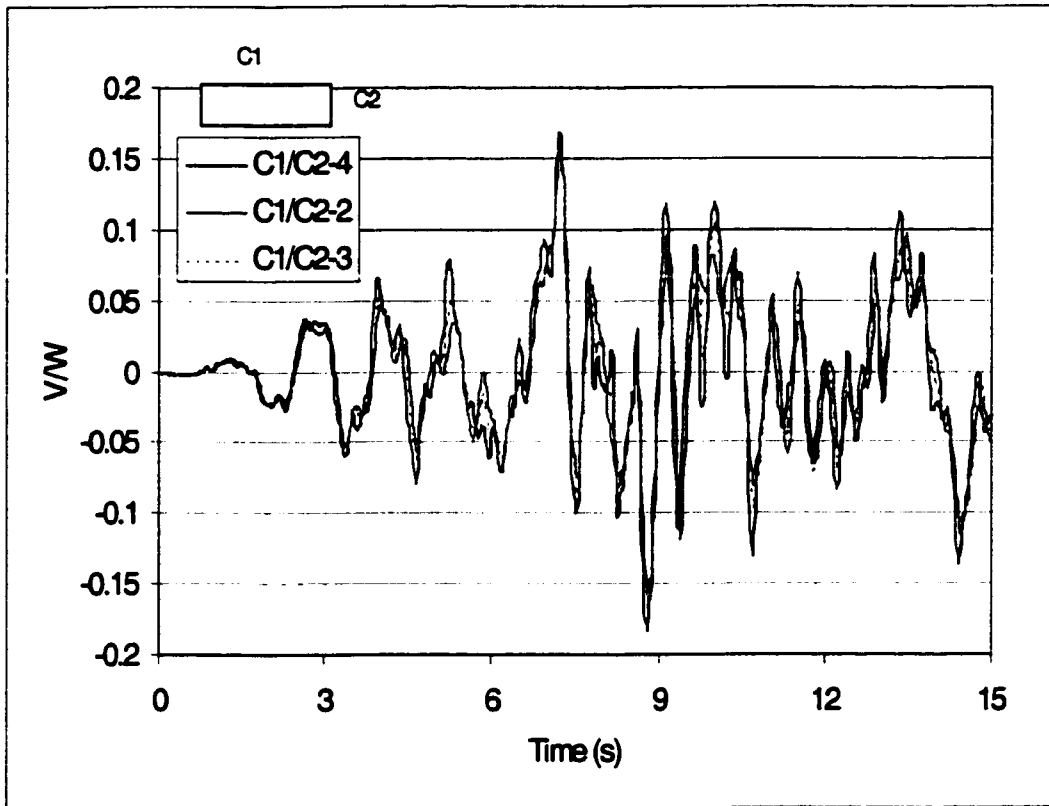


Figure 5.10 Time history of base shear - different column aspect ratios.

5.2.4.2 Connection Rigidity (End Eccentricity)

Plastic hinges in frames and in coupled frame-shear wall structures are expected to form near the faces of the connection rather than at the theoretical joint centerline. This effect can be approximated by considering rigid connections between the nodes and the element ends. The structure consequently is expected to be stiffer because element lengths are reduced to the clear distance between elements. The period of the structure was larger when end eccentricities were

ignored (Runs 10 and 12) (Table 5.1). Figure 5.11 shows peak roof displacement was 25% larger when end eccentricities were not considered.

In Fig. 5.12, peak base shears were similar, but there were noticeable differences at some points in the time history.

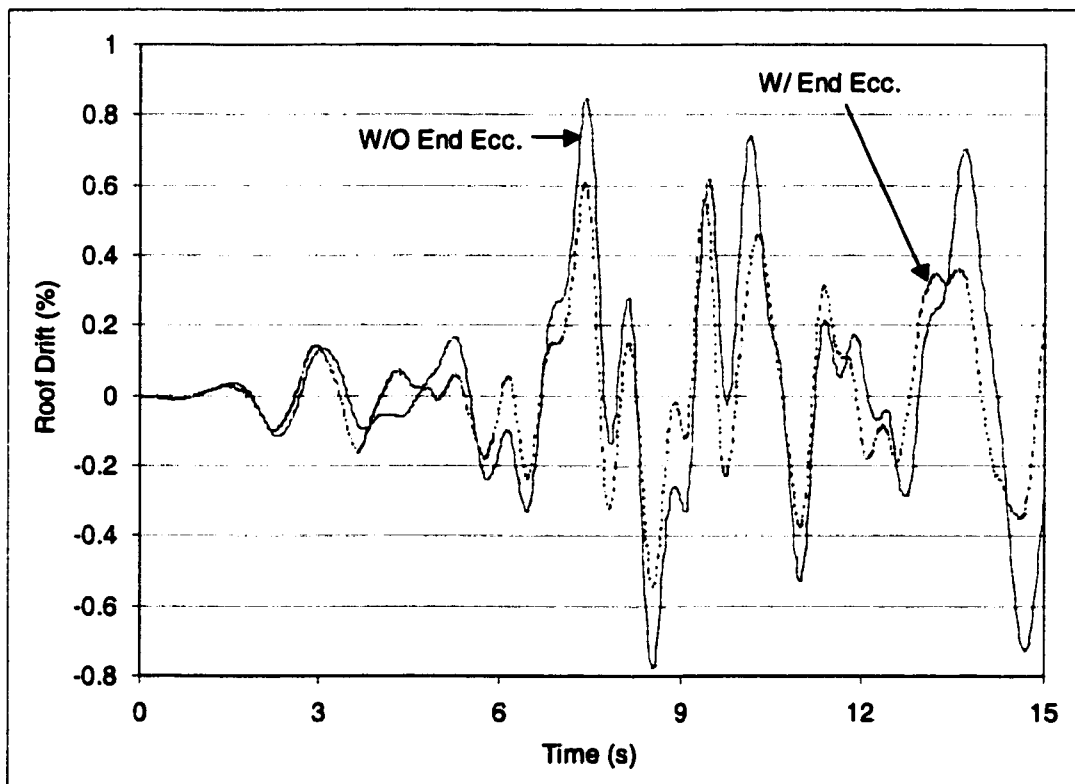


Figure 5.11 Time history of roof drift - with and without end eccentricities.

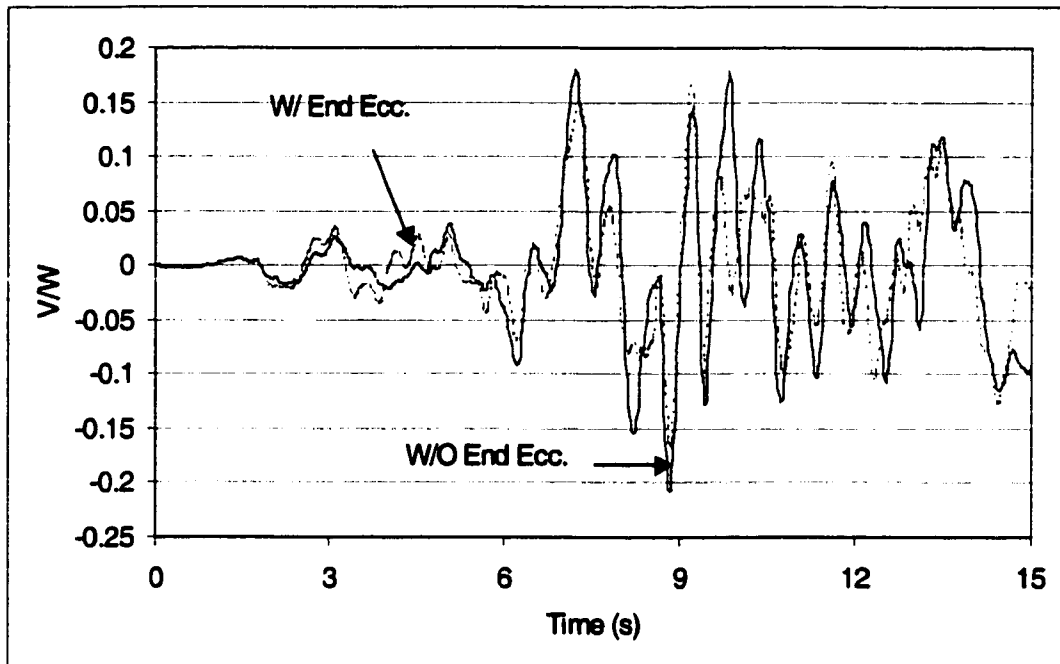


Figure 5.12 Time history of base - with and without end eccentricities.

5.2.4.3 Variation in Column Dimensions over Height of Structure

The response with column dimensions the same at all levels (UNIFORM) was compared with that using smaller size columns from level 5 to the roof (TAPERED) (Runs 13 and 19).

For economy, column dimensions may be reduced on upper floors in a structure because gravity load is smaller and reinforcement ratio on lower floors may be close to minimum code requirements. However, by reducing the size of columns on upper floors, a weak story can be created. Two structures described as soft first story structures with infill walls on the second floor to the roof were analyzed and the results were compared in Figs. 5.13 through 5.16.

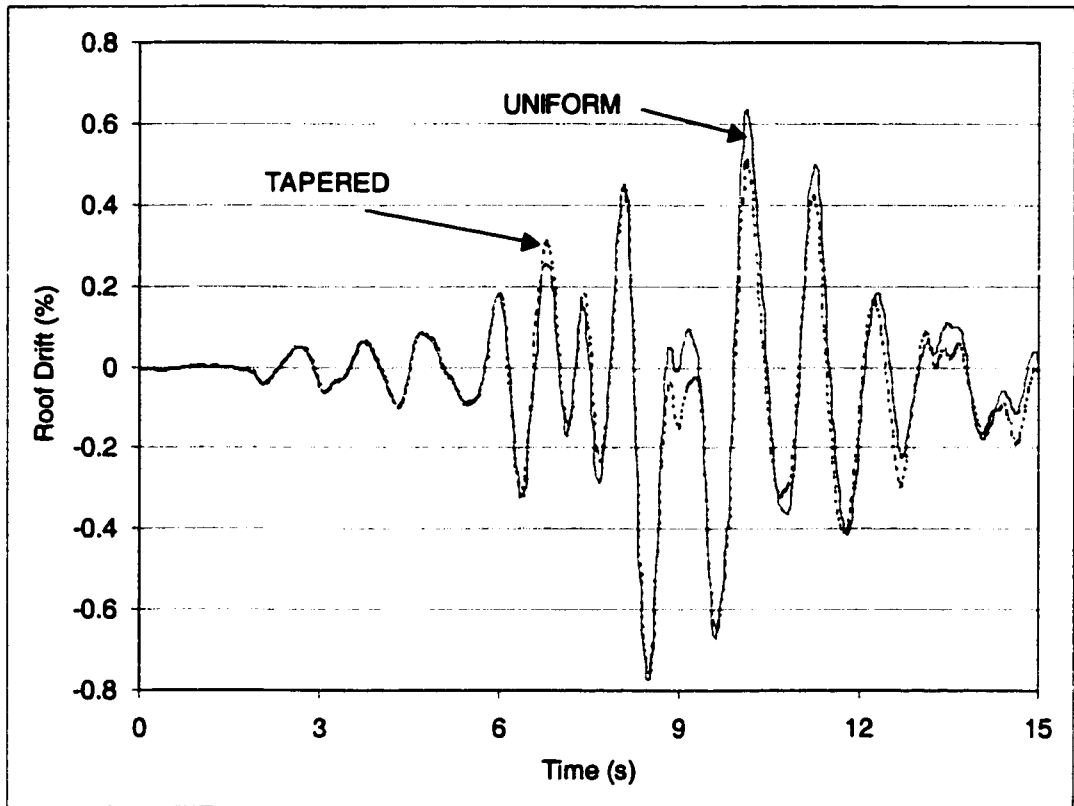


Figure 5.13 Time history of roof drift – uniform and changing column size over height of structure.

As shown in Fig. 5.13, the roof drift for both structures is almost identical. When the shear in a column reached the shear capacity, the column capacity dropped to the residual value and the column was considered as failed in shear. The columns on the 5th story of the TAPERED structure failed in shear at 6 seconds. At 6.35 seconds, the columns at the 4th story of the UNIFORM structure yielded at ground level, leading to slightly higher drifts in the UNIFORM structure than in the TAPERED. After shear failure of the 4 interior columns of the 5th story in the TAPERED structure (beyond 6.35 seconds), the peak base shears in the

UNIFORM structure were slightly larger than for the softened TAPERED structure (Fig 5.14).

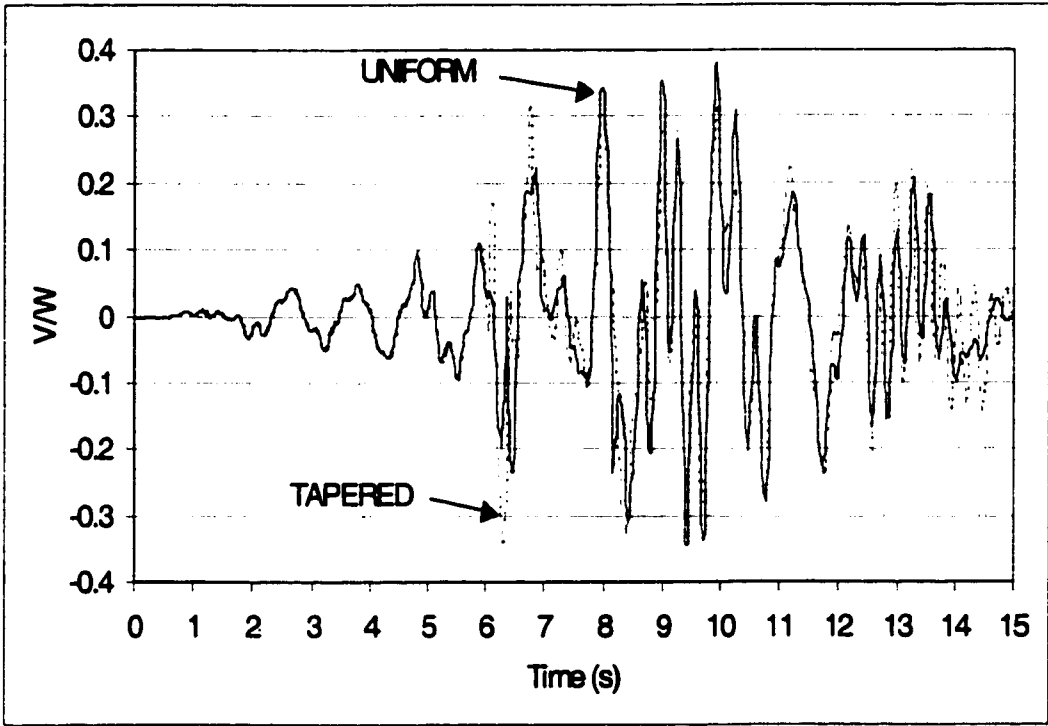


Figure 5.14 Time history of base shear – uniform and changing column size over height of structure.

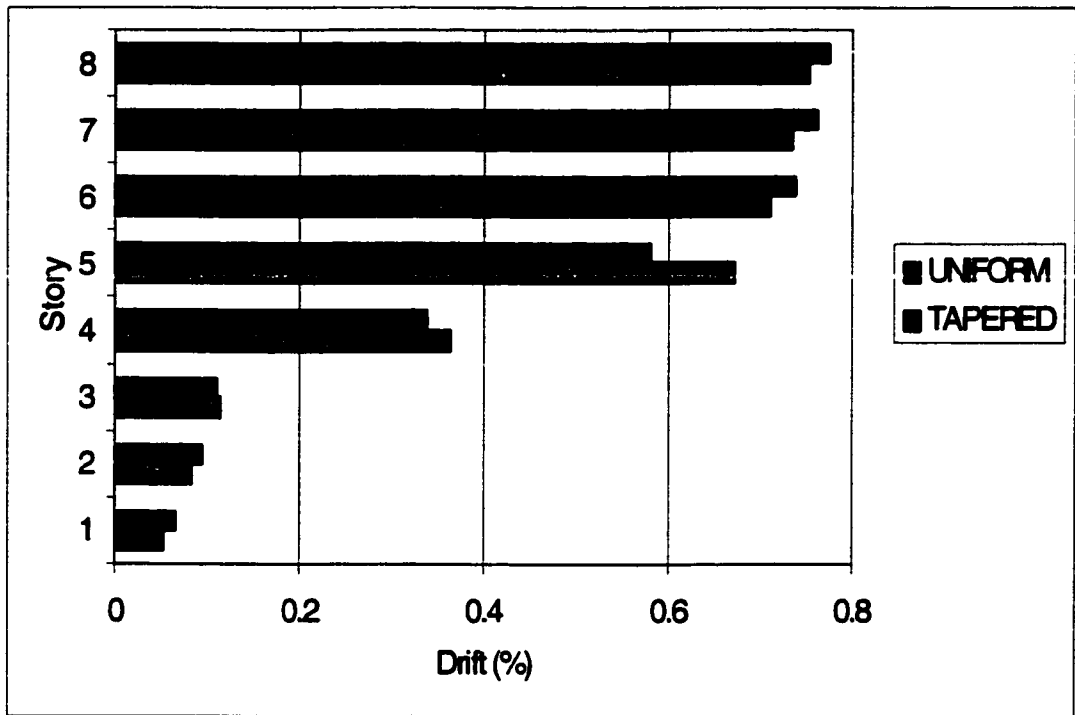


Figure 5.15 Maximum story drift – change in column size over height of structure

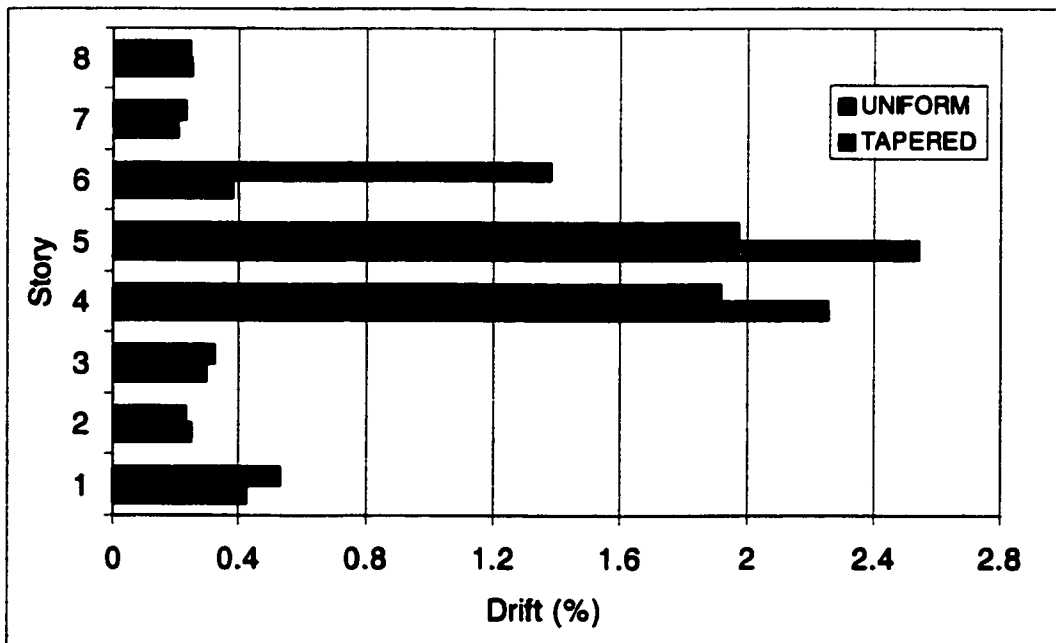


Figure 5.16 Maximum interstory drift – change in column size over height of structure

The infill panels reach failure (cease carrying lateral forces) when an interstory drift of 0.4% is reached (FEMA 273). From Fig. 5.16, it can be seen that infill panels failed on the 4th and 5th story for the TAPERED structure and on the 4th, 5th and 6th story for the UNIFORM structure, thereby softening those stories. The fact that interstory drifts reach higher values on middle stories rather than at the bottom is an indication of higher mode effects. The high interstory drift on the first floor is expected from the soft story effect. The shear failure of columns on the 5th story in the TAPERED structure can be attributed to the change in column shear capacity at the 5th floor level (weak story effect).

5.2.4.4 Column Layout

The orientation of columns is based on architectural requirements rather than structural. In the present study a comparison between regular and irregular column layout is made to emphasize the importance of column orientation. Two structures had identical characteristics except for the orientation of the interior four columns in a frame (Runs 19 and 20). Both frames had infill panels on the 2nd floor to the roof. In FSS (_III_), the strong axis of the interior 4 columns was perpendicular to the plane of the frame and in SSS (I____I), the strong axis of the interior 4 columns was in the plane of the frame, as shown in Fig 5.1. In the plane of the frame, SSS was stiffer than FSS and had larger strength capacity.

As shown in Fig 5.17, peak roof displacements were larger for SSS than

for FSS. Damage is expected to occur in SSS. It can be observed from Fig. 5.18 that the stiffer structure, SSS, attracts considerably higher base shear than FSS.

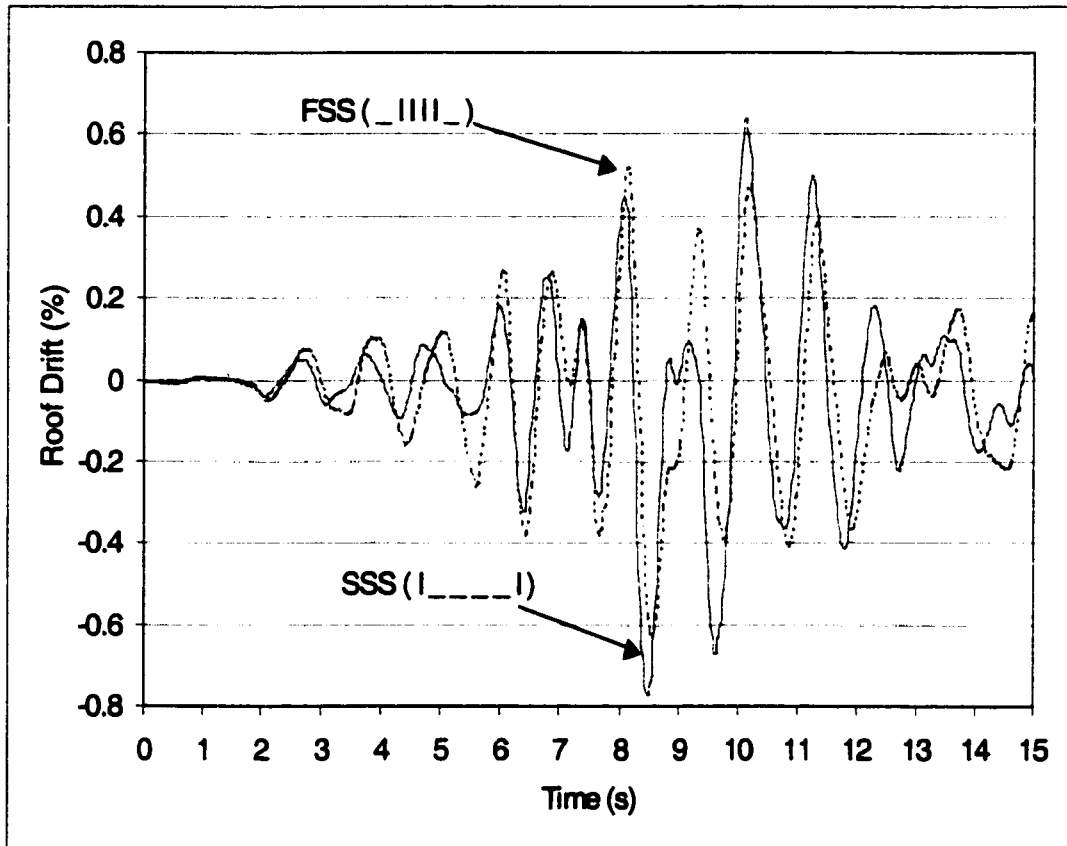


Figure 5.17 Time history of roof drift - different column orientation.

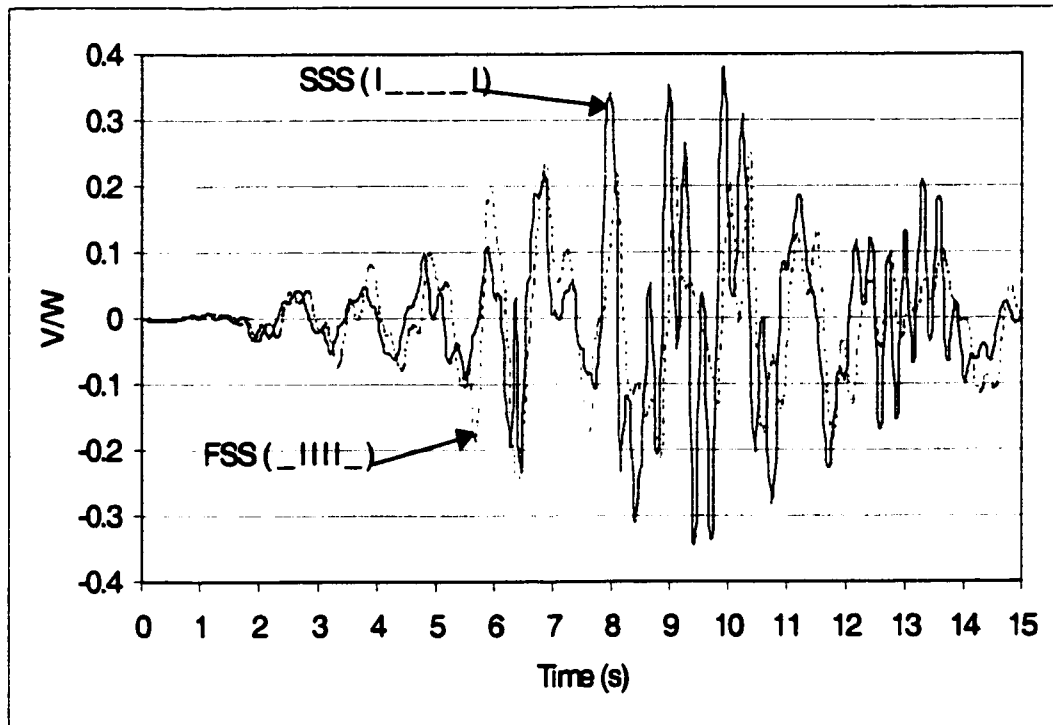


Figure 5.18 Time history of base - different column orientation.

From the results shown in Fig.5.20, failure of the infill panels is expected at the 4th, 5th and 6th stories in SSS, and at the 4th and 5th stories in FSS. The higher story drift on the upper levels in SSS as compared to FSS could be due to the failure of infill panels at the 6th story in SSS. No shear failure was observed in either structure although exterior columns on the 1st and on the 5th story in FSS experienced flexural hinging at both ends. No shear failure was observed because the capacity of the exterior columns is controlled by flexure. A larger first story drift was observed in FSS, which could be expected since the 1st story in FSS was more flexible than the 1st story in SSS.

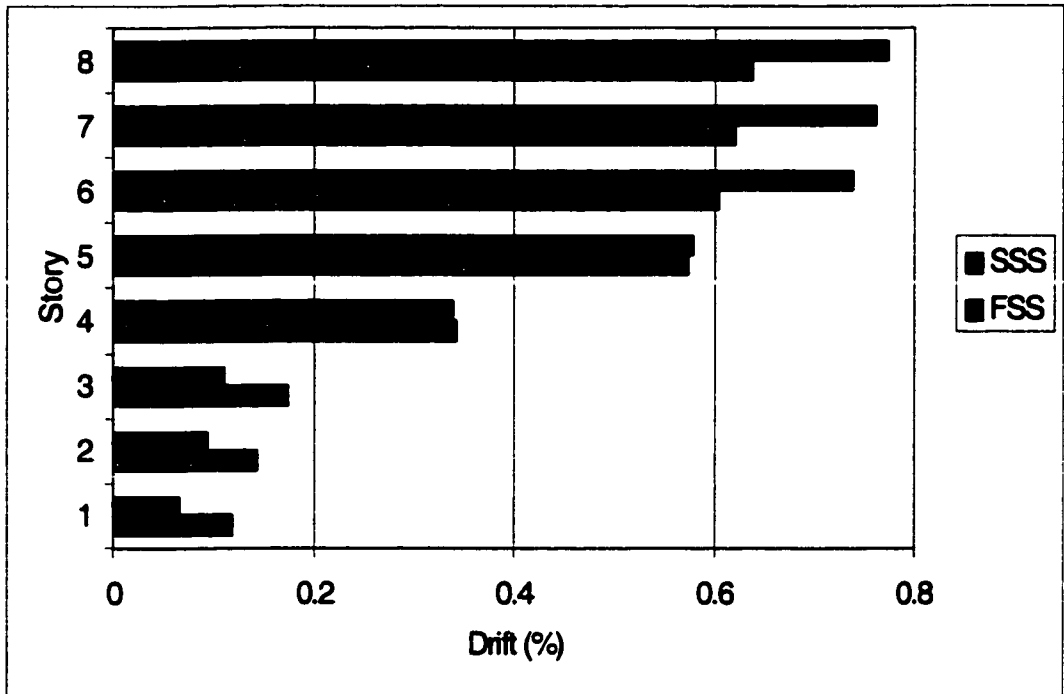


Figure 5.19 Maximum story drift - with different column orientation.

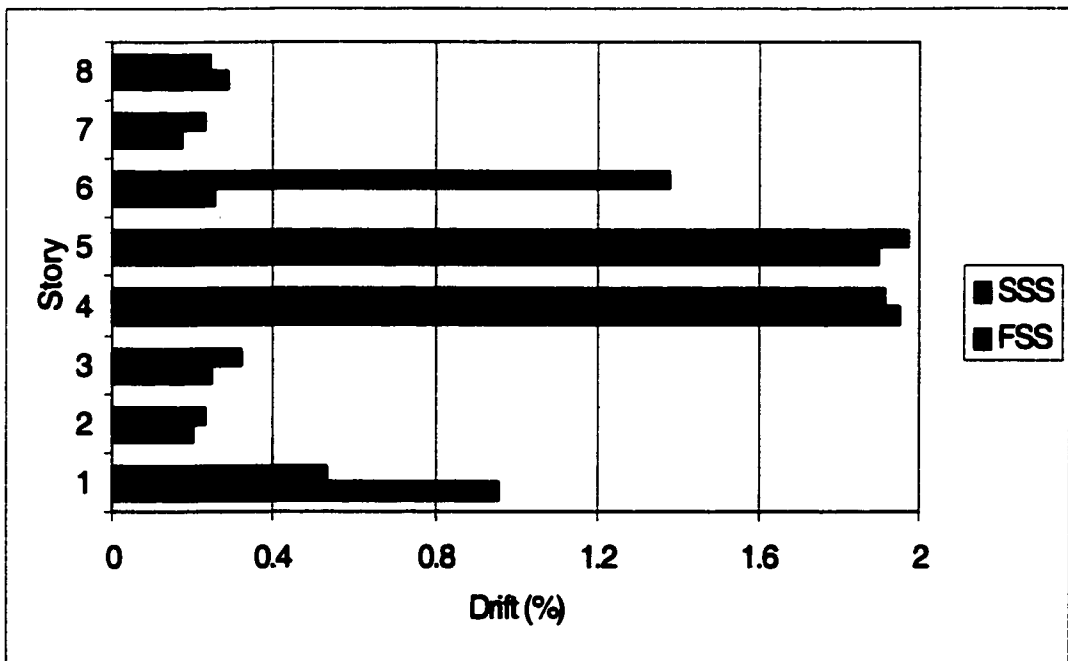


Figure 5.20 Maximum interstory drift - with different column orientation.

5.2.5 Mass Distribution

5.2.5.1 General

The distribution of mass to the frame being analyzed was based on a constant mass to stiffness ratio determined from an elastic dynamic analysis using $0.5E_cI_g$ for beams and $0.7E_cI_g$ for columns (E_c is the modulus of elasticity for the concrete and I_g is the moment of inertia of the gross section). Hence, the fraction of total building mass assigned to each frame was proportional to the base shear resisted by the corresponding frame. The same mass was assigned to all floors except a smaller mass was assigned to the roof. In a real system, the distribution of mass among various lateral-load resisting elements would be changing with time as the stiffness of various elements change during an earthquake. For simplicity, such changes were not included in the analyses conducted herein.

Two structures were analyzed and results were compared. Structures AI and SSS (Fig 5.1) with infill panels were assigned 15 or 20% of total building mass (Runs 13, 14, 15 and 18).

5.2.5.2 Analysis Results

Maximum story drifts, maximum interstory drifts and time-history of base shear to weight ratio were calculated for all models and are shown in Figs. 5.21 through 5.26.

Figures 5.21 and 5.22 show that models with lower assigned mass had

slightly higher base shear to weight ratios. Table 5.1 shows that the fundamental periods of structures AI and SSS were shorter when they were assigned less mass. Therefore, the peak response to the selected earthquake motion was higher.

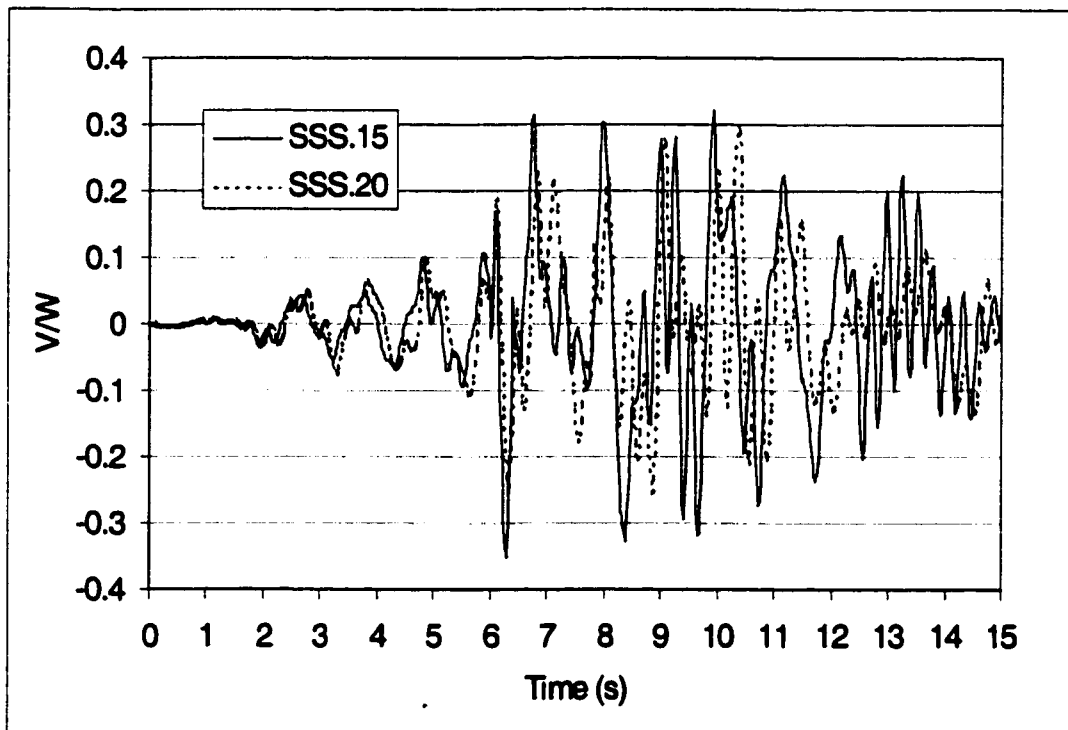


Figure 5.21 Time history of base shear for SSS structure with different assigned masses.

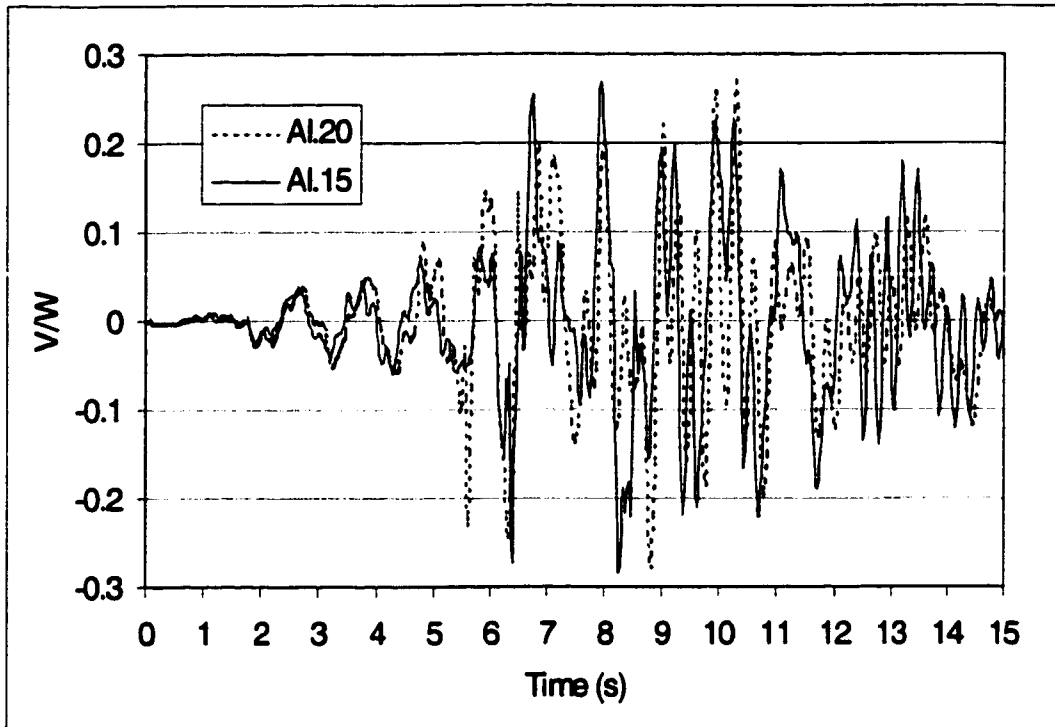


Figure 5.22 Time history of base shear for AI structure with different assigned masses.

Infill panels failed at interstory drifts in excess of 0.4%. Figures 5.23 and 5.24 show that the panels failed at the 4th, 5th and 6th stories in SSS.20, AI.15 and AI.20 and at the 4th and 5th stories in SSS.15.

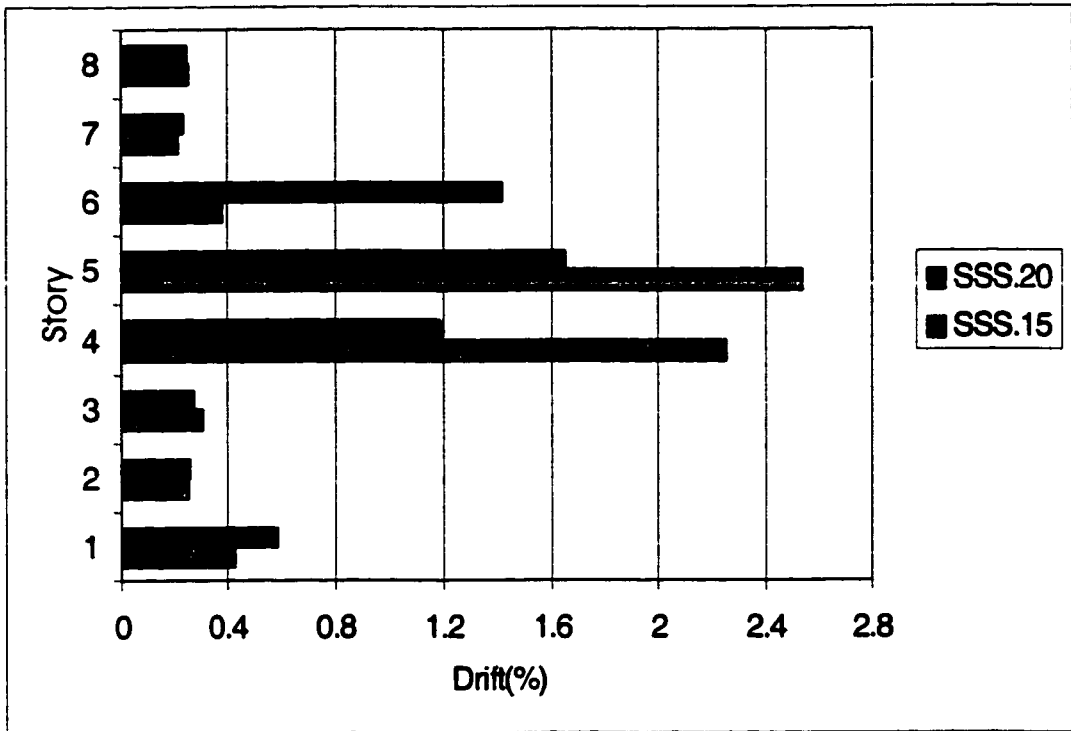


Figure 5.23 Maximum interstory drift for SSS structure with different assigned masses.

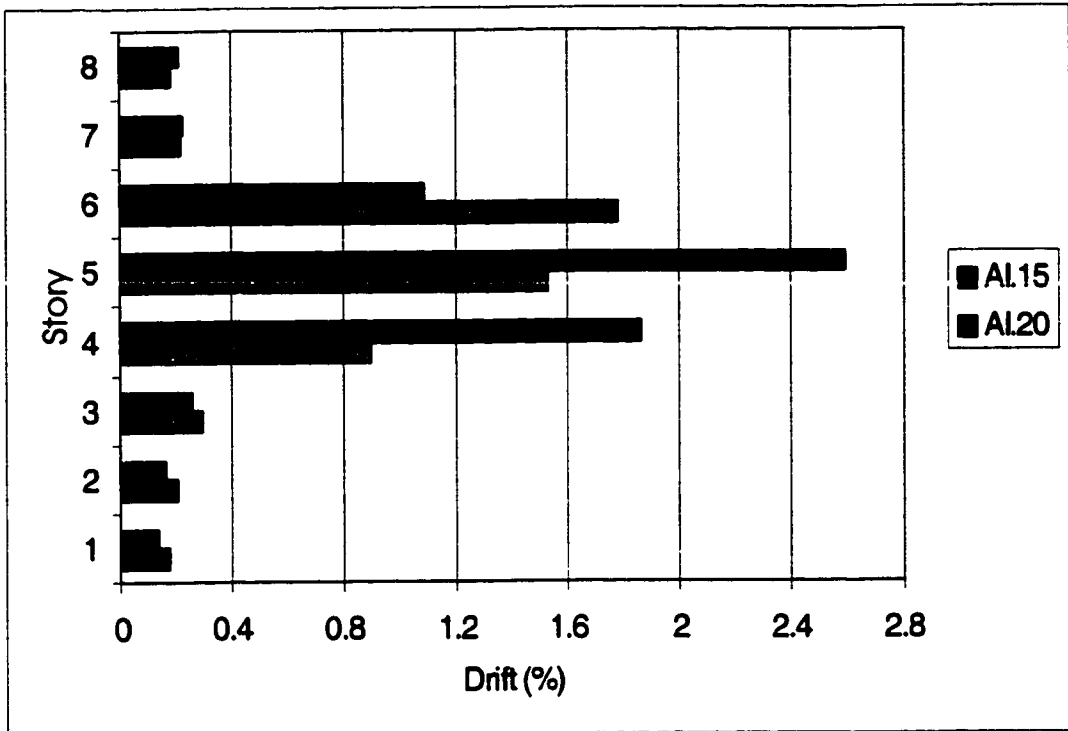


Figure 5.24 Maximum interstory drift for AI structure with different assigned masses.

After infill panels failed on the 4th story in all structures, the 4th story became soft with respect to the 3rd story. There was a significant increase in maximum story drift from the 3rd story to the 4th story in SSS.15, SSS.20, AI.15 and AI.20 as shown in Figs. 5.25 and 5.26.

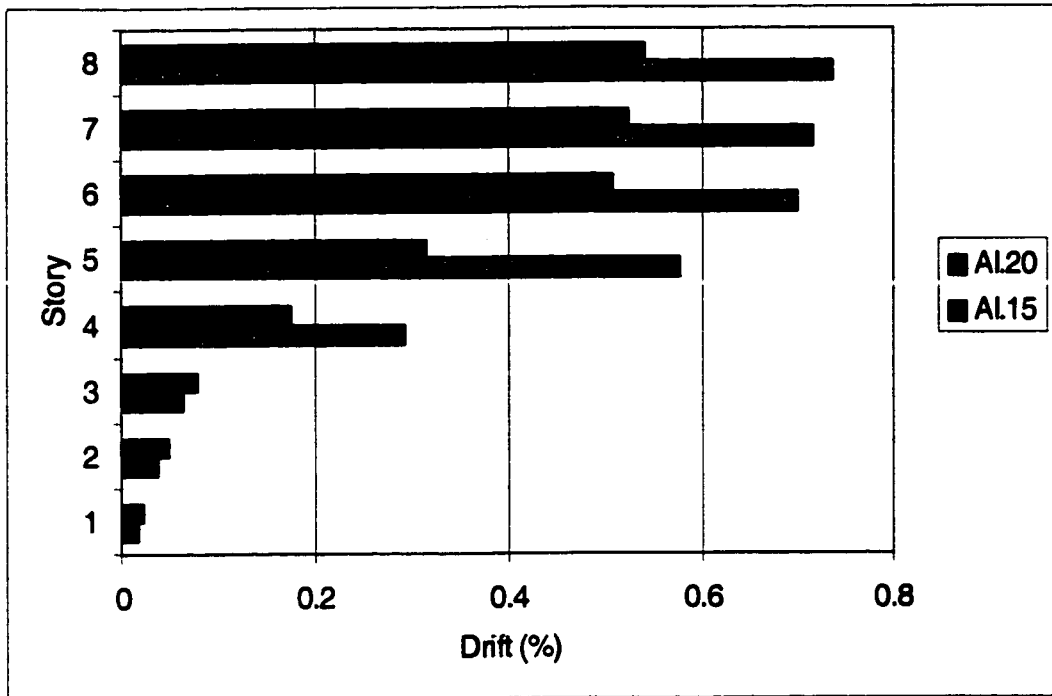


Figure 5.25 Maximum story drift for AI structure with different assigned masses.

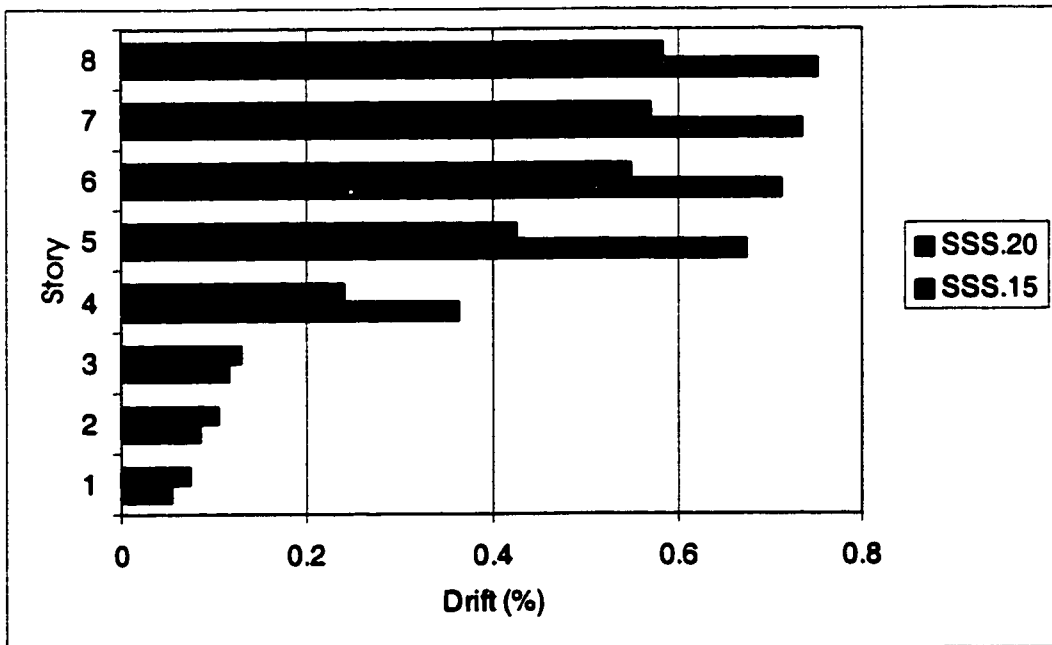
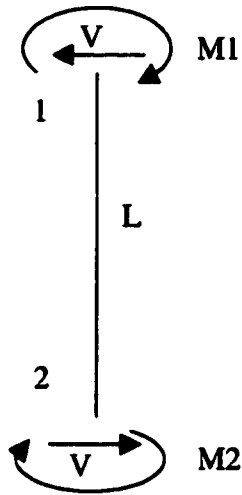


Figure 5.26 Maximum story drift for SSS structure with different assigned

masses.

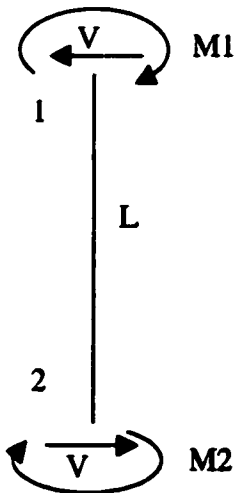
An acceptable measure of damage can be related to the drift sustained by the structure. Interstory drift provides information on the eventual failure mode of structural members. Column failure at the 6th story in AI.20 was identified from the analysis. The corresponding interstory drift was the largest for AI.20 on the 6th story. Column failure on the 5th story in SSS.15 was identified. The corresponding interstory drift was the largest for SSS.15 on the 5th story. AI.15 and AI.20 have the same material and physical properties except for the mass. Column failure could be identified at an interstory drift of 1.8% in AI.20, while no failure was indicated in AI.15 although a 2.6% interstory drift was calculated. The moments at the end of failing columns in AI.20 were almost equal and opposite in sign, indicating that shear had reached the maximum capacity of the column before flexural yielding of the column occurred (Fig.5.27 (a)). Some columns reached yield moment at one end, leading to large interstory drifts, however, the shear resisted by the column did not exceed the shear capacity (Fig. 5.27 (b)). Thus, no failure was observed although interstory drifts were large.



$$M1 \leq M1y \text{ and } M2 \leq M2y$$

$$V = \frac{M1 + M2}{L} \geq V_{\max}$$

(a) Shear Failure



$$M1 \leq M1y \text{ and } M2 \geq M2y$$

$$V = \frac{M1 + M2}{L} \leq V_{\max}$$

(b) Hinging at one end

Figure 5.27 Sketches of two different scenarios for large drift

Where,

M1, M2 = moment at end 1 and end 2 respectively;

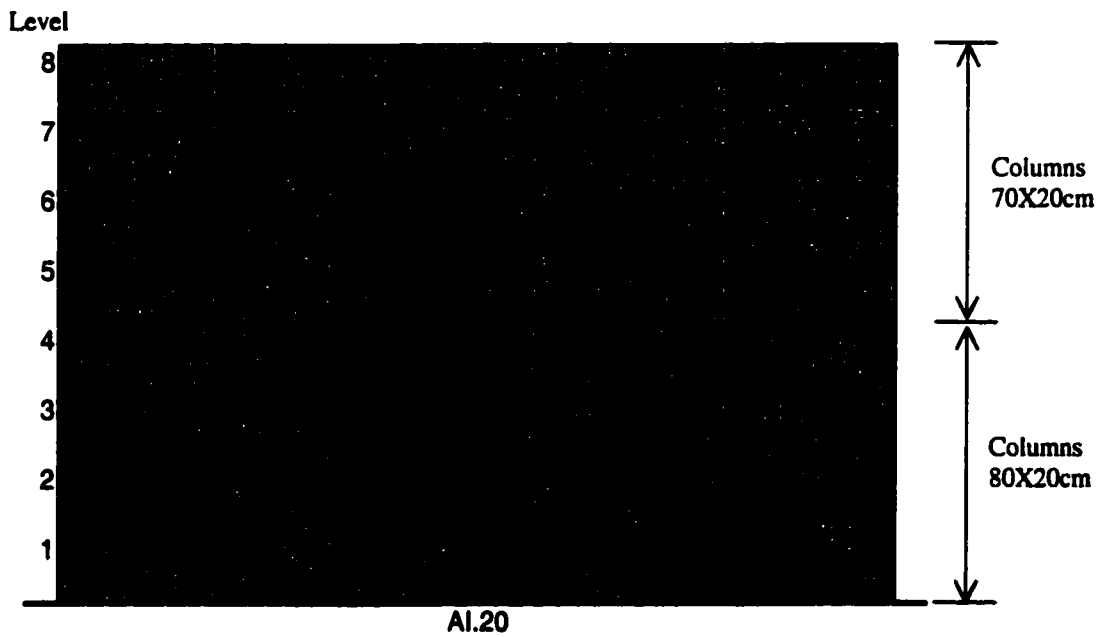
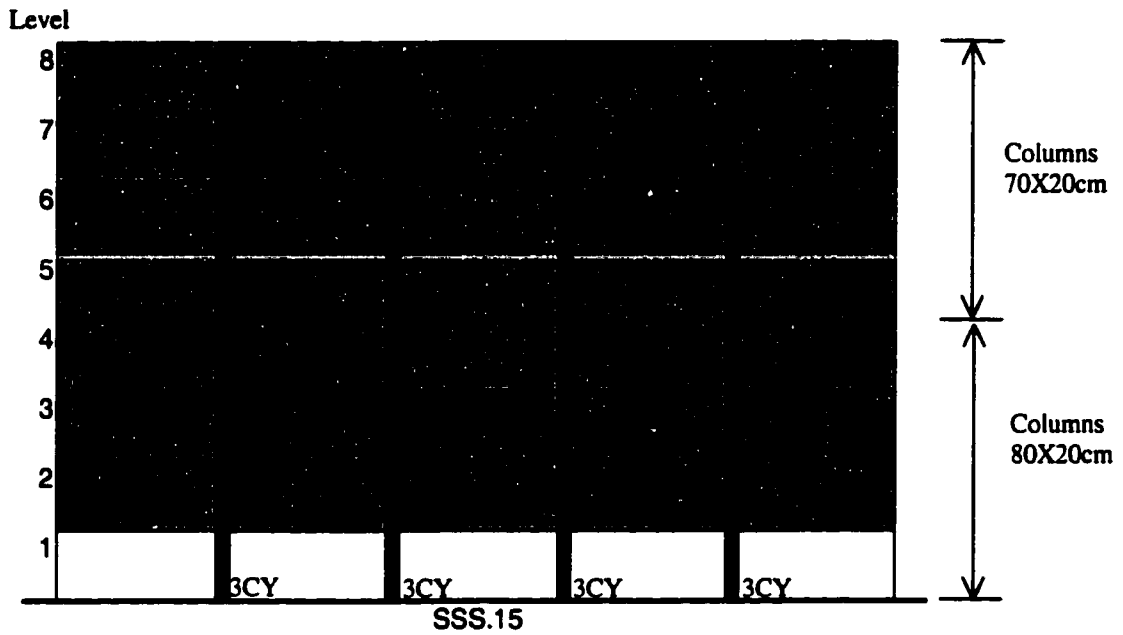
M1y, M2y = yield moment at end 1 and end 2 respectively;

L = length of the column;

V = shear in the column;

Vmax = shear capacity of the column.

Figure 5.28 shows the failure sequence in SSS.15 and AI.20. The infill panels were the first elements to fail when interstory drift of 0.4% was reached. In SSS.15, first the infills failed on the 5th story, next column shear failure occurred on that same story. The event is similar to the failure of a soft 5th story. In AI.20, first the infills failed on the 4th story, no column shear failure occurred on that same story. Next another soft story formed on the 6th floor after infills had failed on the 6th story. Column shear failure followed infill failure on the 6th floor. Column shear failure occurred at the 6th story but not on the 4th story because the 6th story is weaker given the smaller size of columns and therefore lower shear capacity at the 6th story with respect to the 4th story.



Notation

CY is Column Yield

CS is Column Shear Failure

BY is Beam Yield

W is Infill Panel Failure

The number in front of the notation indicate the sequence number of the event

Figure 5.28 Failure sequence for SSS.15 and AI.20

In these analyses, the distribution of total building mass to the section was an important parameter in determining the sequence of failure in a building. The base shear to weight ratio was almost unchanged for AI.15 and AI.20. There was close agreement in the shape of the story drift, however, the magnitude of drifts were different for different assigned masses due to different sequence of failure and different inertial forces. The difficulty in assigning a mass to the analyzed section is similar to the difficulty faced when assigning a load pattern in performing a static nonlinear analysis or pushover analysis of a structure. The mode shapes of the structure vary as some elements of the structure undergo cracking, yielding or failure. Thus, assigning a constant mass for a section will be accurate only if the section is isolated from the rest of the structure.

5.2.6 Residual Column Strength

5.2.6.1 General

Test results^{24, 61} have shown that after shear failure, columns may still carry some load but the strength and stiffness of the columns are reduced substantially (Fig. 5.29). Two values of residual strength were considered in the present investigation. SSS.15RS.1/3 and SSS.15RS.2/3 (Runs 13 and 16) are soft story frame structures with infill walls on the second floor to the roof. AI.20RS.1/3 and AI.20RS.2/3 (Runs 15 and 17) are frame structures with infill walls at all levels. Each pair of structures has the same parameters except for the residual

strength that is 1/3 and 2/3 times the initial shear capacities.

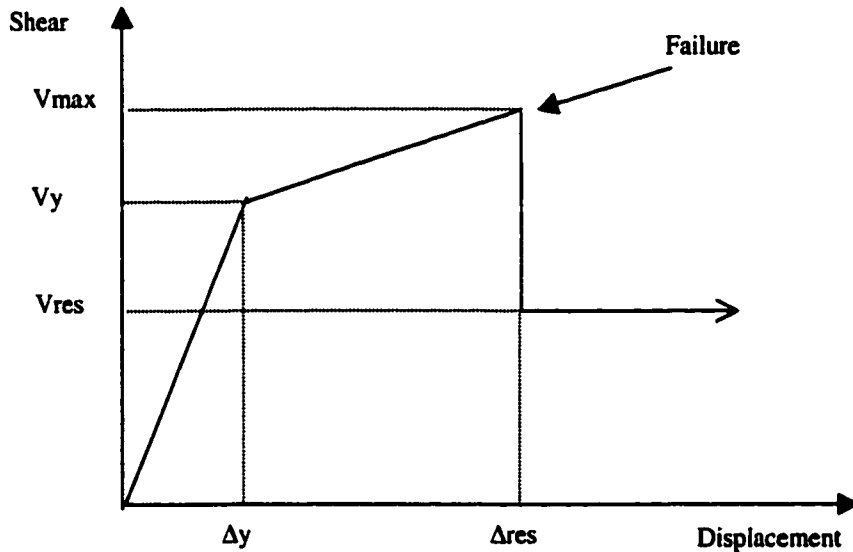


Figure 5.29 Force-displacement relationship for the parallel element¹⁴

5.2.6.2 Analysis Results

The time history of base shear and roof displacement, and the maximum interstory drift and maximum story drift were calculated for the four structures. No clear trends are evident in base shear values. However, Figs 5.30 and 5.31 show that with lower residual shear capacity, the period of the structure after column shear failure occurred was slightly greater. Li and Jirsa¹⁴ made the same observation for a frame structure with no infill walls. The period of the structure seemed to increase after shear failure occurred. Such changes could be expected since the stiffness of the failing elements decreases and thus the stiffness of the structure decreases.

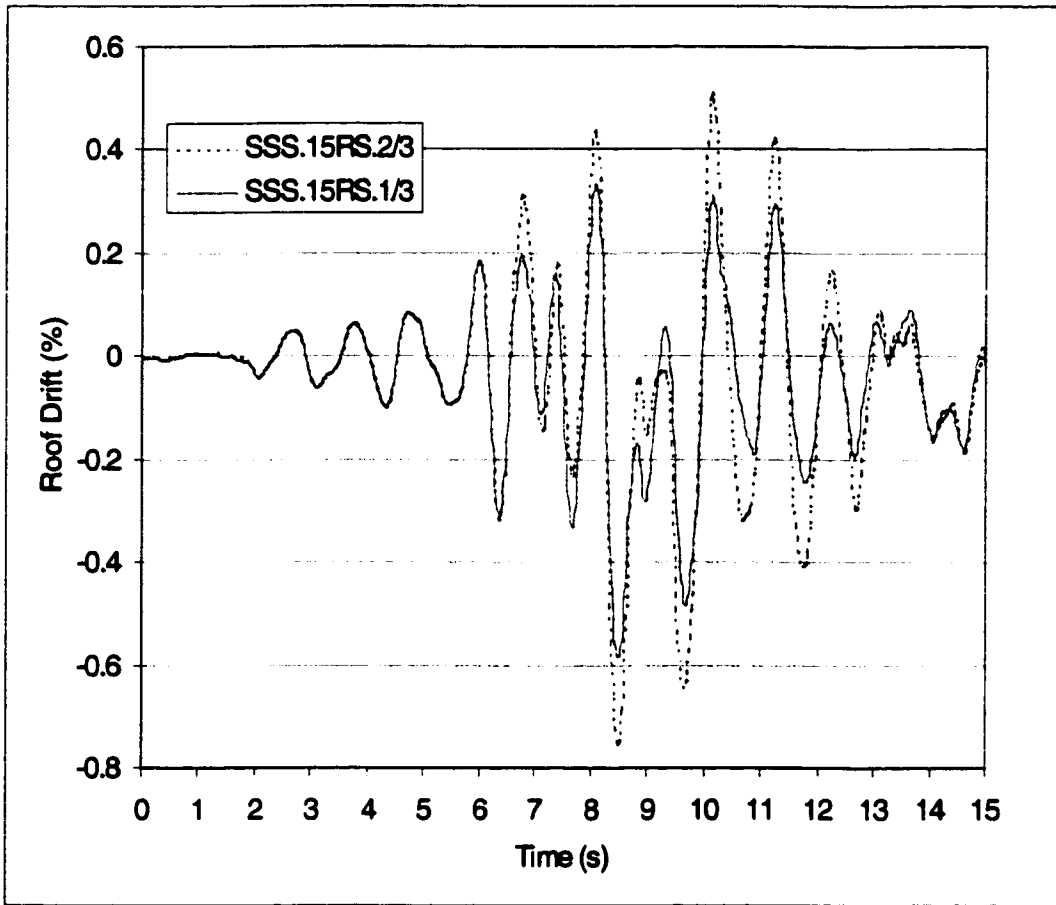


Figure 5.30 Time history of roof displacement for Soft Story System

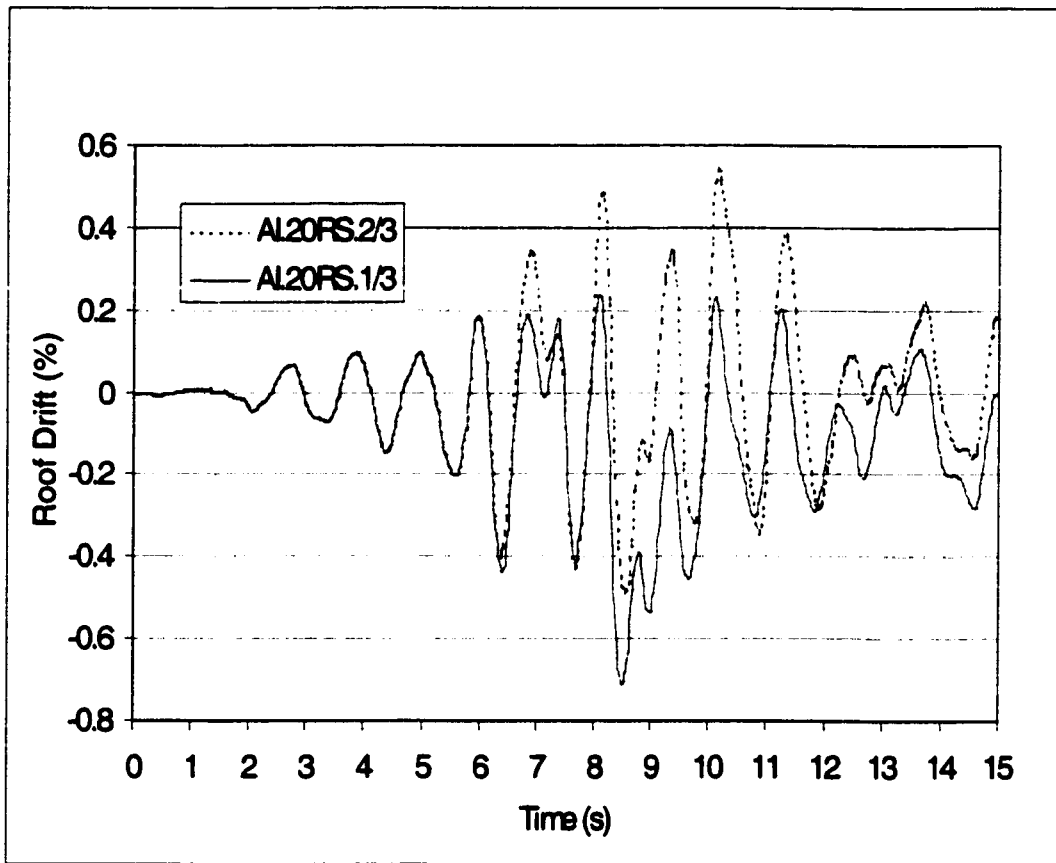


Figure 5.31 Time history of roof drift for All Infill structure

Figures 5.32 and 5.33 showed close agreement in the shape of the story drift for SSS structures and AI structures respectively. However, magnitudes of drifts were different for different assumed residual strengths.

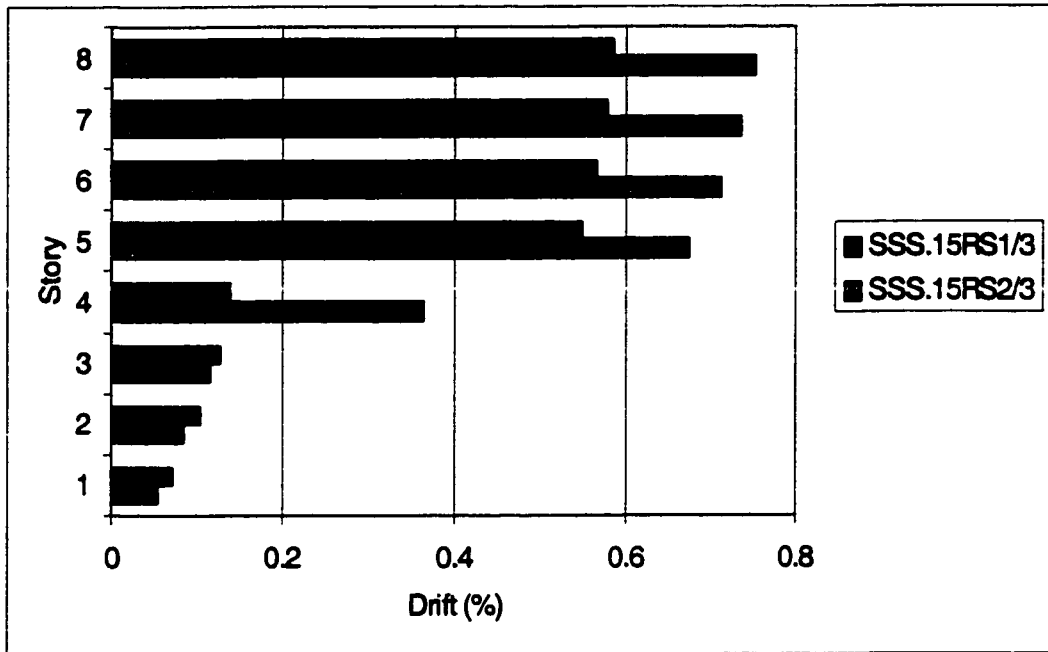


Figure 5.32 Maximum story drift for Soft Story System

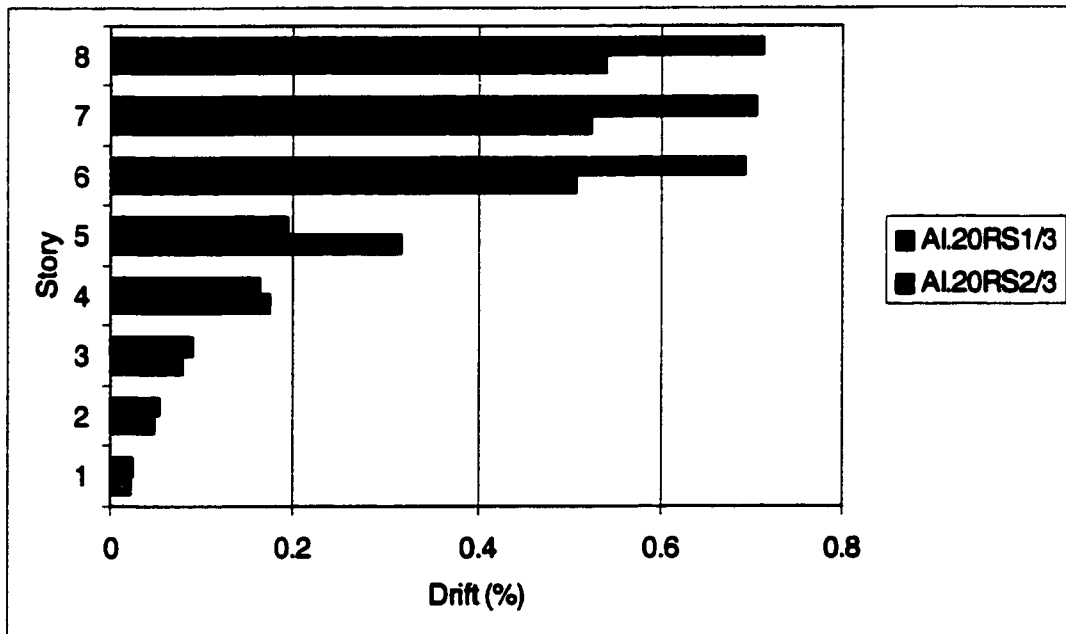


Figure 5.33 Maximum story drift for All Infill structure

Infill walls failed when interstory drift in excess of 0.4% was reached. Figure 5.34 shows that infill walls failed on the 4th and 5th stories for SSS.15RS.2/3 and on the 5th story only for SSS.15RS.1/3. Figure 5.35 shows that infill walls failed on the 4th, 5th and 6th stories for AI.20RS.2/3 and on the 4th and 6th stories only for AI.20.RS.1/3.

The analytical results showed that the interior four columns on the 5th story in SSS.15RS.1/3 and SSS.15RS.2/3 failed in shear at 6 seconds. At 7.7 seconds, the exterior columns on the 5th story in SSS.15RS.1/3 failed in flexure. After shear failure of the interior columns, a dramatic decrease in the stiffness occurred causing the shear to be distributed to the exterior columns. The same effect was observed on the 6th story for AI.20RS.1/3 and AI.20RS.2/3.

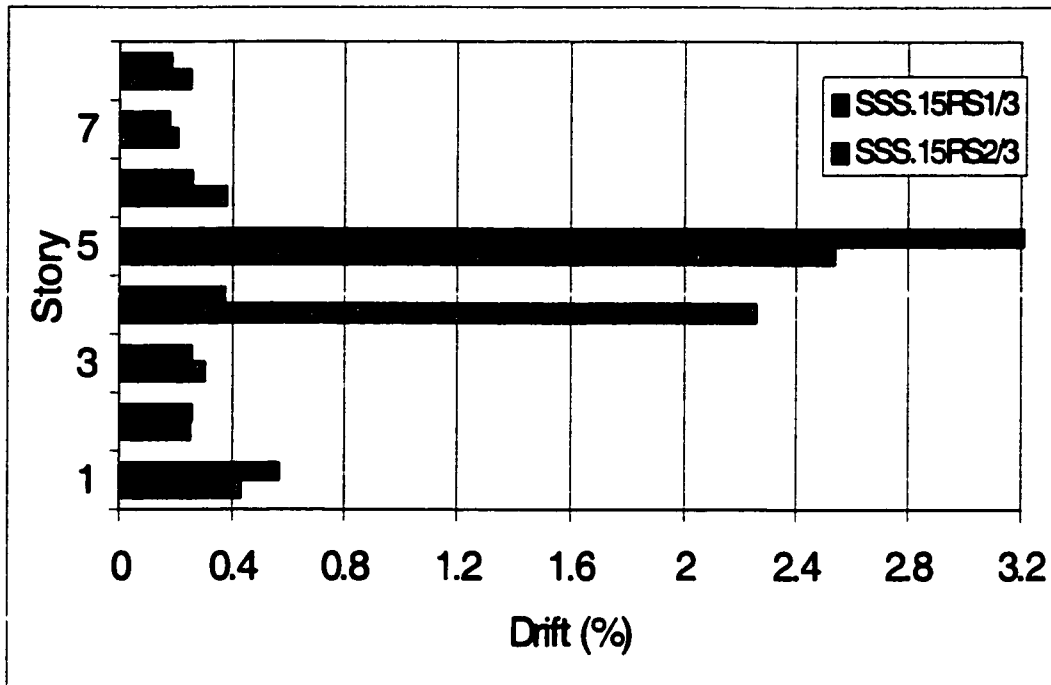


Figure 5.34 Maximum interstory drift for Soft Story System

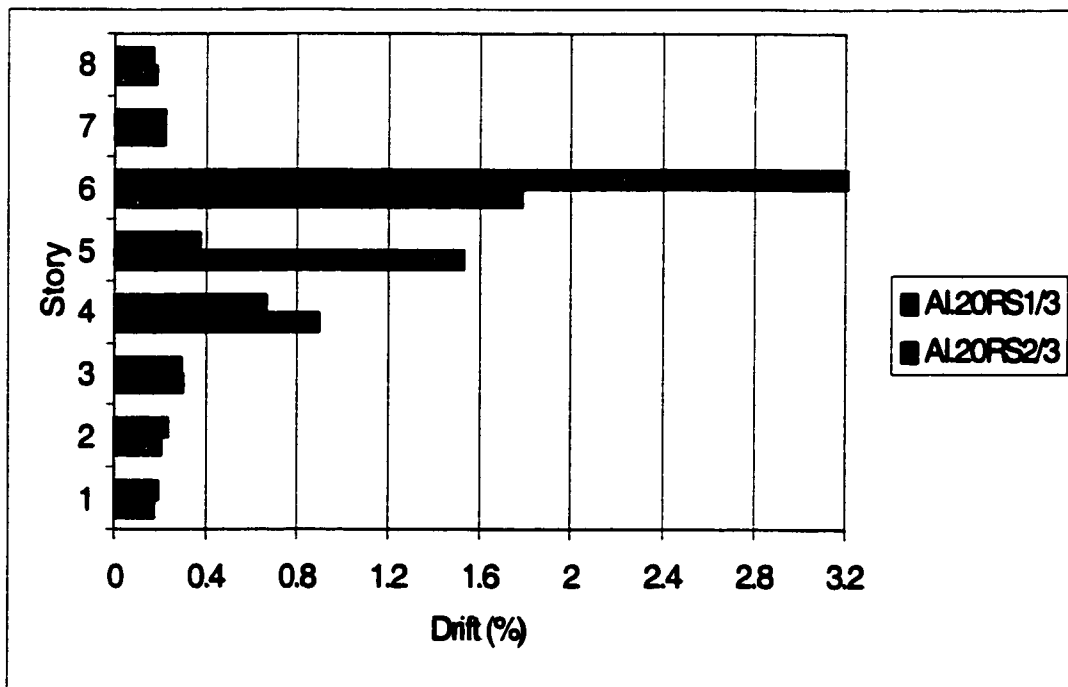


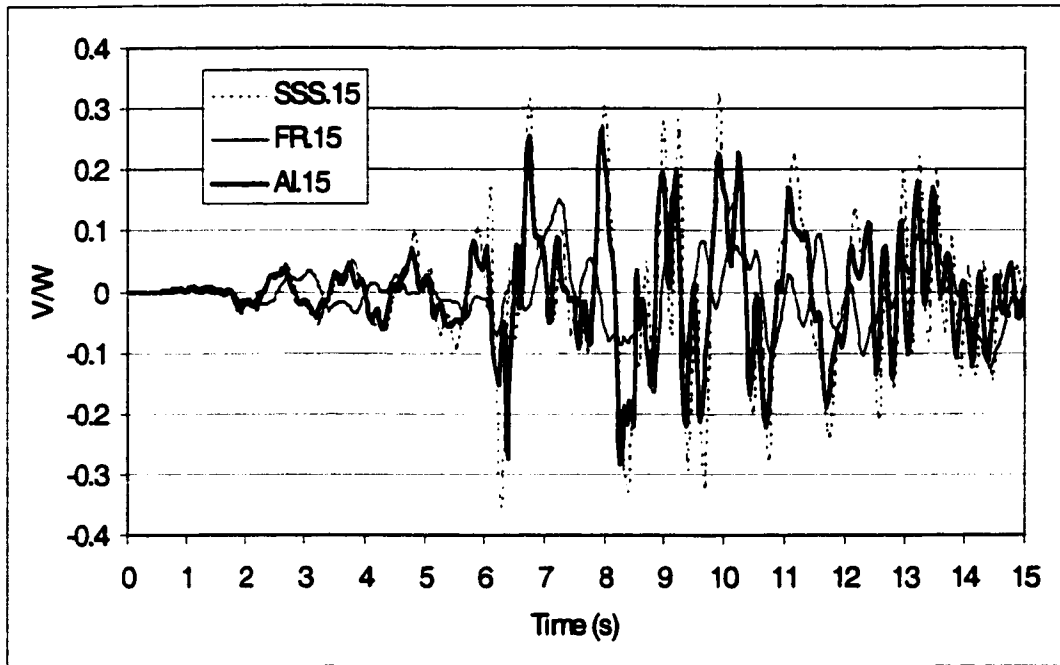
Figure 5.35 Maximum interstory drift for All Infill structure

5.2.7 Infill Action

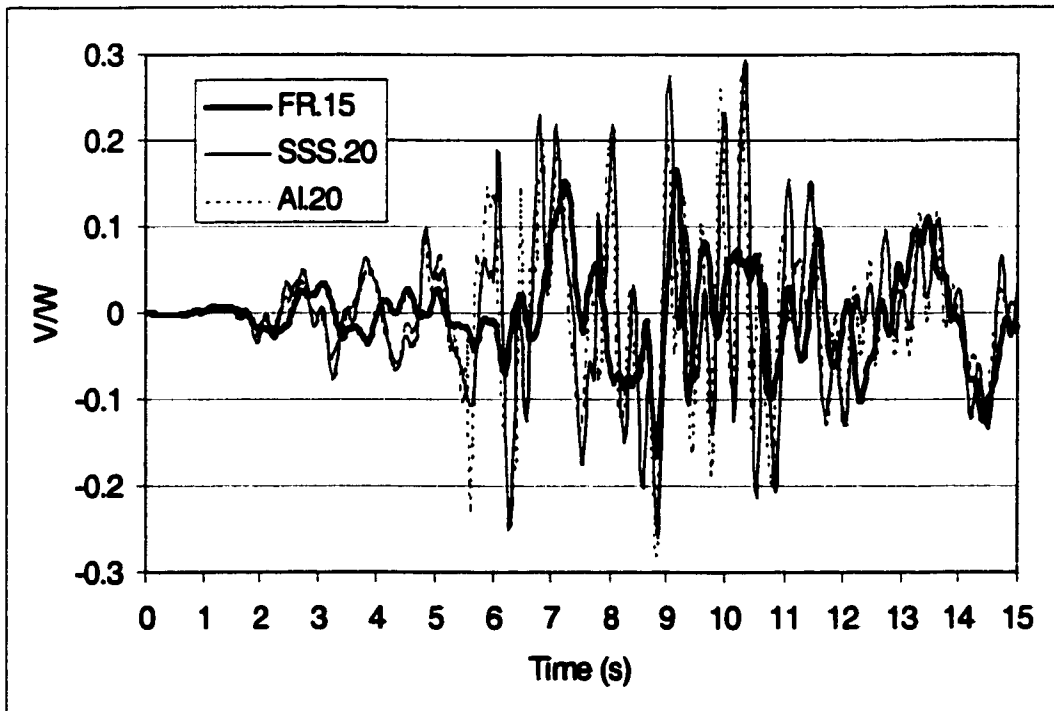
To investigate the effect of infills, behavior of two sets of three structures were compared: (FR.15, SSS.15 and AI.15, Runs 12, 13 and 18) and (FR.15, SSS.20 and AI.20, Runs 12, 14, and 15). In the first set, the three structures had the same material properties and characteristics, except that FR.15 is a frame with no infill, SSS.20 is a frame with infill walls from the second floor to the roof and AI.20 is a frame with infills at all levels. In the second set, the same configuration was used as in the first set except that the attributed mass to structures with infill walls was changed to 20% of total building mass instead of 15%, so that the mass was increased as the stiffness increased.

Maximum story drifts, maximum interstory drifts and time-history of base shear to weight ratio were calculated for all structures and are shown in Figs. 5.36 through 5.38. Figures 5.36 a and b show the much larger base shear for structures with infill walls. The first mode was predominant in the response of FR.15 (Figs.5.37a and 5.37b) because the story drift was almost an inverted triangle. Although AI and SSS were stiffer than FR, deformations were larger at upper floors after infill panels failed (Fig. 5.37a). At lower floors where no panel failure occurred, AI was stiffer than both SSS and FR. As expected, deformations of the first story of the SSS systems were greater than FR because of the soft first story. Column shear failure occurred in the interior four columns on the 5th story in SSS.15 while no shear failure was observed in AI.15. Column shear failure was identified in the

calculations for the interior four columns on the 6th story in AI.20 while no shear failure was observed in SSS.20. Therefore, including infills carrying shear only can alter the location and the sequence of failure in the structure. These phenomena were interpreted in section 5.3.5.2 and will be discussed in greater detail in Chapter 7 (section 7.4.3).

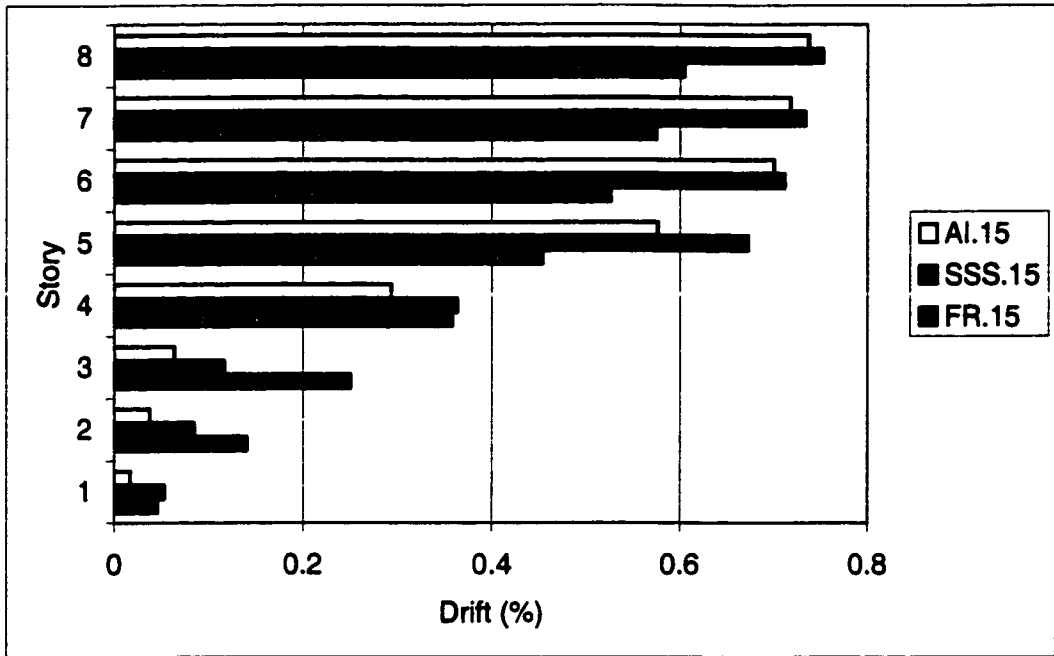


(a) FR.15, SSS.15 and AI.15

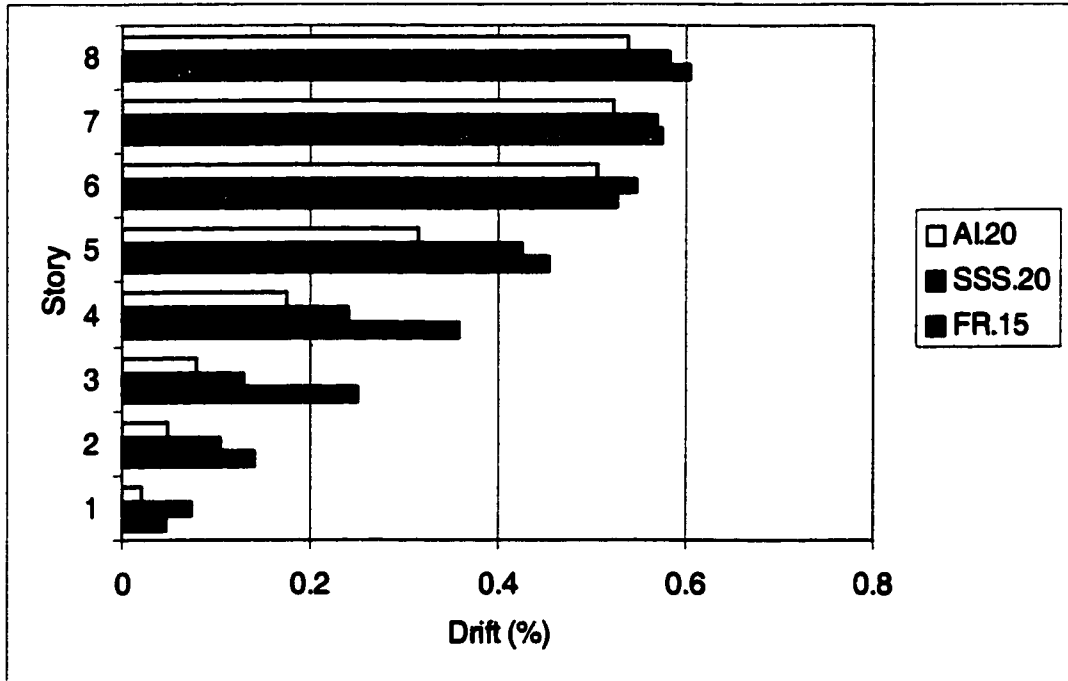


(b) FR.15, SSS.20 and AI.20

Figure 5.36 Time history of base shear

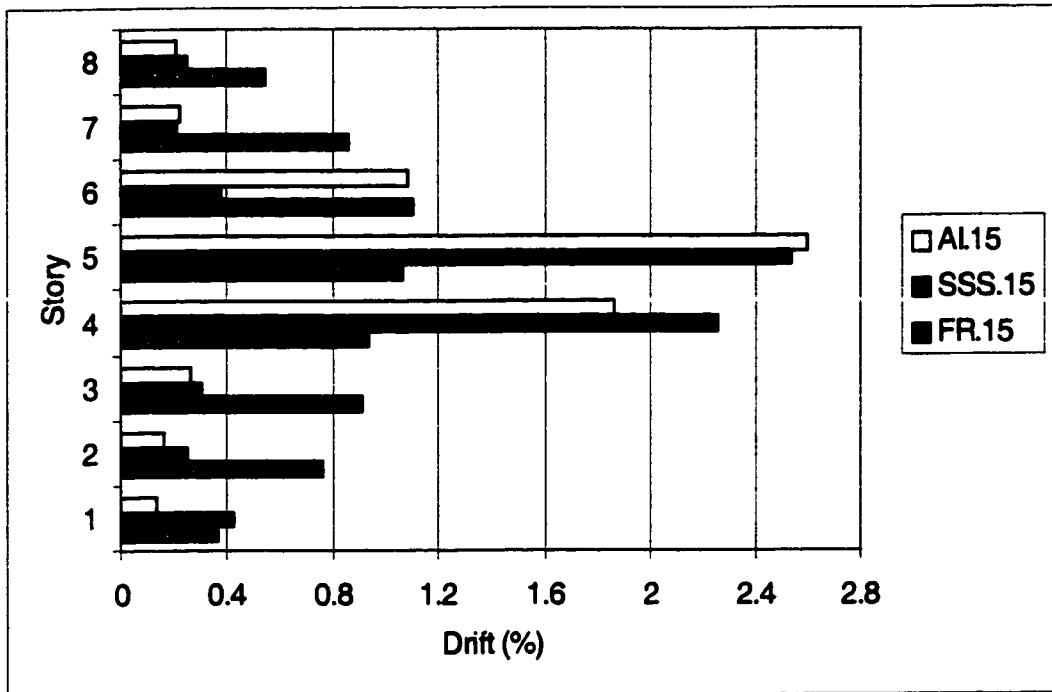


(a) FR.15, SSS.15 and AI.15

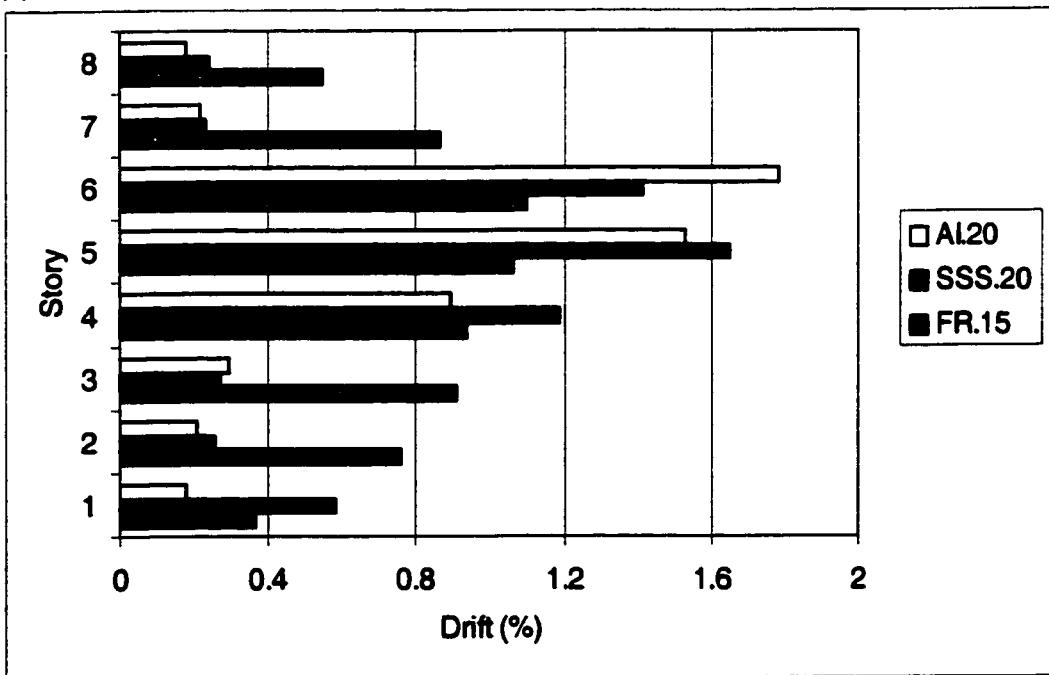


(b) FR.15, SSS.20 and AI.20

Figure 5.37 Maximum story drift



(a) FR.15, SSS.15 and AI.15



(b) FR.15, SSS.20 and AI.20

Figure 5.38 Maximum interstory drift

5.2.8 Variations in Ground Motions

5.2.8.1 Ground Motion Characteristics

In order to assess the importance of the ground motion record as input for conducting a time history analysis, four ground motion records were used in studying the response of the prototype structure. The ground motion records were scaled so that the peak ground acceleration was 0.45g, the peak ground acceleration expected in several areas of Turkey with a 10% probability of exceedance in 50 years, i.e. with a return period of 475 years^{62,63}. The S00E component of the El Centro, Imperial Valley Earthquake, of May 18, 1940 (the first complete earthquake ground motion accelerogram recorded) was selected for this study. It has been widely used as a typical earthquake ground motion in past research, with strong shaking that lasted more than 20 seconds (Fig. 5.39). The three other records used were the 1994 Northridge earthquake because of the similarity of the Levant fracture system and the San Andreas Fault system, the 1998 Ceyhan earthquake and the 1999 Izmit earthquake in Turkey (Figs 5.40, 5.41 and 5.42).

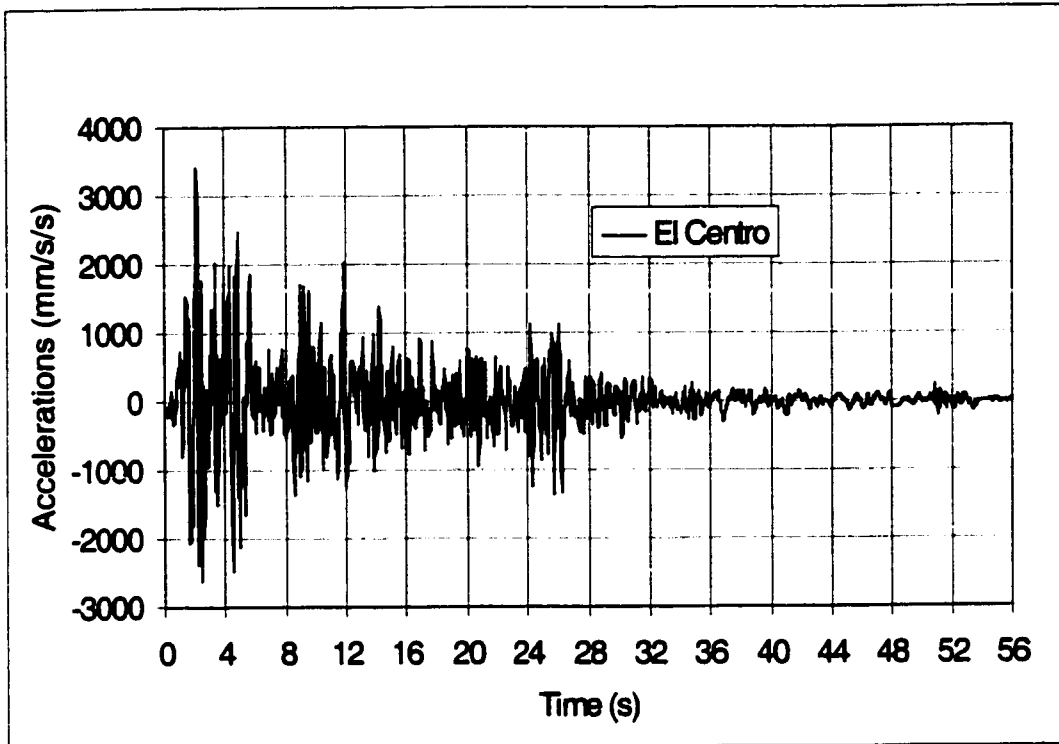


Figure 5.39 Ground acceleration time history of the 1940 Imperial Valley Earthquake at El Centro (S00E direction)

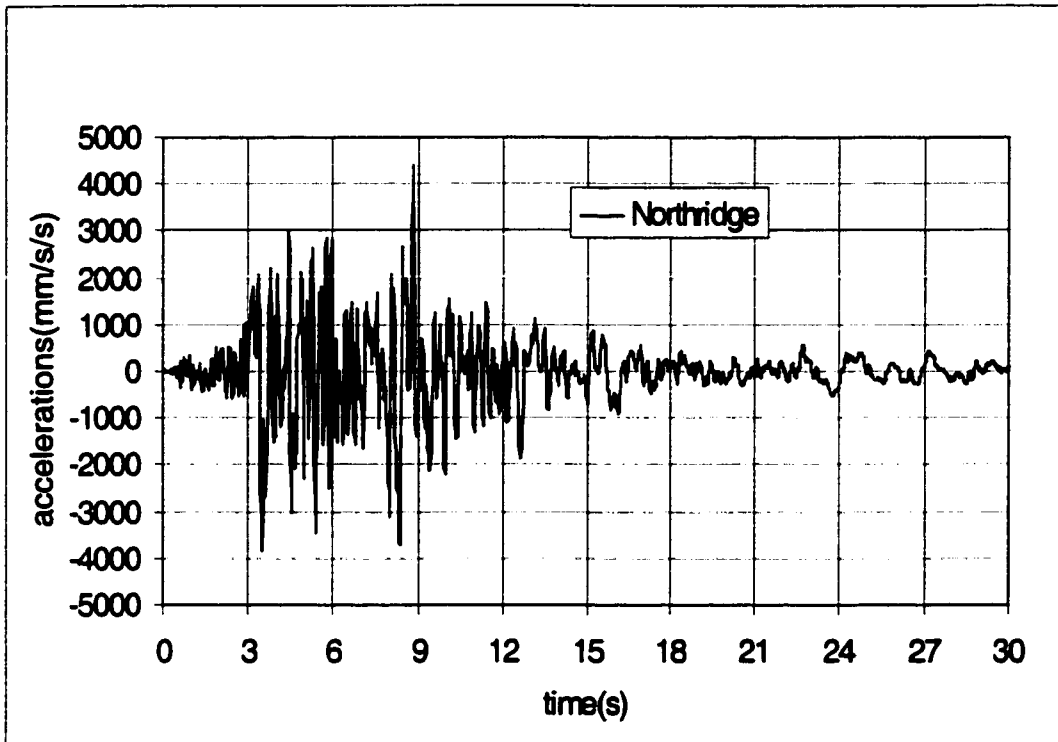


Figure 5.40 Ground acceleration time history of the 1994 Northridge Earthquake (E-W direction).

The Northridge record was obtained from the E-W accelerogram that was recorded at the base of a seven-story hotel at 8244 Orion Avenue, Van Nuys, California. The hotel was located at approximately 4.5 miles east of the epicenter of the 1994 Northridge earthquake.

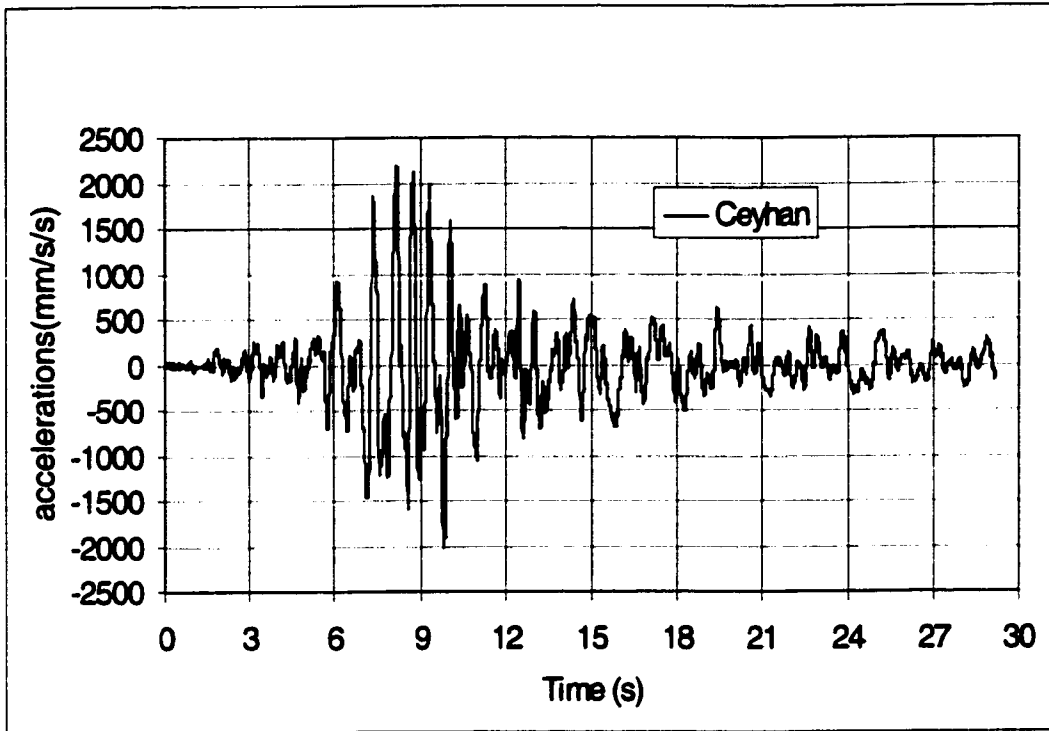


Figure 5.41 Ground acceleration time history of the 1998 Ceyhan Earthquake in Turkey (Direction: N-S. Location: CEYHAN TARIM ILCE MD.LUGU)

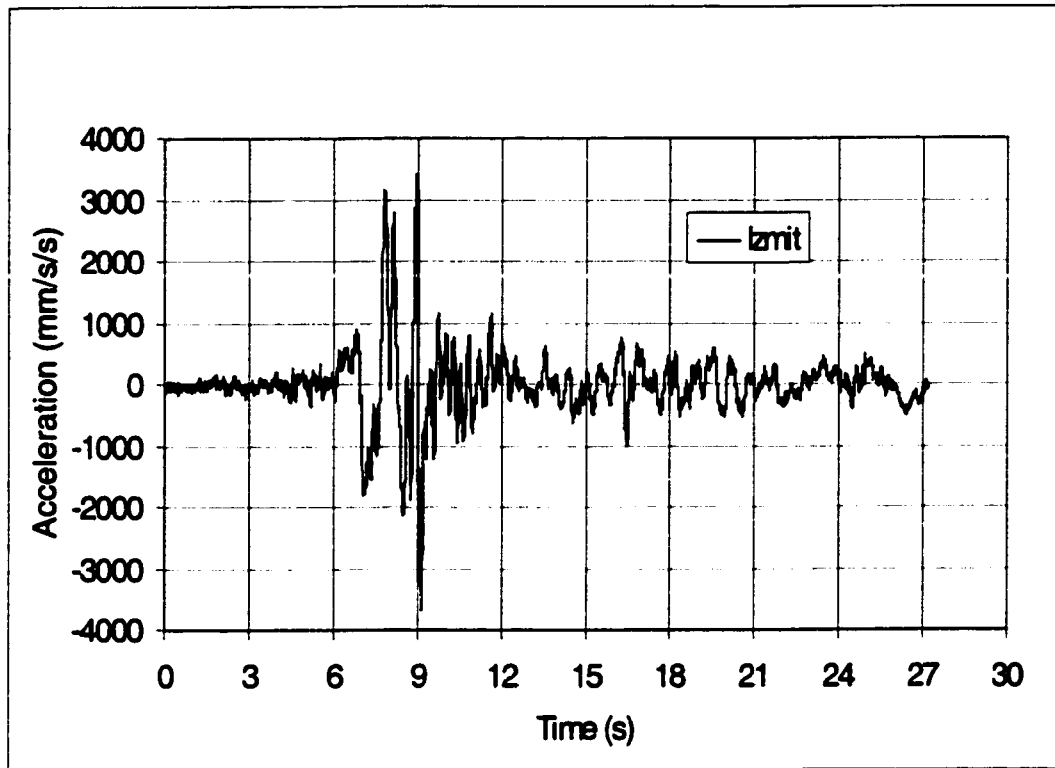


Figure 5.42 Ground acceleration time history of the 1999 Izmit Earthquake in Turkey
(Direction: E-W. Location: DUZCE METEOROLOJI ISTASYONU)

Figures 5.43, 5.44 and 5.45 show respectively the acceleration, the displacement and the velocity response spectra for all of the ground records scaled to the Northridge earthquake. The longitudinal component of the Ceyhan earthquake was scaled by a factor of 2, Izmit by 1.19 and El Centro by 1.28 so that peak ground acceleration equals 0.45g. The response spectra for Northridge and Izmit earthquakes are similar as are the Ceyhan and El Centro earthquakes.

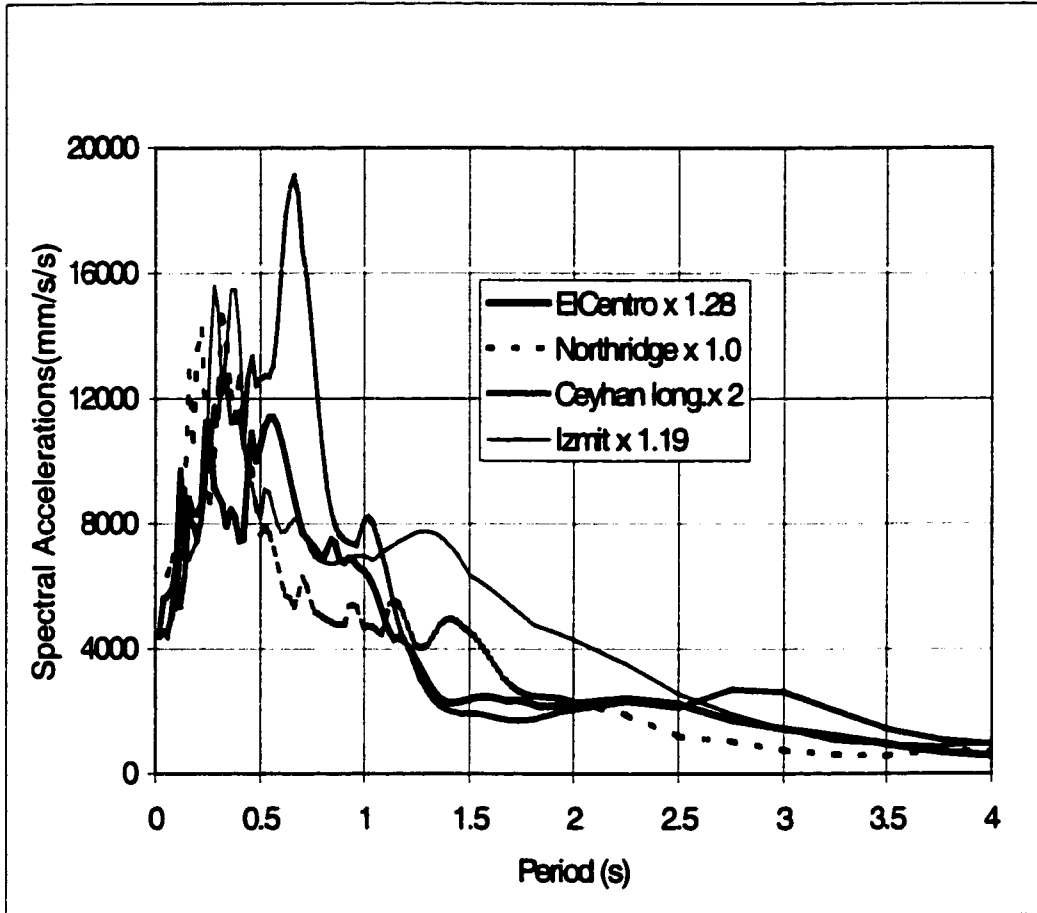


Figure 5.43 Acceleration response spectra for El Centro, Northridge, Ceyhan and Izmit earthquakes with 5% damping ratio.

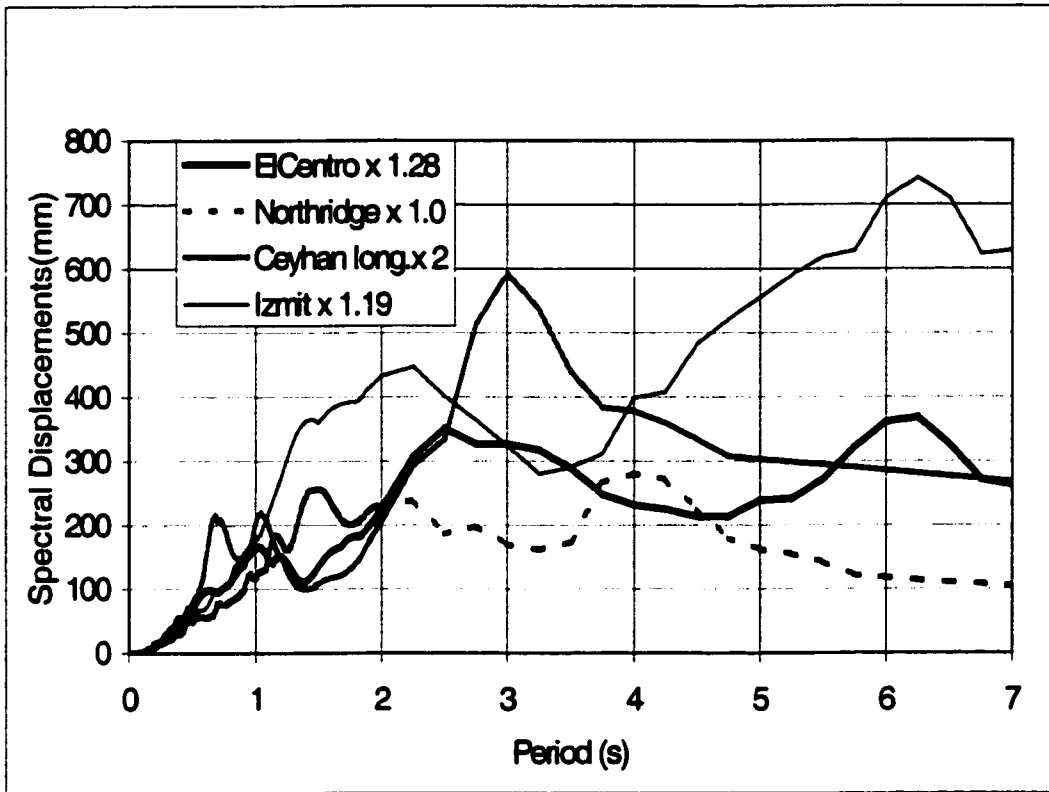


Figure 5.44 Displacement response spectra for El Centro, Northridge, Ceyhan and Izmit earthquakes with 5% damping ratio.

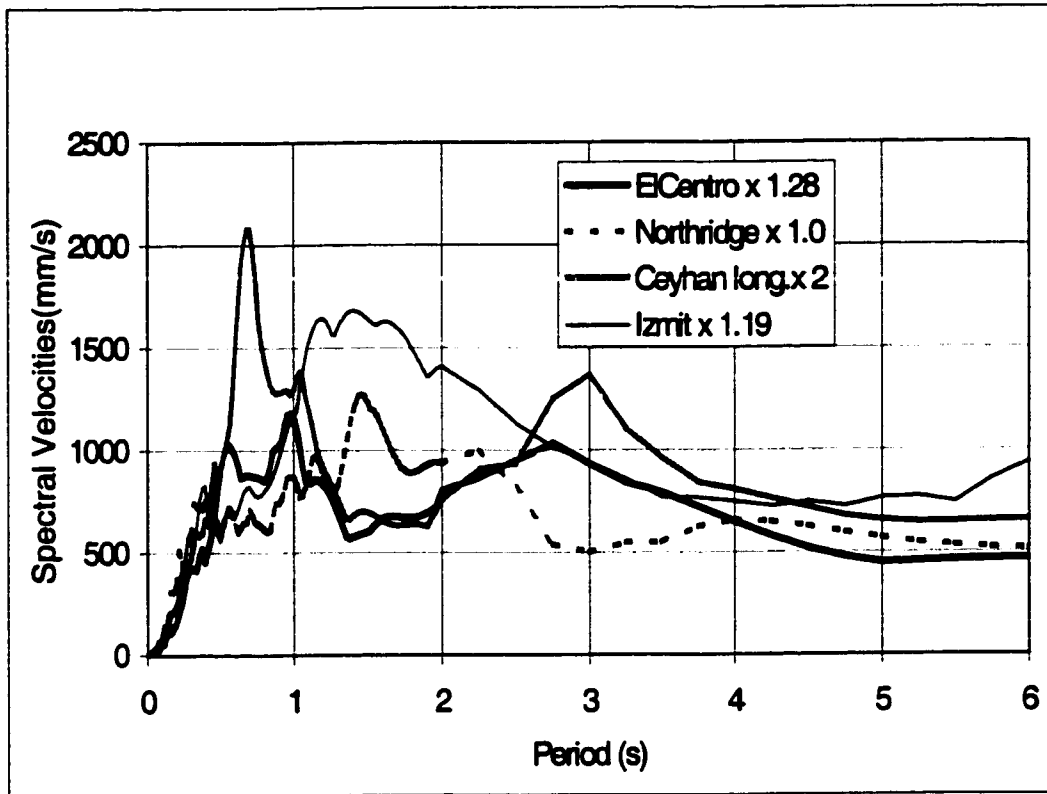


Figure 5.45 Velocity response spectra for El Centro, Northridge, Ceyhan and Izmit earthquakes with 5% damping ratio.

5.2.8.2 Structure Characteristics

The structure subjected to the different ground motion records was SSS.15RS2/3 (Run 13). It had infill walls on the 2nd floor to the roof. The effective stiffness in SSS.15RS2/3 was assumed to be 0.5 times the stiffness of the concrete gross section for beams, and 0.7 times the stiffness of the concrete gross section for columns. The residual strength after column shear failure was assumed 2/3 of the

maximum capacity of the column. Concrete strength was taken equal to 0.9 times the design strength and the steel strength was taken equal to $\frac{4}{3}$ times the design strength. The structure was assigned 15% of the total building mass. The fundamental period for SSS.15RS2/3 was 0.95 seconds and the second mode period of vibration was 0.28 seconds. The acceleration response spectra for all the records considered indicates high responses in the 1st and 2nd modes of the structure. Therefore, the structure is expected to be subjected to significant forces during the earthquakes selected.

5.2.8.3 Analysis Results

The time history of base shear and roof displacement, and the maximum interstory drift and maximum story drift were calculated for SSS.15RS.1/3 subjected to the scaled El Centro, Northridge, Ceyhan and Izmit earthquakes. The results are plotted in Figs. 5.46, 5.47 and 5.48.

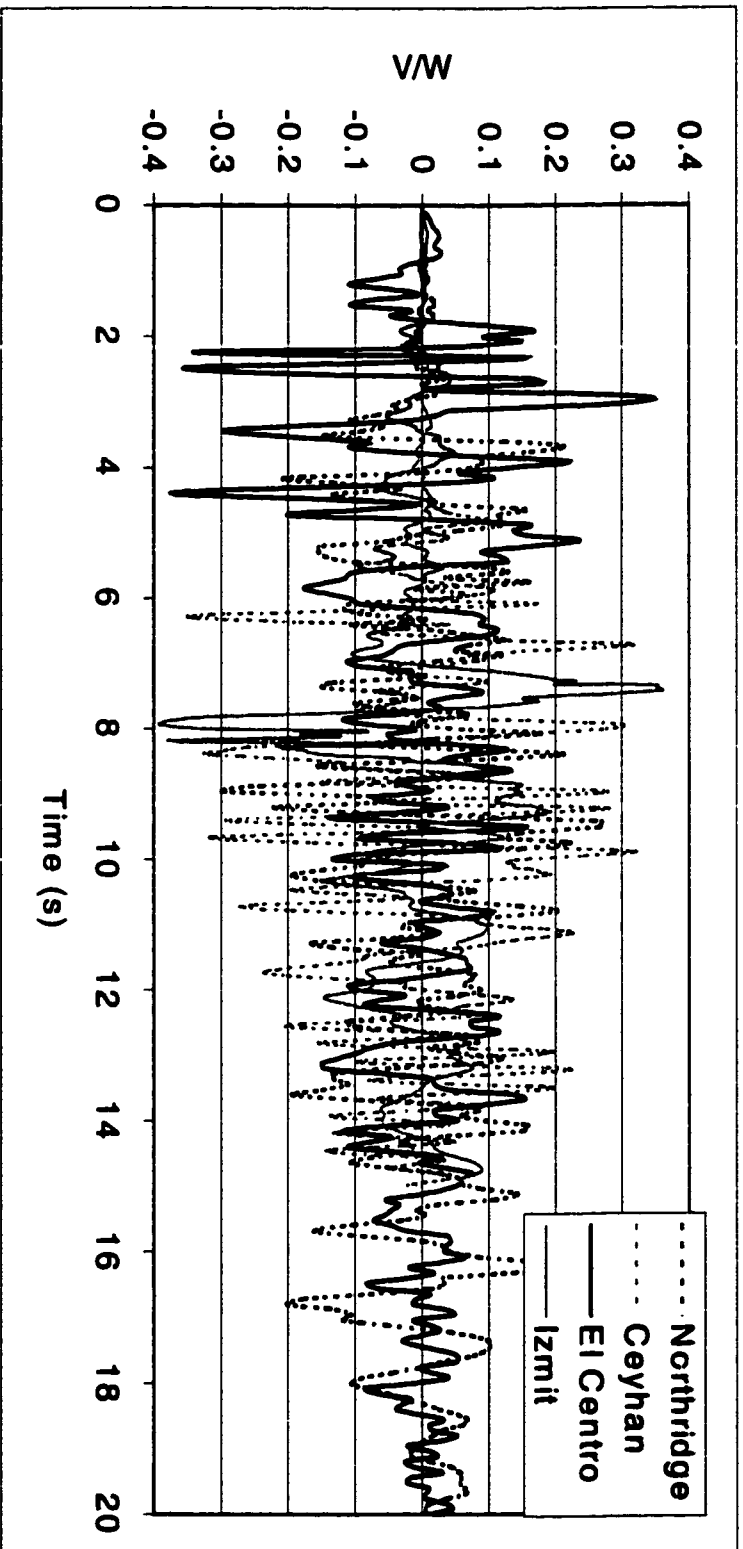


Figure 5.46 Time history of base shear for SSS.15RS.2/3 subjected to Northridge, Ceyhan, El Centro and Izmit earthquakes.

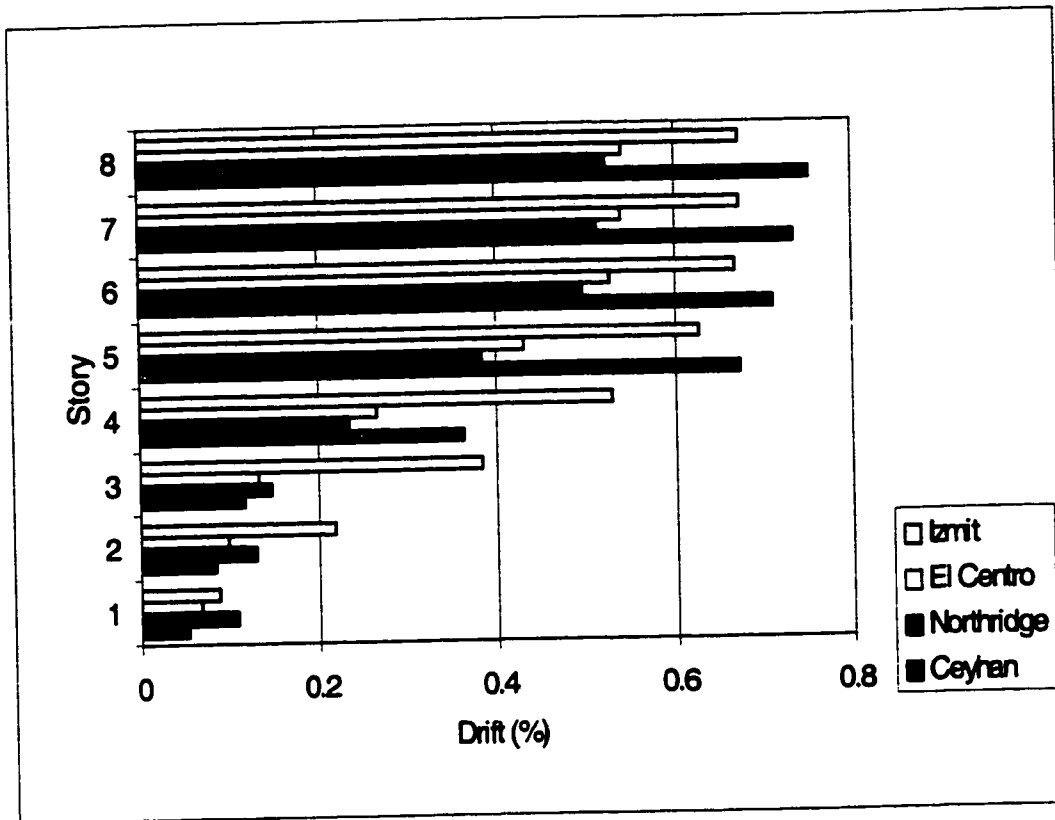


Figure 5.47 Maximum story drifts for SSS.15RS.2/3

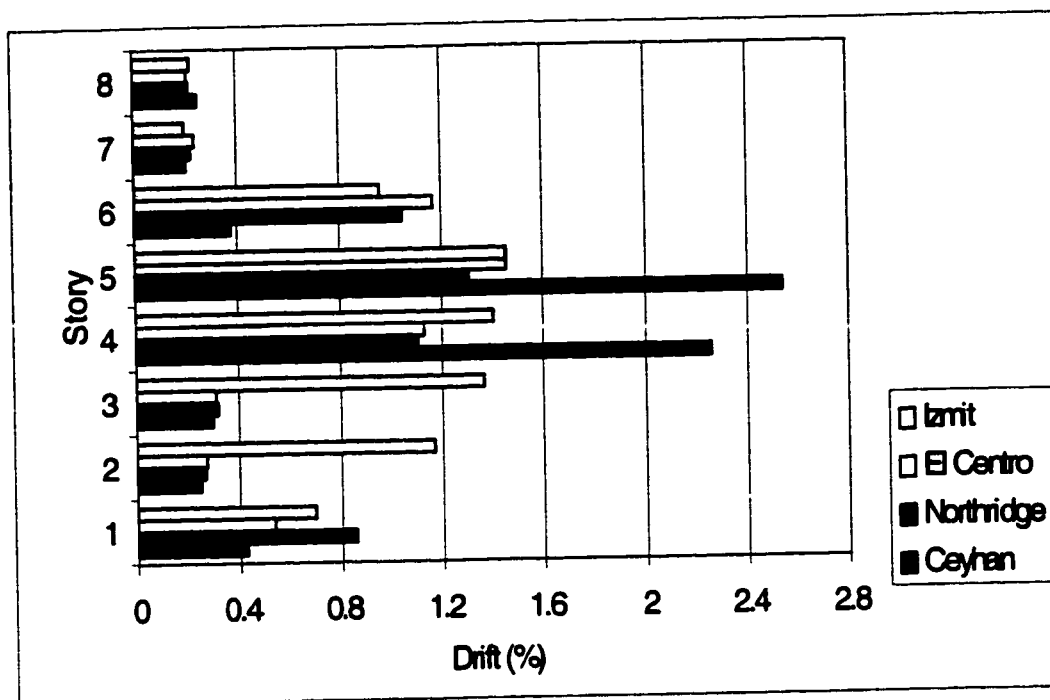


Figure 5.47 Maximum interstory drifts for SSS.15RS.2/3

Even though the peak ground acceleration was the same for all four records, Fig 5.46 shows the maximum ratios of shear to weight of the structure reached at the base of the structure were 0.37 using El Centro ground motions, 0.39 with Izmit, 0.34 with Ceyhan and 0.3 with Northridge. Figure 5.47 shows a close agreement in the general shape of the maximum story drifts using different ground motion records, however, the values of drifts were significantly different especially for the stories above the level infill walls failed. Figure 5.48 indicates infill failure from the 2nd floor to the 7th using Izmit ground motions (interstory drift larger than 0.4%). Infill walls failed on the 4th and 5th stories using Ceyhan earthquake. And EL Centro and Northridge shaking caused infill failure on the 4th, 5th and 6th stories. Analytical

results indicate column shear failure on the 5th story using Ceyhan, and on the 1st story using Northridge, and no column shear failure using Izmit or El Centro. Note the large interstory drift from Northridge on the 1st story and from Ceyhan on the 5th story.

The results were very sensitive to the input ground motions. Failure sequence, location of failure and maximum base shear were significantly different for different earthquakes of the same intensity.

In summary, as expected, a nonlinear dynamic simulation of the response of a structure using models with load-deformation characteristics representing as many key features of the behavior of the real members as possible are expected to reproduce the behavior of the structure with acceptable accuracy. The results of the simulation depend highly on the assumptions, the analytical limitations, the model and the ground motion input used, especially in predicting the sequence and location of structural member failure.

CHAPTER 6 NONLINEAR STATIC ANALYSES

6.1 General

As described in section 2.4.6.3, a nonlinear static analysis procedure, commonly referred to as a pushover analysis, was included in the “Guidelines for the Seismic Rehabilitation of Buildings”¹. It is intended to be a technique that provides the designer with an estimate of the response of a structure under monotonically increasing lateral forces. The method consists of applying a specified lateral load distribution along the height of the structure. The lateral load is increased until either a mechanism forms or a target displacement or deformation of a specific part of the structure is reached. A pushover analysis is expected to establish the sequence of component yielding and/or failure, the global ductility, and the adequacy of the structure by providing a relationship between drift, generally the roof displacement, and the base shear of the structure.

In this chapter, analyses are conducted to compare the results from pushover analyses with the results from nonlinear time history analyses. For consistency, the same structural models used for dynamic analysis are used for the pushover analysis. DRAIN-2D was used to perform the analyses. A brief evaluation of the pushover analysis in Nonlinear Push SAP2000 was conducted.

6.2 Drawbacks of the Pushover Procedure

Previous studies^{14,64,65,66} concluded that the pushover method is sensitive to structural modeling, lateral load distribution and site characteristics.

It is important to note that based on a pushover analysis, nearly any model of member response will provide the same peak lateral capacity of a structure if the load level representing the “yield plateau” is about the same^{14,67} and if there is insufficient ductility of all critical elements. The deformations at which the peak load is reached may be quite different and can be misleading when used to determine deformation capacity of the system, especially when comparing that capacity against deformation demands determined from ground motions. As a result, the failure sequence and locations in a structure from a pushover analysis may differ significantly as more sophisticated structural models⁶⁴ that simulate observed strength-deformation relationships more closely are used.

Although structural capacity and earthquake demand are expected to be interrelated⁶⁵, a pushover procedure that is based on a constant load pattern assumes that the structural capacity and earthquake demand are independent.

Current pushover analysis techniques are two-dimensional procedures. Programs such as SAP2000 that incorporate three dimensional interaction effects seem to be incomplete. Using a 2-D model to simulate the behavior of a 3-D structure is too simplistic in many cases and fails to represent the effects of torsion. It

is impossible to represent completely a 3-D structure using only two parameters, base shear and roof displacement.

6.3 Load Pattern

Two major difficulties are encountered in performing a pushover analysis: determining a representative structural model and an appropriate load pattern. The load pattern is intended to reproduce the inertial lateral forces on the structure due to ground accelerations. In reality, such forces vary as some components of the structure undergo cracking and yielding. There are several patterns used, including uniform distribution, inverted triangular distribution and modal adaptive distribution⁴. The former two patterns bound the response and are the most commonly used. The modal adaptive distribution captures the different modes of deformation and the influence of higher modes in the response but is more difficult to implement in existing analytical programs, as it needs to be updated at each event in the analysis. Results from a pushover analysis using the modal adaptive distribution are in good agreement with time history analysis for the same structure using the acceleration response spectrum corresponding to the ground motion record^{68, 69}. In the current study, “uniform”, “inverted triangle” and “modal” load patterns were investigated (Figs. 6.1 and 6.2). The “modal” pattern was similar to the method suggested in FEMA 273 as the pattern corresponding to the initial elastic modal response. FEMA 273 suggests that inertial forces on each floor be computed from the elastic modal response. The simplification to the method in FEMA 273 was

to use the deformed shape of the structure from elastic modal response and to assume only lateral translational stiffness for each story. The force, F_i on floor i , can be computed using Eq (6.4) which is developed as follows:

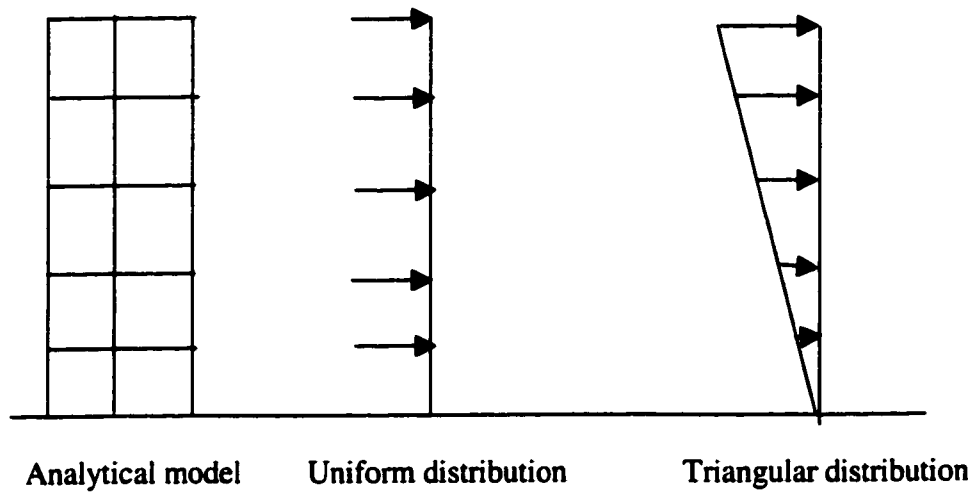


Figure 6.1 Load patterns, “uniform” and “triangle”

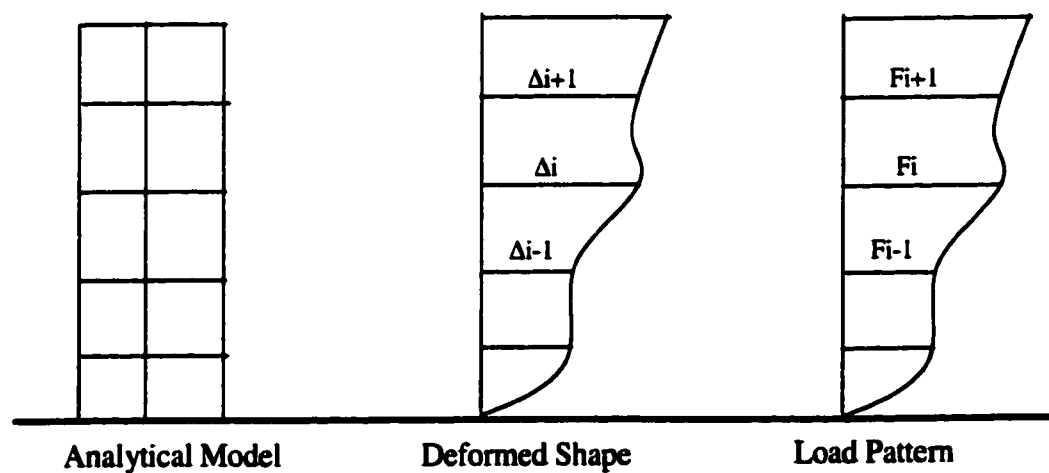


Figure 6.2 Suggested load pattern for “modal” distribution

$$F_R = K(\Delta_R - \Delta_{R-1}) \quad \text{Eq (6.1)}$$

$$\sum_{j=i}^R F_j = K(\Delta_i - \Delta_{i-1}) \quad \text{Eq (6.2)}$$

$$\sum_{j=i+1}^R F_j = K(\Delta_{i+1} - \Delta_i) \quad \text{Eq (6.3)}$$

Subtracting Eq(6.2) from Eq(6.3) and substituting K by $\frac{F_R}{(\Delta_R - \Delta_{R-1})}$ from Eq (6.1)

$$F_i = \frac{F_R}{(\Delta_R - \Delta_{R-1})} (2\Delta_i - \Delta_{i-1} - \Delta_{i+1}) \quad \text{Eq (6.4)}$$

Where,

R is the roof,

i,j are floor levels i and j.

6.4 Comparison Study

6.4.1 DRAIN-2D

DRAIN-2D was used to evaluate the role of structural modeling and load pattern on the behavior of the structure. In order to normalize the base shear, the weight of the structure was assumed equal to 2920 kN = 15% of the total building weight. The following parameters were used for all the structures unless specified otherwise. The residual strength of columns failing in shear was 2/3 of their maximum shear capacity. The concrete strength was 2.25 ksi or 90% of the specified design strength, and the steel strength was 80 ksi or 4/3 the specified design strength.

The effective stiffness of beams was based on half the moment of inertia using the concrete gross section and the columns on 70% of the gross section. The beam column joints were assumed rigid.

6.4.1.1 Frame Structure

The structure was modeled as frame FR shown in Fig 5.1 (Run 12 from Table 5.1). All other properties were as defined in section 6.4.1.

According to FEMA 273¹, for life safety, FR is required to sustain a drift, δ_t , defined by Eq.(6.5).

$$\delta_t = C_0 C_1 C_2 C_3 S_a \frac{T_c^2}{4\pi^2} g \quad \text{Eq. (6.5)}$$

C₀ is a modification factor to relate spectral displacement and likely building roof displacement¹;

C₁ is a modification factor to relate expected maximum inelastic displacements to displacements calculated for linear elastic response¹;

C₂ is a modification factor to represent the effect of hysteresis shape on the maximum displacement response¹;

C₃ is a modification factor to represent increased displacements due to dynamic P-Δ effects¹;

S_a is the response spectrum acceleration, at the effective fundamental period and damping ratio of the building in the direction under consideration¹;

T_e is the effective fundamental period in the direction under consideration¹.

For Ceyhan site,

$S_{XS} = 1.4$ g (spectral response acceleration at short periods);

$S_{X1} = 0.65$ g (spectral response acceleration at one-second period);

$T_0 = 0.6$ seconds (period at which the constant acceleration and constant velocity regions of the design spectrum intersect);

For FR, $T = 1.61$ seconds (from a dynamic analysis);

$C_0 = 1.46$ (FEMA 273 Table 3-2)

$C_1 = 1.0$ (FEMA 273 section 3.3.1.3, $T > T_0$);

$C_2 = 1.1$ (FEMA 273 Table 3-1 Performance Level = Life Safety);

$C_3 = 1.0$ (FEMA 273 section 3.3.1.3);

$S_a = 0.4$ (FEMA 273 section 2.6.1.5 at Ceyhan site);

$T_e = T$ (using the TRIANGLE pattern for FR structure, Fig.6.3).

Therefore, $\delta_t = 414.2$ mm

$\delta_t / H = 1.62\%$

Where H is the height of the building (25600 mm).

The results shown in Fig. 6.3 indicate that the load pattern has a great deal of influence on the base shear and the roof displacement of a frame structure. For the FR structure, the modal pattern, MODAL, which is supposed to include the contribution of more modes than the inverted triangle pattern, TRIANGLE, was the most conservative. The capacity and the stiffness of the structure were significantly

affected by the distribution of lateral forces. The softening of the structure can be observed after yielding was initiated in some elements.

The story drift and interstory drift using different load patterns had the same general shape. The magnitudes at the first story were significantly different (Figs. 6.4 and 6.5). It is likely that failure sequence and location of failing elements will be different for each load pattern.

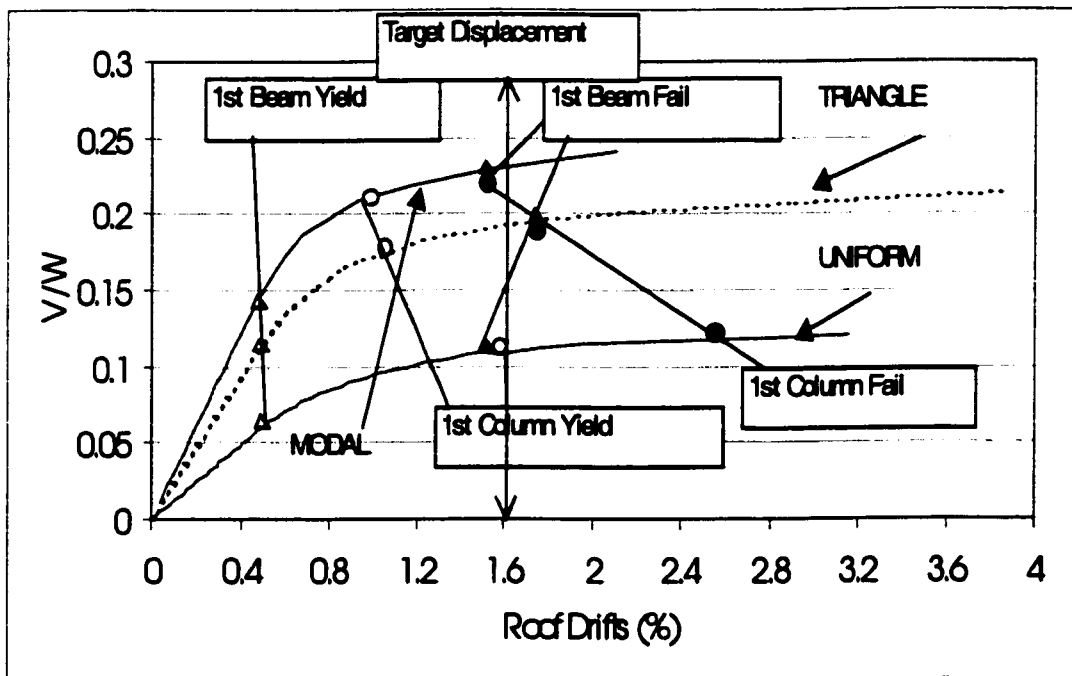


Figure 6.3 Base shear vs. roof drift for FR structure – Different load patterns

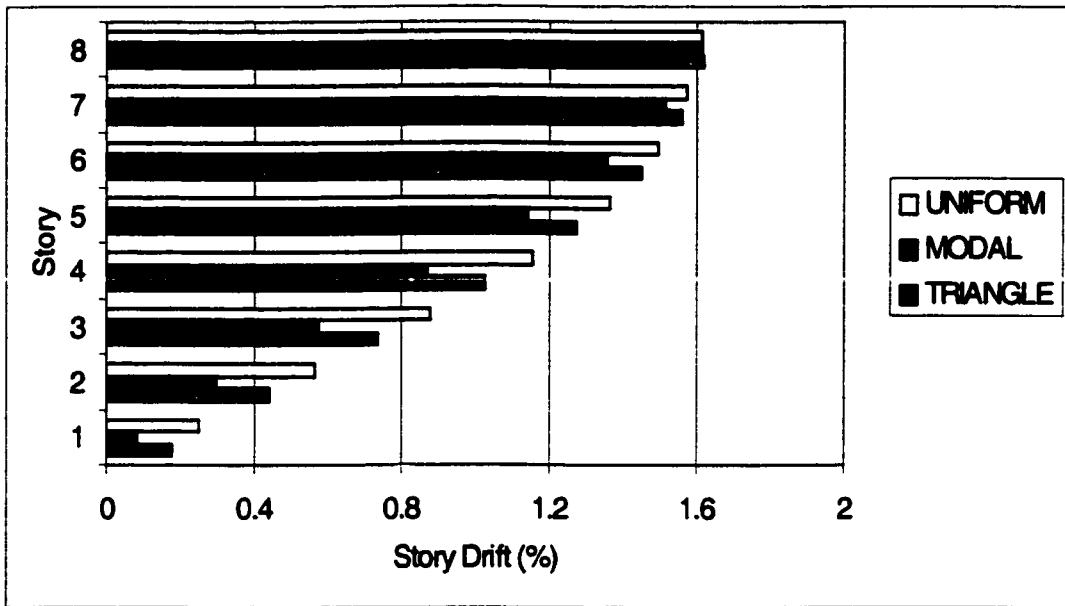


Figure 6.4 Maximum story drift for FR structure at a target roof drift (1.62%, from FEMA 273) – Different load patterns

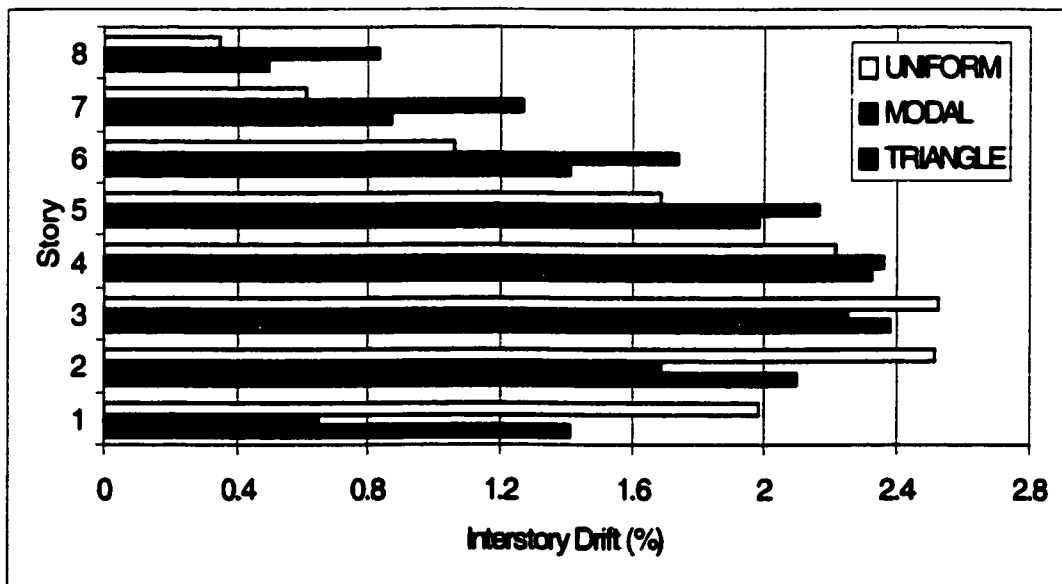


Figure 6.5 Maximum interstory drift for FR structure at target roof drift (1.62%, from FEMA 273) – Different load patterns

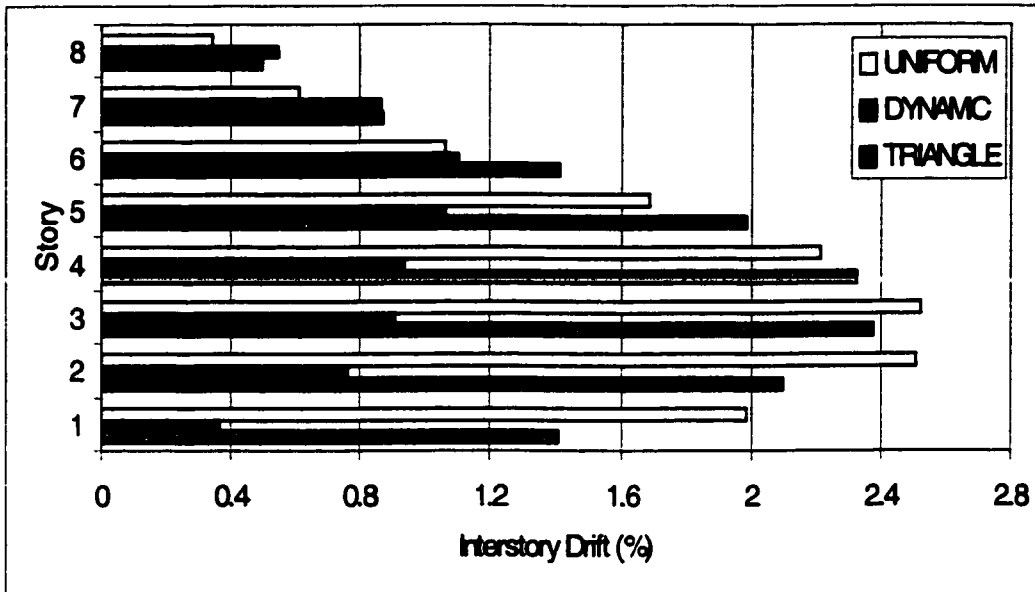


Figure 6.6 Maximum interstory drift for FR structure at target roof displacement.

Maximum interstory drifts for structure FR when roof target displacement was reached from pushover analysis using the inverted triangle pattern, TRIANGLE, are shown in Fig. 6.6. Also shown in Fig. 6.6 are the maximum interstory drifts from the nonlinear time history analysis and the pushover analysis using uniform pattern. Figure 6.6 indicates that, on most floors except the 7th and 8th, interstory drifts from pushover analyses (using different load patterns) were equal or larger than those from nonlinear time history analysis, suggesting that more damage in the structure is expected from pushover analyses than from nonlinear dynamic analysis. The pushover procedure may lead to more conservative design than nonlinear time history analysis.

6.4.1.2 Soft Story Frame Structure

The structure was modeled as a frame with infill walls from the second floor to the roof, SSS as shown in Fig 5.1 (Run 13 from Table 5.1). All other properties were as defined in section 6.4.1.

For SSS, $T = 0.95$ seconds (from Dynamic analysis);

$C_0 = 1.46$ (FEMA 273 Table 3-2)

$C_1 = 1.0$ (FEMA 273 section 3.3.1.3, $T > T_0$);

$C_2 = 1.1$ (FEMA 273 Table 3-1 Performance Level = Life Safety);

$C_3 = 1.0$ (FEMA 273 section 3.3.1.3);

$S_a = 0.68$ (FEMA 273 section 2.6.1.5 at Ceyhan site);

$T_c = T$ (using the TRIANGLE pattern for SSS structure).

Therefore, $\delta_t = 246.7$ mm, and

$\delta_t / H = 0.96\%$ is the roof drift that SSS must sustain for life safety according to FEMA 273.

Figure 6.7 shows that the pushover curve for SSS changed dramatically depending on the load pattern used. Stiffness and strength capacity seemed to be load pattern dependent. SSS failed before the target displacement determined from FEMA 273 was reached. The failure was in the analysis rather than in the structure: several elements failed causing the stiffness to become negative and analyses gave meaningless results. Because the analyses were conducted using DRAIN-2D, the

pushover was force controlled. Therefore, when failure was reached, even an infinitesimal increment of lateral load caused the program to fail.

Figures 6.8 and 6.9 show the maximum story and interstory drifts for SSS structure just before failure. All three load patterns resulted in the same shape of the story and interstory drift curves. As expected the first story drift was significantly larger than the second story values due to the soft first story (no infills) (Fig 6.9). The analyses indicated instability and loss of capacity, which is labeled “end of analysis” on the curves. Therefore, the results give no information regarding the strength of the structure. The largest interstory drift would be expected to occur in the soft first story. However, Fig. 6.9 shows larger drifts at higher levels in the structure. The reason could be attributed to the shear failure in columns at upper floors after infills failed at low base shear.

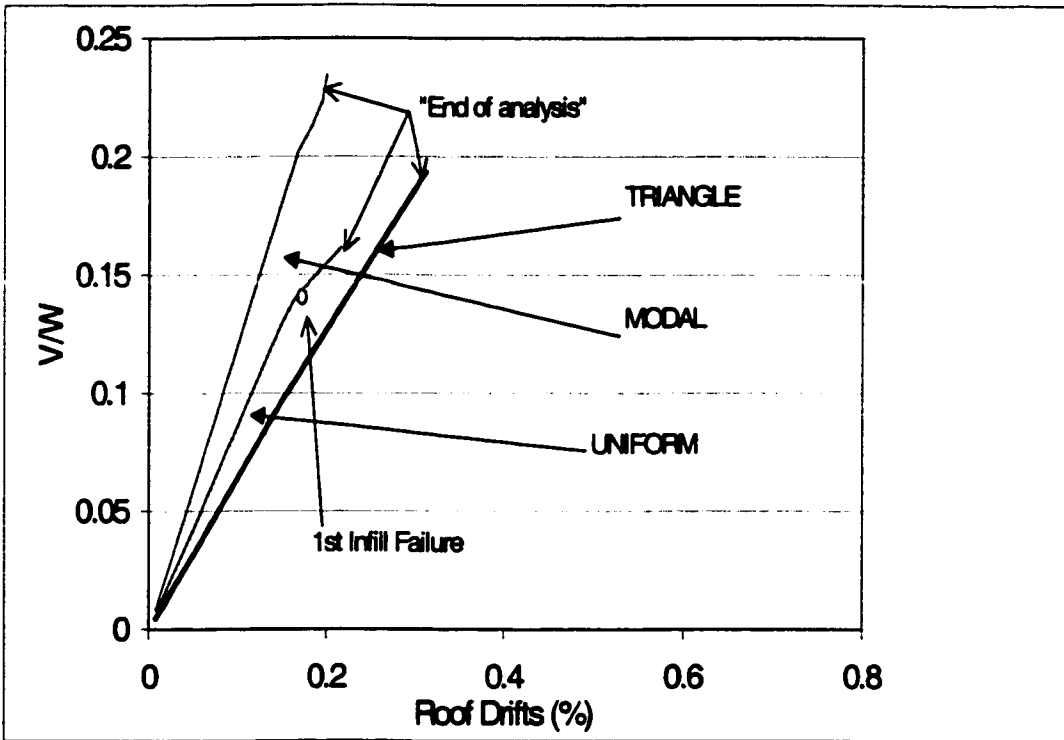


Figure 6.7 Base shear vs. roof drift for SSS structure – Different load patterns

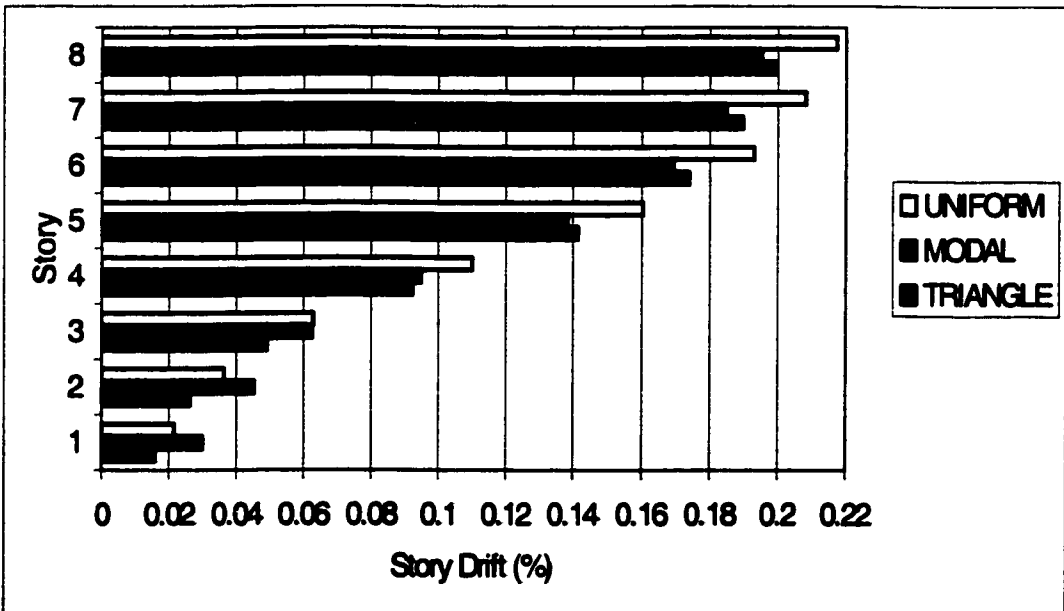


Figure 6.8 Maximum story drift for SSS structure – Different load patterns

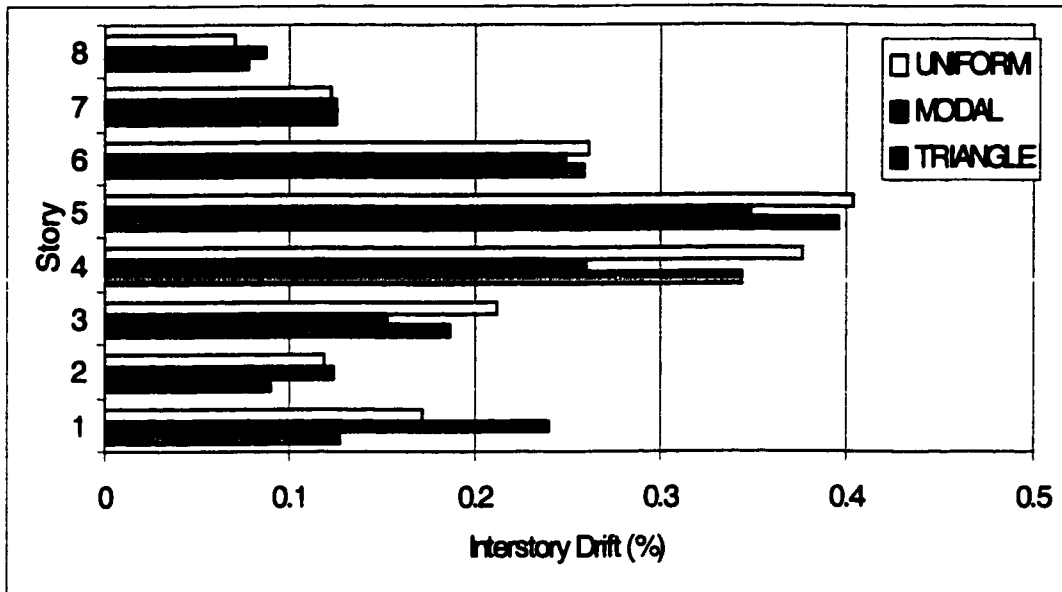


Figure 6.9 Maximum interstory drift for SSS structure – Different load patterns

Figure 6.10 shows the locations of “failure”(end of analysis) in SSS using the inverted triangle load pattern (TRIANGLE). As soon as one element failed, it triggered a load redistribution, which caused failure to spread instantaneously to other adjoining elements. The sequence of failure could not be determined as the analysis was interrupted when such instability occurred. However, the pushover analysis of SSS using the inverted triangle pattern indicated that column failure is likely on the 5th story after the infill walls reach a critical interstory drift of 0.4% (the reliability of this indication is questionable). This is in agreement with the nonlinear time history analysis of the same structure under the Ceyhan ground motions with peak ground acceleration of 0.45g. (See Fig. 5.28 SSS structure)

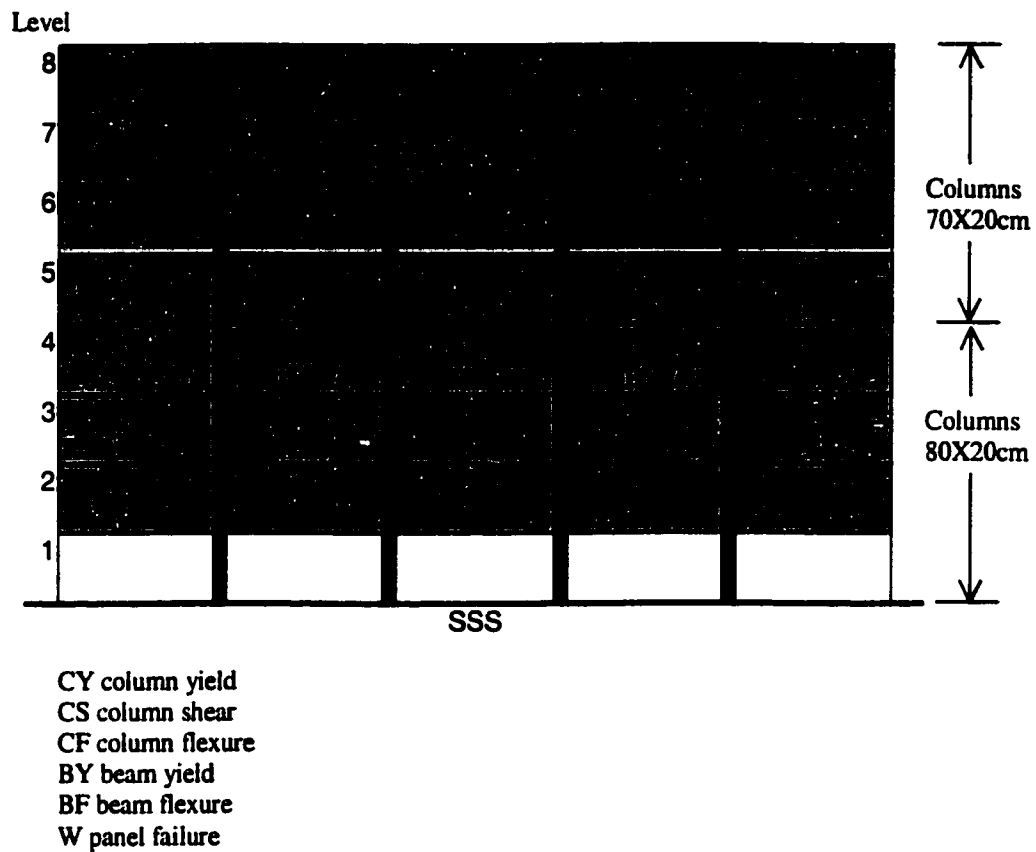


Figure 6.10 Locations of failure in SSS structure using TRIANGLE load pattern

6.4.1.3 All Infill Frame Structure

The structure was modeled as a frame with infill walls at all levels, AI (Run 15), as shown in Fig 5.1. The mass of the structure was assumed equal to 20% of the total building mass. All other properties were as defined in section 6.4.1.

For AI, $T = 1.05$ seconds (from Dynamic analysis);

$C_0 = 1.46$ (FEMA 273 Table 3-2)

$C_1 = 1.0$ (FEMA 273 section 3.3.1.3, $T > T_0$);

$C_2 = 1.1$ (FEMA 273 Table 3-1 Performance Level = Life Safety);

$C_3 = 1.0$ (FEMA 273 section 3.3.1.3);

$S_a = 0.62$ (FEMA 273 section 2.6.1.5 at Ceyhan site);

$T_e = T$ (using the TRIANGLE pattern for AI structure).

Therefore, $\delta_t = 272.6\text{mm}$, and

$\delta_t / H = 1.06\%$, is the roof drift that is required by FEMA for AI to satisfy life safety requirements.

It should be noted that the fundamental period for AI is larger than for SSS because the mass of AI is larger than that of SSS. However, for comparison with SSS, the base shear was normalized by dividing it by the same weight used in SSS, that is, weight was relative to the tributary area (FEMA 273).

Figure 6.11 indicates that the capacity of structure AI depended on the load pattern used in the pushover analysis. Using the inverted triangle pattern, TRIANGLE, the pushover curve for AI showed gradual softening of the structure as cracking, yielding and failure of some of its components were reached. A mechanism was reached at a displacement larger than the target displacement for life safety performance determined from FEMA 273. Using a UNIFORM pattern results in an instability of the analysis before the target displacement was reached (Fig. 6.11).

Maximum story drift from the nonlinear time history analysis, DYNAMIC, and at roof target displacement from pushover analysis using inverted triangle are

shown in Fig. 6.12. It can be seen that the pushover analysis using the inverted triangle pattern, TRIANGLE, and the nonlinear time history analysis, DYNAMIC, gave the same trend in story drift for structure AI. Infill panels failed when interstory drift reached 0.4%. Infill panels failed on the 4th story (Fig. 6.13) from both procedures, nonlinear dynamic and nonlinear static using inverted triangle load pattern causing the 4th story to become more flexible than the 3rd story (soft 4th story with respect to the 3rd). The increase in drift from the 3rd story to the 4th can be related to the softening of the 4th story after infill panel failure.

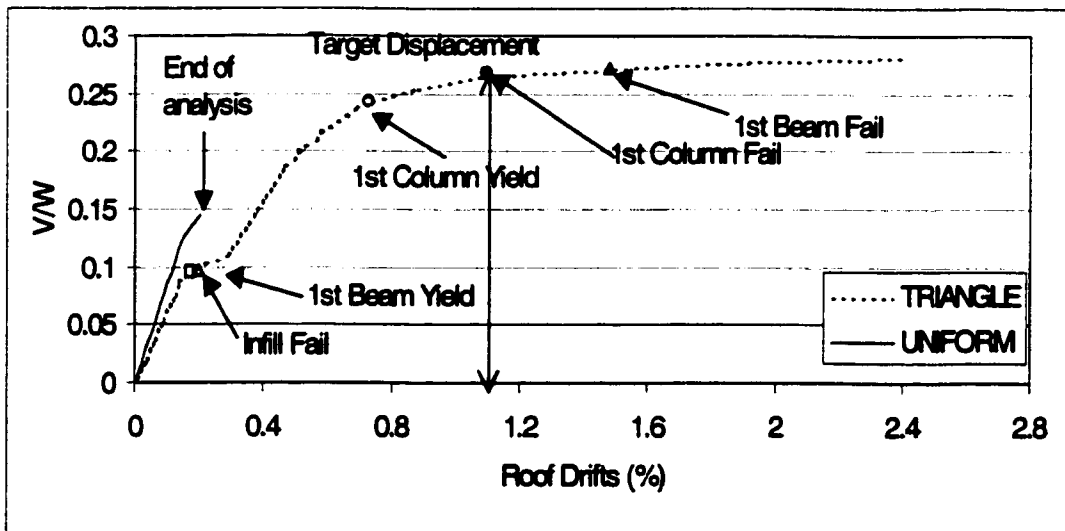


Figure 6.11 Base shear vs. roof drift for structure AI – Different load patterns

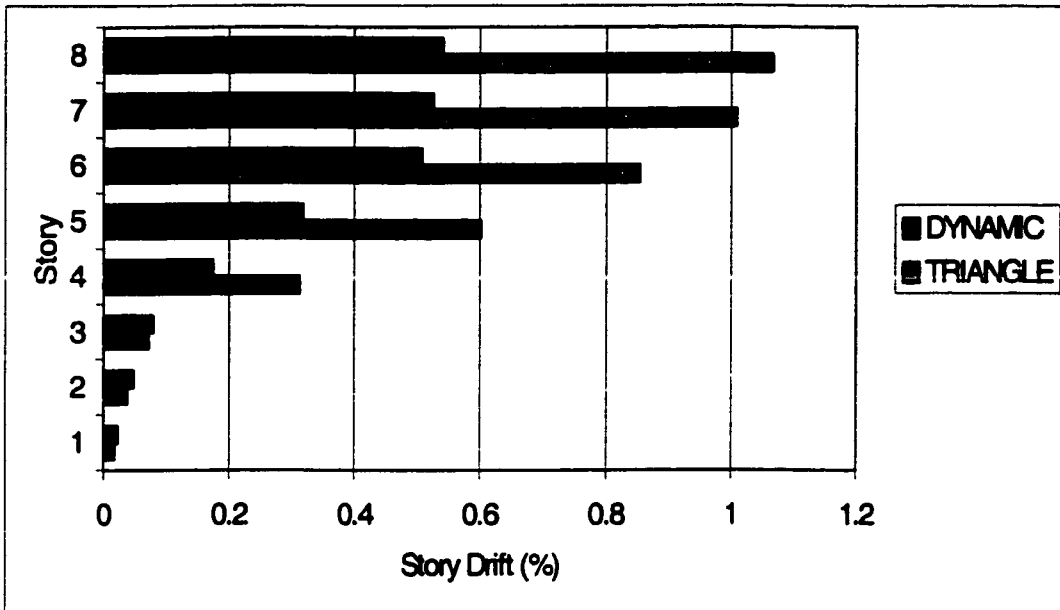


Figure 6.12 Maximum story drift for AI structure at roof target displacement

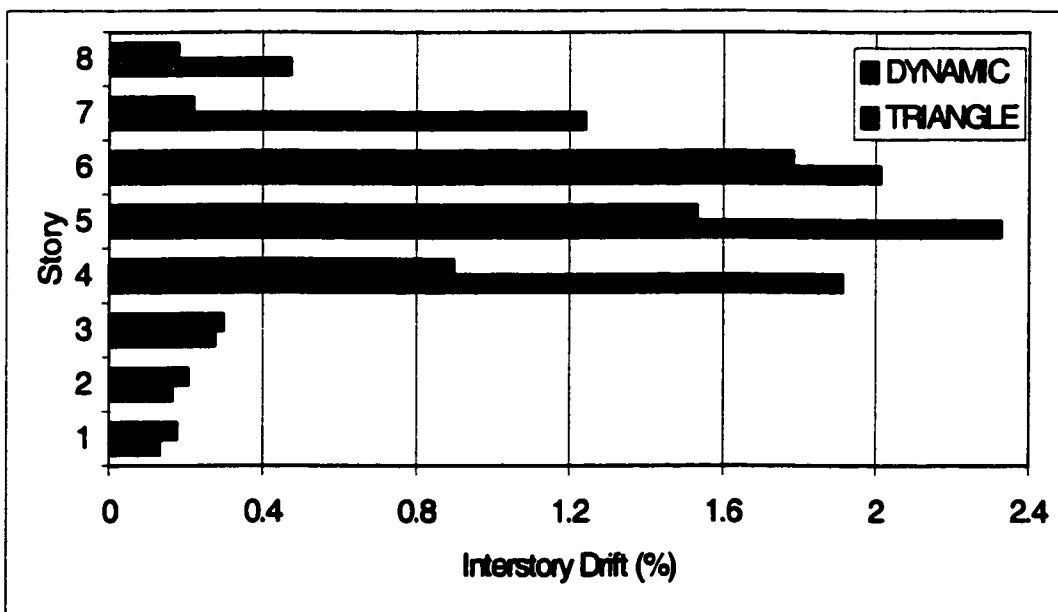


Figure 6.13 Maximum interstory drift for structure AI at roof target displacement

Maximum interstory drifts for structure AI when roof target displacement was reached from pushover analysis using the inverted triangle pattern, TRIANGLE, are shown in Fig. 6.13. Also shown in Fig. 6.13 are the maximum interstory drifts from the nonlinear time history analysis. Figure 6.13 indicates that the inverted triangle pattern produced infill failure at the upper floors, such failure can be indicator of weak upper story. Infill panels failed on stories where interstory drift exceeded 0.4%. It can also be seen that, on stories where infill panels failed, the interstory drift values from pushover analysis, TRIANGLE, exceeded those from the nonlinear time history analysis, DYNAMIC, suggesting that more damage in the structure is expected from pushover analysis than from nonlinear dynamic analysis. The pushover procedure may lead to more conservative design than nonlinear time history analysis.

Interstory drifts for structure AI are shown in Fig. 6.14 at the time when the maximum roof drift was reached during a non-linear time history analysis, DYNAMIC. The dynamic and the static analyses gave a similar pattern of interstory drift, however, the values of the drifts were very different. Hence, using the base shear versus roof drift to approximate damage is too simplistic and therefore its accuracy is questionable particularly when higher mode effects are not negligible.

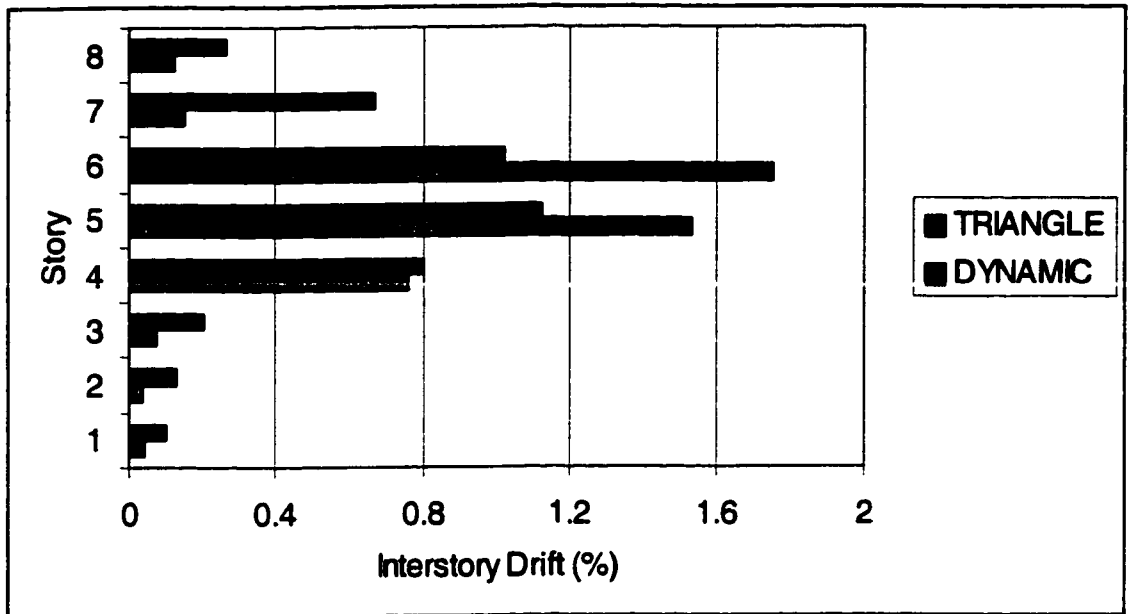


Figure 6.14 Interstory drifts for structure AI at maximum roof drift during nonlinear time history analysis, DYNAMIC.

Figure 6.15 shows the location of failure that was produced in structure AI when the structure was increasingly pushed, using the inverted triangle load pattern, until a mechanism was formed. Shear failure in columns was identified in the pushover analysis of structure AI. However, the location of failure occurred on the 4th story (Fig. 6.15), while column shear failure was identified on the 6th floor from the dynamic analysis. The difference in prediction of the failure sequence between dynamic and pushover analysis may be attributed to higher mode effects that could not be reproduced with a load pattern that has the same shape throughout the load history. Failure would be expected at the first story in a static pushover analysis. However, the contribution of infills to the shear strength at the base of the structure

and the failure of the infill panels at the upper floors at low base shear might have been the reason why column shear failure occurred on the 4th story level.

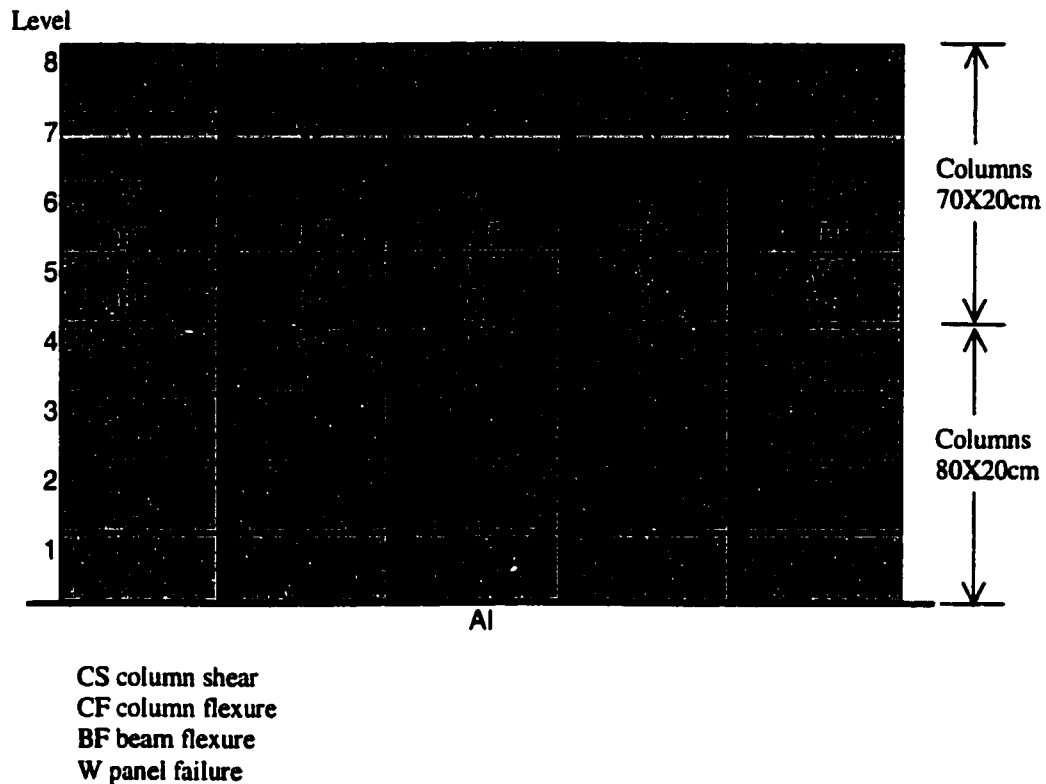


Figure 6.15 Location of failure in AI structure using inverted triangle load pattern, TRIANGLE.

6.4.1.4 Residual Strength

Two sets of models were considered for this section. The first set comprised two structures SSS (Runs 13 and 16) and the second two structures AI (Runs 15 and 17) having the same characteristics except for the residual strength of columns failing in shear. The analyses were performed using DRAIN-2D which is capable of

force controlled analyses only. When column shear failure occurred for both structures SSS and AI, the stiffness of the structure was negligible (Figs. 6.7 and 6.11), deflections were very large and the results were not reliable. The analysis was interrupted due to instability.

6.4.1.5 Geometric Variations

Two models, SSS (Run 19) and FSS (Run 20), having the same characteristics except for the column layout, were analyzed. SSS was a soft story frame structure with infill walls from the 2nd floor to the roof and the long direction of the interior four columns in the plane of the frame (Fig. 5.1). FSS was a soft story frame structure with infill walls on the 2nd floor to the roof and the long direction of the interior four columns normal to the plane of the frame (Fig. 5.1).

Inverted triangle and uniform load pattern were used for pushover analysis and the results are shown in Figs. 6.16 and 6.17. The capacity curves showed that SSS is stiffer than FSS and has a higher base shear capacity (Figs. 6.16 and 6.17). Flexural failure at both ends of all the columns on the third story in FSS was reached using inverted triangle load pattern and could be identified from the large interstory drift at the 3rd story in Fig. 6.18. Since the columns at the 1st story level have the same capacity as those on the 3rd level, failure would be expected at the lower floor. However, the analysis was ended abruptly. Therefore, the results may be questionable. The failure determined from the pushover analysis was reached at a

roof drift of 0.18%, while the building sustained a roof drift of 0.64% with no flexural failure during the nonlinear time history analysis using the Ceyhan earthquake record. Flexural yielding of exterior columns on the 5th story was observed in the nonlinear time history analysis. The discrepancy in the sequence of failure between the dynamic and the static analyses may be attributed to higher mode effects that are vaguely approximated with the inverted triangle loading. Uniform loading predicted flexural failure on the 5th story exterior columns only.

It should be noted that the capacity curves in Figs. 6.16 and 6.17 are terminated at the points shown. In reality, the program generated larger displacements, but failure caused the analysis to be unstable.

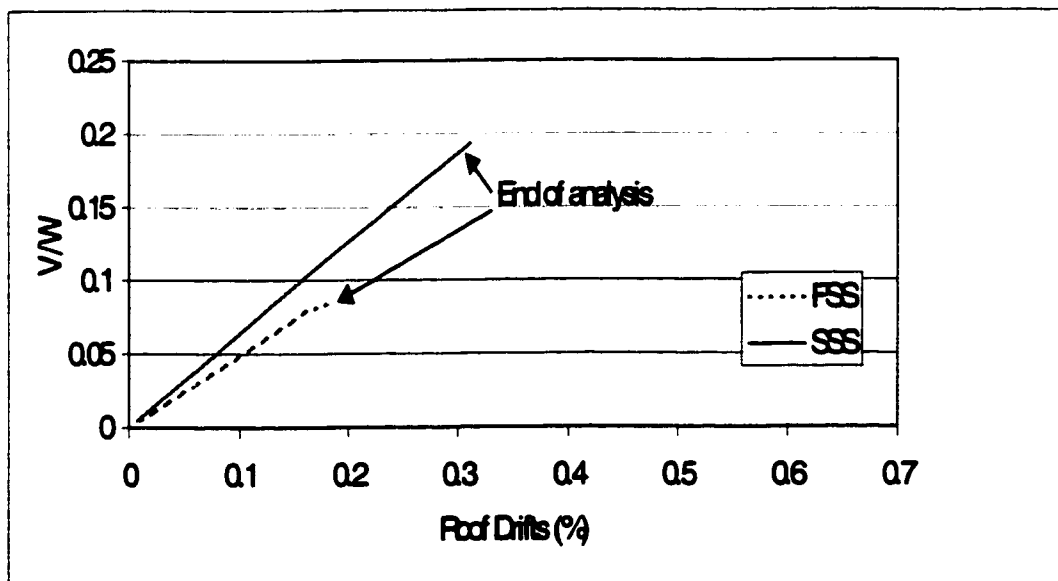


Figure 6.16 Base shear vs. roof drift for SSS and FSS using inverted triangle load pattern

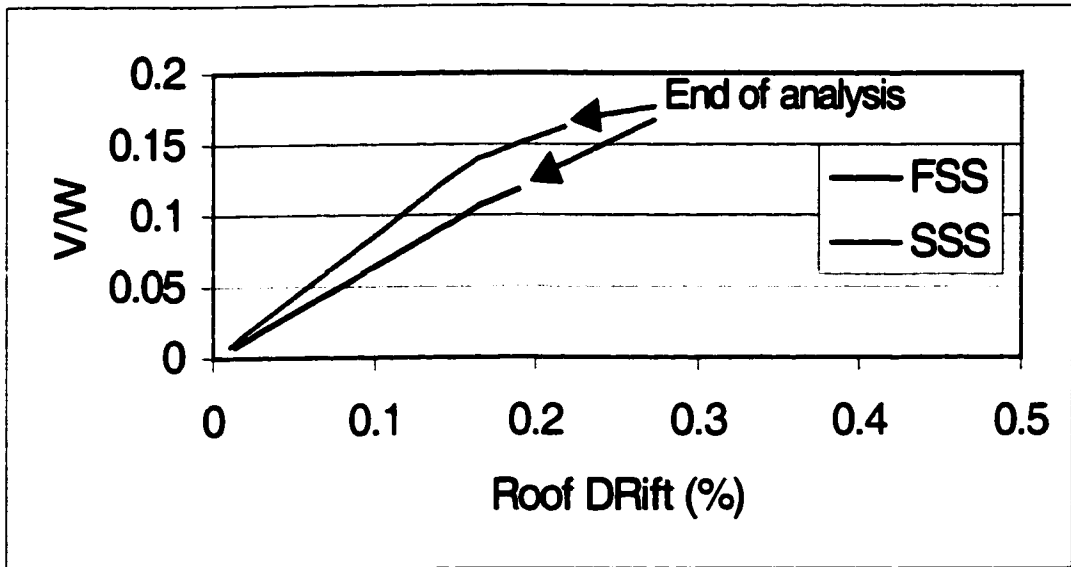


Figure 6.17 Base shear vs. roof drift for FSS and SSS using uniform load pattern

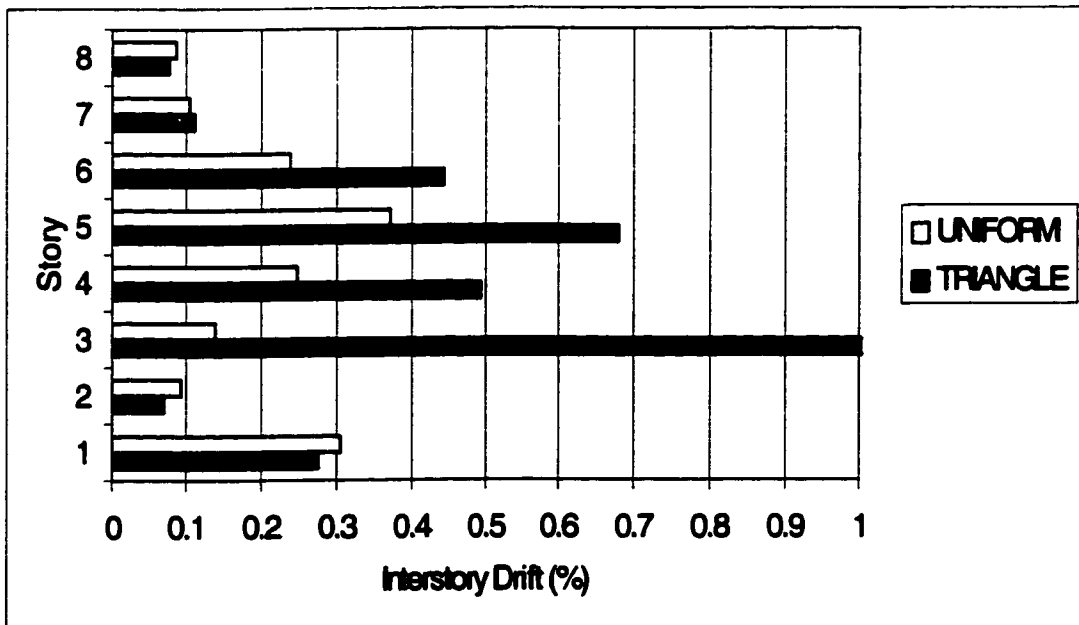


Figure 6.18 Maximum interstory drift for FSS using inverted triangle and uniform load patterns

6.4.2 SAP2000

A user-friendly program with visualizing capacities such as SAP2000 has been used in design. In this section, the results using SAP2000 were compared to the results from DRAIN-2D.

6.4.2.1 Modeling Assumptions

It was found that the SAP2000 package is still incomplete for performing pushover analysis on buildings with panel (shell) elements. In SAP2000, Pushover analysis can be applied to frame structures only. Inelastic behavior is limited to beams, columns and truss elements.

Structure FR was analyzed using SAP2000. Geometric characteristics and material properties were input and the program determined the inelastic hinges. The same modeling assumptions as in DRAIN-2D were used, namely that hinge rotations occurred at the end of the elements and shear hinges in columns were located in the middle of the column element. A large discrepancy in the results was found due to the shear capacity calculated in SAP2000. The shear capacity V_{max} computed using SAP2000 is given by Eq. (6.6)

$$V = 2 \frac{A_g}{1.2} \sqrt{f_c'} \quad \text{Eq. (6.6)}$$

Where A_g = concrete gross area;

f'_c = concrete strength.

This value of shear is only an approximation of the concrete contribution to the shear capacity of the structure. The shear capacity of a typical column in the lower floors of FR is 284 kN from hand calculations using ACI318-95 code⁹, and 88.6 kN from SAP2000 calculations. Therefore, the hinge properties used in SAP2000 were input by hand.

6.4.2.2 Results

Figure 6.19 shows that DRAIN-2D and SAP2000 gave the same results until the maximum capacity of members was reached. The discrepancy between DRAIN-2D and SAP2000 may be explained by two reasons:

- SAP2000 allows deformation-controlled analysis. The analysis is stopped when a target displacement is reached or a mechanism is formed. Thus, for increasing displacements, lower values of base shear may be obtained, DRAIN-2D is force controlled. Therefore, an increase of base shear is associated with an increase in displacement and analysis is stopped when a target base shear is reached or a mechanism is formed.
- The model used in DRAIN-2D has no limitations on the plastic rotation. SAP2000 allows limiting the plastic rotation as shown in Fig. 6.20.

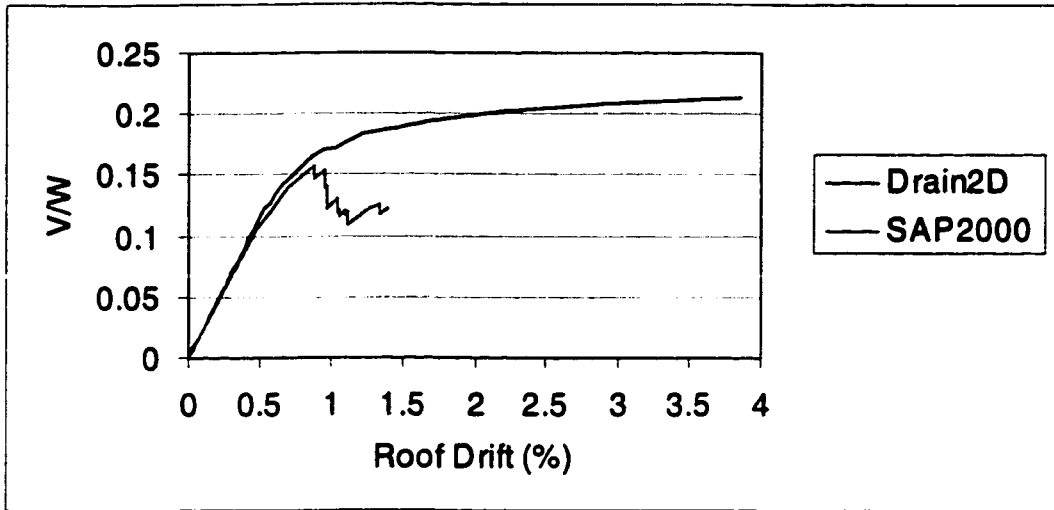


Figure 6.19 Base shear vs. roof drift for FR using SAP2000 and DRAIN-2D

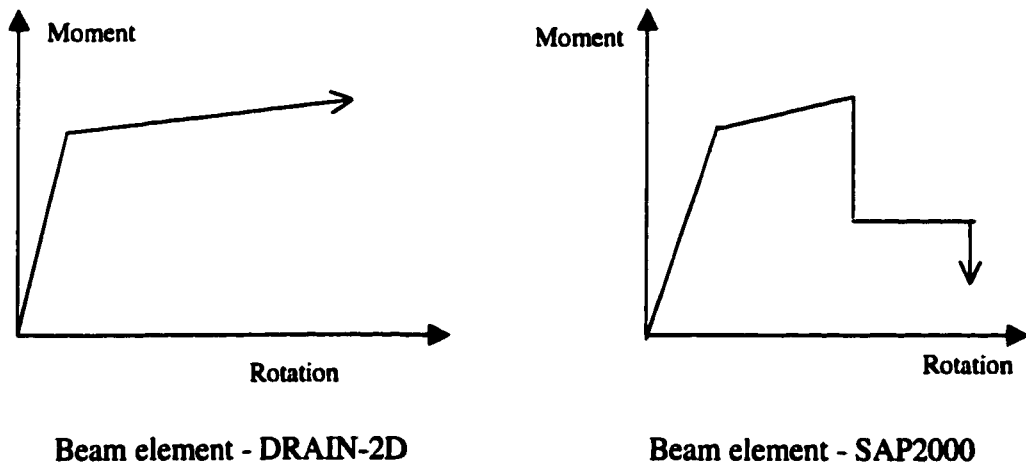


Figure 6.20 Force deformation characteristics

For the same model and same hinge properties, the run time for the pushover analysis using SAP2000 was more than 10 times longer than running a time history analysis with a ground motion record of 3000 points using DRAIN-2D. SAP2000 is

certainly easier to use than DRAIN-2D but the package is not complete yet, and some calculation subroutines, particularly for section properties need to be verified.

In summary, pushover analysis may not be as simple as has been assumed by many users. It is sensitive to the properties of the components of the lateral force resisting system and the load pattern. Section properties are needed as in a nonlinear time history analysis. A constant load pattern may underestimate the effect of higher mode effects. A load pattern that varies as the structure undergoes cracking and yielding (modal adaptive) is site dependent as is the ground record input in dynamic analysis. Therefore, the author believes that non-linear static analysis cannot reliably replace nonlinear dynamic analysis.

CHAPTER 7

RETROFIT AND PERFORMANCE ENHANCEMENT SCHEMES FOR THE PROTOTYPE BUILDING

7.1 General

In the previous chapters, it was shown that a non-linear dynamic or static analysis is expected to be sensitive to structural characteristics and site specific ground motions or seismic properties. In this chapter, structural characteristics of the building were chosen such that it would represent, as closely as possible, a typical building. The Ceyhan ground motion record was used. Evaluation of the performance of the building was conducted and different possible retrofit and enhanced design schemes are presented.

7.2 Performance of a Typical Building

7.2.1 Modeling Assumptions

Simple models were used to represent the nonlinear behavior of beams, columns, infill panels and shear walls.

Beam-column connections were assumed rigid. As shown in Fig. 7.1 beams were modeled as bilinear elements with no limit on the deformation capacity. The linear degradation of beam strength was ignored to avoid instability in the analyses

due to negative stiffness. Therefore, maximum plastic rotations of elements had to be checked to determine the reliability of the results.

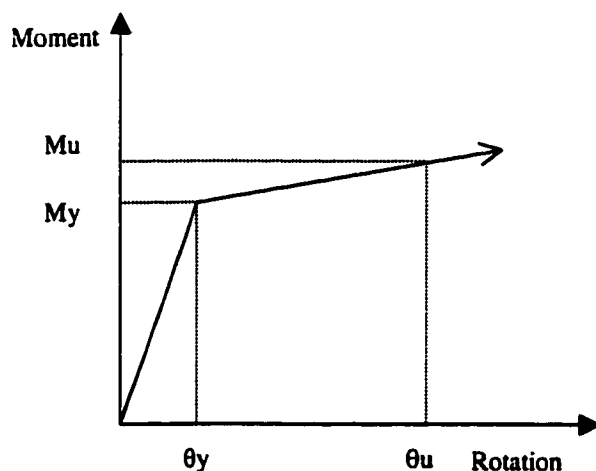


Figure 7.1 Load-Deformation characteristic for a beam

The load-deformation characteristic for columns failing in shear is shown in Fig. 7.2. The residual strength is expressed in the analysis as a fraction of the maximum strength. The residual strength level is an upper bound on the column capacity for all deformations greater than those at which the peak is reached. This model was first suggested by Li et al.¹⁴, and is referred to as the parallel element model. The parallel element was detailed in section 4.3.1.2 and summarized in Fig. 7.3. This model is acceptable if the column fails when the moments at its ends are both below their yield value. In some instances, a column shear might reach a maximum value when one end of the column has reached flexure yield (Fig. 5.27).

The parallel element model was modified so that boundary conditions could be respected and the inconsistency removed. The inconsistency in the original parallel element model occurs when element2 fails after element1 goes into plastic range. Since element1 and element2 are comprised between the same nodes, the plastic rotation at one end should be the same for both elements 1 and 2. The modified parallel element is shown in Fig. 7.4.

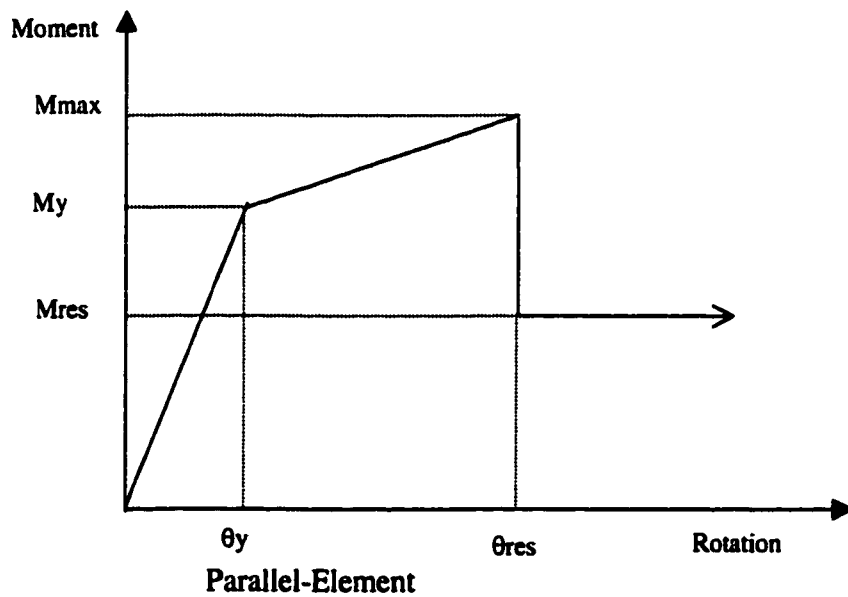


Figure 7.2 Load-Deformation characteristic for the parallel element

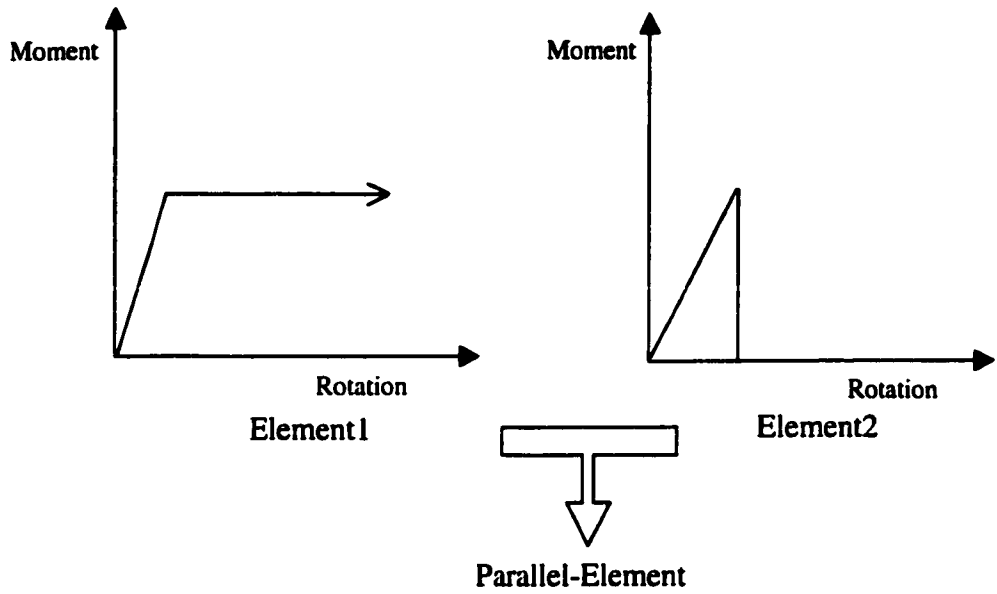


Figure 7.3 Original Parallel-Element¹⁴

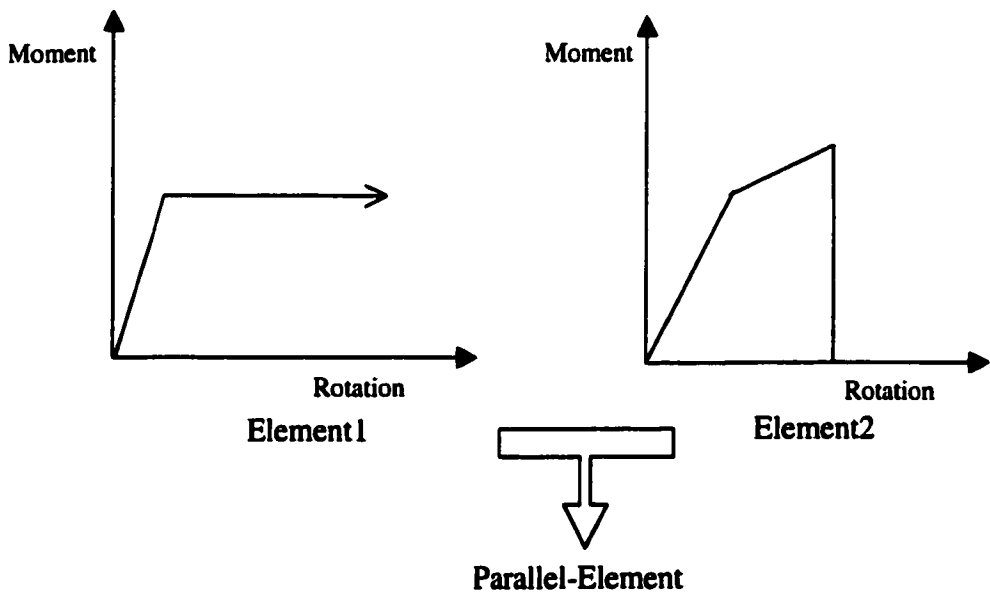


Figure 7.4 Modified Parallel-Element

The model used for the infill panels is shown in Fig.7.5. The infill panel is assumed to have shear stiffness only. The strain hardening is assumed equal to 1% of the initial stiffness and the strain at failure was assumed equal to 0.4% (FEMA 273). The infill panel element can not be used to represent “accurately” a shear wall because the flexural stiffness of a shear wall is not negligible.

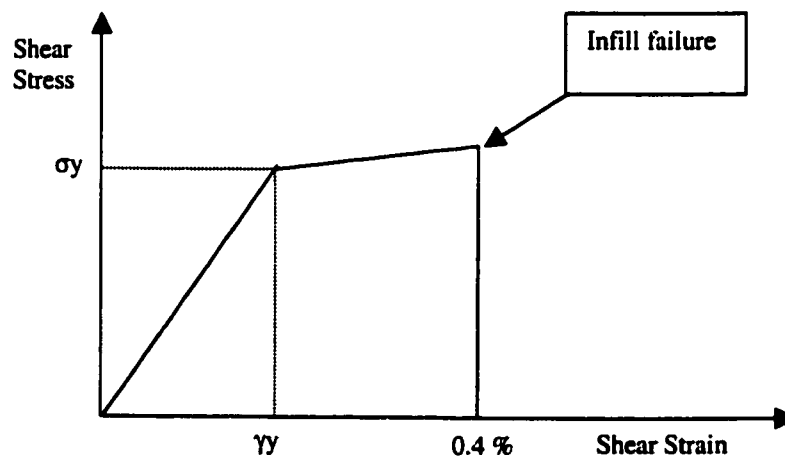


Figure 7.5 Stress-Strain characteristic of infill panel element³

7.2.2 Input and Building Description

A frame structure with infill walls from the 2nd floor to the roof (SSS structure Fig. 5.1, Run 13 from Table 5.1) was analyzed. Material strengths were taken as 2.25 ksi or 90% of the nominal design strength for concrete and 80 ksi or 4/3 the design strength for reinforcing steel. The effective stiffness was assumed $0.5E_cI_g$ for beams and $0.7E_cI_g$ for columns. Beam-column joints were assumed rigid

and fixed end moments were computed at the face of the connection. The residual strength of columns susceptible to fail in shear was assumed equal to $2/3$ the maximum strength capacity. The mass attributed to the frame was assumed equal to 15% of the total building mass (based on tributary area). Geometric aspects and orientation of sections were as described in chapter 3. The foundation was assumed to be rigid. The building was subjected to the ground shaking record from the Ceyhan Earthquake. The magnitude of ground accelerations was scaled to achieve a peak ground acceleration of 0.2g, 0.25g and 0.45g. The performance of the structure was evaluated for each of the peak ground accelerations.

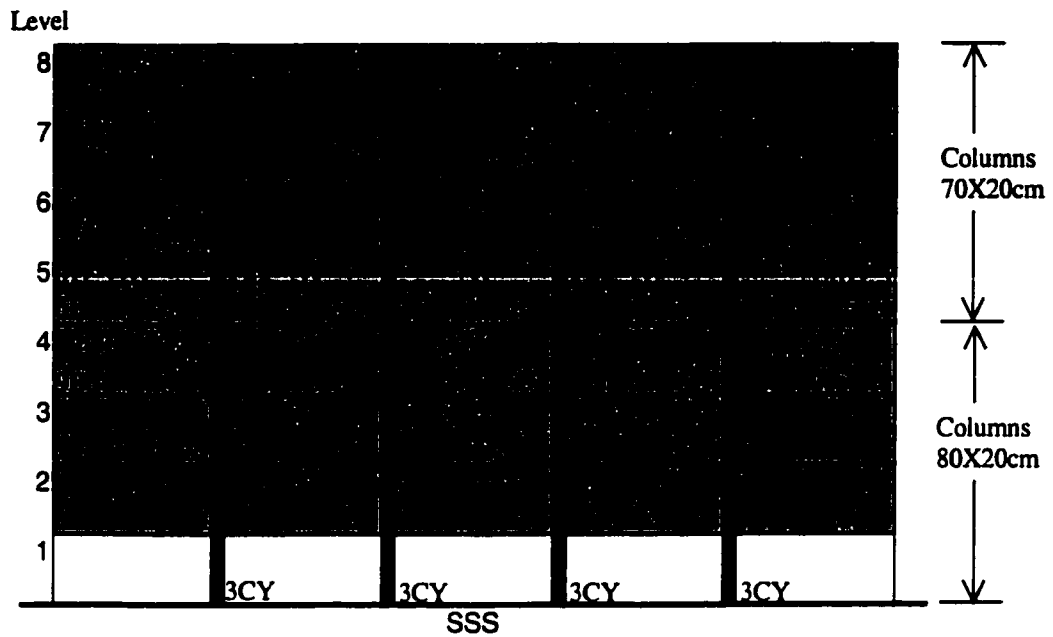
7.2.3 Results

When the structure was subjected to the Ceyhan ground acceleration with 0.2g as a peak, the structure experienced minor damage to structural elements. The infill walls between the 4th and the 7th floor failed, while beams on the 5th floor yielded. The columns did not yield at any location.

When a 0.25g peak Ceyhan ground acceleration was used, beams on the 5th and on the 6th floors reached yield. The interior four columns also yielded at the base of the structure. The infill walls between the 4th and the 7th floor failed. The inelastic deformations of all structural members were still within the life safety range for the acceptance criteria given in FEMA 273¹.

Using the ground acceleration record from the Ceyhan earthquake scaled to a peak of 0.45g, SSS sustained structural damage and the structure did not meet the acceptance criteria for life safety in FEMA 273. Infill walls between the 4th and the 7th floor failed. Beams on the 5th and 6th floors reached yield. On the 5th story, the interior four columns failed in shear and the exterior columns reached yield at the top end. Figure 7.6 shows the failure sequence and location in SSS subjected to 0.45g peak ground acceleration from the Ceyhan earthquake.

Column shear failure on the 5th story was observed when a peak ground acceleration of 0.4g or higher was used.



The number preceding the notation shows the sequence of events.

Figure 7.6 Failure sequence in SSS structure – Ceyhan Earthquake with 0.45g peak ground acceleration.

Figures 7.7 to 7.10 indicate that base shear or roof displacement are not proportional to the peak ground acceleration. After the structure had sustained some damage from yielding and/or failing elements, its behavior ceased to be linear and it had a longer period. It was found that, with a peak ground acceleration of 0.2g, only beams on the 5th floor yielded and Fig. 7.10 shows significant interstory drifts on stories 4 and 5. With 0.25g peak acceleration, beams on the 5th and 6th floors yielded and Fig. 7.10 shows large interstory drifts on stories 4, 5 and 6. With 0.45g peak

acceleration, beams on the 4th and 5th floor yielded, column shear failure occurred on the 5th story and Fig. 7.10 shows the largest interstory drift at the 5th story.

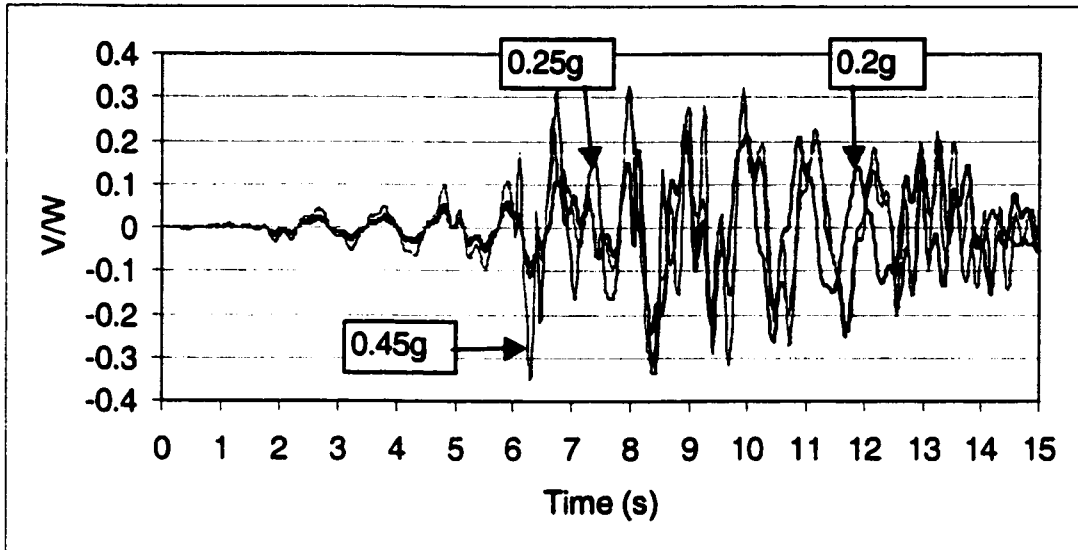


Figure 7.7 Time history of base shear for SSS structure – Different peak ground accelerations.

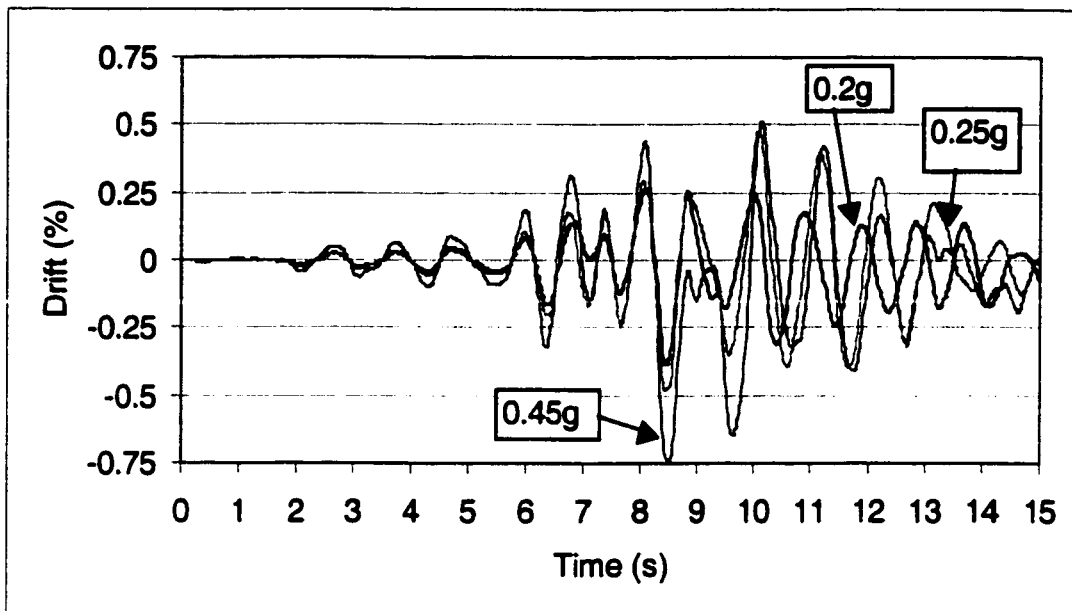


Figure 7.8 Time history of roof drift for SSS structure – Different peak ground accelerations

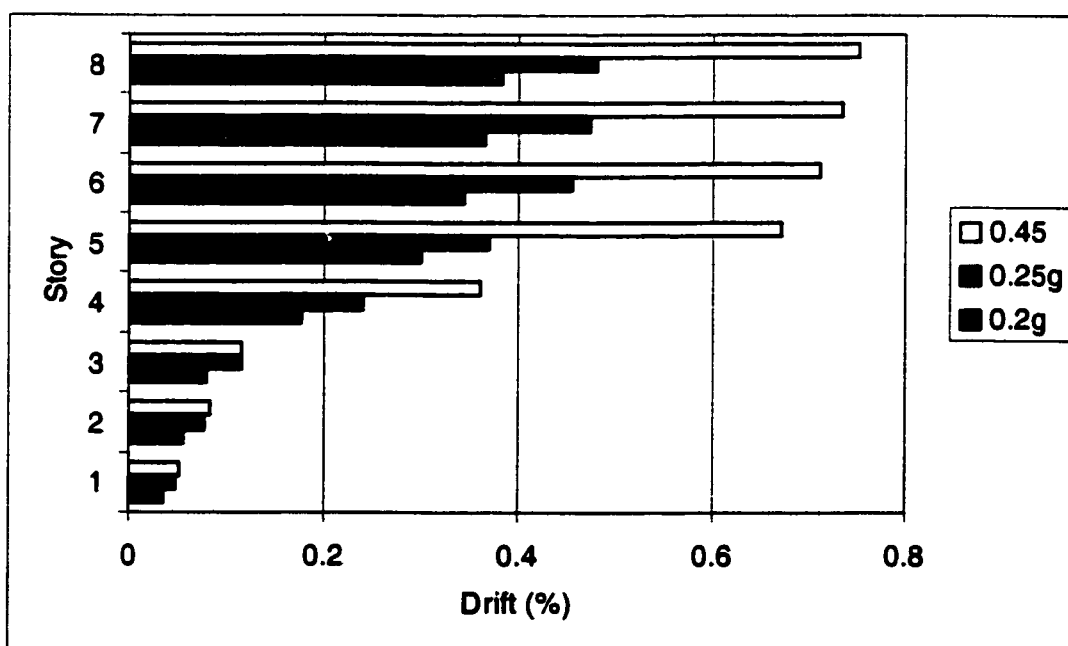


Figure 7.9 Maximum story drift for SSS structure – Different peak ground accelerations

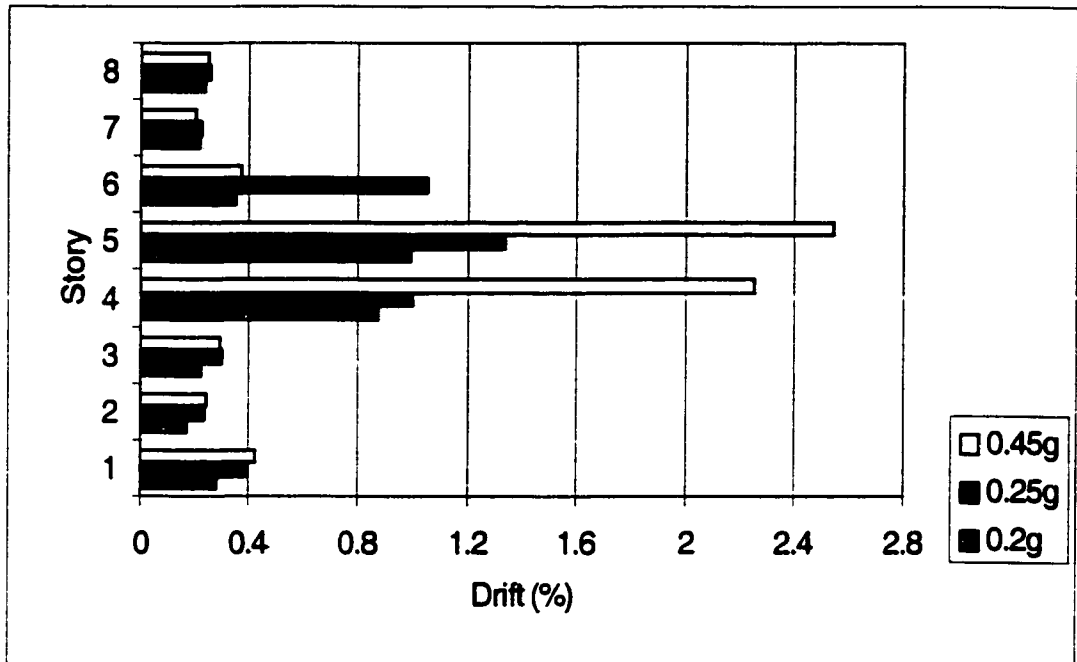


Figure 7.10 Maximum interstory drift for SSS structure – Different peak ground accelerations

From Fig. 7.11, it can be observed that failure on upper floors was independent from the base shear. Column shear failure on the 5th story occurred when the interstory drift on this story reached 0.75% for the first time. The failure corresponded to the first peak roof displacement.

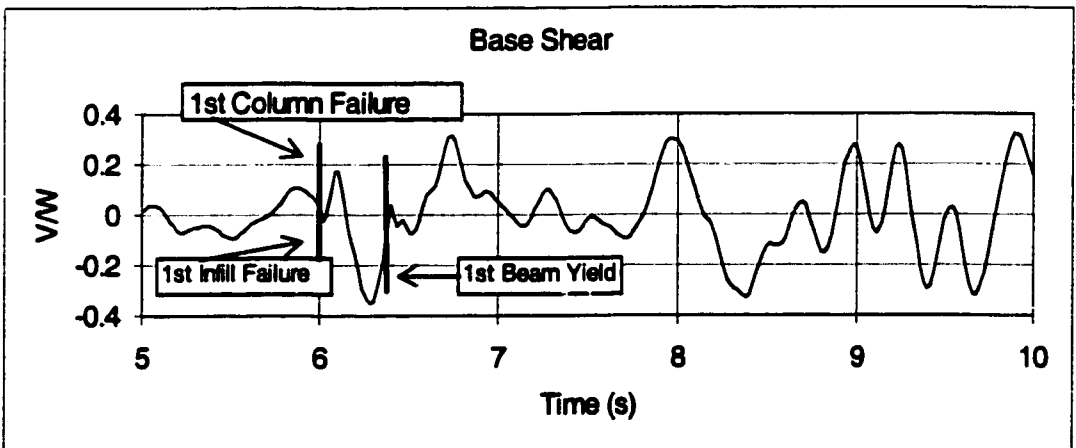
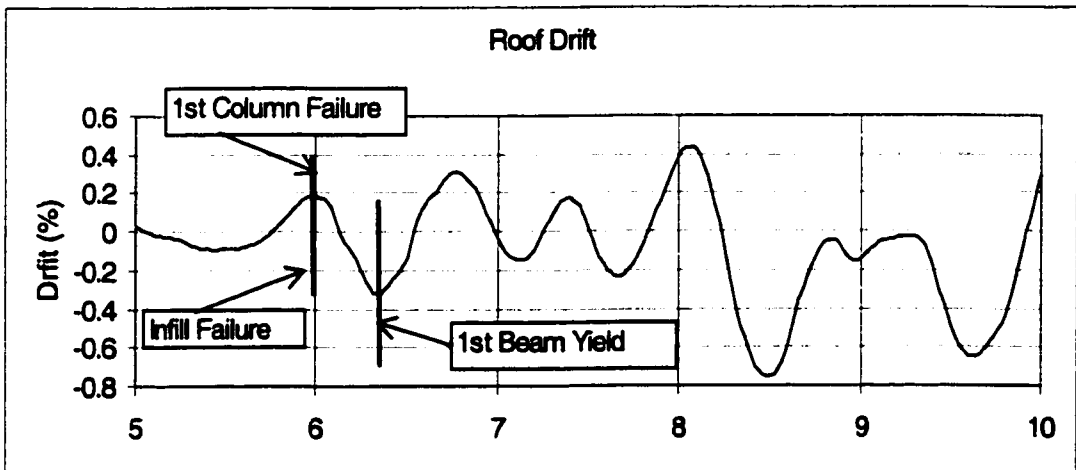
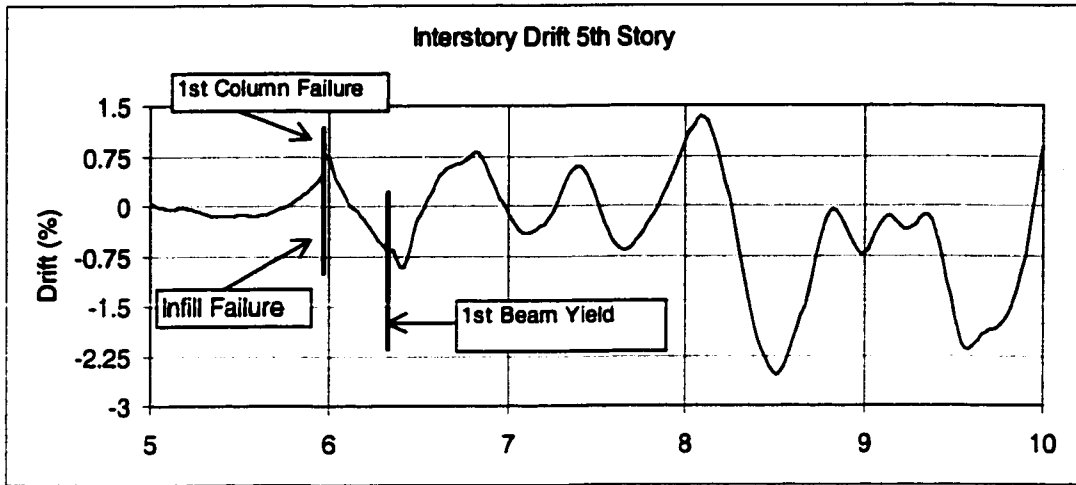


Figure 7.11 Sequence of failure in structure SSS with 0.45g peak ground acceleration from the Ceyhan Earthquake

Figure 7.12 displays the time history of roof drift and the time history of the interstory drift between the 5th and 6th floors (interstory drift on the 5th story) when SSS was subjected to the Ceyhan ground accelerations with a peak value of 0.25g. Note that roof drift was normalized by dividing the roof displacement by the height of the building, and the interstory drift on the 5th story was normalized by dividing the differential displacement of the 5th and 6th floor by the height of the 5th story. It can be observed that an interstory drift larger than 0.75% was reached on the 5th story and no shear failure was observed. Although, it is believed that damage/failure is related to interstory drift⁴⁸, the observation just mentioned proves that interstory drifts are not enough to determine failure.

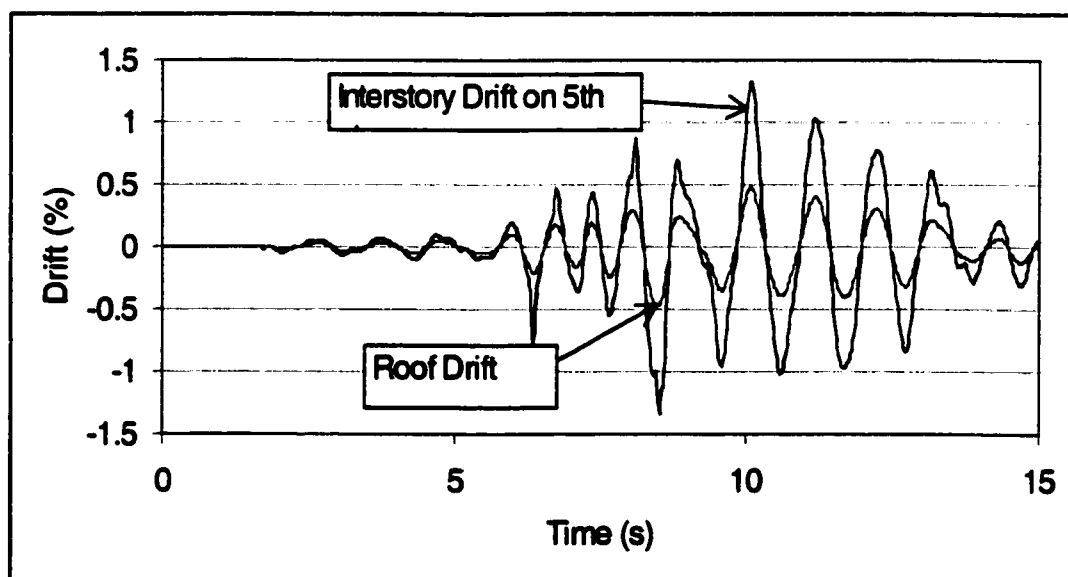


Figure 7.12 Time history of roof drift and 5th story interdrift for SSS with 0.25g peak ground acceleration from the Ceyhan Earthquake.

7.3 Retrofit

7.3.1 Conditions

The extensive damage and economic losses which occurred during the 1994 Northridge and other recent moderate earthquakes have promoted structural engineers to consider protecting economic investment in addition to meeting life safety requirements of structures.

The damage may be due to strength deficiency, inadequate stiffness or lack of deformation capacity. Appropriate retrofit systems have been developed in research and used in practice to enhance the performance of structures. FEMA 273 provisions and guidelines were developed to serve as guidance to the seismic evaluation and rehabilitation of structures^{1,70}.

7.3.2 Design Strategy for Seismic Retrofit

The choice of a retrofit scheme depends on economic, architectural, structural and feasibility constraints. In this section, structural aspects in the design strategy for retrofit are discussed. Retrofit strategy serves to determine whether strengthening, stiffening, or enhancing the deformation capacity or a combination of all three is needed to retrofit the structure. In order to select a retrofit strategy, it is necessary to establish the performance objectives desired for the building and the existing deficiencies. ATC 40⁷⁰, a document developed by the Applied Technology Council, provides guidelines for the selection of a retrofit strategy.

In most cases, strengthening and stiffening of a structure are inseparable. The effect of this retrofit strategy is expected to lower the lateral deflection of the structure and to increase its capacity.

Enhancing the deformation capacity of a structure is produced by increasing the ductility of the structural components or by the application of base isolation. Enhancing the ductility of structural components is adequate if only a few existing elements are deficient. Base isolation is efficient if the structure is very stiff with respect to the base isolation components.

7.3.3 Retrofit Options/Techniques

A retrofit system or technique is a specific method used to achieve a selected strategy. Based on the objectives of the building owner, the current state of the structure and the economic constraints, retrofit techniques may target strengthening, stiffening or enhancing the deformability of the structure. Techniques that are commonly used include, base isolation, addition of mechanical dampers (energy dissipation devices), addition of structural walls or braces, element jacketing and ultimately, demolition of part of the structure or reducing the stiffness of some elements.

Base isolation is an expensive technique. It is suitable for stiff structural systems. The theory of base isolation is founded on concentrating the inelastic

deformation at the base in the special elements or isolators, and reducing the seismic demand by lengthening the fundamental period of the structure.

Mechanical dampers are typically installed as part of a bracing system. They are most effective in structures with significant deformation capacity. They are intended to increase viscous damping in the structure and hence, reduce seismic demand and increase the energy dissipation capacity of the structure.

Element jacketing can be used for both concrete and steel frame elements. Jacketing can provide an increase in strength, stiffness and ductility⁷¹. When elements are jacketed, the structural system of the retrofitted building remains unchanged.

Bracing is extensively used in steel frame structures and can be used for concrete frame structures also. The use of bracing was found to improve the lateral stiffness and strength a structure^{15, 72}. However, the ductility of a braced frame relying on both tension and compression in the braces may be unreliable and such systems should be used with caution⁷².

The addition of structural walls or infill panels is a common technique for improving lateral strength and stiffness. Connecting the additional wall elements is essential in transferring the lateral forces between the wall and the existing structural elements. Therefore, quality control is of primary importance. In an infill wall scheme, existing columns act as boundary elements and therefore are subjected to large compressive or tensile axial forces. Consequently, the benefits of adding infill

walls will be limited by the failure of columns unless existing columns are strengthened as well⁷³. Depending on the size of the added wall(s), the behavior of the retrofitted frame structure may be controlled by the structural wall(s). Because walls are much stiffer than frame elements, they attract most of the lateral forces and therefore may require modifications to the foundation.

The demolition of part of a structure is intended to reduce the inertia forces by removing a fraction of the building mass. The decrease in element stiffness may be achieved by cutting a wall into two walls for instance or cutting some longitudinal reinforcing bars. The intent of reducing the stiffness of some elements is to reduce their share in resisting the lateral forces on a local scale. On a global scale, the period of the structure is lengthened when stiffness of the structure is reduced and hence, the acceleration demands on the structure are reduced but displacements increased. A retrofit technique based on reducing stiffness depends heavily on the site characteristics and the structure's modal properties and may not be applicable to all kind of structures.

7.3.4 Application of Retrofit

Two retrofit techniques were chosen to be analyzed, namely the addition of a structural wall and stiffness reduction. The same SSS building analyzed earlier in the present chapter was considered with the following modifications:

- A separation space was assumed between the frame of the structure and the infill walls. The space was assumed large enough so that the infill panels would not contribute to the lateral resistance of the building. Infill walls added only weight to the structure and no lateral load resistance. The model is noted FR15 (Fig.5.1) corresponding to a frame structure with attributed mass equal to 15% the total building mass (Run 12).
- A structural wall connected to the existing columns was added to the SSS structure in the central bay (Fig. 7.13). The wall is a 20 cm reinforced concrete. The vertical and horizontal reinforcement in the web of the wall consisted of one layer of bars 12 mm in diameter spaced at 45 cm in both directions. The connected columns were considered as boundary elements for the wall. The mass distribution was based on a constant ratio of mass to initial stiffness of the structure. Therefore, the mass of the section analyzed was assumed equal to 30% the total building mass. For the analyses using DRAIN-2D, the wall sections were modeled by a deep beam controlled by flexure. Two possibilities were considered for the wall foundation, namely a rigid foundation (SSS.FW, Run 23) and a pin (SSS.PW, Run 24). The addition of wall panels between existing columns without retrofitting the foundation was assumed as pinned base wall.

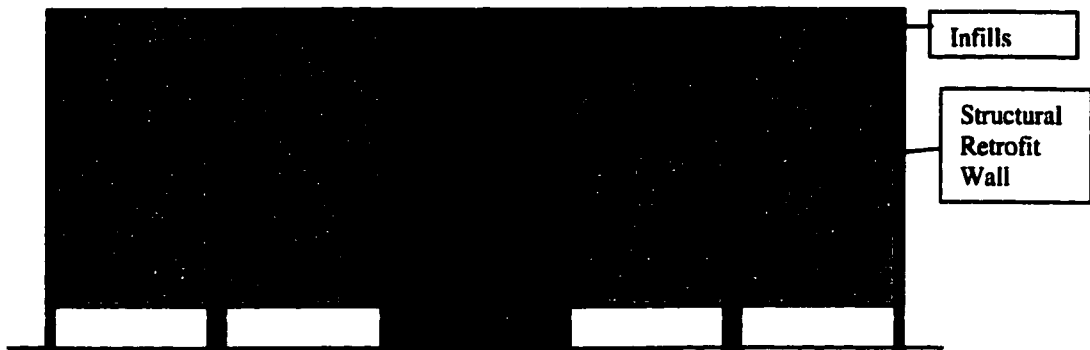


Figure 7.13 Wall retrofitted structures SSS.FW and SSS.PW

7.3.4.1 Addition of Shear Walls

The computed fundamental periods of SSS.FW and SSS.PW were 0.51 and 0.77 seconds respectively.

SSS.FW and SSS.PW were subjected to the ground accelerations from the Ceyhan earthquake scaled to a maximum peak acceleration of 0.45g. Fig. 7.14 shows the time history of base shear for SSS, SSS.FW and SSS.PW. The stiffer structure (SSS.FW) experienced the largest base shear. However, the largest base shear in SSS occurred after column shear failure on the 5th story.

Figures 7.15 and 7.16 indicate that the structure SSS.FW, which was initially the stiffer, experienced the largest peak roof drift (at 8.52 seconds, Fig. 7.15). This paradox may be due to the yielding of the wall on the 5th and 6th stories (at 8.38 seconds) and the plastic hinge that formed when the base of the wall reached yield at

6.1 seconds in SSS.FW. Flexural yielding of the wall occurred only on the 5th story (at 8 seconds) in SSS.PW.

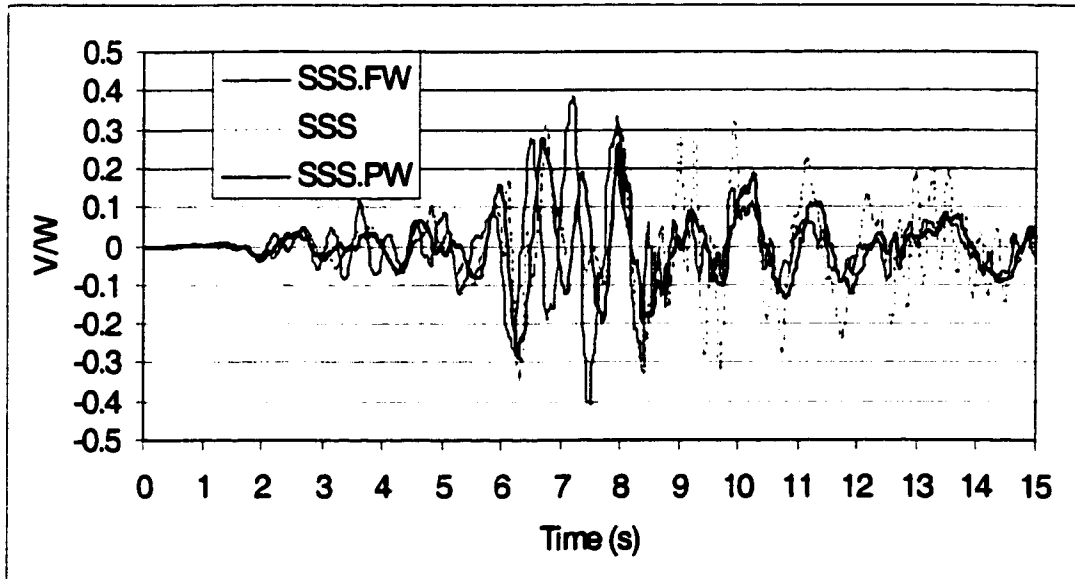


Figure 7.14 Time history of base shear for SSS, SSS.FW and SSS.PW

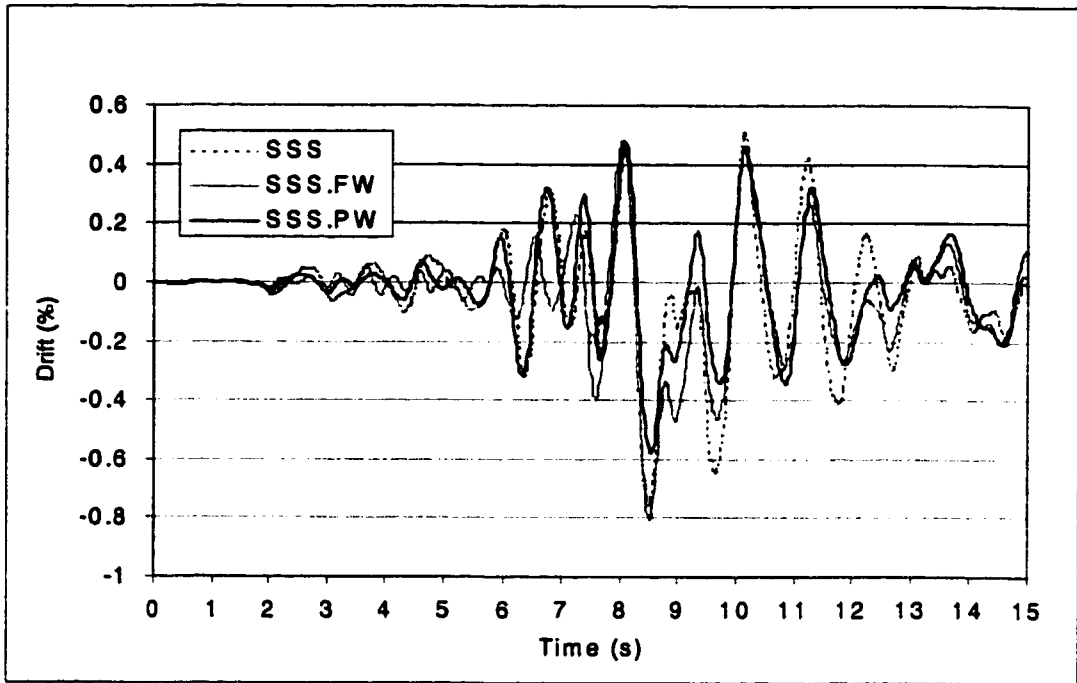


Figure 7.15 Time history of roof drift for SSS, SSS.FW and SSS.PW

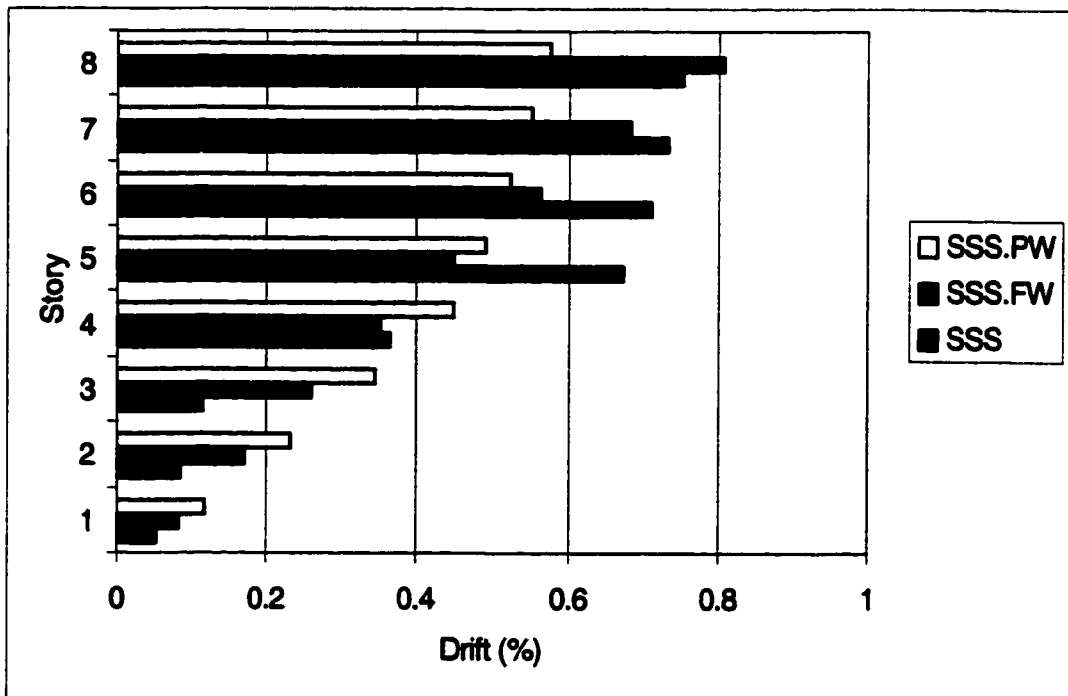


Figure 7.16 Maximum story drift for SSS, SSS.FW and SSS.PW

Figure 7.17 indicates infill failure at all levels in SSS.FW while infill failure (interstory drift greater than 0.4%) was reached on stories 2 to 4 in SSS.PW.

When the walls were added, the existing columns were assumed to act as boundary elements for the added walls. Columns on the 5th floor to the roof had smaller size and capacity than those between floors below. The wall flexural yield on the 5th story in SSS.FW and SSS.PW is due to the weaker boundary elements on this story for both structures.

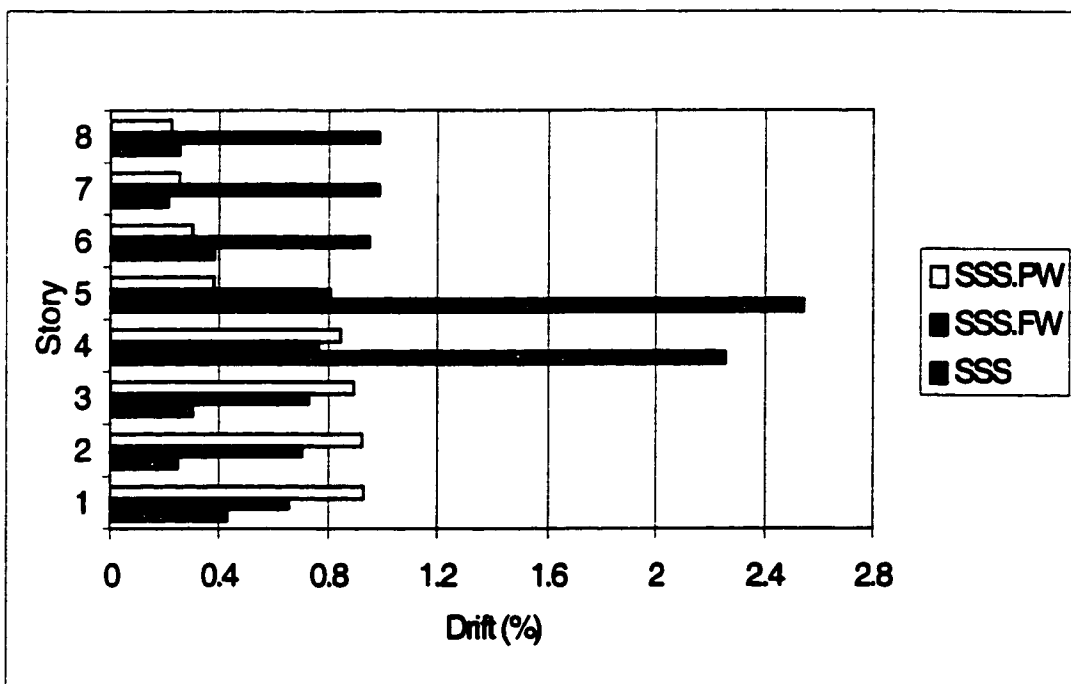
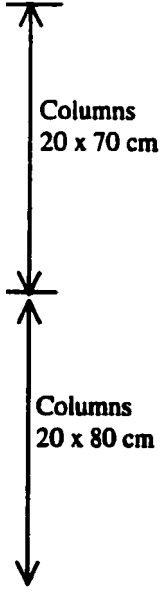
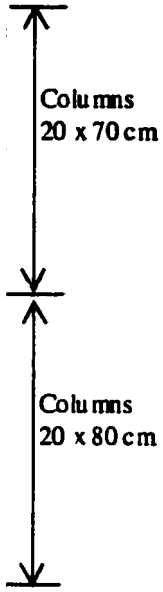


Figure 7.17 Maximum interstory drift for SSS, SSS.FW and SSS.PW

Flexural yielding of certain columns at the base of structures SSS.FW and SSS.PW can be seen in Figs. 7.18 and 7.19. When the wall reached yield at the base of the structure, its tangent stiffness decreased. As the base shear increased after the base of the wall yielded, the added shear was distributed to the remaining resisting

element in proportion to their stiffness. Columns that had their long direction in the plane of the frame were stiffer than those with long direction normal to the plane of the frame (Figs. 7.18 and 7.19) and attracted more shear which lead to their yield.



In this case study, it seems that the addition of a shear wall as a retrofit scheme is adequate in providing life safety performance of the structure. However, architectural damage may still be significant (Figs. 7.17 and 7.18). The added wall with a rigid foundation had lower performance than the wall with pinned base. The addition of walls provided strength and stiffness increase. The added strength was beneficial in eliminating the shear failure in columns. The added stiffness with pinned-base wall reduced the deformations in the structure at upper levels only, but the added stiffness with fixed-base wall caused higher inertial forces and did not reduce the deformations in the structure.

7.3.4.2 Stiffness Reduction

Assuming the space between the framing system and the infill walls is large enough so that the infill contribution is absent, structure FR15 appears to satisfy the performance criteria for immediate occupancy level, set by FEMA 273, when subjected to the Ceyhan ground acceleration with a peak ground acceleration of 0.45g. The analyses indicated that some beams on the 3rd and 4th floors barely reached yield. FR15 met the performance criteria for life safety when the Ceyhan ground accelerations were scaled to a peak of 0.8g. The interior four columns reached yield at the base of the structure and the beams on all floors yielded but did not reach the life safety limit for plastic rotation (0.02 rad, FEMA 273).

As expected, Figs.7.20 and 7.21 show that peak roof displacements and peak base shear were larger using a peak ground acceleration of 0.8g. However, neither displacements nor base shears were proportional with respect to peak ground accelerations for FR15. Proportionality would be expected only if the structure remained totally in the elastic range.

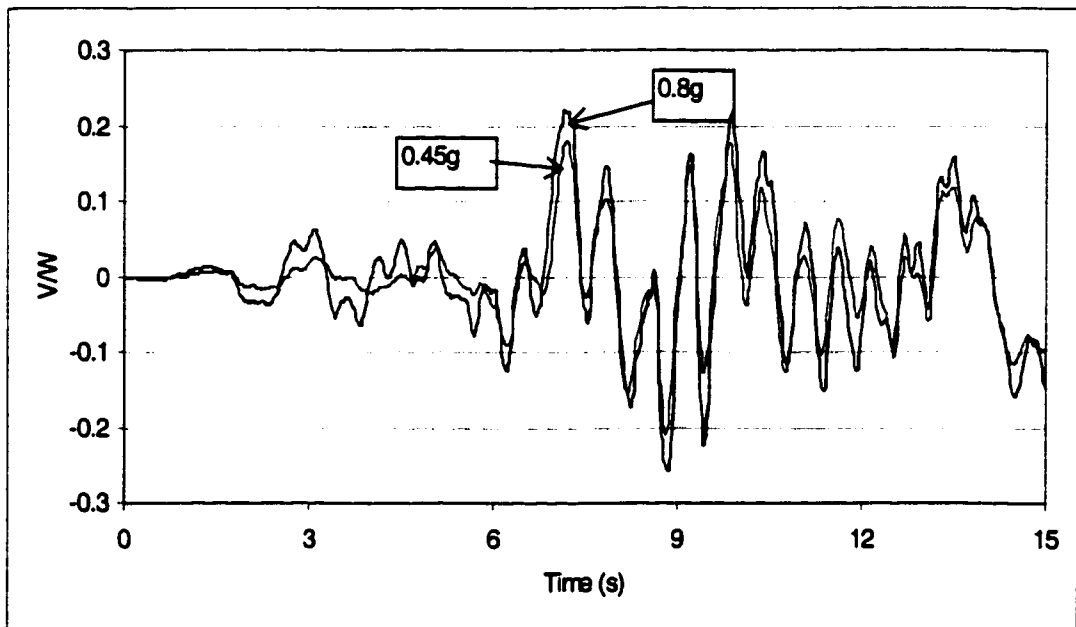


Figure 7.20 Time history of base shear for FR15 using different peak ground accelerations scaled from the Ceyhan earthquake

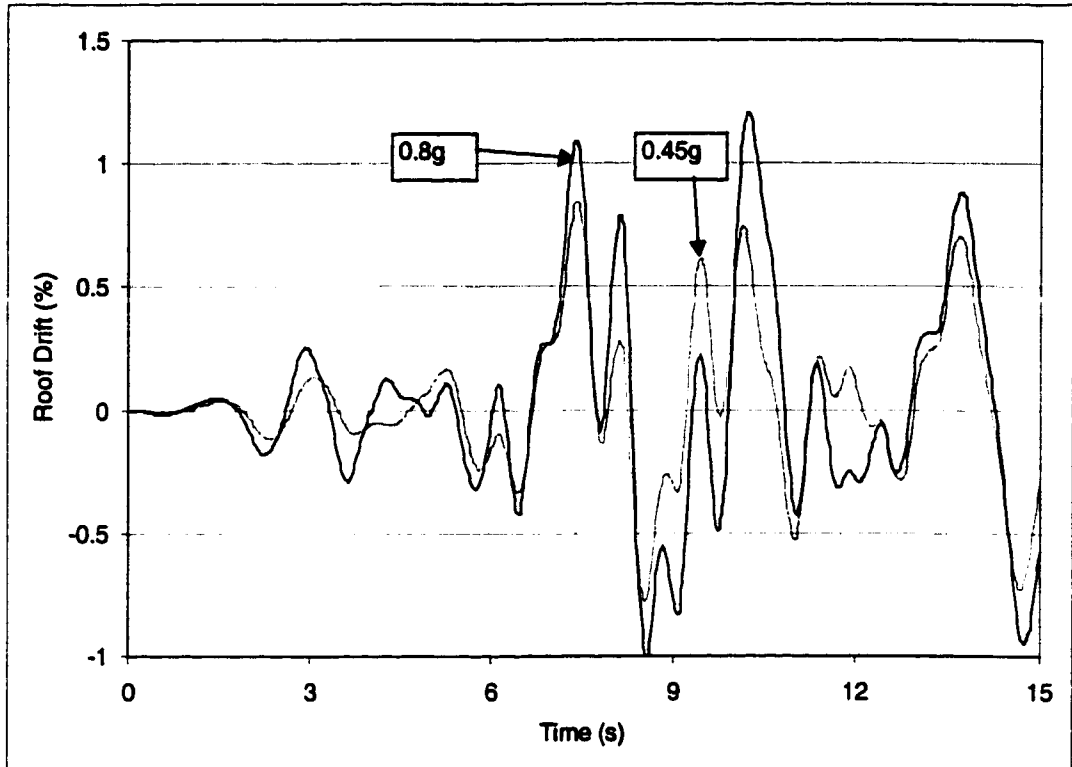


Figure 7.21 Time history of roof drift for FR15 using different peak ground accelerations scaled from the Ceyhan earthquake

Figure 7.22 indicates the predominance of the first mode in the shape of maximum drifts for the frame structure FR15. The general shape of maximum story drifts and maximum interstory drifts were about the same using 0.8g and 0.45g, but the values were significantly different (Figs. 7.22 and 7.23). The interstory drifts shown in Fig. 7.23 indicate that a space of approximately 3.3 cm or 1.3 in (1.1% x 300 cm) between the infill walls and the adjacent columns is needed on the 6th floor assuming the peak ground acceleration is 0.45g. Similarly, a space of approximately 5.7 cm or 2.3 in (1.9% x 300 cm) between the infill walls and the adjacent columns is needed on the 5th floor assuming the peak ground acceleration is 0.8g. In practice,

such a space becomes critical for many reasons: structurally, the infill walls need to be stabilized against motions in the direction perpendicular to the plane of the panel. Architecturally, the space between infill walls and exterior frame may not be appealing. From the construction point of view, there may be a potential risk of water and tightness of the building.

The failure of infill panels was assumed to occur when an interstory drift of 0.4% was reached. Hence, assuming the same interstory drifts for FR15 with infill walls as for FR15, Fig. 7.23 indicates that infill panels would have failed on the second story up to the roof using a peak ground acceleration of 0.45g. However, the contribution of infill to the stiffness of the structure is not negligible, consequently, the assumption that SSS structure will behave as FR15 since interstory drifts for FR15 exceed 0.4% would be wrong. The behavior of SSS is expected to approach the behavior of FR15 if the interstory drifts for SSS exceed 0.4% at all levels with infill walls.

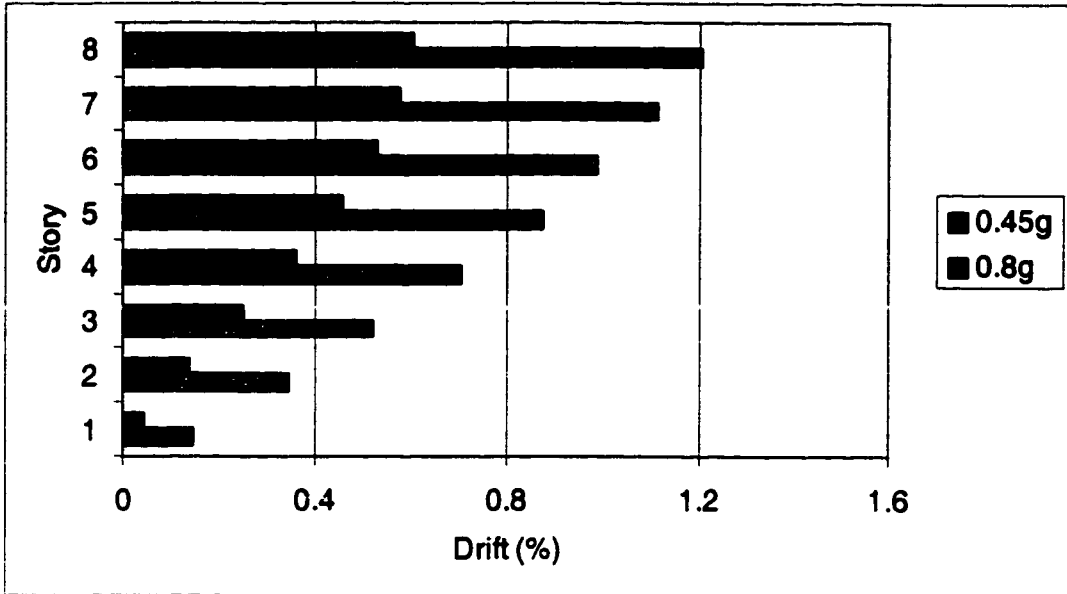


Figure 7.22 Maximum story drifts for FR15 using different peak ground accelerations from the Ceyhan earthquake

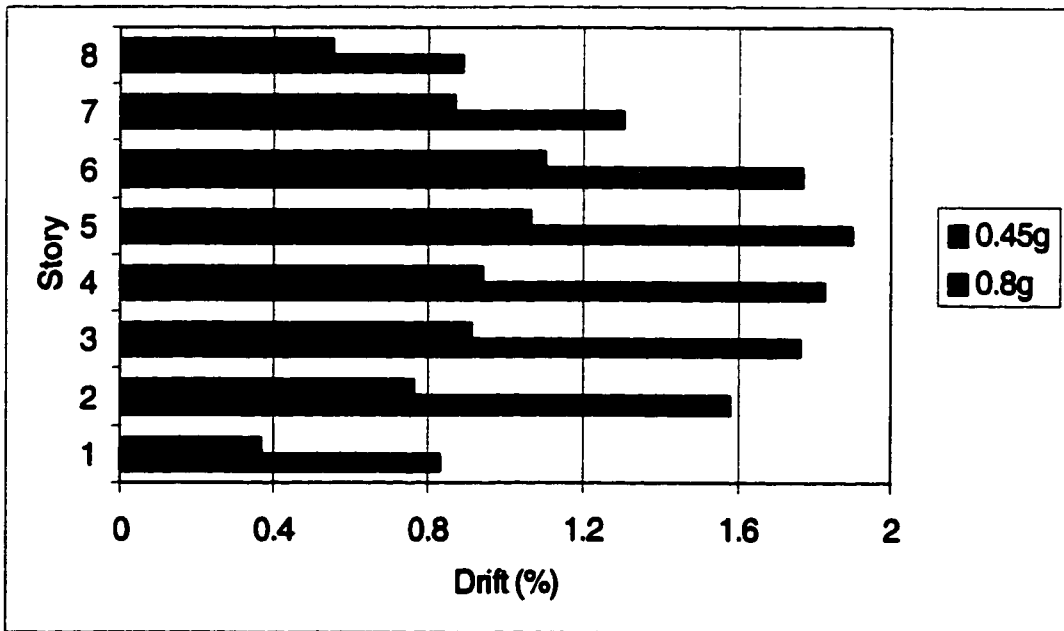


Figure 7.23 Maximum interstory drifts for FR15 using different peak ground accelerations from the Ceyhan earthquake

7.3.5 Enhanced Design

7.3.5.1 Conditions

Two soft first story frame structures, REGULAR.LONG (Run 21) And REGULAR.SHORT (Run 22), with regular column layout were analyzed and the results compared to those from the prototype SSS building. REGULAR.LONG had the larger shear capacity in the direction of loading and REGULAR.SHORT the smaller. REGULAR.LONG was assigned 20% of total building mass, and the long direction of all columns was in the plane of the frame. REGULAR.SHORT was assigned 15% of total building mass, and the long direction of all columns was normal to the plane of the frame. All other parameters were the same for both regular buildings. The fundamental periods of REGULAR.LONG, REGULAR.SHORT and SSS were 1.05, 1.35 and 0.95 seconds respectively.

7.3.5.2 Results

Maximum story drifts and interstory drifts for REGULAR.LONG, REGULAR.SHORT and SSS are shown in Figs. 7.24 and 7.25. As expected, REGULAR.SHORT was the most flexible and had the largest story drifts at the lower stories. Yielding of columns on upper floors in the three structures indicated the higher mode effects. Column size, shear and flexure capacities were smaller from the 5th floor to the roof than the columns below. Shear failure occurred on the 5th floor in the four interior columns in SSS.

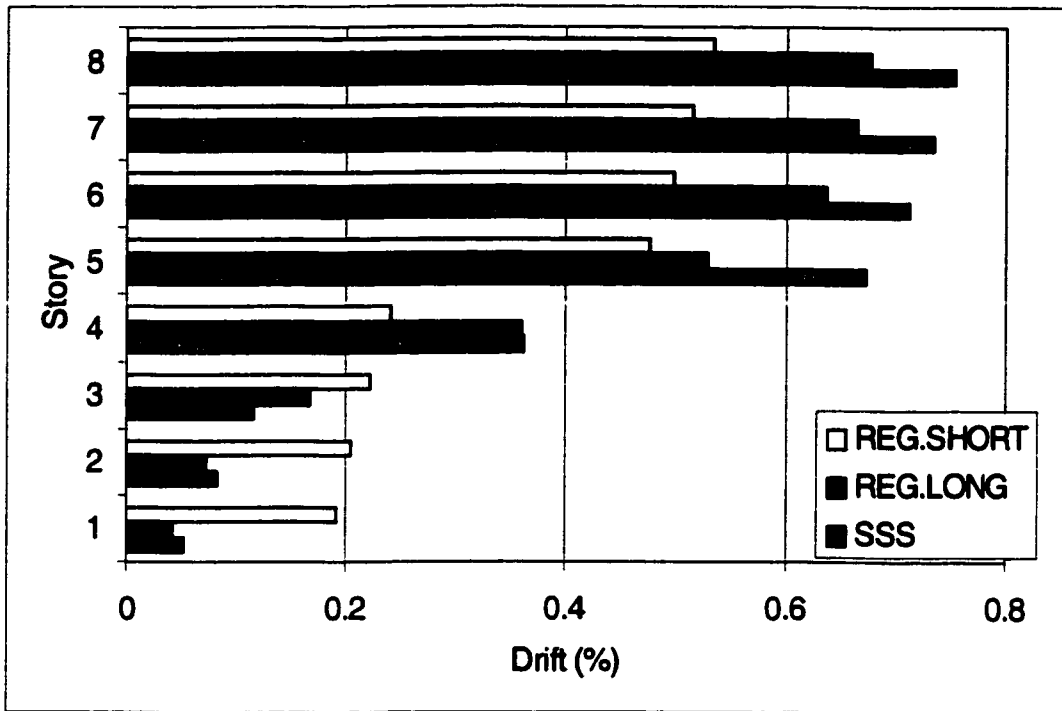


Figure 7.24 Maximum story drift for SSS, REGULAR.LONG and REGULAR.SHORT

The first story columns in REGULAR.SHORT met the life safety requirements for components set by FEMA 273 although interstory drift on the first floor was larger than 1.5%. The inelastic rotations at the base of columns in REGULAR.SHORT were 0.003 (<0.01 set by FEMA) and the major portion of the drift was due to the elastic deformation of these flexible columns.

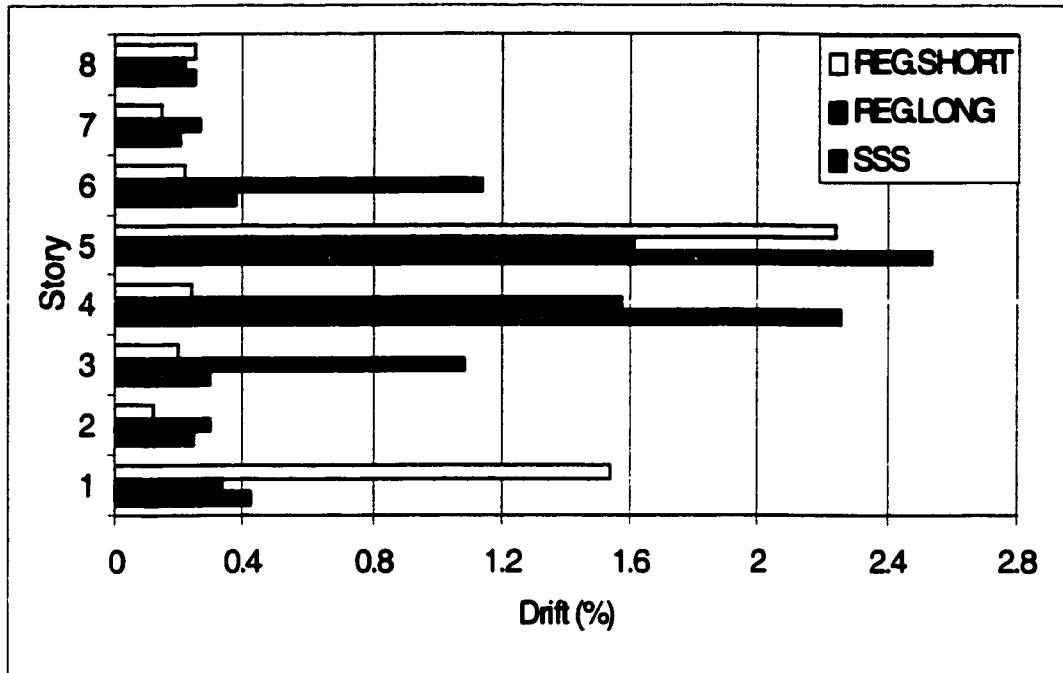
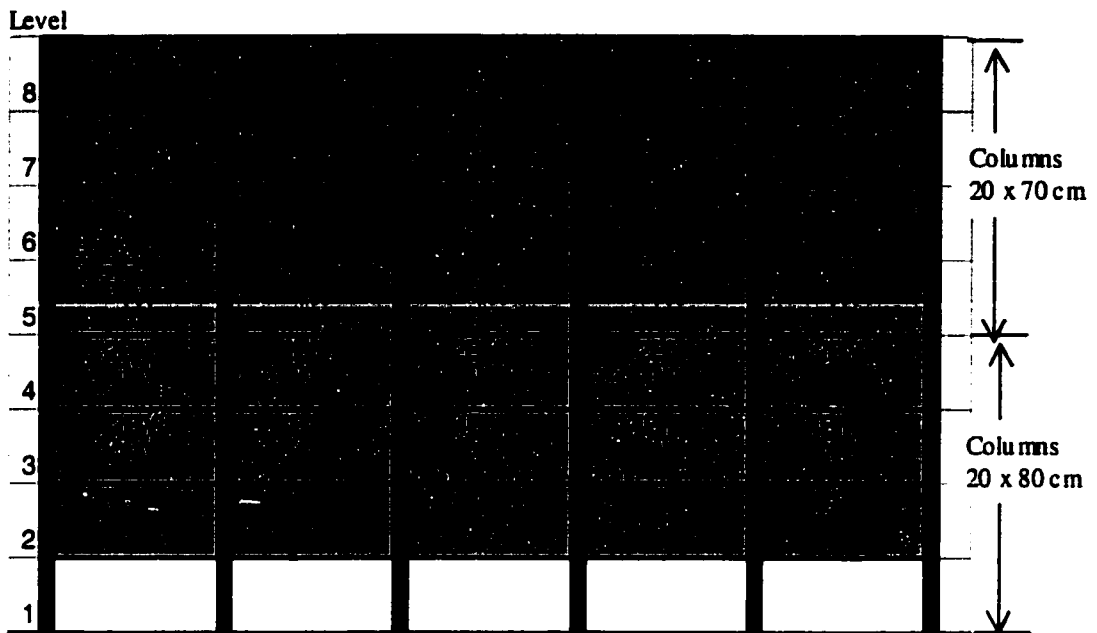
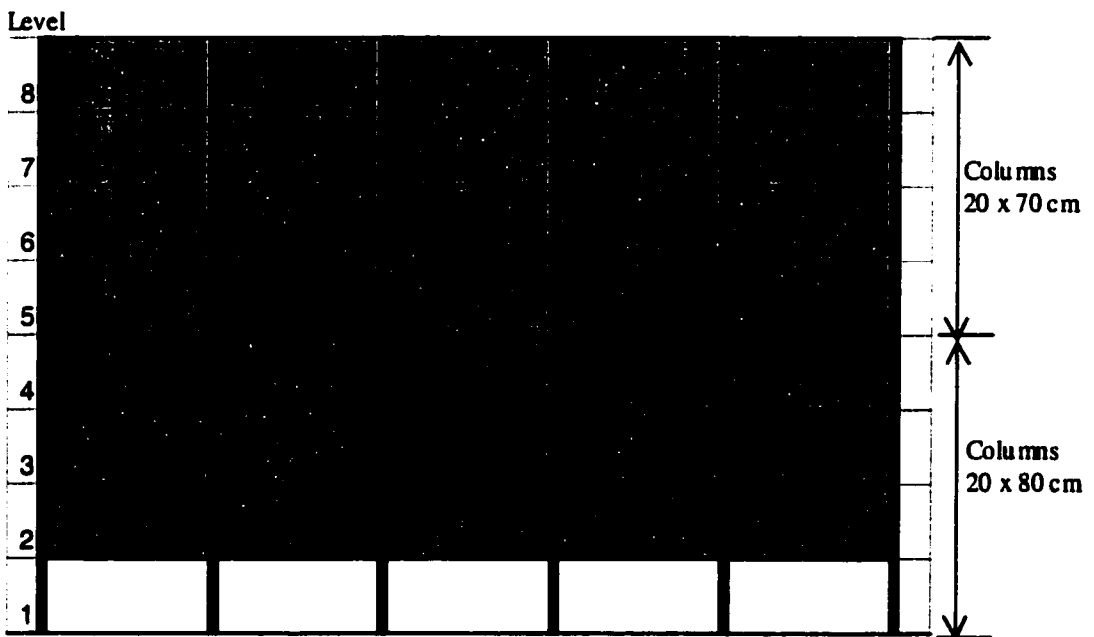


Figure 7.25 Maximum interstory drift for SSS, REGULAR.LONG and REGULAR.SHORT

Figures 7.26 a and b show the location and the sequence of failure in Structures REGULAR.LONG and REGULAR.SHORT. As expected, it appears that structures with regular column layout performed better than irregular structures. In this particular case, and for life safety, no structural upgrading of the structure would be needed if the column layouts were regular.



(a) Structure REGULAR.LONG



CY Column Yield
 BY Beam Yield
 W Infill Failure

The number preceding the notation indicates the sequence of the event

(b) Structure REGULAR.SHORT

Figure 7.26 Locations and sequence of failure

7.4 Discussion and Design Implications

The present parametric study was conducted using simple modeling assumptions. When studying the effect of one parameter, the remaining parameters were held constant. However, the suggested values for the parameters were hypothetical, yet care was taken to choose parameters representative of the “real” or expected field values. No field data were available at the time the analyses were performed. Therefore, uncertainty in the structural properties and earthquake input were unavoidable, but to be expected in practice. Also, limitations of the element models and the capacity of the analytical tools were a challenge.

7.4.1 Uncertainties

Uncertainties derive from both the structure and its location. Only a few of these uncertainties are approached in this section:

The foundation was assumed on bedrock and in most cases rigid (except for SSS.PW). Vertical accelerations were ignored because in a previous study³², the effect of vertical accelerations appeared to have no major impact on the response of the structure except for the axial force in columns.

The acceleration record used in most of the analyses was the longitudinal component of the Ceyhan earthquake. For the same location, the spectral characteristics of the transverse component were significantly different from the longitudinal component (Figs. 7.27 and 7.28).

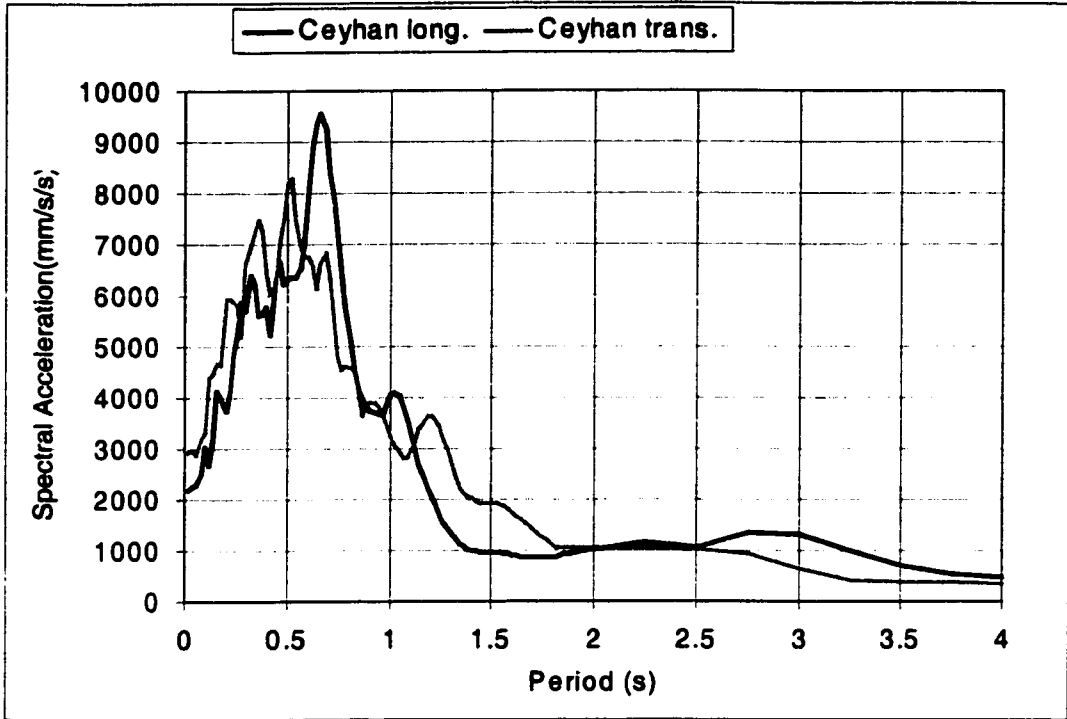


Figure 7.27 Acceleration response spectra at 5% damping for the longitudinal and the transversal components of the Ceyhan earthquake

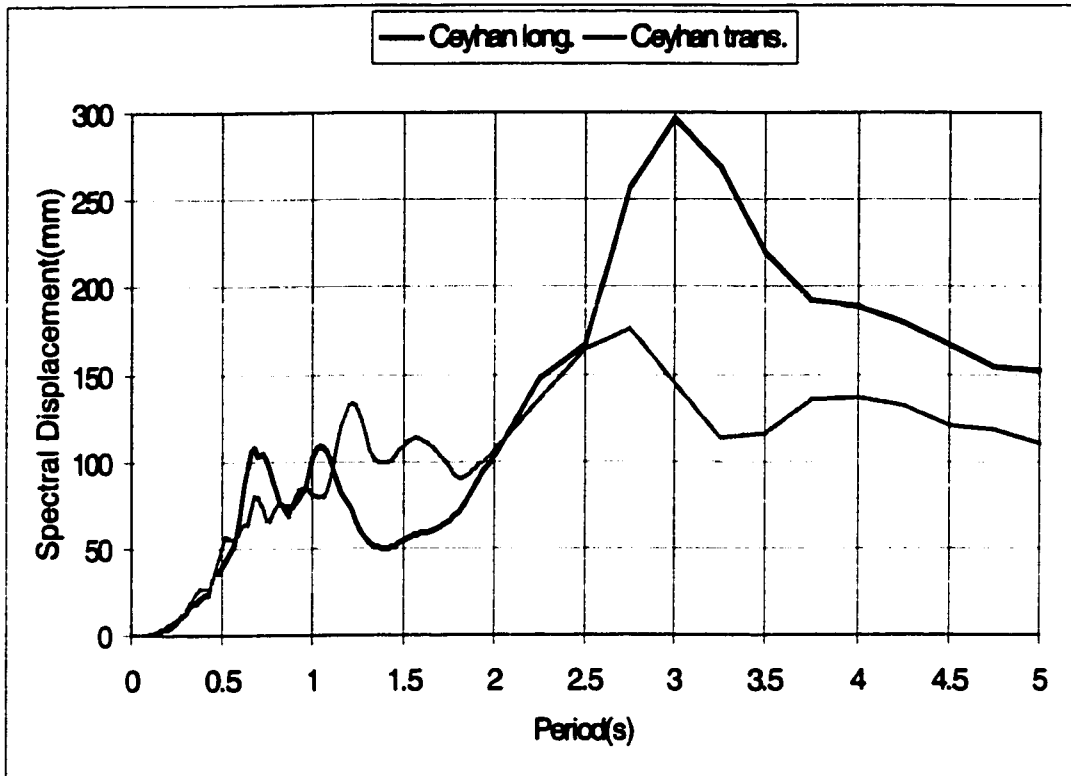


Figure 7.28 Displacement response spectra at 5% damping for the longitudinal and the transversal components of the Ceyhan earthquake

Numerous assumptions were made in modeling the structural properties of the building. No tests of typical ribbed slab wall-type column connections used in the structural system were found. It was assumed that the slab action was restricted to the concealed beams (main beams) framing between columns and the influence of the ribs was ignored (the ribs were normal to the concealed beams and the plane of the frame). However, previous studies^{14,32,74} showed that the slab contribution increased somewhat both the stiffness and the strength of beams.

The effective stiffnesses of the structural components were assumed to have constant values. The effective stiffness was expressed as fraction of the stiffness of the gross section of concrete. The same fraction was assumed at all levels. A previous study¹⁴ showed that the response is expected to be different if “softening” of the elements were considered as drift levels increase. The overall stiffness is expected to decrease as components crack, yield or fail.

The distribution of mass to different portions of the lateral load resisting systems of the building was proportional to stiffness. The stiffness of the frame was determined based on the fraction of shear resisted by this frame from a linear dynamic analysis. Therefore, a constant mass was used during the time history analyses whereas in a real structure, the distribution of mass between lateral-load resisting elements would be changing with time if elastic limits of various elements were exceeded.

7.4.2 Limitations

Limitations of the analytical tools include a very limited library of element models, instability of the programs when several elements fail simultaneously, and the approximations needed to convert an irregular 3D-structure using a 2D model.

The limitations in the existing elements in DRAIN-2D were discussed in section 7.2.1. DRAIN-2D appears to be more appropriate for time history nonlinear analyses rather than static nonlinear analyses for two reasons.

- Only force controlled analyses can be performed using DRAIN-2D. Therefore, a drop in the force with an increase in displacement is not possible, hence a residual strength cannot be visualized in the pushover curve computed using DRAIN-2D. Also, several elements may fail during the same force increment, consequently a sudden instability of the program causes the analysis to stop.
- DRAIN-2D does not have a modal adaptive load pattern for static analysis.

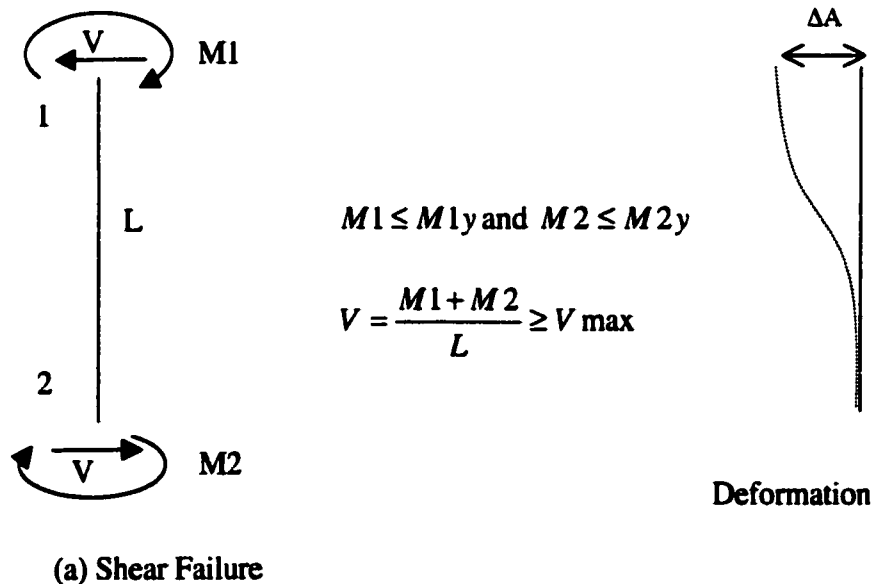
The nonlinear analysis in SAP2000 seems to be incomplete at the present stage. The pushover analysis is limited to frame structures and no models for wall panels are included. The nonlinear element models have only bilinear (or exponential) characteristics. Such models can only determine the maximum lateral capacity of the structure⁶⁴. No degradation in strength or stiffness is considered in SAP2000. However, previous studies^{14,32,64} have shown that degradation in stiffness and strength has a major effect on the displacement response of the structure and the determination of failure sequence and location. Also the pushover analysis in SAP2000 is limited to frame structures. Although SAP2000 includes a preprocessor for the determination of section properties given the geometry of the section and the material properties, the determination of shear capacity does not seem to be accurate because the transverse reinforcement participation seems to be ignored.

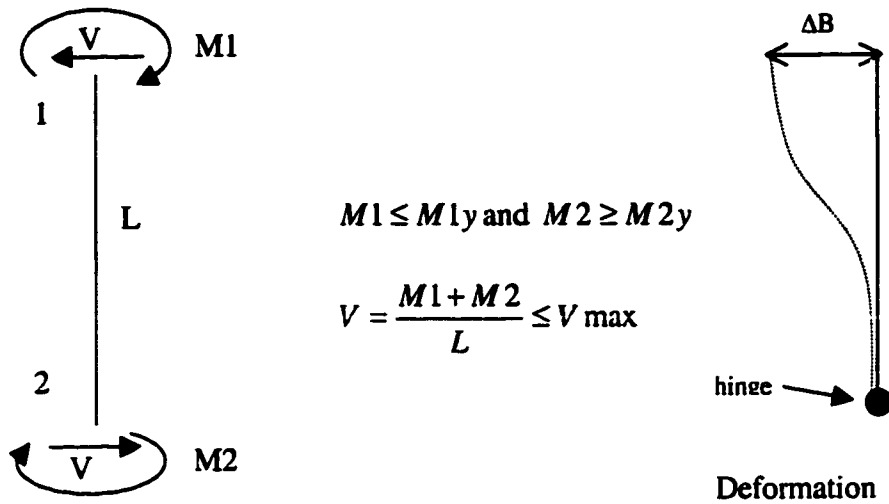
It seems that with DRAIN-2D and SAP2000, nonlinear static analysis is more appropriate for regular low-rise frame structures rather than for structures including

panel elements. The reason may be the limitation in element models and in lateral load patterns available for use with DRAIN-2D and SAP2000. Low-rise frame structures are dominated by the first mode response.

7.4.3 Design Implications

It appears that drift can be a good measure of damage in non-structural elements. Infill panels failed at 0.4% interstory drift set in the analytical model (FEMA 273). However, it was found that drift was not a precise indication of structural damage. Columns between stories that may have reached a differential drift of 2.6% did not fail in one case and in another case failed at a differential drift of 1.8%. This was interpreted and discussed in section 5.3.6.2 and summarized below in Fig. 7.29.





$$M_1 \leq M_{1y} \text{ and } M_2 \geq M_{2y}$$

$$V = \frac{M_1 + M_2}{L} \leq V_{\max}$$

(b) Hinging at one end

$$\Delta A \leq \Delta B$$

Where,

M_1, M_2 = moment at end 1 and end 2 respectively;

M_{1y}, M_{2y} = yield moment at end 1 and end 2 respectively;

L = length of the column;

V = shear in the column;

V_{\max} = shear capacity of the column.

Figure 7.29 Sketches of two different scenarios for large drift

Infill panels were controlled by shear only. Therefore, one variable, such as interstory drift is enough to predict failure of infills. For structural components such as columns and beams involving both shear and flexure capacities at both ends, interstory drift is not sufficient to predict failure.

CHAPTER 8 CONCLUSIONS

8.1 Summary

The performance of typical structural system used in the Eastern Mediterranean was studied. These structural systems are flexible but have low ductility and strength. Extensive damage, loss of life, and economic disruption that have occurred several times in Greece, Turkey, and other locations in that region indicate the need for evaluation and retrofitting of existing structures. In the absence of field data, a parametric study with representative values was conducted using nonlinear analyses to assess the significance of the parameters considered. Information on deformation demands, internal force distributions and locations of failure in elements of the lateral force resisting system can be obtained from nonlinear dynamic analyses. Verification of nonlinear static and nonlinear dynamic procedures were included in this study.

Objective

The objective of this study was to evaluate the influence of earthquake ground motions, geometry of the structure, and material characteristics on the response of concrete structures. The results provide data that may be helpful for guiding nonlinear dynamic analyses for design of new buildings or for evaluation and retrofitting of existing structures.

Parametric Study

A prototype basic reinforced concrete frame structure was analyzed using a scaled ground acceleration record from the Ceyhan (Turkey, 1998) earthquake. Variations in the basic structure include different mass distributions, variation of the column dimensions, orientation of the rectangular columns, or inclusion of infill walls.

Analytical Tools and Models

Two nonlinear programs were studied, DRAIN-2D and SAP2000. DRAIN-2D was used for both nonlinear static and dynamic analyses. Section characteristics were determined using RCCOLA and the structural component models were selected from the available elements in DRAIN-2D library of elements. The NLLink in SAP2000 was not used because it does not include strength or stiffness degradation. SAP2000 was used for pushover analysis only because it offers the possibility of using the component modeling defined in FEMA273. DRAIN-2D was used for the parametric study and the verification of the pushover procedure in SAP2000.

Beams and columns controlled by flexure were modeled using the beam element available in DRAIN-2D. The beam element is a linear elastic element with nonlinear spring elements attached to each end. Inelastic behavior is concentrated at the end to represent stiffness degradation.

Infill walls were modeled using the infill panel element available in DRAIN-2D. The infill panel model has shear stiffness only and the load-deformation is bilinear with a defined deformation limit. If deformation reaches the limit defined, the panel is considered to have failed and is ignored in subsequent loading history.

Columns controlled by shear were modeled using the parallel element developed by Li and Jirsa and modified to satisfy boundary conditions. The original parallel element assumed equal moments at both ends of the member. The modified parallel element allows the member to reach yield at one end before failing in shear, or to reach yield at both ends thereby precluding a shear failure.

Parametric Study

The structural parameters investigated using nonlinear time history procedures included variations in material and geometry. The material strength and ductility had little influence on the behavior of the frame structure in the range of ground accelerations used for the investigation. The effective stiffness of beams and columns had a significant effect on the response of the structure. The use of column dimensions with different width to depth ratios had little influence on the response if the orientation was the same (strong or weak axis in direction of loading).

It was found that the rigidity of beam-column connections significantly influenced the global stiffness of the structure and the associated displacement. As long as beam-column connections do not fail, the assumption of rigid connection

seems acceptable. In the prototype structure, joints are unlikely to fail because of their geometry and the low strength of the beam and column elements at the connection.

The variation in column size over the height of the structure did not seem to alter the general response of the structure. However, shear failure in columns was predicted on the 5th story for the structure with smaller size columns from the 5th floor to the roof.

The column layout may alter the response of the structure because the stiffness of the structure changes significantly depending on the orientation of the column long axis (for rectangular columns). As expected, the stiffer elements attracted more shear and may fail even if shear capacity in that direction is larger. As expected, better performance was achieved using regular column layout (all rectangular columns having the same orientation).

The distribution of mass to the different frames in a building was found to have an important influence on the behavior of the structure. A larger mass produces larger inertial forces and longer periods. Two options were used for the distribution of mass to different portions of the lateral load resisting systems of the building: a constant value proportional to the initial stiffness of the frame or a constant value proportional to the tributary area for gravity load assigned to the frame. The “all infill” (AI) structure experienced column shear failure on the 6th story when the mass distribution was based on a constant value proportional to the initial stiffness of the

structure. No shear failure was calculated when the mass was based on a constant value proportional to the tributary area. However, the “soft story” (SSS) structure experienced column shear failure when the mass was based on tributary area, while no shear failure was calculated when the mass was based on stiffness. Therefore, it is recommended that both cases be considered for design and/or evaluation, because in a real structure, the distribution of mass is expected to vary as components crack, yield or fail.

The infill walls were found to produce failures at different locations than might be anticipated. Unless there is a sufficient gap between infills and frame elements to allow large interstory drifts without the frame bearing on the infills, the effect of infills must be included.

The residual shear level for a column depends on the amount of transverse reinforcement and the axial load in the column. The lower the residual strength the more vulnerable the structure to total collapse.

Ground Motions

To compare the effects of ground motion, four earthquake records were selected and scaled to the same peak ground acceleration. The frame structure with infill walls from the 2nd floor to the roof was subjected to the four records and analyzed using the nonlinear time history procedure. The responses varied significantly. Response spectra were helpful in understanding the differences.

The ground motion record from the Ceyhan earthquake was scaled to three different peak ground accelerations namely, 0.2g 0.25g and 0.45g and the performance of the building was evaluated using the scaled records. It was found that shear failure occurred in columns on the 5th story only after peak acceleration of 0.4g was applied.

The lack of soft-first-story response for the prototype building may be because shear failure occurred first in columns on upper floors. The base motion used may have dominated the parametric study.

Retrofit Schemes

Two retrofit schemes were analyzed. One retrofit system consisted of adding a shear wall to the structure in the central bay. Another retrofit system consisted of separating the infill walls from the frame so that there was no frame-wall interaction. The walls were considered to add mass only.

The addition of the shear wall eliminated column shear failure and reduced the damage to structural components, however the infill walls failed because interstory drifts exceeded the limit deformation capacity for infills.

When infill walls were separated from the frame, large interstory drifts were observed. Minor structural damage occurred in the beams because the beams (floor system) were very flexible. The frame structure (with no infill contribution to the

lateral load resisting system) performed very well. However, the space between infills and columns may be too large to be a practical option.

The assumption of the structure with infill behaving like a frame structure after the infill has failed is not acceptable because infill panels do not fail at all floor levels at the same time. Therefore, the system with failed infill panels may resemble a structure with soft stories at levels where infills have failed. The addition of a shear wall as a retrofit scheme can provide life safety level of performance and the preference for such retrofit is supported by the extensive use of walls in retrofit projects all over the world.

8.2 Conclusions

Based on the assumptions made and the limitations of the analytical procedures used for the prototype flexible structural system, the following conclusions and recommendations were made:

Important Material and Geometric Parameters

1. The effective stiffness was an important factor in determining the response of the prototype structure. Ideally, an effective stiffness that changes as the analysis progresses should give the best results. Alternatively, a constant value for the effective stiffness could be used provided low values are assigned to elements expected to experience large forces and cracking. Effective stiffness values

suggested in FEMA 273 and ACI 318-95 gave nearly the same results in this case study.

2. Failure of columns in a softened story (after the infills have failed) was caused by irregular column layout rather than by large displacements consistent with a reduction in stiffness at that level. The column layout controlled the response of the structure. For an irregular column layout, the stiffer columns in the plane of the frame attract more shear force and are susceptible to failure depending on the shear capacity provided.
3. When different column sizes were used over the height of the structure, failure was more likely at the level where the size (and capacity) was reduced. It was of interest to observe that the reduction in shear capacity of the smaller columns was about 10% (<25%, the criteria for weak story as by FEMA 273) but lead to dramatic difference in the failure pattern. A uniform column size over the height of the structure is always desirable.
4. The distribution of mass to the different frames in a structure is an approximate procedure. It is recommended that at least two cases be analyzed, namely a distribution based on tributary area and a distribution based on constant mass proportional to initial stiffness, where stiffness is based on an elastic dynamic analysis.
5. Infill walls altered the behavior of the structure and lead to failure in cases where the structure without infills (bare frame) would sustain only minor damage.

Although the structure may resemble analytically a frame structure after infill walls have failed, the sequence of failure causes the behavior of the structure with infills to be different from that of the frame structure.

Earthquake Ground Motions

1. Ground accelerations from different earthquakes were scaled to the same peak and were used to evaluate the performance of the prototype structure. Severe damage to possible column shear failure was predicted with different earthquakes of the same intensity. The use of several earthquake records is recommended to fully understand the range of response possible. Recent earthquakes have provided new records that indicate different response at a given site depending on the location of the triggering event.
2. The response of the prototype structure could be explained using acceleration response spectra and the first two modes of the structure, suggesting that acceleration spectra can be used for an approximate solution that provides acceptable accuracy.

Analytical Tools and Procedures

1. SAP2000 does not seem to be suitable for nonlinear analyses at its current stage of development. The nonlinear time history portion needs a better element library with degrading strength and stiffness models. The nonlinear static analysis

portion of SAP2000 is very promising since it allows the direct input of the component characteristics and acceptance criteria described in FEMA 273. However, it seems to be adequate for frame structures only. It is recommended that component characteristics be input manually rather than generated automatically by the SAP2000 processor. Computation of shear capacity by SAP200 processor seems to be incomplete.

2. The nonlinear time history procedure yields information on internal forces and deformations that are needed to determine location and sequence of failure/damage. Once again, a range of input assumptions and properties may be needed to bracket behavior.
3. Nonlinear static procedures provide a relationship between base shear and roof displacements needed to establish performance of the structure. The pushover analysis is load pattern dependent with the lateral capacity depending on the load pattern used. It is recommended that nonlinear static procedures be used with caution and for low-rise frame structures.
4. For the same peak roof displacements, interstory drifts from pushover analyses were equal or larger than those from nonlinear time history analyses, suggesting that more damage in the structure is expected from pushover analyses than from nonlinear dynamic analyses. The pushover procedure may lead to more conservative design than nonlinear time history analysis.

Performance and Retrofit

1. Using nonlinear time history analysis, the frame structure with infills on the 2nd floor to the roof was found to meet the performance criteria for:
 - Immediate Occupancy when subjected to the ground shaking from Ceyhan earthquake with peak acceleration of 0.2g
 - Life Safety level with peak acceleration of 0.25g
 - Collapse Prevention level with peak accelerations of 0.45g.
2. The separation of infills from the frame components to provide enough space so that no infill action is possible was considered as a retrofit scheme. The retrofitted structure was found to meet the life safety level of performance set by FEMA273 with peak accelerations in excess of 0.45g. However, displacements were quite large.
3. The addition of shear walls provided a life safety level of performance with peak ground acceleration of 0.45g. It seemed to be the most appropriate retrofit system considering economy and structural performance factors.

8.3 Assumptions and Uncertainties

Nonlinear time history analyses provide information on internal forces and deformations necessary for design and evaluation of structures. However, the results presented in this study were very sensitive to assumptions and initial conditions. Therefore, engineering judgement of the computed results and a verification of the

initial modeling assumptions were crucial in assessing the credibility of the analytical results. At the present time, the analytical techniques available do not provide a range of variables or parameters to be considered to cover all the possible responses of a structure. Given all the uncertainties in the input data and the numerous assumptions involved in nonlinear analyses, the credibility of such sophisticated techniques is questionable.

8.4 Suggestions For Further Research

After completing the research for this study, it was concluded that research in the following areas would allow more rapid implementation of analytical procedures:

1. Field data are critical for calibration of non-linear time history procedures. A study of the behavior of structures with concentric and eccentric beam-column connections with wide shallow beams and wall-like columns is needed.
2. A preprocessor is needed for the computation of the properties of any arbitrary section properties. The preprocessor should enable the user to define the stress-strain relationship for steel and concrete materials. Such a processor should be included as an internal subroutine in DRAIN-2D or similar programs for nonlinear time history analysis. A subroutine that updates the stiffness of the element at different sections as the element undergoes cracking is needed to reduce uncertainties in the input of structural properties. A user-friendly interface for DRAIN-2D is very desirable. More element models are needed, in particular

a panel element that handles both shear and flexural stiffness of the element. The parallel element model would be enhanced by including a limit on the inelastic deformation.

3. A three-dimensional non-linear time history analysis program is needed for analyzing irregular structures. Such a program should account for torsion effects and biaxial interaction.

References

1. Building Seismic Safety Council, NEHRP Guidelines for the Seismic Rehabilitation of Buildings (FEMA273) and Commentary (FEMA274), Washington, D.C., October 1997.
2. Seismology Committee, Structural Engineers Association of California, "Recommended Lateral Force Requirements and Commentary", San Francisco, California, 1989.
3. Kanaan and Powell, G. H., "DRAIN2D: A General Purpose Program for Dynamic Analysis of Inelastic Plane Structures", *Reports No. EERC 73-06 and EERC 73-22*, University of California at Berkeley, April 1973 (Revised September 1973 and August 1975).
4. R. E. Valles, C. Li, A. Madan, Sashi, K. Kunnath and Andrei M. Reinhorn, "IDARC2D Version 4.0: A Computer Program for the Inelastic Damage Analysis of Buildings", State University of New York at Buffalo, *Technical Report NCEER-96-0010*, June 3, 1996.
5. Park, Y. J., Reinhorn, A. M., and Kunnath, S. K., "IDARC: Inelastic Damage Analysis of Reinforced Concrete Frames-Shear wall Structures", *Technical Report NCEER-87-0008*, State University of New York at Buffalo, Buffalo, NY, 1987.
6. Ray W. Clough and Joseph Penzien, "Dynamics of Structures", McGraw-Hill Book Co., New York, NY, 1993.
7. Chopra, A. K., "Dynamics of Structures, A Primer", *Monograph Series*, Earthquake Engineering Research Institute, Berkeley, CA, 1981.
8. SAP2000 –"Integrated Structural Analysis and Design Software", Computers and Structures, Inc., Berkeley, California, 1997.
9. ACI Committee 318, "Building Code Requirements For Structural Concrete (ACI318-95) ad Commentary (ACI318R-95)", American Concrete Institute, Farmington Hills, MI, 1995.
10. International Conference of Building Officials (ICBO), Uniform Building Code, Whittier, California, 1994.

11. Building Officials & Code Administrators International, The BOCA National Building Code, Country Club Hills, IL, 1993.
12. Southern Building Code Congress International (SBCCI), Standard Building Code, Birmingham, AL, 1993.
13. Building Seismic Safety Council, NEHRP Recommended Provisions for the Development of Seismic Regulations for Buildings, FEMA-222, Washington, DC, 1994.
14. Li, Y. R., "Nonlinear Time History and Push-Over Analyses for Seismic Design Evaluation", *PhD Dissertation*, The University of Texas at Austin, December 1996.
15. Pincheira, J. A., "Seismic Strengthening of Reinforced Concrete Frames Using Post-Tensioned Bracing System", *PMFSEL Report N.92-3*, The University of Texas at Austin, Austin, TX, December 1992
16. Farahany, M. M., "Computer Analysis of Reinforced Concrete Cross Sections", *M.Sc. Thesis*, The University of Texas at Austin, May 1983
17. Alvarez, R. J., and Brinstiel, C., "Inelastic Analyses of Multistory Frames", *Journal of Structural Division*, ASCE, 95(11), 1969, pp. 2477-2503
18. Fardis, M. N., and Calvi, M. G., 1994, "Member-type Models for the Nonlinear Seismic Response of Reinforced Concrete Structures", *Experimental and Numerical Methods in Earthquake Engineering*, Editors Donea, J., and Jones, P. M., Kluwer Academic Publishers, Dordrecht, The Netherlands.
19. Filippou, F. and Issa, A. , "Nonlinear Analysis of Reinforced Concrete Frames under Cyclic Load Reversals", *Report No. UBC/EERC88/12*, Earthquake Engineering Research Center, University of California at Berkeley, CA, September 1988, 114 pp.
20. Newmark, N. M., "A Method of Computation for Structural Dynamics", *Transactions ASCE*, Vol. 127, Part I, 1962, pp. 1406-1435.
21. Giberson, M. F., " Two Nonlinear Beams with Definition of Ductility", *Journal of the Structural Division*, ASCE, Vol. 95, February 1969, pp. 137-157.

22. Takeda, T., Sozen, M. A. and Nielsen, N., "Reinforced Concrete Response to simulated Earthquakes", *Journal of the Structural Division*, ASCE, Vol. 96, Dcember 1970, pp. 2557-2573.
23. Edward L. Wilson, "Three Dimensional Dynamic Analysis of Structures with Emphasis on Earthquake Engineering", Computers and Structures, Inc. Berkeley, CA. 1997. "Damping and Energy Dissipation", http://www.csiberkeley.com/Tech_Info/dampEnergyDiss.html., November 1998.
24. Umehara, H. and Jirsa, J. O., "Shear Strength and Deterioration of Short Reinforced Concrete Columns under Cyclic Deformations", *PMFSEL Report 823*, The University of Texas at Austin, July 1982, 256 pp.
25. Kent, D. C. and Park, R., "Flexural Members with Confined Concrete ", *Journal of the Structural Division*, ASCE, Vol. 97, No. ST7, July 1977.
26. Applied Technology Council, Tentative Provisions for the Development of Seismic Regulations for Buildings, ATC 3-06, Washington, DC, 1978.
27. American Society of Civil Engineers, Handbook for the Seismic Evaluation of Buildings- A Prestandard, FEMA310, Washington, D.C., January 1998.
28. A. Biddah and A. Heidebrecht, "Seismic Performance of Moment-Resisting Steel Frame Structures Designed for Different Levels of Seismic Hazard", *Earthquake Spectra*, Vol.14, No. 4, November 1998.
29. P. Negro and A. Colombo, "How Reliable Are Global Computer Models? Correlation with Large-Scale Tests", *Earthquake Spectra*, Vol.14, No. 3, August 1998.
30. Veletsos, A. S., "Dynamics of Structure Foundation Systems", Structural and Geotechnical Mechanics, A Volume Honoring N. M. Newmark, edited by W. J. Hall, PrenticeHall, 1977, pp. 333-361.
31. "Designer's Guide to the Dynamic Response of Structures", Jeary, F.A.P, Routledge, 1st edition, 1998.
32. Mary Beth D. Hueste and James K. Wight, "Evaluation of a Four-Story Reinforced Concrete Building Damaged during the Northridge Earthquake", *Earthquake Spectra*, Vol. 13, No. 3, August 1997.

33. J. P. Moehle, "Displacement-Based Design of RC Structures Subjected to Earthquakes", *Earthquake Spectra*, Vol. 8, No. 3, 1992.
34. Vision 2000 Committee, "VISION 2000, Performance Based Seismic Engineering of Buildings", Structural Engineers Association of California (SEAOC), Sacramento, California, April 1995.
35. Applied Technology Council, "Post-Earthquake Safety Evaluation of Buildings", ATC-20, Redwood City, CA, 1989.
36. Peter Fajfar, "Trends in Seismic Design and Performance Evaluation Approaches", *Proceedings of the Eleventh European Conference on Earthquake Engineering*, September 1998, Paris, France.
37. Newmark, N. M., and Rosenblueth, E., "Fundamentals of Earthquake Engineering", Prentice-Hall, Inc., Englewood Cliffs, NJ, 1971.
38. Housner, G. W., "An Investigation of the Effects of Earthquakes on Buildings", *Ph.D. Thesis*, California Institute of Technology, Pasadena, CA, 1941.
39. Biot, M. A., "A Mechanical Analyzer for Prediction of Earthquake Stresses", *Bulletin of the Seismological Society of America*, Vol. 31, pp. 151-171, 1941.
40. Biot, M. A., "Analytical and Experimental Methods in Engineering Seismology", *Proceedings of ASCE*, Vol. 68, pp. 49-69, 1942.
41. Seed, H. B., Ugas, C., and Lysmer, J., "Site-Dependent Spectra for Earthquake-Resistance Design", *Bulletin of the Seismological Society of America*, Vol. 66, pp. 221-243, 1976.
42. Moghadam, A.S. and Tso, W.K., "Seismic Response of Asymmetrical Buildings Using Push-Over Analysis". *Proceedings of the Workshop on Seismic Design Methodologies for the Next Generation of Codes*, Bled, Slovenia 1997. Rotterdam: Balkema.
43. Joe Nicoletti, "Static Nonlinear Pushover Analysis", Appendix G, Vision 2000, Performance Based Seismic Engineering of Buildings. Sacramento, CA. SEAOC 1995.
44. Sigmund A. Freeman, "Development and Use of Capacity Spectrum Method", *Proceedings from the Sixth U.S. National Conference on Earthquake Engineering*, EERI, May 31st-June 4th, Seattle, WA., 1998.

45. Bathe, K. J., "Finite Element Procedures in Engineering Analysis", Prentice-Hall, Inc., Englewood Cliffs, NJ, 1982.
46. Newmark, N.M. and Hall, W.J., *Earthquake Spectra and Design*, Earthquake Engineering Research Institute, Oakland, California, 1982.
47. Priestley, M.J.N., Kowalsky, M.J., Ranzo, G., Benzoni, G., "Preliminary Development of Direct Displacement-Based Design for Multi-Degree of Freedom Systems", *Proceedings 65th Annual SEAOC Convention*, pp 47-66, October 1-6, 1996, Hawaii.
48. Mete A. Sozen, "A Frame of Reference", *The Art and Science of Geotechnical Engineering at the Dawn of the Twenty-First Century. A Volume honoring Ralph B. Peck*. Editors: E.J Cording, W.J. Hall, J.D. Halmiwanger, A.J. Hendron Jr., G. Mesri. Prentice Hall, 1989 pp. 240-247.
49. Hamburger, R.O., "Defining Performance Objectives". *Seismic Design Methodologies for the Next Generation of Codes*. Editor: Peter Fajfar and Helmut Krawinklet. A.A. Balkema, Rotterdam, Brookfield, 1997.
50. Plassard, J. and Kogoj, B., 1981, "Seismicite du Liban", *Collection des Annales-Memoires de l'Observatoire de Ksara*, 4. Troisieme edition, Conseil National de la Recherche Scientifique , Beirut, 47pp.
51. Ambraseys, N. and Barazangi, M., 1989, "The 1759 Earthquake in Bekaa Valley: Implications for Earthquake Hazard Assessment in the Eastern Mediterranean Region", *Journal of Geophysical Research*, Volume 94, No. B4, pp. 4007-4013.
52. Ambraseys, N. and Melville, C.P., 1988, "An Analysis of the Eastern Mediterranean Earthquake of 20 May 1202", *Historical Seismograms and Earthquakes of the World*, Academic Press Inc. Harcourt Brace Jovanovich Publishers, pp. 181-200.
53. Jackson, J. and McKenzie, D., 1988. "The Relationship Between Plate Motions Seismic Moment Tensors, and the Rates of Active Deformation in the Mediterranean and Middle East". *Geophysical Journal* 93, pp. 45-73.
54. Harajli, M.H., Tabet, C., Sadek, S., Mabsout, M., Moukaddam, S. and Abo, M., 1994. "Seismic Hazard Assessment of Lebanon: Zoning Maps, and Structural Seismic Design Regulations", *Research Report*, submitted to the Directorate of Urbanism, Ministry of Public Works, Beirut, Lebanon, pp. 195.

55. El-Khoury, N.D. and Harajli, M.H.,1997. "Seismic Risk Assessment of Existing Building Structures in Lebanon", *Research Report*, submitted to the National Council for Scientific Research, Beirut, Lebanon.
56. Moghadam, A.S., Tso, W.K., "Pushover Analysis for Asymmetrical Multistory Buildings". *Proceedings from the 6th National Conference on Earthquake Engineering*. EERI. May-June, 1998.
57. Bertero V., "Lessons Learned from Recent Earthquakes and Research and Implications for Earthquake-Resistant Design of Building Structures in the United States", *Earthquake Spectra Journal*, 2 (4), 1986. pp. 825-858.
58. Pauley, T. and Priestly, M. J. N., "Seismic Design of reinforced Concrete and Masonry Buildings", John Wiley and Sons, Inc., 1992.
59. Mirza, S.H., Hatzinikolas, M. and MacGregor, J.G., "Statistical Description of the Strength of Concrete", *Journal of the Structural Division*, ASCE, June 1979, pp. 1021-1037.
60. Mander, J. et al. 198, "Seismic Design of Bridge Piers", *Report 84-2*, Department of Civil Engineering, University of Canterbury, New Zealand.
61. Lu, Zhan-Qin and Chen Jia-Kui, " Aseismic Behavior of RC and SRC Short Columns", *Concrete Shear in Earthquake*, Elsevier Applied Science, London, and New York, 1992, pp. 65-74
62. Wasti, S.T. and Sucuoglu, H., "Rehabilitation of Moderately Damaged R/C Buildings after 1 October 1995 Dinar Earthquake", *Report No. METU/EERC 99-01*, April 1999, Ankara, Turkey.
63. Gulkan, P. et al., "Turkish Seismic Zones Map", *Report No. 93-01*, Earthquake Engineering Research Center, Middle East Technical University, 1993.
64. JoAnn Browning, Y. Roger Li, Abraham Lynn, Jack P. Moehle, "Performance Assessment for a Reinforced Concrete Frame Building",. *Seismic Design Methodologies for the Next Generation of Codes*, *Fajfar and Krawinkler*. 1997 Balkema, Rotterdam, ISBN 90 5410 928 9.
65. Bertero, V. V., Anderson, J., C., Krawinkler, H. and Miranda, E., "Design Guidelines for Ductility and Drift Limits", *UBC/EERC-91/15*, Earthquake Engineering Research Center, University of California, Berkeley, CA. 1991.

66. Kim, S. and D'amore, E., "Push-over Analysis Procedure in Earthquake Engineering", EERI, *Earthquake Spectra*, Vol. 15, No. 3, August 1999.
67. Jirsa, J. O. and Feghali, H. L., "Simulation of Seismic Response of Reinforced Concrete Structures", *Proceeding of the Ugur Ersoy Symposium on Structural Engineering*, Ankara, Turkey, July 1999.
68. Kunnath, S.K., "IDASS Version3.0: Inelastic Damage Analysis of Structural Systems", University of Central Florida, July 1999.
69. Gupta, B., "Enhanced Pushover Procedure and Inelastic Demand Estimation for Performance-Based Seismic Evaluation of Buildings". *PhD Dissertation*, University of Central Florida, Orlando, Florida, 1998.
70. Applied Technology Council, "Seismic Evaluation and Retrofit of Concrete Buildings". *Report No. SSC 96-01*, November 1996, Redwood City, CA.
71. Alcocer, S. M. and Jirsa, J. O., "Reinforced Concrete Frame Connections Rehabilitated by Jacketing," *PMFSEL Report 911*, The University of Texas at Austin, July 1991, 221 pp.
72. Badoux, M. E., "Seismic Retrofitting of Reinforced Concrete Structures with Steel Bracing Systems," *PhD Dissertation*, The University of Texas at Austin, May 1987, 275 pp.
73. Gaynor, P. J., "The Effect of Openings on the Cyclic Behavior of Reinforced Concrete Infilled Shear Walls," *M.Sc. Thesis*, The University of Texas at Austin, August 1988, 245 pp.
74. French, C. W. and Moehle, J. P., "Design of Beam-Column Joints for Seismic Resistance," *SP123-9*, ACI, Detroit, 1991, pp. 225-258.
75. Wood, S. L., Course CE384R, Class Notes. Summer 1996.

VITA

Habib Labib Feghali was born in Kfarabida, in the North of Lebanon on August 1st, 1971, the son of Labib Salloum Feghali and Amale Youssef Cherabieh-Feghali. After completing his school work at College des Freres Mont LaSalle at Ain Saade, Lebanon, he entered Lycee Louis Le Grand in Paris in 1990, where he took the preparatory classes for the French Grandes Ecoles and was admitted to Ecole Centrale in 1993. In 1995, he entered the University of Texas at Austin. In 1996, he received his French Diploma of Engineering (general engineering) from Ecole Centrale and his Master of Science in Engineering from the University of Texas at Austin. In spring 1997, he was admitted to the PhD program at the University of Texas at Austin.

Permanent address: In Lebanon

Building Labib Feghali, Al-Shwar street, Dbayeh, Lebanon

P.O.Box 70048 Antelias Lebanon

Habib.Feghali@alumni.utexas.net

In the United States

11660 Porter Valley Dr.

Northridge, CA, 91326

This dissertation was typed by the author.